0-18-71

A15-05058 N71-36/17

NASA CR 72973

FINAL REPORT

DEVELOPMENT OF LOW-COST ABLATIVE NOZZLES FOR LARGE SOLID PROPELLANT ROCKET MOTORS

CASE FILE COPY

Prepared by:

J. D. Sohl

Aerojet Solid Propulsion Company Advanced Technology Operations Sacramento, California

National Aeronautics and Space Administration Lewis Research Center Cleveland, Ohio

Technical Management
J. J. Notardonato, Project Manager

NOTICE

This report was prepared as an account of Government-sponsored work. Neither the United States, nor the National Aeronautics and Space Administration (NASA), nor any person acting on behalf of NASA:

- A.) Makes any warranty or representation, expressed or implied, with respect to the accuracy, completeness, or usefulness of the information contained in this report, or that the use of any information, apparatus, method, or process disclosed in this report may not infringe privately owned rights; or
- B.) Assumes any liabilities with respect to the use of, or for damages resulting from the use of, any information, apparatus, method, or process disclosed in this report.

As used above, "person acting on behalf of NASA" includes any employee or contractor of NASA, or employee of such contractor, to the extent that such employee or contractor of NASA or employee of such contractor prepares, disseminates, or provides access to any information pursuant to his employment or contract with NASA, or his employment with such contractor.

NASA CR 72973

FINAL REPORT

DEVELOPMENT OF LOW-COST ABLATIVE NOZZLES FOR LARGE SOLID PROPELLANT ROCKET MOTORS

Prepared by:

J. D. Sohl Aerojet Solid Propulsion Company Advanced Technology Operations Sacramento, California

January 1971

Contract NAS3-12038

Prepared for:

National Aeronautics and Space Administration Lewis Research Center Cleveland, Ohio

Technical Management
J. J. Notardonato, Project Manager



ABSTRACT

The objective of this program was to evaluate selected low-cost ablative materials at a scale and under conditions relevant to large solid-rocket motor nozzle design. In addition, acquisition of processing and performance data on a trowelable chamber insulation system was required.

Two 13-in.-dia (33 cm) nozzles were tested in the firing of Algol-sized motors. The first firing resulted in a chamber burnthrough early in the test because of an undetected flaw in the bond joint between the igniter cavity restriction and the forward boot. Valid performance data on the low-cost ablative nozzle materials were obtained from the second test. These data were used in the design of a full-scale nozzle, suitable for use on a 260-FL motor.

Thermal and stress analyses were conducted on the full-scale nozzle design, which incorporates a flexible seal for TVC purposes and a 9:1 contoured exit cone. Fabrication specifications and a detailed cost estimate were also prepared for this design. Extensive use of canvas-duck phenolic and the less expensive carbon tapes results in an ablative material cost savings of about 35% compared with a similar design utilizing conventional carbon and silica phenolic composites.

			445
			e ·

TABLE OF CONTENTS

				Page
I.	Sum	mary		1
	Α.		I - Nozzle and Test Motor Design, Analysis, Fabrication	epones of the state of the stat
	В.		II - Nozzle and Trowelable Insulation em Evaluation	3
	С.		III - Full Scale Nozzle Design, Analysis, Fabrication Planning	. 3
II.	Int	roduct	ion	4
III.	Tec	hnical	Discussion	5
	Α.	Prog	ram Objectives	5
	В.		I - Nozzle and Test-Motor Design, Analysis, Fabrication	6
		1.	Motor Design and Description	6
		2.	Nozzle Design	12
		3.	Motor Processing	25
		4.	Nozzle Fabrication	36
		5.	Ablative Materials Characterization	42
	С.	Task	: II - Nozzle and Insulation System Evaluation	48
		1.	Test Plan	48
		2.	Motor LCAN-01 Test Results	51
		3.	Motor LCAN-02 Test Results	57
	D.		: III - Full Scale Nozzle Design and rication Planning	67
		1.	Evaluation of High Nozzle Throat Erosion Rates on Motor Performance and Cost	67
		2.	Design Criteria	70
٠		3.	Other Factors Affecting the Design	71
		4.	Design Description	74
		5.	Design Verification	79
		6.	Fabrication Plan for Ablative Components	84
		7.	Full-Scale Nozzle Cost Estimate	89
		8.	Other Factors Influencing Large Nozzle Fabrication Costs	96
		9.	Alternative Exit Cone Fabrication Methods	97
IV.	Con	clusio	ons and Recommendations	99

TABLE LIST

	Table
IBT-100/IBT-106 Insulation System Design Summary for LCAN Motor	1
Calculated Weight Summary of IBT-100/IBT-106 Insulation	
System for Algol Nozzle Test Motors	2
Effects of Curing Agent Level, Cure Temperature, and Cure Time on the Mechanical Properties of ANB-3347	3
Effect of PBAN Terpolymer Lot on Mechanical Properties of ANB-3347 Propellant	4
Effect of Oxidizer Blend Ratio on Mechanical Properties of ANB-3347 Propellant	5
Summary of Significant ANB-3347 Propellant Characteristics	6
Grain Stress Summary	7
NASA-LeRC Nozzle and Test Motor Design Criteria	8
Candidate Low Cost Ablative Materials for the Algol Test Nozzles	9
Cost Effectiveness Comparison of Ablative Materials Considered in 13-india (33 CM) Nozzle	10
Initial Boundary Layer Conditions	- Para-
Heat Transfer Analysis Summary, Nozzle No. 1	12
Heat Transfer Analysis Summary, Nozzle No. 2	13
Heat Transfer Analysis Summary, Carbon Phenolic Throat, Candidate Nozzle	14
Structural Analysis Summary, Nozzle No. 1	15
Stress Analysis Summary, Nozzle No. 2	16
Qualification Data for LCAN-02 Insulation System	17
Qualification Data for ANB-3347 Propellant	18
Mechanical Property Data for ANB-3347 Propellant Batches	19
Pre-Preg Materials Used in Test Nozzles	20
Pre-Preg Material Properties	21
Fabrication Data for Nozzle Components	22
Billet Tag-End Properties	23
Mechanical Properties of SP-8030-96 Silica Composite	24
Mechanical Properties of MXSC-195 Carbon-Silica Composite	25
Mechanical Properties of 4KXDO2 Canvas Composite	26
IBT-106 Bond Test Data	27
Ballistic Performance Summary, Motor LCAN-02	28
LCAN-02 Nozzle Material Performance Summary	29

TABLE LIST (cont)

	<u>Table</u>
Compressive Strength of Charred Carbon Silica in 45 Degree-to-Ply Direction	30
Comparison of Nozzle Entrance Conditions and Configuration Between Algol IIB and LCAN-02	31
Effect of Nozzle Erosion Rates on 260/SIVB Vehicle Payload Capability	32
260-in-dia (6.6 m) Motor Weight and Cost Increase Required to Achieve Baseline Payload	33
Ablative Material Cost Comparison for 260-FL	0.4
Nozzle De signs	34
Exhaust Gas Composition - ANB-3374 Propellant (HTPB)	35
Weight Summary, Full-Scale Nozzle	36
Exit Cone Weight Summary	37
Thermal Analysis Stations and Boundary Conditions - Full-Scale Nozzle	38
Heat Transfer Correction Factor Schedule	39
Expected Performance of Full-Scale Nozzle	40
Structural Material Properties	41
Carbon Phenolic Material Properties	42
Canvas-Duck Phenolic Material Properties	43
Maximum Stress and Strain Conditions in Exit Cone Thermal Stress Analysis Summary	44
Full Scale Nozzle Cost Summary	45
Ablative Material Cost Summary	46
Pre-Preg Prices Applicable to Full-Scale Ablative Nozzles	47
Tooling Requirements, 260-FL Nozzle Fabrication	48
New Facility Requirements and Estimated Cost	49

FIGURE LIST

	Figure
LCAN Test Motor Assembly	1
Trowelable Insulation Configuration	2
Propellant Initial Modulus vs Cure Agent Concentration	3
Effect of Oxidizer Blend Ratio on the Solid Strand Burning Rates of ANB-3347 Propellant	4
Algol Test Motor Grain Design	5
Predicted Pressure and Thrust-vs-Time, LCAN Motors	6
Nozzle No. 1	7
Nozzle No. 2	8
Nozzle No. 2 - Reworked Configuration	9
Erosion, Char, and Thermal Zone at Throat, Nozzle No. 1	10
Erosion, Char Depth and Thermal Zone Depth at Throat Station, Nozzle No. 2	11
Erosion, Char, and Thermal Zone Depth Throat Station, Candidate Nozzle	12
Thermal Response Profile, Nozzles No. 1 and 2	13A
Thermal Response Profile, Nozzle No. 2 - Reworked Configuration	13B
Sidewall Dispenser	14
Fwd Dome Sweep Template	15
Aft Dome Sweep Template	16
Sidewall Dispenser Orientation	17
Aft Flange Insulation Details	18
View of Completed Insulation, Motor LCAN-01	19
Aft Step Joint and Boot, Motor LCAN-02	20
Motor LCAN-02 Rework	21
Test Specimen Design	22
Thermal Conductivity of MXSC-195 Carbon-Silica Composite	23
Specific Heat of MXSC-195 Carbon Silica Phenolic Composite	24
Thermal Expansion of MXSC-195 Carbon-Silica Composite	25
Thermal Conductivity of 4KXD02 Canvas Composite	26
Specific Heat of 4KXD02 Canvas Composite	27
Thermal Expansion of 4KXD02 Canvas Composite	28
Profile Mapping of LCAN-01 Nozzle	29

FIGURE LIST (cont)

	Figure
Thermal Sensor Assembly	30
View of Motor LCAN-01 Prior to Test Firing	31
Ignition Transient - Motor LCAN-01	32
Forward Head Configuration - Motor LCAN-01	33
Pressure and Thrust vs Time, Motor LCAN-01	34
Posttest View of Motor and P-3 Test Facility	35
Chamber Fragment From Area of Major Failure	36
Pressure and Thrust vs Time, Motor LCAN-02	37
Posttest View of LCAN-02 Nozzle	38
Erosion Rate-vs-Area Ratio for Canvas-Duck Phenolic	39
View of Sectioned Exit Cone	40
Nozzle Throat Section Fragments	41
Entrance Insulation at Location of Failure	42
Posttest Nozzle Insulation Profile	43
Charred MXSC-195 From Entrance Section Tag-End	44
Chamber Temperature 289 in. Forward of Aft Flange	45
Posttest View of LCAN-02 Chamber	46
Trowelable Insulation Performance Data	47
Thrust-vs-Time Performance Comparison for Full-Length 260-india (6.6 m) Motors	48
First Stage Cost Increase vs Throat Erosion Rate	49
Predicted Pressure vs Time Performance 260-FL Motor (260/SIVB Study)	50
Low-Cost Nozzle Design, 260-FL Motor	51
Low Cost Exit Cone Design, 260-FL Motor	52
Erosion, Char and Thermal Gradient - Full-Scale Nozzle	53
Erosion, Char and Thermal Gradient - Full-Scale Exit Cone	54
Predicted Thermal Response at Throat Station - Full Scale Nozzle	55
Predicted Thermal Response at Exit Cone Area Ratio of 2.5:1	56
Predicted Exit Cone Erosion vs Area Ratio at End of Firing	57
Finite Element Model - Nozzle Shell	58
Finite Element Model, Throat Support Structure	59
Calculated Deflections at Outer Joint	60

FIGURE LIST (cont)

	rigure
Maximum Tensile Strain Distribution at Exit Cone ϵ = 2.3	61
Maximum Hoop Stress Distribution at Exit Cone ϵ = 2.3	62
Maximum Tensile Strain Distribution at Exit Cone ϵ = 3.85	63
Maximum Hoop Stress Distribution at Exit Cone ϵ = 3.85	64
As-Wrapped Closure Insulation Billet Configuration	65
As-Wrapped Submerged Insert Billet Configuration	66
As-Wrapped Nose Insert Billet Configuration	67
As-Wrapped Entrance Insert Billet Configuration	68
As-Wrapped Throat Insert Billet Configuration	69
Nozzle Fabrication Schedule - Option A	70
Nozzle Fabrication Schedule - Option B	71

I. SUMMARY

The Low-Cost Ablative-Nozzle Development Program, conducted under Contract NAS3-12038, was initiated for the purpose of acquiring performance data on promising low-cost materials under conditions applicable to large solid rocket motors. To accomplish this objective, two intermediate size (Algol) motors, containing approximately 20,500 lb (9300 Kg) of a PBAN type propellant, were processed and test-fired. Each motor contained an IBT-100/106 insulation system troweled onto the internal chamber surfaces.

Selection of the ablative materials to be incorporated into each of the two test nozzles was made from a listing of several candidate materials included in the contract work statement. Utilization of conventional tape-wrapping and autoclave cure fabrication procedures were program requirements.

The program effort was organized in three tasks, as discussed below:

A. TASK I - NOZZLE AND TEST MOTOR DESIGN, ANALYSIS, AND FABRICATION

The first nozzle had a silica (SP-8030-96) and carbon-silica (MXSC-195) entrance insert, a carbon-silica throat, and an exit cone having a forward flame liner of carbon silica and an aft ablator of canvas-duck phenolic (4KXD02). Asbestos phenolic (MXA-6012) was used in the overwrap on each ablative insert.

The second test nozzle was an "all-white" design, having a silicaphenolic (MX-2600-96) throat, entrance, and forward exit cone liner and a canvasduck phenolic (4KSD02) aft exit cone liner. Canvas-duck was also used for the parallel-to-surface overwrap on all components. After the first motor test, the completed throat and entrance sections of the second nozzle were removed and replaced with inserts having the same materials as the first nozzle, except that MX-2600-96 silica was used in the entrance section instead of SP-8030-96 and the overwrap was of canvas-duck phenolic rather than asbestos phenolic.

Comprehensive thermal and stress analyses were performed on each nozzle design, using established computer routines, to determine the adequacy of the selected configuration and materials under the test firing conditions.

Although some minor problems were encountered during the wrapping of the carbon-silica throat section for the first nozzle, the processing qualities of the low-cost materials were generally satisfactory. In fact, the heavyweight silica and the canvas-duck materials had excellent fabrication characteristics. The asbestos overwrap of the exit cone for the first nozzle delaminated during the high temperature cure of the glass structural wrap. It was subsequently removed and replaced with an ambient curing epoxy-glass hand lay-up.

Application of the trowelable insulation system was accomplished using the technique described in Report NASA CR-72584 $^{(1)}$. Ultrasonic and radiographic inspection of the insulated cases revealed numerous small voids that were repaired prior to propellant loading.

Each insulated Algol chamber was loaded with ANB-3347 propellant using standard production Algol tooling and procedures. ANB-3347 propellant has a combustion temperature and exhaust gas composition similar to those of the ANB-3301 and -3354 propellants used in the 260-in.-dia (6.6 m) short length (260-SL) motors. The test motors were designed to operate at an average pressure of about 500 psia (345 N/cm^2) over a web duration of 40 sec.

Radiographic inspection of each loaded motor was accomplished and no discrepancies were detected.

Subsequent to the first motor failure (see Section I.B, below), the second motor was reworked to ensure a full-duration firing. Modifications included potting behind each boot and enlarging of the forward-grain igniter cavity.

An evaluation and characterization study was conducted by the Battelle Memorial Institute to further define the thermal and mechanical properties of the low-cost ablative materials. Thermal conductivity, specific heat, and thermal expansion measurements were obtained of the carbon-silica and canvas-duck materials in both the virgin and charred condition. Tensile, compressive, and shear strength data were also obtained for these materials and for the heavyweight silica phenolic. The very fragile nature of the charred carbon silica precluded acquisition of valid tensile and shear data on this material. All other results were satisfactory and comparable to data from other investigators.

I. Summary (cont)

B. TASK II - NOZZLE AND TROWELABLE INSULATION SYSTEM EVALUATION

The first motor firing resulted in a chamber burnthrough at 5.635 sec after fireswitch. This malfunction was caused by abnormal propellant ignition in the forward-boot/igniter-sleeve area. A localized pressure differential was created across the forward propellant web, which, in turn, initiated a massive failure of the insulation or primer bond to the case wall. No nozzle performance data were obtained.

Valid performance data on the low-cost nozzle ablatives were obtained from the second nozzle-evaluation motor firing. Motor operation was normal for 26.8 sec at which time a burnthrough occurred in the nozzle entrance section. Poor physical properties of the carbon-silica char, combined with the severe exhaust impingement and flow pattern in line with the grain valleys, caused the burnthrough. Performance of both the silica-phenolic and canvas-duck phenolic ablative liners in the exit cone was better than expected. The trowelable insulation system satisfactorily protected the case during the motor action time, demonstrating the potential of this type insulator for large motor application. Hot spots were formed on the case during the latter portion of the tail-off period and during the extended heat soak in areas where undetected thin spots and voids existed in the insulation.

C. TASK III - FULL SCALE NOZZLE DESIGN, ANALYSIS, AND FABRICATION PLANNING

A nozzle was designed that incorporated low-cost ablative materials suitable for use on a 260-in.-dia (6.6 m) full length (260-FL) motor. Heat-transfer and stress analyses were conducted that verified the adequacy of the design for the expected motor operating conditions. Fabrication plans and procedures were prepared for the manufacture of 30 nozzles over a 5-year period. Conventional tape wrapping and cure processes were specified, except in the aft exit cone where a tension overwrap technique replaces the autoclave method for achieving the desired final composite density. Tooling and facility requirements were identified and costs were calculated.

A detailed cost estimate for production of the nozzle was accomplished, and on the basis of the 30-nozzle fabrication schedule, a unit cost of \$899,334 was

developed. The ablative materials represent about 25% of this cost. The extensive use of the low-cost canvas-duck and lower-price carbon materials results in an ablative cost reduction of 35% in comparison with the more conventional materials used to date in nozzles of similar design. The overall nozzle cost savings would be about 9%.

ability of a 260/SIVB vehicle when high throat erosion rates (to 0.025 in./sec [0.063 cm/sec]) of the solid motor nozzle were encountered. The weight and cost of the additional propellant and motor inerts required to regain the mission capability of the base-line motor with a nozzle having a carbon throat, which erodes at 0.006 in./sec (0.015 cm/sec), were determined and compared to the cost-savings achieved through use of the low-cost ablative materials. It was conclusively shown that the most economical approach retains carbon, or an equivalent performing material, in the throat area but incorporates the lower cost ablatives in other sections of the nozzle.

II. INTRODUCTION

This report presents the results of the Low-Cost Ablative-Nozzle Development Program. The work was conducted by the Aerojet Solid Propulsion Company (ASPC) for the National Aeronautics and Space Administration, Lewis Research Center, under Contract NAS3-12038. The program was initiated in June 1969 to obtain performance data on low-cost ablative materials which could be used on large rocket motor nozzles in place of the more expensive conventional materials used previously. The quantities of these materials required are such that the cost of the ablative components represents a significant element of the motor unit cost.

Recent programs (2)(3) have identified ablative materials and fabrication techniques that may reduce the costs of ablative components significantly without introducing excessive performance penalties. Laboratory evaluations and small nozzle tests have been conducted to characterize the most promising low-cost materials. This program accomplished the next logical step in materials development by testing the most promising materials at firing conditions and on a scale relevant to the 260-FL class motors.

II. Introduction (cont)

The data obtained from the static firing of the subscale test motors and from the cost/performance trade studies were used in the design of a low-cost nozzle for a 260-FL motor. Design verification analyses, fabrication plans, and a detailed cost estimate for this nozzle were completed. The full-scale nozzle design described in this report makes maximum use of the most promising low-cost ablative material (canvas-duck phenolic) which was evaluated in the subscale tests. A material cost reduction of about 9.0% may be achieved over a similar design which uses carbon-phenolic and silica-phenolic composites exclusively in the ablative liners.

Supplement Agreement No. 1, dated 28 July 1969, to the basic contract provided for a demonstration of the processing feasibility and performance of a trowelable internal insulation system in the two nozzle test motors.

III. TECHNICAL DISCUSSION

A. PROGRAM OBJECTIVES

The overall objective of this program was the development of low-cost ablative nozzles for the large, solid-propellant rocket motors. To accomplish this objective, the following basic program requirements were established:

- 1. Evaluate the performance of the most promising low-cost ablative materials at a scale and under firing conditions relevant to large solid motors.
- Characterize the thermal and physical properties of these materials.
- 3. Using the data from the above two tasks, design and analyze a low-cost, full-scale nozzle.
- 4. Prepare manufacturing plans, specifications, and a cost estimate for the full-scale nozzle.

III.A. Program Objectives (cont)

A secondary objective concerned evaluation of the processing and performance characteristics of a trowelable insulation system in the motor chamber.

B. TASK I - NOZZLE AND TEST-MOTOR DESIGN, ANALYSIS, AND FABRICATION

1. Motor Design and Description

The nozzle test motor consisted of an Algol II chamber, a trowelable insulation system, a propellant type igniter, a PBAN propellant grain cast with a modified Algol II core, and the nozzle to be evaluated. The PBAN propellant is similar to the ANB-3105 and -3254 propellants used in the 260-SL motors that have been tested. The two test-nozzle configurations are described in Section III.B.2. The motor assembly is shown in Figure 1; the major components are discussed in the following paragraphs.

a. Chamber

The Algol IIB motor chamber, PN 360344-9, is fabricated of rolled-and-welded AISI 4130 steel, heat-treated to 180,000 to 200,000 psi (124000 to 136000 N/cm²) ultimate tensile strength in the sidewall section. The chamber is 318.4 in. (8.08 m) long, the outside diameter is 40 in. (1.02 m), and the nominal wall thickness in the cylindrical section is 0.112 in. (0.284 cm). The igniter is fastened to the forward-dome igniter boss by a snap ring, and the nozzle is secured to the aft-closure nozzle boss by a bolted joint. Both joints are sealed by 0-rings. Identical forward- and aft-skirt rings are provided for lifting and handling.

The chamber was hydrostatically tested to 725 to 750 psig (500 to 517 $\rm N/cm^2$) and has a burst strength capability in excess of 800 psig (551 $\rm N/cm^2$).

b. Trowelable Insulation System

(1) Introduction

Work completed under Contract NAS3-11224, "Development of Cost-Optimized Insulation System for Use in Large Solid Rocket Motors," led to the selection of trowelable insulation as a cost-effective system for 260-in.—dia (6.6 m) motor applications. A logical follow-on to the foregoing program was to demonstrate the installation process and performance of the selected trowelable insulation system in an intermediate size motor. The opportunity to accomplish this follow-on effort presented itself in processing of the two Algol ablative-nozzle test motors required for the subject contract.

The insulation system for the Algol nozzle-test motors (as contracted) was of standard Gen-Gard V-44, as used in the Algol IIB production motors. ASPC proposed and was granted a contract change to insulate the two Algol test motors with the selected insulation system derived under Contract NAS3-11224.

(2) Design

The insulation system design for the Algol test motor is shown in Figure 2. The significant motor performance parameters affecting insulation design were as follows:

	9	
Web	Average Pressure, psia (N/cm²)	502 (346)
Web	Duration, sec	40.1
Tota	al Duration, sec	63
Prop	ellant	ANB-3347
	Type	PBAN
	Aluminum Content, %	15
	Combustion Temperature, °F (°K)	5463 (3290)

The aluminum content and combustion temperature of the selected propellant, ANB-3347, are very similar to those of the 260-SL propellants, ANB-3105 and ANB-3254. Therefore, no design correction factor was necessary to account for

propellant flame composition and temperature differences. An adjustment in insulation performance was necessary to account for the lower web average pressure. Thickness loss rate data for the proposed materials were obtained from 260-SL and Contract NAS3-11224 motor tests, where the average operating pressure was approximately 600 psia (413 N/cm^2) . The correction factor applied was as follows:

$$\left(\frac{P_{c} \text{ motor}}{600}\right)^{0.3}$$

A design thickness calculation summary is shown in Table 1; a conservative safety factor of 2.0 was used.

The forward-dome insulation of IBT-106 tapered from a thickness of 0.40 in. (1.06 cm) at the igniter boss to 0.20 in. (0.53 cm) at the chamber tangent plane. The chamber sidewall insulation from the forward tangent to 14.0 in. (35.6 cm) forward of the aft joint was 0.20-in.-thick (0.53 cm) trowelable IBT-106. Insulation in the aft dome and nozzle forward shell varied in contoured thickness and because of the high gas velocities expected in these areas, trowelable IBT-100 was specified.* The critical insulation thickness was 1.30 in. (3.30 cm) at the 26-in.-dia (63.5 cm) location of the aft step-joint. All other areas in the aft dome and nozzle had excess material to maintain a smooth contour. The propellant boots were 0.25-in.-thick (0.635 cm) trowelable IBT-106, with a 10-in.-long (25.4 cm) bond line to the sidewall insulation. A calculated insulation weight summary is shown in Table 2.

c. Propellant Selection and Tailoring

The propellant selected for loading of the two Algol cases was ANB-3347. This propellant is basically a low-burning-rate version of the ANB-3254 propellant used in Motor 260-SL-3. It contains 84 wt% total solids

^{*} IBT-100 is a trowelable, cure-in-place insulation based on an epoxy-cured PBAN binder filled with asbestos fibers, antimony oxide, and carbon black. IBT-106 is essentially the same except for shorter asbestos fiber length which makes it easier to process and apply but less resistant to erosive conditions.

(AP/A1, 69/15) and utilizes a PBAN binder, cured with DER-332 and plasticized 15% with DOA. There are no burning rate additives. Available data had indicated that the target liquid strand burning rate of approximately 0.21 in./sec (0.533 cm/sec) at 500 psia (345 N/cm 2) could be achieved with an oxidizer blend composed of +48/Ung/MA in a 50/30/20 ratio.

To determine the curing agent concentration required to provide a propellant with the desired initial modulus of 450 to 500 psia (310 to 345 N/cm^2), a series of laboratory scale, 10-lb size (4.54 Kgm), batches were prepared with five levels of DER-332 epoxide ranging from 90 to 110 equivalents. On the basis of mechanical properties data from these batches (Table 3 and Figure 3), a curing agent level of 110 equivalents was selected.

Since the inner bore hoop strain in the Algol motors could be reduced by curing the propellant at 110°F (317°K) instead of the usual 135°F (331°K) (for PBAN propellants), samples of each of these batches were cured at both of these temperatures. The data (Table 3) indicate that the propellant initial modulus and tensile strength reached approximately the same level at either cure temperature, but the propellant strain capability was significantly less when when cured at 100°F (311°K) rather than at 135°F (331°K). All batches appeared to be fully cured after 10 to 11 days at 135°F (331°K), and there was no significant change in properties after an additional 7 days cure. Based on this data, a cure cycle of 10 to 11 days at 135°F (331°K) was selected for the Algol motor.

The binder ingredient that exerts the greatest effect on propellant mechanical properties is the PBAN terpolymer. Since there was not sufficient PBAN available from a single lot of material to make all of the propellant required for this program, it was necessary to utilize a blend of two lots (691 and 725A). All the small-scale development batches described above utilized a blend of these two lots in the proper ratio. To determine the effects of possible incorrect blending on propellant properties, a 10-1b (4.54 Kgm) batch of ANB-3347 propellant was prepared with each lot of PBAN by itself (691 and 725A). The data (Table 4) indicate that these two particular lots produce virtually identical propellant and errors in blending would not be expected to have any significant effect on propellant properties.

Although the 50/30/20, +48/Ung/MA oxidizer blend ratio provided approximately the desired propellant burning rate, final selection of the blend ratio to be used in the two Algol motors was made on the basis of solid strand and 3KS-500 size motor burning rates of the propellant made in the first production size (scale-up) batch. To provide a sound basis for selection of this oxidizer blend ratio, a series 10-1b (4.54 Kgm) propellant batches was prepared with blends ranging from 80/20, +48/MA to 80/20, Ung/MA to establish a correlation between strand burning rate and oxidizer blend. The results of this work are shown graphically in Figure 4. At 500 psia (345 N/cm²) the solid strand burning rate range is 0.195 to 0.240 in./sec (0.495 to 0.610 cm/sec). These batches were also tested for mechanical properties, and the data (Table 5) indicate no significant effect due to variation of the oxidizer blend.

The significant propellant characteristics are summarized in Table 6.

d. Grain Design

A cast-in-case, internal-burning grain design with forward and aft release boots was selected to provide the required ballistic performance in conjunction with the ANB-3347 propellant. The standard Algol IIB grain configuration consists of a Maltese cross perforation extending to within 9.0 in. (22.9 cm) of the forward end of the grain. The cross configuration is tapered so that the flow area increases toward the aft end, allowing for maximum propellant loading while minimizing erosive burning. The grain design is defined in Aerojet Drawing 1147611 (Figure 5).

The grain design is identical to that of the Algol IIB except for the incorporation of fillets between each of the four cross tips in the aft 75 in. (190 cm) of the bore. Each flat fillet has a maximum depth of 1.0 in. (2.54 cm) at the aft end and tapers linearly to zero depth 75 in. (190 cm) forward. The extra cross-sectional flow area provided by the additional tapering of the bore results in an aft end port-to-throat area ratio of 1.34.

Like the Algol IIB, the grain is case-bonded with the exception of forward and aft end boots. Since the stress and strain levels are essentially the same as these experienced in the Algol IIB motor, the allowable mechanical properties of ANB-3347 propellant were compared with those of the Algol propellant. This comparison verified that the margins of safety for the low-cost ablative nozzle (LCAN) motor were all positive. A summary of maximum stresses and strain-vs-propellant allowable mechanical properties is presented in Table 7.

e. Igniter

The ignition system consists of a modified Algol IIB propellant igniter (PN 1128253-49) with two initiators. The system was selected because of its availability, prior qualification, and demonstrated ability to ignite the motor with Algol IIB propellant. The pyrotechnics consist of a primary charge of 100 gm of BPN pellets and a main charge of about 5.5 lb (2.5 Kgm) of ANP-2758 Mod I propellant.

Two propellant-loaded igniter chambers, residual to a previous Algol IIB program, were modified from the standard configuration for use in this program. About 40% of the igniter propellant charge was removed by machining away 2/3 of each of the 18 grain rays. This was done to reduce the mass-flow added to the motor at ignition where the predicted pressure peak was approaching the case proof pressure. Analysis verified that the remaining propellant charge would provide adequate energy for positive motor ignition. A 0.25-in.-thick (0.64 cm) coating of IBT-106 insulation was applied to the outer surface of both igniter chambers for protection during the firing.

f. Ballistic Performance

The Algol nozzle test motors were designed to subject the low-cost ablative nozzles being evaluated to motor firing conditions representative of large solid rocket boosters. Exhibit A to the contract work statement stipulated the principal operating parameters that provided the design criteria of the motor (Table 8). An average chamber pressure of 600 ± 100 psia ($414 \pm 69 \text{ N/cm}^2$) over a web time of 40 sec (min) was required.

Using the actual solid strand burning rate of the propellant cast into Motor LCAN-O1, and the expected throat erosion rate of 11.7 mils/sec (28.7 cm/sec), a ballistic performance prediction was accomplished. The Algol IIB Simulation Program that was used takes into account the expected erosive burning effects on motor performance. The results of this analysis indicated that a web action time of 38.6 sec at an average pressure of 532 psia (366 N/cm 2) could be expected. The combination of a slightly higher than desired propellant burning rate and the initial high pressure due to erosive burning contributed to the web-duration being less than the target value. However, the predicted chamber pressure was 500 psia (345 N/cm 2) or greater for 39.6 sec, which is very close to the required 40 sec. Average chamber pressure for the duration of the motor analysis (41 sec) was 530 psia (365 N/cm 2) with a corresponding average thrust of 4.38 x 10 6 lbf (19.5 x 10 6 N). The predicted pressure and thrust curves, which are applicable to both motors, are shown in Figure 6.

2. Nozzle Design

a. Requirements

Exhibit A to the contract work statement established the basic ground rules of the low-cost ablative nozzle design consistent with the objective of acquiring performance data on low cost ablative materials suitable for use in future large solid motor nozzles. A nonsubmerged nozzle having a throat diameter of 13 to 16 in. (33 to 40.6 cm), a 6:1 expansion ratio, and a conical exit cone with a divergence angle of 17.5° (0.306 rad.) was specified. It was further required that conventional tape wrapping and pressure/heating cure techniques be employed. A listing of acceptable candidate materials was provided (Table 9) with actual selection of materials subject to approval of the NASA-LeRC Project Manager.

The nozzle was to be of flight-weight design, having maximum safety factors of 1.3 on structural components and 2.0 on ablative components. These requirements were subsequently relaxed, with the approval of the NASA-LeRC Project Manager, in the intent of increasing the probability of success in the

tests. Therefore, no effort was attemped to optimize the design to a flight-weight configuration. Primary considerations in the design were that the interface between the ablative flame liner and the insulation overwrap did not exceed 100°F (312°K) during the firing and that strain in the ablatives did not exceed 0.25%.

b. Material Selection

(1) Nozzle No. 1

On the basis of nozzle material cost trade studies conducted on a base-line 260-FL nozzle design, conclusion was made that the use of carbon-silica phenolic, double-weight silica, and canvas-duck phenolic showed the most potential for overall nozzle-cost reduction. These materials would be substituted for the MX-4926 carbon phenolic and FM-5131 silica phenolic materials that have been used previously in the large motor nozzle assemblies. Although subsequent trade studies (discussed in Section III.D.1) indicated that the use of a carbon-phenolic material in the throat was the most economical approach in reducing overall large-motor cost, it was felt that additional characterization of carbon-silica would be beneficial. If the actual throat erosion of this material could be demonstrated to be lower than expected (as determined from limited subscale-motor test data) it could be an atractive replacement for carbon-phenolic on the basis of its lower cost of \$5.00 to \$6.00/lb. However, its most probable application would be in the lower erosion areas of the nozzle entrance sections and forward exit cone.

In the less-severe environments of the nozzle and exit cone, the use of heavyweight silica and canvas-duck phenolic showed the greatest potential as a cost-effective ablative material. These materials had not been tested previously on a large scale motor having propellant exhaust characteristics essentially the same as would be experienced on the 260-in.-dia (6.60 m) motors. Other low-cost materials on the NASA-LeRC listing of acceptable alternatives, such as FM-5272 paper phenolic and the asbestos phenolics, do not possess any significant cost, performance, or processing advantage over the canvas-duck materials and were not considered for evaluation as ablators.

III.B. Task I - Nozzle and Test-Motor Design, Analysis, and Fabrication (cont)

For the reasons stated above, the following material selections were made:

Component	Area Ratio	Material	Acceptable Grades
Entrance Section	-3.49 to -1.73	Silica Phenolic	MX-2600-96
		(double-weight)	SP-8030-96
			WB-2233-96
			FM-5504-96
Entrance Section	-1.73 to -1.11	Carbon-Silica Phenolic	MXSC-195
Throat Inse rt	-1.11 to +1.17		4C 2530
Exit Cone Fwd Liner	+1.17 to +1.60		WB-8251
Exit Cone Aft Liner	+1.60 to -6.00	Canvas Duck Phenolic	KF-418
	•		4KXD02
			CA-2213
Overwrap	NA	Asbestos Phenolic	MXA-6012
,			FM-5525

Selection of asbestos phenolic for the overwrap was based primarily on the desire to investigate the fabrication compatibility between a low-cost asbestos-phenolic system and the selected liner materials. Asbestos and canvas duck phenolic are equivalent in terms of mechanical properties and cost, while the asbestos is a slightly better insulator. Both materials are well suited for the overwrap application and each material was incorporated into the two nozzles for evaluation in this program.

To further substantiate the nozzle material selections, a comparison of the relative cost and performance of the candidate materials was made. A Cost Effectiveness Index (CEI) rating was formulated which takes into account the predicted material loss and char, the specific gravity, and pre-preg cost per pound. This, in effect, compares the unit cost of material which must be provided to meet design requirements. The results are summarized in Table 10 and show little apparent difference between carbon and carbon-silica in the higher erosion areas of the nozzle. Conversely, canvas duck has a distinct cost/performance advantage over silica in the exit cone.

(2) Nozzle No. 2

Selection of suitable materials for evaluation on the second test nozzle was primarily to establish the limits within which very low cost ablative materials can be used in the various regions of the nozzle. On the basis of current experience in nozzle design, the very low cost types of ablative materials, i.e., silica, asbestos, and canvas phenolics, have been used only in the high expansion-ratio areas of the nozzle. Results of a cost effectiveness study (Table 10), indicated that a saving in nozzle cost would be realized by using silica in the throat and low area ratios of the nozzle. Although a subsequent motor performance trade study showed that the most economical approach is a nozzle design where throat area change is at minimum, it is nevertheless desirable to obtain factual performance characteristics of these material types at the throat and low area ratios of the nozzle. On the basis of results for erosion characteristics, intelligent selection of these materials for the full scale nozzle design of Task III can be made.

After consideration of various low-cost materials, a nozzle design incorporating a silica-phenolic throat, entrance section, and forward exit cone with a canvas duck-phenolic aft exit cone and overwrap was selected. This comprised an "all white" nozzle for the second evaluation test.

Considerable data are currently available on the thermal and physical properties and performance of the various carbon phenolic materials. However, there has been very little experience to date on the use of silica-phenolic materials in rocket motor nozzle throat sections. Thermal analysis and design confirmation is handicapped by the lack of adequate material characteristics in this environment. If the erosion rate of a 260-FL motor nozzle throat made of silica phenolic were demonstrated to be only 0.013 in./sec (0.033 cm/sec), rather than the 0.017 in./sec (0.043 cm/sec) predicted, a net savings of \$118,600 in motor costs could be realized. This is based on an ablative-material saving of \$303,600 (from the base-line design) less the \$175,000 propellant and case cost that is necessary to recover the same payload capability as the baseline motor, as is explained in Section III.D.1.

It was also felt that the processing properties of the double-thickness silica tapes should be further evaluated since this type of material would contribute to significant labor cost savings during wrapping of full-scale (260-FL) nozzle components.

c. Design Description

The nozzle configuration was of a nonsubmerged design having a 13.0 in. (33.0 cm) initial throat diameter, a 17.5-degree expansion angle, and a 6:1 expansion ratio providing a 31.85 in. (80.8 cm) exit diameter. A conical entrance contour of approximately 35 degrees provides a smooth gas flow surface from the motor chamber to the throat station.

The nozzle assembly was comprised of three ablative liners for the entrance, throat, and exit sections. Each liner component was designed to be fabricated by conventional tape-wrapping methods and cured at 250 to 300 psi (172 to 207 N/cm²) autoclave pressure. The tape orientation angle measured from the nozzle center line was 70, 45, and 0 degrees for the entrance, throat, and exit section components, respectively. Each liner component was designed to be overwrapped with tape parallel to the wrapping surface, with the two materials being cured simultaneously.

The liner components were supported by a structural shell fabricated of AISI 4130 steel (normalized) having a minimum yield strength of about 70,000 psi (48300 N/cm 2). The gap between liner components was filled with a silica rubber. In addition to the three plastic inserts, a trowelable insulation (IBT-100) was used to protect the nozzle approach section forward of the entrance insert.

The fiberglass structural wrap, consisting of 65% roving and 35% cloth in interspersed layers, provided additional strength in the higher stressed area of the exit-cone liner immediately aft of the steel shell. S-994 glass roving (20 end) and No. 143 glass cloth impregnated with epoxy resin were specified. This system required a standard elevated-temperature and pressure-cure cycle.

The above description applies generally to the two nozzles that were fabricated. The significant difference between the two units was in the ablative materials used and the location of material transition interfaces. These features are documented in the fabrication drawings referenced in the following paragraphs:

(1) Nozzle No. 1

Nozzle No. 1 is defined in Aerojet Drawing No. 1147608 (Figure 7). From the listing (on the drawing) of acceptable and equivalent phenolic-resin impregnated ablative tapes, the following materials were actually used: (Choices were made by the fabricator on the basis of best cost and delivery.)

Forward Entrance Section (to ε = 1.67)	SP 8030-96 (Armour) Silica-phenolic
Aft Entrance Section	MXSC-195 (Fiberite) Carbon-silica phenolic
Throat Insert	MXSC-195
Forward Exit Cone Liner (to ϵ = 1.6)	MXSC-195
Aft Exit Cone Liner	4KXD02 (Hexcel) Canvas duck phenolic
Overwrap	MXA-6012 (Fiberite) Asbestos phenolic

(2) Nozzle No. 2

The second nozzle is shown in Figure 8 (Aerojet Drawing 1147609), and the materials used in fabrication of this nozzle are listed below:

Entrance Section	MX-2600-96 (Fiberite) Silica-phenolic
Throat Insert	MX-2600-96
Fwd Exit Cone Liner (to $\varepsilon = 2.01$)	MX-2600-96

Aft Exit Cone Liner

4KXD02 (Hexcel)
Carbon duck phenolic

Overwrap

4KXD02 (Hexcel)

(3) Redesign and Modification of Nozzle No. 2

No nozzle ablative material performance data were obtained from the first test because of the motor malfunction early in the firing.

The first nozzle incorporated the materials that were of greatest interest and the data loss represented a set-back in achieving the basic goals. Since the acquisition of performance data on a silica throat and entrance section (nozzle No. 2) was for experimental purposes (not directly applicable to a 260-FL design), the decision was made to modify the second nozzle to incorporate the same materials in the throat and entrance sections as were used on the first nozzle. The exit cone of nozzle No. 2 was not altered. Therefore, the modified nozzle (PN 1149295-2, Figure 9) represented a combination of the nozzle No. 1 forward section design (including throat) and the nozzle No. 2 exit cone. Materials actually used in the modified nozzle section were:

Forward Entrance Section (to $\varepsilon = 1.67$)

MX-2600-96 (Fiberite)

Silica phenolic

Aft Entrance Section

MXSC-195 (Fiberite)

Carbon-silica phenolic

Throat

MXSC-195

Overwrap

4KXD02 (Hexcel)

Canvas duck phenolic

A brief description of the selected insulation materials and their prior use follows:

(a) Codeposited Carbon-Silica Phenolic

This material, exemplified by WB-8251

(Western Backing Company) was selected for use in the throat insert, the aft

portion of the entrance section, and the forward portion of the exit section (nozzle No. 1). The reinforcement (Averam C/S) was produced by the American Viscose Corporation and contains about 65% SiO_2 and 35% carbon. The material has been used in nozzle components for two previous programs investigating low cost material $^{(2,3)}$. Materials that are equivalent to the WB-8251 and 4C2530 (Coast Manufacturing) and MXSC-195 (Fiberite Corporation). The material cost is about \$15/1b.

(b) Double-Thick Silica Phenolic

This type of material is exemplified by SP-8030-96 (Armour Coated Products). In addition to the low prepregnated cost, economy is achieved because the double tape thickness reduces wrapping time by about 50%. Materials that are equivalent to the SP-8030-96 are MX-2600-96 (Fiberite), WB-2233-96 (Western Backing), and FM-5504-96 (U. S. Polymeric). The material cost is about \$5.50/lb.

(c) Canvas Duck Phenolic

A representative of this type of material is KF-418 (Fiberite). Equivalent grades are 4KXD02 (Coast Manufacturing) and CA-2213 (Western Backing). The material performed well in both the Air Force and NASA programs referenced above. The material cost is about \$1.80/lb.

(d) Crocidolite Asbestos Mat Phenolic

Typical of this material is MXA-6012 (Fiberite). It also has a successful record in the two programs discussed previously. The material is felted, which cures to a lower density (1.60 gr/cc) than the commonly used curysotile asbestos grades (1.8 gr/cc). An equivalent material is FM-5525 (U. S. Polymeric). The cost of these materials is from \$1.85\$ to \$2.00/1b.

d. Design Verification and Performance Prediction

(1) Heat Transfer Analysis

In any nozzle analysis, the local convection heat-transfer coefficients are evaluated independently and utilized as input to the charring-ablation program. Therefore, to provide a realistic basis for a thermal response investigation, certain data on the properties of the heat transfer media must be available. This includes the exhaust gas composition in any region of interest, thermal properties (specific heats, thermal conductivity), and transport properties (diffusion coefficients, viscosity). These data were either available from previously completed programs or were determined during the material characterization task conducted at Battelle Memorial Institute.

The method of analysis for the ablation process, even though the mechanisms are extremely complex, has progressed as a result of extensive development efforts. The basic technique used to evaluate the thermal response of an ablation material is the "Vidya" program. This particular program is available to industry contractors and has been widely used for analyzing ablative components. A modified version is in use at Aerojet.

The procedure used to predict ablative performance is to first estimate the response (chemical or mechanical) of the wall material to the propellant and pyrolysis gases in the boundary layer.

To predict the chemical response of carbon-based material, two separate programs are available. The first program, "The Thermo-Chemical Equilibrium Program" (TEP) computes the equilibrium composition of the gas adjacent to the wall. It considers either (1) no reaction with the wall material, (2) pyrolysis gas blowing with nonreacting wall materials, or (3) pyrolysis gas blowing with a reacting wall material. The second program performs essentially the same calculation; however, instead of the equilibrium assumption, three separate reactions with carbon are considered with each reaction being kinetically controlled.

The two methods predict widely different material loss rates. Recognition of which is the controlling process can be made only by comparison of both to observed data in current applications.

In addition to the chemical attack on carbon-based materials, various other modes of surface loss occur for the other low-cost ablative systems (i.e., silica-carbon, silica, canvas duck). These include (1) erosion from pressure and shear forces acting in the low density char layer, (2) structural failure of the char as the result of thermal stresses, (3) spallation resulting from pressure buildup within the decomposition zone, (4) combinations of chemical and mechanical modes acting on the exposed surface (i.e., particle impacts).

To accurately analyze and evaluate each material removal mode would be a formidable task. This is so because a detailed knowledge of the material's kinetic behavior is required to formulate a model that would clarify the ablation process sufficiently. In lieu of what could be termed a rigorous model for surface regression, a provisional model is used. This model considers (1) all energy transport processes that occur in the virgin, decomposition, and char zones, (2) a basis for the prediction of char rates, erosion rate, and transient temperature distributions, and (3) a treatment of the surface regression by combining all modes of removal into an "effective removal rate," which will be obtained from actual motor firings.

The use of the simplified model is easily accomplished since the basic program assumes that the surface material is removed solely by chemical reaction characterized by a diffusion limited process. The mass transfer is then calculated assuming a unity mixture Lewis number, thereby making the mass transfer and convective heat-transfer coefficients exactly equal. The resulting erosion rate then becomes proportional to the magnitude of the local heat-transfer coefficient with blowing for a particular blowing gas rate.

The surface equilibrium data represent input to the charring material ablation program, which describes the transient response of a composite material that reacts at the surface and decomposes in depth.

In addition to the kinetic constants, it is necessary to provide the (1) thermal conductivity, (2) specific heat, and (3) virgin and char densities of each material being evaluated in order to solve the transient-conduction equation.

Output of the computer analysis provides ablativematerial performance in terms of erosion depth, char depth, pyrolysis gas rate, internal temperature distribution, and local density distribution over any desired time interval.

(2) Predicted Data From the Analytical Model

The preliminary nozzle designs were subjected to a boundary layer analysis to predict the local heat transfer rates. These results are presented in Table 11 together with the input data, namely, nozzle contour and surface Mach number. It is noted that the inlet geometry of the nozzle design is such that the flow is forced to turn sharply in the throat approach, resulting in a transition to supersonic flow well upstream of the geometric throat. The sonic point, which roughly coincides with the peak heat transfer coefficient, occurs at an upstream radius of 6.61 in. (16.8 cm) (area ratio ~ 1.035). At the geometric throat, the local Mach number is noted to be 1.28. This flow field results in the location of the peak heat-transfer coefficient (also erosion) to occur at an area ratio of 1.07.

The three principal nozzle designs that were considered for test and evaluation were analyzed using the charring-ablator program. Therefore, predicted performance data were obtained on nozzles having carbon-silica, silica, and carbon-phenolic throats. Tabulations of the expected erosion and char depth and the location of the 100°F (312°K) thermal gradient at several stations are presented in Tables 12, 13, and 14 for these three nozzle designs. A plot of these parameters vs time at the throat section is shown for each nozzle in Figures 10, 11, and 12. For the carbon-silica throat, an erosion rate of 12.9 mils/sec (0.033 cm/sec) is predicted to occur during web-time, with a total surface loss of 0.586 in. (1.49 cm) during the firing. This compares to the more severe rate of 18.5 mils/sec (0.047 cm/sec) expected

at the silica throat and a 4.0 mils/sec (0.010 cm/sec) loss rate predicted for the carbon-phenolic throat.

The thermal response data summarized in Tables 12 and 13 were plotted on cross-sectional drawings of nozzles No. 1 and 2, and the erosion, char, and 100°F (312°K) isotherm profiles were constructed. Figure 13A is the result of this procedure and depicts the expected nozzle performance. Since the actual nozzle tested on the second motor was a combination of the two designs, its performance profile was predicted to be as shown in Figure 13B.

On the basis of the expected erosion and char penetration, the minimum safety factor in the No. 1 nozzle section was 1.59, located at the aft joint of the throat insert; the minimum safety factor on the exit cone was 1.30, located just aft of the transition to the canvas duck phenolic. As may be seen in Figure 13A, in no case does the 100°F (312°K) isotherm extend into the overwrap, thus satisfying one of the major design criteria.

Figure 13A also shows the more marginal performance of the No. 2 nozzle (all-white) design. A safety factor of only 1.11 exists at the throat-exit cone interface, as compared to 1.59 at the same location in the carbon-silica throat, and the overwrap would be expected to experience temperatures in excess of 100°F (312°K) at this location. However, this line represents the condition expected at T + 60 sec, or well after web burnout. Therefore, this design was considered acceptable from an ablator performance standpoint. Because of the material substitution that was subsequently incorporated into this design, no assessment of the validity of the prediction was possible except in the exit cone area.

(3) Stress Analysis

Extensive use was made of the Aerojet finite element computer routine No. El1405. The finite element technique solves the differential equations governing the stress-strain relationships of an axisymmetrical structure of arbitrary shape when subjected to thermal and mechanical loads. The finite element approach replaces the continuous structure with a system of

elastic quadrilateral rings (elements) interconnected at a finite number of nodal points (joints). Equilibrium equations, in terms of unknown nodal point displacements, are developed at each nodal point with the solution of these equations being the solution of the system. Displacements, loads, or stresses to which the structure is subjected are replaced by equivalent values acting at the nodal points of the finite element system. Since each element may have separate mechanical properties and loading, composite or anisotropic structures of arbitrary geometry can be evaluated. The effects of finite length, curved boundaries, variable end conditions, linear and nonlinear variation of modulus of elasticity, and coefficients of thermal expansion with temperature can be completely accounted for in the solution.

The E11405 program allows the use of complete anisotropic (hoop, meridional, and radial) material properties. The effects of ablation can be considered by degrading the material properties above the ablation temperature (as used in this analysis), or by using the ablated geometry at the instant considered in the analysis.

Analyses were conducted for both the nozzle No. 1 (carbon-silica throat) and nozzle No. 2 (silica throat) designs. The ablator inner-surface configuration and internal thermal gradient existing at T + 40.5 sec, as determined by the heat-transfer analysis, was used in conjunction with nozzle pressure loads at a chamber pressure of 600 psia (413 $\rm N/cm^2$) as the input conditions causing material stress or strain. The validity of the analysis was compromised slightly by a lack of adequate physical properties data on the carbon-silica phenolic char at elevated temperature. Characterization of this material by Battelle was not time-phased to be of use in the design verification analyses, therefore, available data were extrapolated to the temperature levels existing within the part.

The results of the analyses, as summarized in Table 15 (nozzle No. 1) and Table 16 (nozzle No. 2) verified that both nozzle designs were structurally sound. The hoop strain in all ablative liners was determined to be below 0.25%, the normal maximum allowable value for plastic parts.

The thickness of the ablative parts is usually determined by the expected heat transfer and regression rates, and not by structural considerations. For this reason, structural safety margins often exist that are higher than would be necessary to satisfy the structural requirements only. This condition is evident on both nozzles, where, on most components, safety factors exceed the maximum desired values stated in the contract work statement. With the approval of the NASA-LeRC Program Manager, no attempt was made to optimize the design of the nozzles to attain lower "flight-weight" margins.

3. Motor Processing

a. Chamber Preparation

The two Algol IIB motor chambers were prepared for application of the trowelable insulation system in a similar manner, with one exception. Motor No. 1, hereafter referred to as LCAN-01, utilized a new chamber manufactured by the same supplier and from the same production run as the current Algol IIB motor contract. Motor No. 2 (LCAN-02) used a case that was Government furnished as a surplus, loaded Algol motor. Therefore, the existing propellant and insulation had to be removed from this motor as the first step in the preinsulation procedure. When this had been completed (using a high pressure water jet) both chambers were subjected to the following sequence of operations:

- (1) The interior surfaces were solvent wiped.
- (2) These same surfaces were lightly grit-blasted and again solvent wiped.
- (3) An epoxy-resin corrosion-inhibiting primer (Fuller 162-Y-22) was applied by brushing.
- (4) The primer was cured at ambient temperature, and the chamber openings sealed.

b. Chamber Insulation Processing

The overall planned sequence of operations for installing IBT-100 and IBT-106 materials was as follows:

- Design, fabricate, and check-out process equipment
- Grit-blast, clean, and prime Algol chamber
- Install and cure forward dome insulation
- Install and cure sidewall insulation
- Install and cure aft dome insulation
- Install and cure forward and aft boots.

(1) Process Equipment

Four major items of process tooling or shop aids were required; the design concepts for these items were derived from the work accomplished under Contract NAS3-11224. The process equipment used is identified below:

Description	Tool/I.D. No.	Configuration Shown in
Sidewall Dispenser	T-1023503	Figure 14
Fwd Dome Sweep Template	*	Figure 15
Aft Dome Sweep Template	*	Figure 16
Aft Step-Joint Mold	*	NA

The sidewall dispenser (Figure 14) consists of a 5-gal (0.019 m 3) Binks pressure pot (150 psig) (103.4 N/cm 2) mounted on a base plate equipped with swivel casters. The casters can be adjusted and locked in two positions: (1) for movement into and out of the chamber, and (2) for dispensing material when the chamber is rotated. A 5-degree (0.011 rad) caster

^{*}These items were defined as expendable shop-aids, therefore a tooling accountability number was not required.

deflection was incorporated in the dispenser to provide a 10.5-in. (26.7 cm) lateral movement of the dispenser for each rotation of the case. As shown in Figure 17, the 10.5-in. (26.7 cm) lateral movement for each rotation produced a continuous spiral application, with the required 1.0 ± 0.5 -in. (2.54 ± 1.27 cm) overlap between adjacent spiral passes.

Flow into the trowel from the bottom drawoff of the Binks pot was controlled by a "speed-ball" rotary valve. In the "off" position, the handle was rotated so that the slots in the tube were misaligned with the housing inlet and trowel outlet. Flow control was possible also by adjusting the pot pressure through a regulator installed on the GN_2 pressure line.

The forward and aft dome sweep template configurations are shown in Figures 15 and 16, respectively. The trowel portion of each template was adjustable, so that the standoff distance between the chamber and the trowel could be changed. After the forward and aft dome insulation was installed and cured, the standoff distance between the insulation and trowel was adjusted to 0.25 in. (0.64 cm) for propellant-boot application. A mahogany mold, also shown in Figure 16, was machined to the required aft step-joint configuration and mounted to the aft flange. The sidewall dispenser drawoff configuration was modified to include a 4.6 ft (1.17 m) flexible hose and shutoff valve for dispensing material onto the forward dome. Material for the aft dome was dispensed directly from the 300-gal (1.14 m³) mix bowl.

Processing operations were accomplished in Building 006, Line 1. This area was the Algol IIB motor production facility and included a top-loading, horizontal oven with turning rollers.

(2) Motor LCAN-01 Insulation Processing

Insulation of the first Algol chamber (SN 27) was begun on 11 September 1969. The primed chamber was installed on turning rollers that had been modified to permit a minimum rotation of 1/2 rpm. The forward dome sweep template was installed and adjusted to give the desired stand-off distance between the trowel edge and the dome. The measured mimimum

stand-off distances were 0.40 in. (1.02 cm) at the igniter boss and dome mid-point, and 0.20 in. (0.51 cm) at the sidewall tangent.

IBT-106 insulation was transferred from the mixing bowl to the small, mobile 5-gallon (0.019 m^3) dispenser, moved into the chamber, and troweled onto the forward dome. When the insulation contour matched that of the template, the trowel was removed and the surface was solvent-wiped to provide a smooth surface. A total of 43 lb (19.5 kg) of material was installed in the forward dome.

During a special IBT-106 sidewall dispenser dry-run in a 54-in.-dia (1.37 m) chamber*, it was determined that a 0.30 in. (0.76 cm) trowel standoff setting was necessary to achieve the required 0.20 in. (0.51 cm) insulation thickness.

A mobile dispenser, loaded with IBT-106, was moved into the chamber so that the edge of the trowel assembly was approximately 12 in. (30.5 cm) aft of the forward tangent. The casters were locked in the 5 degree (0.017 rad) spiral attitude, and the pot was pressurized to 40 psig (27.6 N/cm²). As the valve was opened, chamber rotation (1/2 rpm) was started and material application began. A total of 395 lb (179 Kg) of IBT-106 was applied to the sidewall.

Following the sidewall operations, IBT-100 was applied to the aft dome interior. As shown in Figure 16, the step-joint contour was controlled by a wooden mold mounted to the aft flange. Difficulty was encountered in troweling the IBT-100 into the narrow area adjacent to the flange (shown as the shaded area in Figure 18A). Visual inspection after cure and mold removal revealed several voids and deformations; these were surface defects, however, and did not extend into the material beyond the shaded area. The defective areas were trimmed out and fresh IBT-100 was applied. Then the mold was reinstalled, extruding excess repair material from between the mold

^{*}This chamber previously used for Task II, Process Evaluation, Contract NAS3-11224.

and cured insulation. This repair method was effective in producing a sound, defect-free joint. For the second motor, IBT-100 was troweled on the aft flange as shown in Figure 18B to a thickness greater than required to fill the area adjacent to the flange. Then, as shown in Figure 18C, the wooden mold was installed, extruding excess material onto the aft dome.

Forward and aft propellant-boot installation was accomplished as planned. IBT-106 was applied over the cured insulation surface after application of DC-Q92, a silicone -based release agent. The sweep templates were used to obtain the required thickness. After cure, the boots were manually pulled away from the released insulation surface. The boots retained their position without application of external force.

The following significant problem areas were encountered during the insulation process:

- (a) Good thickness control was obtained on the forward dome, except at the chamber tangent point where a ridge build-up occurred. The ridge was removed by hand trimming after cure. In Motor LCAN-02, the ridge was smoothed off with a spatula prior to cure.
- (b) The template contour did not exactly match that of the forward dome, and there was insufficient horizontal adjustment capability. These deficiencies were corrected prior to boot installation.
- (c) Poor thickness control was experienced initially during sidewall application with measured thicknesses ranging from 0.2 to 0.5 in. (0.53 to 1.27 cm). Slippage between the motor handling rings and the turning roller surfaces at 1/2 rpm resulted in a corrugated surface effect. There was no apparent method of correcting this situation.
- (d) An excessive build-up of material between spiral passes was experienced. This condition was caused by overflow around the edge of the trowel. Extensive effort was expended in trimming away these ridges in Motor LCAN-01. To prevent overflow and excessive ridge build-up in the second motor, a plate was welded to the end of the trowel.

(e) During initial operation of the sidewall dispenser, the trowel, valve, and housing section tended to rotate and float as a result of drag caused by material build-up in the trowel. This problem was solved by incorporating a U-clamp brace between the valve housing and the pot platform.

(f) By far the most significant problem was air entrapment in the sidewall insulation caused by GN₂ pressurization gas leakage past the diaphragm, or by GN₂ blow-through when the dispenser was emptied or when the diaphragm became misaligned. As shown in Figure 14, three guides were bolted to the diaphragm to reduce instances of misalignment. Because of the small dispenser-pot capacity, 40 lb (18.2 kg), the frequent refills resulted in significant air entrapment and even though the operator tried to anticipate dispenser depletion, blow-through was encountered frequently.

The forward and aft sections of the insulated motor were inspected by tangential radiography every 60 degrees (1.05 rad) around the circumference. Two thin areas of 0.25 in. (0.635 cm) each and approximately 8 in. (20.8 cm) in diameter, were detected in the sidewall adjacent to the forward and aft propellant boots. The forward insulation contained a few small, flattened voids, randomly scattered through the material. These defects were generally from 0.25 to 0.50 in. (0.635 to 1.27 cm) long and less than 0.02 in. (0.51 cm) thick, and were caused by material overlapping during the troweling process. Since these defects were buried in the material and were few in number, they presented no hazard to insulation performance and no repair effort was attempted. The forward visual inspection (confirmed later by X-ray) revealed one thin area approximately 6 in. (15.2 cm) in diameter in the aft boot adjacent to the step-joint. There were no backside defects. A 2 in. (5.04 cm) diameter thin area was found in the forward boot, and there was also a back-side defect associated with this thin area. Both of these defects were repaired with fresh IBT-106.

Several voids to 0.5 in. (1.27 cm) in dia were detected in the aft dome insulation, generally in areas adjacent to the dome wall. Apparently some air entrapment occurred when the initial layer of

IBT-100 was applied. As was discussed previously, it was difficult to trowel IBT-100 into the narrow area adjacent to the aft flange. The effort required to move material into the joint area may have led to air entrapment in the aft dome. The defects were located in a noncritical area where the material thickness needed to provide a smooth contour far exceeded the performance thickness requirements. Thus, no repair effort was necessary.

a 100% ultrasonic inspection of the case sidewall insulation system was performed. For the most part, the defects noted turned out to be small voids, less than 0.50 in. (1.27 cm) in diameter and near the case bond line. The defects were caused primarily by ${\rm GN}_2$ leakage past the dispenser diaphragm or by blow-through when the dispenser was empty. All the foregoing defects and thin areas were trimmed out and repaired with fresh IBT-106.

V-44 sleeve and fiberglass aft-boot extension were installed, the interior surface was cleaned, and precast operations were initiated. A total of 774 lb (351 kg) of insulation, including propellant boots, was installed. This amount was approximately 80 lb (36.3 kg) more than the amount calculated. A photograph of the completed insulation system is shown in Figure 19.

(3) Motor LCAN-02

Insulation operations for the second motor were started on 28 October 1969. The forward dome and sidewall insulation were installed in three consecutive days beginning 28 October. Installation operations were accomplished much more efficiently than with Motor LCAN-01, especially for the sidewall. In particular, the plate that was welded to the end of the dispenser trowel was effective in eliminating the material build-up between spiral passes. Although the technique of handling and operating the sidewall dispenser was improved significantly, problems concerning GN₂ leakage around the diaphragm and blow-through when the dispenser pot emptied were still not overcome. This was evidenced by ultrasonic inspection which revealed numerous small voids similar to those found on the first motor. The defect areas were trimmed out and repaired with fresh IBT-106.

Installation of the aft dome insulation and forward and aft boots installation were accomplished as planned. Visual inspection after aft-dome cure and mold removal revealed several deformations in the aft step-joint insulation surface, but these surface defects were not as severe as those experienced in the first motor. Figure 20 shows four of these surface defects and the aft insulation/boot configuration after cure. The changes in the IBT-100 installation process discussed in the previous section were successful to the extent that the quantity and depth of the defects were reduced; however, it does appear that thick sections of IBT-100 must be built up layer by layer to avoid air entrapment caused by material folding upon itself. No difficulties were encountered during propellant boot installation.

The forward and aft sections of the insulated motor were inspected by tangential radiography every 60 degrees (1.05 rad) around the circumference. The following defects were noted:

(a) Aft Dome

 $\underline{1}$ A 5-in.-long (12.7 cm) area of thin insulation, approximately 0.10 in. (0.25 cm) thick, located 16 in. (40.7 cm) forward of the aft tangent at 270 degrees (4.71 rad).

 $\underline{2}$ A 3-in.-dia (7.62 cm) area of flat voids, 10 in. (25.4 cm) forward of the aft tangent at 90 degrees (1.57 rad).

 $\underline{3}$ Flattened voids in the IBT-100 near the chamber wall at the thickest section of insulation.

(b) Forward Dome

 $\underline{1}$ An irregularly shaped void measuring 0.8 by 0.6 in. (2.03 by 1.52 cm) located 5.5 in. (13.9 cm) aft of forward tangent at 330 degrees (5.76 rad).

 $\underline{2}$ An irregularly shaped void measuring 0.6 by 0.5 in. (1.52 by 1.25 cm) located 16 in. (40.7 cm) aft of forward tangent at 30 degrees (0.525 rad).

 $\underline{3}$ Some small flattened voids well scattered throughout the material.

The noted defects were trimmed out where required and repaired with IBT-106.

(c) Boots

The propellant boots were free of defects. After cure of the dome repairs, the forward V-44 sleeve and fiberglass aft boot extension were installed, the interior surface was cleaned, and precast operations were initiated. A total of 884 lb (402 kg) of insulation, including propellant boots, was installed. Qualification data for the insulation material used in the second motor is shown in Table 17.

A leak-check was conducted to determine the integrity of the forward propellant boot and the bond between the V-44 rubber sleeve and the boot. The test agent was ammonia gas; the indicator was phenolphthalein, which turns a deep-purple color when exposed to traces of $\mathrm{NH}_{\mathrm{B}}^{\circ}$. Ammonia gas from a pressurized cylinder was introduced into the cavity between the boot and the forward insulation. White cloths, wet with phenolphthalein, were laid over the boot and sleeve. There were no indications of leakage.

c. Propellant Loading and Preassembly Operations

(1) Motor LCAN-01

The modified Algol IIB core was installed in the insulated case and the entire assembly positioned vertically (aft-end up) in a vacuum casting bell. Four 5600 lb (2550 kg) batches of ANB-3347 propellant were mixed and loaded into the motor on 27 October 1969.

The core was removed with no difficulty following an 8-day cure at +135°F (331°K) and a 36 hr cool-down at 80°F (300°K). The

aft face of the grain was trimmed to the configuration of Drawing No. 1147611 following core removal. The final propellant grain weight was 20,478 lb (9330 kg).

A 100% radiographic inspection of the completed motor was performed. There was no evidence of any propellant voids, cracks, or unbonding from the insulation surfaces. No gas path was visible between the forward or aft boot voids and the propellant. The inspection results verified the integrity of the insulated and loaded motor and confirmed its acceptability for test firing.

(2) Motor LCAN-02

Loading of this motor with ANB-3347 propellant was completed on 8 December 1969. Loading was accomplished in the same manner as described for Motor LCAN-01. An 11 day cure period at 135°F (331°K) was accomplished followed by normal core removal and aft-grain face-trimming operations. The net propellant weight in this motor was 20,404 lb (9260 kg).

Again, radiographic inspection of the completed motor verified the acceptability of the propellant/insulation system.

Qualification data for the four LCAN-02 propellant batches is presented in Table 18. Data from the previous motor and the scale-up batches are included for comparison. A slightly higher liquid strand burning rate in the second motor propellant was the only significant difference noted. However, the average solid strand burning rate at 500 psia (345 N/cm²) is lower for LCAN-02 propellant, 0.205 in./sec vs 0.237 in./sec (0.52 cm/sec vs 0.60 cm/sec) and is a better indicator of what could be expected as the static burning rate in the full-scale motor.

Mechanical properties data for all ANB-3347 propellant batches processed on this program are summarized in Table 19; the consistency of data between batches was very good.

d. Modification and Rework of Motor LCAN-02

Because of the failure of Motor LCAN-01 during static test firing (see Section III.C.2), several modifications were made to the completed second motor to prevent a similar failure.

The rework that was performed is discussed below and shown in Figure 21.

The forward igniter bore was enlarged by hand trimming to about 7.0 in. in dia (17.8 cm). This involved removal of the entire V-44 sleeve and the bond joint between it and the forward boot. The exposed propellant surface was restricted with IBT-113 trowelable insulation.

The boot release voids at the forward and aft heads of the motor were filled with an epoxy-based potting compound (MK-599). This was done with the motor in a vertical position under vacuum conditions and with the propellant cooled to 60°F (289°K).

The exposed portion of the igniter adapter was insulated with IBT-106.

When these rework operations had been completed, a comprehensive radiographic inspection of the forward and aft sections of the motor was performed. With the exception of one small area near the igniter boss (subsequently repaired) the MK-599 potting compound had completely filled the boot cavities as intended. The quality of igniter bore restriction and its bond to the propellant were also verified by the X-rays.

e. Motor Final Assembly

Prior to motor final assembly, two modifications were made to reduce the initial high chamber pressure caused by erosive burning. These were the application of a restriction material to the aft face and aft 3 ft (0.91 m) of the grain bore and the removal of about 40% of the igniter

propellant grain. The grain restrictor of SD-830, an epoxy-cured polysulfide potting compound, was brushed on to a thickness of 0.05 to 0.10 in. (0.13 to 0.25 cm).

Final assembly of both motors was completed in accordance with the requirements of Drawing No. 1149067. A dry fit of the nozzles confirmed the expected 0.05 to 0.10 in. (0.13 to 0.25 cm) gap between the IBT-100 insulation step-joint mating faces. AGC-34076 silicone rubber sealant was applied to this area during nozzle installation.

The assembled motors were leak-tested at 30 psig (20.7 $\rm N/cm^2)$ using a leak detecting solution. No leakage was found.

The motors were maintained in a 70 to 85°F (294 to 303°K) controlled environment during all processing, storage, and pretest operations.

4. Nozzle Fabrication

Two nozzle assemblies were manufactured to evaluate the low-cost ablative material performance capabilities. The assemblies were identical with respect to dimensional configuration, and the components for each were fabricated using similar wrapping procedures. Three sets of entrance and throat inserts were fabricated for the two nozzle assemblies; the second set was removed from assembly and replaced by the third set as a result of the first motor firing. All nozzle fabrication was performed by Haveg Industries, Inc., of Santa Fe Springs, California.

a. Materials

The pre-preg materials that were used to fabricate the nozzle components are listed in Table 20. Also shown are the suppliers and the reinforcement-resin systems of each pre-preg material. The parenthetical numbers in the "Where Used" column refer to the particular nozzle assembly - 2i being the set that was initially installed in the second nozzle assembly. Three of the five materials had been evaluated in previous low-cost nozzle

evaluation programs ^(2,3); the remaining two (4KXDO2 and MXSC-195) were considered to be equivalent to KF-418 and WB-8251, both of which had been previously evaluated. The measured and desired properties of the pre-preg materials are shown in Table 21. In most cases, the desired range of each property was met, although the spread of measured values was greater for the AVCERAM C/S (carbon-silica) and canvas duck pre-preg materials. Since these materials have but recently been used in ablative applications, it appears that their impregnating parameters have not yet been standardized.

b. Fabrication

The nozzle components were designed to consist of flame liners with plies oriented at a specified angle to the center line of the nozzle and overwrapped with a combined insulative-structural material. Excess material was provided at one or both ends of the wrapped component for evaluating the properties of the cured composite. Following the removal of this excess material, the components were machined to produce the finished parts. These were then dry-fitted and assembled to form the nozzle.

The general fabrication procedure for the ablative nozzle inserts was as follows:

- (1) The flame liner materials were wrapped onto a steel mandrel with the tape plies oriented to yield the specified angle after completion of cure. The aim was to achieve an as-wrapped density of 87% for the high-angle plies and 93% for the parallel-to-center line plies.
- (2) The flame liner was compacted (debulked) in an autoclave at a temperature of $170^{\circ}F$ (350°K) and a pressure of 250 psig (172.4 N/cm²). The exterior surface was then machined.
- (3) The flame liner was covered with the insulative material wrapped parallel to the machined surface.

- III.B. Task I Nozzle and Test-Motor Design, Analysis, and Fabrication (cont)
- (4) The overwrapped flame liner was cured in an autoclave at a temperature of 300°F (422°K) and a pressure of 250 psig (172.4 $\,\rm N/cm^2)$.
- (5) The excess material was parted from the insert and evaluated. The insert was machined for assembly.

The specific parameters used to fabricate each of the components are shown in Table 22. Wrapping, one of the three principal operations (the others are debulking and curing) is essentially a manual operation. Consequently, the wrapping parameters are subject to more fluctuation than those of the other two operations. Despite the wide variation in tape temperature and roller pressure, the as-wrapped densities met the target values, except for the canvas-duck in Exit Cone No. 2, which had an as-wrapped density of 92%.

The properties of the cured composite are shown in Table 23. Test procedures were conducted in accordance with the requirements of Specification AGC-36413. The minimum requirements were met or exceeded for all composites except the canvas duck. The measured values of hardness, uncured resin content, and volatile content of this material indicate that either the cure process was not as complete as desired, or that the property limits require some alteration for specification purposes.

c. Assembly

The nozzle components were bonded to a steel shell using the epoxy adhesive Epon 913. Joints between the ablative components were filled with the silicone rubber compound PR-1910. The sequence of bonding was (1) exit cone to shell, (2) throat to shell and exit cone, and (3) entrance to throat and shell. The adhesive was cured by heating to 180°F (355°K). After each ablative component was cured, it was machined at the forward face to match the adjacent, next-to-be-bonded, component.

After all nozzle components were bonded to the shell, glass/epoxy roving was wrapped over the steel shell and a portion of the exit cone (Nozzle No. 1 only). The nozzle assembly was then autoclave-cured at $300^{\circ}F$ (422°K) and $100^{\circ}F$ (69 N/cm²) for 2 hours.

Following cure, the nozzle was set up in a lathe and the internal contours of the entrance and throat were machined to the drawing dimensions.

d. Fabrication Problems

(1) Nozzle No. 1 Exit Cone Delaminations

The most severe problem encountered during any of the nozzle manufacturing procedure concerned processing of the glass structural overwrap, as discussed in the previous section.

A separation between the asbestos-phenolic overwrap and the canvas duck-phenolic exit-cone liner was discovered after completion of the glass overwrap cure. Three areas of separation between the two materials were apparent at the exit plane of the nozzle. Radiographic and ultrasonic inspection of the assembly indicated that 60 to 80% of the exit cone aft of the steel shell had delaminated at the asbestos overwrap interface. Limitations of inspection equipment prevented a satisfactory verification of this bond forward of the aft end of the shell, although the X-rays did show the separation ending about 2 in. (5.08 cm) aft of the steel shell.

The separation of the asbestos overwrap from the canvas duck flame liner was observed after completion of the glass overwrap cure cycle and subsequent cool-down. The cure cycle consisted of a temperature rise at a rate of 1°F/sec to 180°F (356°K) with a hold at 180°F (356°K) for 2 hours followed by a further increase at the same rate to 300 \pm 10°F (422 \pm 261°K) for 2 hours (min). This was all accomplished with the part under vacuum-bag pressure of 20 in. Hg (6.75 N/cm²) and an autoclave pressure of 100 \pm 10 psig (69 \pm 6.9 N/cm²).

Using the available data on the coefficient of thermal expansion of canvas- and asbestos-phenolic composites and the actual exit cone geometry, a stress analysis was conducted to determine if the failure was caused by the differential expansion of the liner and overwrap during this cure cycle. The results show a tensile hoop stress of 2000 psi (1378 $\rm N/cm^2)$ and a shear stress of 500 psi (345 $\rm N/cm^2)$ occurring at the bond interface during the increasing-temperature portion of the glass-cure cycle. The ultimate room-temperature tensile strength of an asbestos-phenolic laminate, perpendicular to the wrap, is 1500 psi (1033 $\rm N/cm^2)$). The bond failure thus appears to be the result of the tensile hoop stress resulting from differential thermal expansion.

The X-rays taken to define the extent of the exit cone overwrap separation revealed two additional defects. The more serious of the two was a possible delamination between plies of the canvas-phenolic exit cone liner at an area ratio of 2.8:1. The extent of this condition circumferentially was not established due to the limited number of exposures taken. However, the presence of the delaminations was verified visually after removal of the asbestos overwrap. Four defects measuring 4 to 7 in. (10.15 to 17.78 cm) in length were noted. These did not extend to the inner surface of the liner, but could possibly have been exposed during the course of the firing. In addition, a delamination in the glass structural overwrap was found. This defect extended over the full length and circumference of the material.

The delaminations in the canvas-phenolic liner are believed to be the result of high tensile loads induced in the parallel-to-center line wrap at the point where good bonding to the asbestos existed adjacent to a separated area. The delamination in the glass overwrap cannot be explained.

The following repair procedure was established in conjunction with Haveg and was approved by the LeRC Program Manager. Prior to implementation of the repair, a preliminary stress analysis was conducted that verified the structural adequacy of the proposed approach.

- III.B. Task I Nozzle and Test-Motor Design, Analysis, and Fabrication (cont)
- (a) All the glass roving and HT-424 adhesive was removed from the outside surface of the exit cone and metal housing.
- (b) All MXA-6012 asbestos overwrap aft of the metal housing was machined from the outside surface of the canvas duck exit-cone liner. The remaining asbestos overwrap surface was tapered parallel to the nozzle center line from the metal housing to the canvas duck liner.
- (c) The entire outside surface of the exit cone was inspected by acetone-penetrant testing to determine the location and magnitude of any delaminations in the canvas duck liner.
- (d) The four liner delaminations detected were impregnated with Epon 828 resin, vacuum-bagged, and subjected to a 100 psi (69 N/cm^2) autoclave pressure for 30 min.
- (e) A hand lay-up of glass cloth (Type 182) and an ambient-curing epoxy resin (Epon 828) was applied, covering the entire exit cone to a thickness of 0.15 in. (min) (0.38 cm).
- (f) The part was vacuum-bagged and cured at room temperature and 100 psi (69 $\mbox{N/cm}^2)$ for 24 hours.

Subsequent to repair of the exit cone, a finite-element analysis of this area was conducted in which it was assumed that the noted delaminations in the canvas extended completely through the part. The calculated hoop stress and strain in the glass overwrap were only 4000 psi (2754 N/cm^2) and 0.133%, respectively, well below allowable limits.

Radiographic inspection of the entire nozzle at Aerojet verified acceptable bonding of the glass overwrap to the exit-cone liner and the steel shell and confirmed the integrity of the asbestos-overwrap bond to the entrance and throat inserts. The delaminations in the canvas liner were also seen to end at least 1/2 in. (1.27 cm) from the inner surface of the part.

(2) Carbon-Silica Wrapping Difficulties (Nozzle No. 1)

During the initial wrapping of the MXSC-195 carbon-silica entrance section, and prior to the debulk cycle, a delamination (or unbonding) between plies occurred. A "predebulk" cycle of 1 hr at 150° F (339 °K) and 100 psi (69 N/cm²) was used to successfully repair this condition.

Cracking at the O.D. surface of the pre-preg tape was experienced during wrapping of the carbon-silica throat insert. This was traced to overadvancement in the resin. To achieve the requirement of 6% maximum volatile content in the pre-preg, it was necessary for Fiberite to take their standard material and dry it further, at a temperature below 200°F (367°K). This reduced the formability. It appears that the volatile content for this pre-preg should be between 6 and 9%.

(3) Nozzle No. 2

No significant fabrication discrepancies were encountered during the processing of this unit. As on the first nozzle, the volatile content and acetone-extraction level of the cured canvas duck-phenolic material (4KXDO2) slightly exceeded the specification requirement. The removal of the bonded silica-phenolic entrance and throat inserts from the completed second nozzle was accomplished without difficulty subsequent to the decision to replace these parts with components fabricated from carbon silica.

The replacement inserts were processed with no deviations reported. The cured composite properties met all specification criteria.

5. Ablative Materials Characterization

The nozzle components were characterized with respect to chemical, physical, and mechanical properties. The properties of the pre-preg and composites were determined by the pre-preg supplier and component fabricator;

the physical and mechanical properties (of the composite) were determined by Battelle Memorial Institute, Columbus, Ohio. The specimens for all measurements of composite properties were made from test rings removed from the first nozzle components.

a. Pre-Preg Properties

The properties of the pre-preg materials used in the test nozzles are given in Table 21.

b. Composite Properties

Properties of the cured composites are shown in Table 23.

(1) Specific Gravity

The specific gravities of specimens taken from the test extensions were determined in accordance with the weight-volume method of Federal Test Method Standard 406 (FTMS 406, Method 5011). In general, the specific gravities of the composites were normal except for that of the MXA-6012 asbestos. The value of 1.74/1.78 reported herein is higher than the 1.60/1.61 reported previously (2,3).

(2) Hardness

The hardness of the cured composites were determined by the Rockwell 'R' scale, which uses a 0.5-in. (1.27 mm) ball indentor with a 60 kg load. Measurements were taken for informational purposes, and, in general, are similar to those given in Reference (2).

(3) Volatile Content

Volatile content was determined by establishing the weight loss in a specimen heated to $325 \pm 10^{\circ} F$ ($436 \pm 5.6^{\circ} K$) for 24 ± 0.5 hours. Except in the 4KXD02 canvas composite, the volatile contents were all below the 4.0% called out on the nozzle drawing. The volatile contents of the 4KXD02 specimens were between 4.7 and 5.2%, but were considered to be acceptable on the basis of results obtained with high-volatile-content parts tested in solid rocket motors in a recent NASA-funded program (4).

(4) Uncured Resin Content

Uncured resin content in the cured composites was determined by the weight fraction dissolved after extraction of a particulate sample with acetone. The MXA-6012 specimens contained between 0.51 and 0.56% uncured resin, and the 4KXD02 specimen contained between 0.49 and 0.71%. These figures are slightly higher than the 0.5% maximum that is usually specified, but the material was accepted for use.

c. Mechanical Properties

The tensile, compressive, and shear properties of SP-8030-96 silica and 4KXD02 canvas composites were determined at room and elevated temperatures, using specimens of the design shown in Figure 22. All room-temperature measurements were conducted on virgin material, and elevated-temperature measurements were made on material that had been charred at 2750°F (1783°K) prior to test.

Specimen charring was conducted in a graphite, resistance furnace in an atmosphere of flowing argon. The basic char cycle consisted of (1) heating to 1100°F (866.5°K) at the rate of 100°F (56°K) per hour, (2) holding

for 1 hour, (3) heating to 2750°F (1783°K) at the rate of 300°F (167°K) per hour, (4) holding for 4 hours, and (5) furnace cooling in argon. This procedure yielded satisfactory specimens for the silica— and canvas—phenolic materials.

For the carbon-silica phenolic, the above char cycle produced severe distortion and delamination of the test specimens. The cycle was modified to (1) heating to 750°F (672°K) at the rate of 25°F (14°K) per hour, (2) holding for 2 hours, (3) heating to 2750°F (1783°K) at the rate of 200°F (111°K) per hour, (4) holding for 4 hours, and (5) furnace cooling. This cycle eliminated the distortion, but a high incidence of interply cracks was still observed. Consequently, all elevated-temperature strength measurements of this material were omitted from the program.

(1) SP-8030-96 Silica Phenolic

The mechanical properties of the SP-8030-96 composite are shown in Table 24. Also listed are the tensile and compressive properties of material tested in a previous program (2). The values of the two sets of data are quite close except for tensile modulus. The present results appear to be low by a factor of 2.

(2) MXSC-195 Carbon-Silica Phenolic

The mechanical properties of the carbon-silica phenolic are shown in Table 25. Comparative properties are also presented for two similar composites, 4C 2530 and X-5571. Here again, the correspondence of the two sets of data is close except for the tensile modulus. The results with the other, similar composites indicate that if the MXSC-195 had not delaminated during charring, the compressive strength would have been upwards of 1760 psi (1213 N/cm²) at 2750°F (1783°K).

(3) 4KXD02 Canvas Phenolic

The mechanical properties obtained for the 4KXDO2 composite are shown in Table 26. Except for tensile modulus, the results compare closely with those of the previous program. It should be noted that the strength at elevated temperature of the charred canvas material was higher than that of either the charred silica or carbon-silica composites.

d. Physical Properties

The thermal expansion and specific heat specimens were prepared as cylinders, nominally 0.375 in. (0.95 cm) in dia by 2 to 4 in. (5.1 to 10.2 cm) long. The specimens representing the direction parallel to the plies could usually be fabricated in one piece, but those representing the perpendicular-to-ply direction were made of several stacked pieces. The thermal conductivity specimens were prepared as discs, nominally 3 in. (7.5 cm) in dia by 0.50 in. (1.25 cm) thick.

Thermal conductivity of both virgin and charred specimens was measured by a steady-state comparative technique that featured one-dimensional heat flow. In this technique, heat is transferred axially through a specimen and a heat flow meter in series and conductivity is calculated from the relation:

$$K = \frac{q L}{A (\Delta T)}$$

where: K is the thermal conductivity

q is the heat flow rate

A is the cross-sectional area of specimen in test section.

L is the specimen thickness

ΔT is the temperature difference across L

The total of potential errors in conductivity measurements by this technique was determined to be approximately \pm 8%.

Linear expansion of the virgin materials was measured in a standard quartz dilatometer, and expansion of the char was measured in a direct-view dilatometer. In the direct-view dilatometer, dilation of the specimen is measured with telemicroscopes, fitted with filar eyepieces, which track the movement of fiducial marks on the specimen. The specimen is supported on a platform inside a tube furnace and data are recorded when thermal equilibrium is achieved. Dilation of 7×10^{-6} in. $(17.78 \times 10^{-6} \text{ cm})$ can be detected by the direct-view technique; the quartz dilatometer has a sensitivity of 20×10^{-6} in. $(50.8 \times 10^{-6} \text{ cm})$.

Specific heat was calculated from enthalpy data measured in a Bunsen-type ice calorimeter. Briefly, specific heat is the slope of the curve fitted to the enthalpy data. Accuracy of the calorimeter is checked frequently through measurements on standard (NBS) aluminum oxide and by absolute heat-input methods. Results are routinely within 1% of absolute.

Physical properties of the silica phenolic composite were not determined since it was felt that the available data were satisfactory for use.

(1) MXSC-195 Carbon-Silica Phenolic

The thermal conductivity of the virgin carbon-silica composite was of the order of 5 Btu/in./hr-ft²-°F (0.008 W-cm/cm²-°C) in the temperature range from 75 to 500°F (269 to 400°K), and there was only a slight difference between the values parallel to the plies and those normal to the plies. The thermal conductivity of the charred composite exhibited more anisotropicity, the parallel-to-ply values running about four times higher than those in the normal-to-ply direction. The thermal conductivity of the MXSC-195 material is shown in Figure 23.

The specific heat of the MXSC-195 material is shown in Figure 24 over the range from 75 to 2750°F (30 to 1785°K).

The thermal expansion of the MXSC-195 material is shown in Figure 25. In the virgin condition, the expansion and shrinkage in the normal-to-ply direction was about ten times that of the parallel-to-ply direction. The difference in expansion between the two orientations was much less in the charred material.

(2) 4KXD02 Canvas Phenolic

The thermal conductivity of the 4KXDO2 canvas composite is shown in Figure 26. There was pronounced anistropy in both the virgin and charred materials, with the normal-to-ply values running about half those of the parallel-to-ply values.

The specific heat of the 4KXD02 composite is shown in Figure 27. Since the canvas is a cellulose product, its specific heat is higher than that of the MXSC-195 and approaches that of the carbon composites.

The dimensional changes in the 4KXD02 composite are shown in Figure 28. In the charred condition, there is little difference between the two fabric orientations that were examined. In the virgin condition, however, the normal-to-ply orientation exhibited a much greater expansion and shrinkage than the parallel-to-ply direction.

C. TASK II - NOZZLE AND INSULATION SYSTEM EVALUATION

1. Test Plan

a. Nozzle Material Evaluation

The two low-cost ablative nozzles were subjected to special inspection procedures prior to installation on the test motors. These operations were intended to fully document the "as-built" nozzle configuration. The first inspection was in the form of manual measurement and mapping of the ablative interior surface. These pretest reference dimensions would be compared with posttest measurements taken in an identical fashion to

accurately determine the surface material lost during the test. Figure 29 shows this inspection being accomplished on the LCAN-01 nozzle with the use of a Portage layout gage. It was planned to section the nozzles following the posttest profile mapping to allow measurement of the char depth and thermal degraded material.

As an added assurance that valid ablative liner erosion data could be obtained, the nozzle assembly was X-rayed before each test. The thickness of each liner may be accurately determined in this manner using reference scale-blocks (pentrometers). These X-rays were to be duplicated following the test if for any reason the posttest profile measurements were questionable or unobtainable.

b. Determination of Ablator Thermal Gradient

Four instrumented thermal sensors were fabricated and installed in the first nozzle. Each sensor assembly used a 0.50-in.-dia (1.27 cm) plug (machined from a section of the ablative material it was to be installed in) as the body of the device. These temperature sensing probes were developed by Aerojet on an Air Force sponsored program (2) to measure the thermal response of the ablative materials. These data were intended to verify (or provide a basis for modifying) the analytical predictions of the ablation and charring response of composite materials.

Three of the thermal sensing plugs had four thermocouples (two chromel/alumel, and two W-3 rhenium/W-25 rhenium) and 15 eutectic sensors installed; the fourth plug had only three thermocouples (two each chromel/alumel, and one each W-3 rhenium/W-25 rhenium). The thermocouples were made of very fine wire with a welded junction at the center of the plug; leadwires were routed normal to the direction of heat flow. This design provides a very high measurement response rate and increased data accuracy as heat conduction away from the hot-junction is minimized. The tungsten-rhenium thermocouples can accurately measure temperatures to approximately 4200°F (2590°K) and are placed closest to the expected erosion surface; the chromel-alumel thermocouples are used to measure temperatures to 2400°F

 $(1590\,^{\circ}\text{K})$ and are positioned adjacent to the maximum expected char penetration depth.

The eutectic sensors provide a high temperature sensing capability in excess of the thermocouples. These micro sensors were developed under contract as described in Reference (5). Each micro sensor consists of a 0.030-in.-dia (0.076 cm) by 0.010-in.-thick (0.025 cm) graphite cup (with cover) filled with a metal-carbon or carbide-carbon eutectic powder composition having a well defined melting point. Radiographic examination of the sensors, before and after the firing, determines whether the transition temperature of each particular eutectic composition was or was not reached.

A typical thermal sensor assembly is shown in Figure 30 and depicts how the thermocouples and eutectic sensors are installed in the ablative plug. Each completed plug was bonded into a drilled hole in the nozzle liner insert with its top face flush with the inside surface of the ablator.

c. Static Test Firing Procedure

A detailed static test firing plan (Project Directive No. LCAN-05, Revisions 1 and 2) was prepared which defined the requirements of each test. The principal features of this test plan are outlined below:

- (1) The assembled nozzle-test motors were installed on a horizontal ballistic test fixture.
- (2) The motors were maintained at a temperature of 80 \pm 5°F (300 \pm 258°K) for at least 48 hr prior to the test and until T-2 hr on the countdown.
- (3) Chamber pressure was measured by three transducers installed on the igniter adapter.
 - (4) Two channels of axial thrust were recorded.

- (5) Thermocouples were spot-welded to the motor case and to the nozzle shell at locations where the maximum heating was expected. Twenty thermocouples were placed on Motor LCAN-02 as compared to ten on Motor LCAN-01.
- (6) The 15 special thermocouples in the four ablative thermal sensors (LCAN-01 only) were connected to the data recording system.
- (7) A Beckman 210 analog-to-digital conversion (ADC) unit was the primary data recording system. Data were recorded on magnetic tape for subsequent computer reduction and plotting. All major parameters were also recorded on a C.E.C. Model S-119 oscillograph.
- (8) A quench system was provided that was intended to flush the chamber interior with ${\rm CO}_2$ shortly after propellant burnout for extinguishment of residual insulation burning and for chamber cooling.
- (9) Motion picture coverage consisted of six high-speed (200 and 64 fps) cameras operating over the duration of the test.

2. Motor LCAN-01 Test Results

January 1970. The test was conducted at the Aerojet Solid Propulsion Company P-3 test stand in accordance with the test plan summarized in the preceding section. The motor is shown just prior to firing in Figure 31. The firing resulted in a failure of the pressure vessel at T + 5.635 sec because of abnormal exposure of the case wall to high temperature gases. Because of the premature termination of the test, no useful nozzle performance data were obtained. Discussions of the test results, probable cause of the failure and conclusions and recommendations formulated are provided in the following paragraphs.

a. Test Results

Excellent motion picture documentation and recorded data were obtained that describe the sequence of events leading to the final failure. Ignition was normal, and the smooth pressure trace (Figure 32) peaked at 615 psia (424 $\mathrm{N/cm}^2$), almost exactly as predicted. At 0.315 sec, an abnormal pressure rise was measured by the two transducers (P $_{
m c}$ -1 and P $_{
m c}$ -2) mounted on a common boss at the outer periphery of the igniter adapter (Figure 33). The pressure recorded by these two sensors increased from 601 psia (414 N/cm²) at 0.315 sec to 890 psia (614 N/cm^2) at 0.940 sec, at which time an abrupt drop occurred, followed by three lesser pressure reductions at 1.60, 2.16 and 3.42 sec. The measured thrust data do not show increases or decreases with pressure, or in fact show any significant response to changes in pressure. Following the last pressure drop sensed by P_c-1 and -2 (at 3.42 sec), the output of these transducers and the igniter pressure $(P_{\underline{i}})$ instrument were the same. Previous to this time, P; (transmitted through the center of the igniter) did not sense the sharp pressure increase or drops described above, but continued to measure a smooth regression as the igniter grain burned out. This sequence of events was important in the failure analysis, which is described in Section III.C.2.b.

The recorded chamber pressure was smooth, slightly regressive, and about 25 psi (17.3 N/cm^2) below the predicted level from 3.42 secuntil the chamber failed at 5.635 sec. At no time was there any indication of any significant additional propellant surface burning. Pressure and thrust data for the full motor duration are plotted in Figure 34.

The high speed movie film clearly portrays the first chamber burnthrough. This event occurred at about T + 2.3 sec, as determined from a film frame count. The initial failure point was located at the forward equator and at about 20 degrees (0.35 rad) clockwise from the top of the case (standing aft, looking forward). Flame and exhaust gases continued to jet from this small hole until the final case failure. The major chamber burnthrough, and subsequent violent rupture, initiated on the lower right hand side (160 to 170 degrees) (2.79 to 2.97 rad) of the chamber just forward of

the center radial weld. The film exposure is too dark to discern discoloration of the dark green primer on the chamber prior to the failure; however, one small area opposite the location of the major burnthrough is seen to be smoking and an orange glow appears immediately prior to the gross failure.

The nozzle and aft 6 ft (1.83 m) of chamber were the only motor parts remaining in the test stand (Figure 35). Large sections of the failed chamber were found in the general test vicinity, some up to 400 ft (121.9 m) away. One fragment showed definite evidence of a high temperature—type failure, having smooth feathered edges typical of a ductile fracture with evidence of some flow-induced erosion. This piece was probably from the area of the major failure and is shown in Figure 36. Note the absence of any IBT-106 insulation on the inside surface of this section.

All other large metal pieces evidenced only tearing or brittle-fracture type edges. Most pieces had patterns of severe primer discoloration or other evidence of high-temperature exposure on the outside of the case where the major rupture occurred. Very little of the IBT-106 sidewall insulation remained on any of the recovered fragments. In the few cases where it did, the primed metal on the opposite surface was not marred.

The forward igniter boss of the motor, with the igniter adapter still installed, was recovered. The forward section of the adapter showed evidence of a definite gas-flow pattern, from outboard toward the center and generally including a 150 degree (2.62 rad) segment centered about the 160 degree (2.79 rad) radial.

Some fairly large segments of IBT-106 insulation were found in the test bay. All were too severely damaged by the post failure heat and water exposure to permit useful analysis. Unburned and well-bonded propellant was found on one piece of insulation.

b. Analysis of the Motor Failure

From analysis of the evidence provided by the recorded data, movie film, and the recovered motor fragments, the sequence of events

within the motor leading to the failure can be established. The mechanics of exactly how the first hot gas locally ignited propellant bonded to the forward boot or to the chamber insulation is not absolutely known. The conclusions reached and discussed below are based on a knowledge of the as-built motor configuration and a thorough review of the radiographic film and other NDT results.

The configuration of the forward section of the motor, with igniter installed, must be understood to substantiate the failure sequence. As seen in Figure 33, the igniter is positioned within a Gen-Gard V-44 rubber sleeve, which is bonded by epoxy adhesive to the IBT-106 forward boot. The nominal O.D. of the igniter adapter is 4.680 in. (11.9 cm), and the nominal I.D. of the V-44 sleeve is 4.650 in. (11.8 cm). This condition of potential interference is identical to that of the Algol IIA and IIB motor designs, and actual IIB components were used in this area. By examination, in Figure 33, of the relationship of the igniter adapter to the boot-release area, the P_c -1 and -2 pressure port, and the sleeve bond joint, one can readily see how the void in back of the boot can be isolated from the rest of the chamber bore. Any gases being generated by propellant burning at an abnormal location, anywhere from the boot-release point to the sleeve-bond interface, are essentially trapped behind the boot because of the limited clearance (or even interference) between the igniter adapter and the V-44 sleeve. This is the condition that existed in the motor from 0.315 sec, when P_c-1 and -2 first indicated the abrupt pressure rise, until 0.940 sec, when erosion or burnthrough of igniter components first relieved this localized pressure.

The most logical location to suspect the first hot-gas penetration to the propellant surface is through undetected defects in the adhesive bond line between the V-44 sleeve and the forward boot. However, results of X-ray and visual inspection do not reveal this to be a suspect area. The boot itself is known to have been greater than design thickness, and no evidence of voids or internal discrepancies that could present a gas-path were discovered in either the precast or postcast X-rays.

When the pressure behind the boot had increased to its maximum level of 890 psia (614 N/cm²) at 0.94 sec, a pressure differential of about 310 psi (214 N/cm²) existed at the chamber equator, or end of the boot release surface. The resulting aftward force, which tended to further open the boot separation, was probably sufficient to cause propagation of the release line until the pressure found or opened a path to the propellant surface at or near the first-observed case burnthrough in the upper, forward-equator area. Ignition of a small, localized, and confined propellant surface would tend to produce a torching effect, quickly burning through the insulation and case wall.

The same mechanism, a substantial pressure differential and a gas path to the case wall, was responsible for the gross failure experienced at 5.635 sec. At the area where the chamber eventually burned-through and rupture initiated, (a significant distance down the case from the original burnthrough), propellant again must have been ignited and the resulting failure was inevitable. Most likely, this ignition occurred at a location where the insulation fractured because of high bond-strength areas existing adjacent to those of lesser quality.

Because little insulation was found on any of the chamber fragments and because of the nature of the midchamber overheating condition, a poor steel-to-primer (Fuller 162-Y-22) bond, or cohesive failure within the primer itself, is the most probable contributor to the progressive mode of failure. Small pieces of the IBT-106 material still bonded to the steel case could be pulled off without too much difficulty, and the primer would generally come off with it, still adhering to the insulation. An investigation of data concerning prior use of the Fuller primer revealed that during the 260SL-3 nozzle fabrication process, inconsistent and sometimes very low peel and shear strengths resulted for test specimens prepared at different times or from different lots of primer. For this reason, the Fuller primer was not used to protect the inner surface of the SL-3 nozzle shell. In the Algol test motor application, under normal operation conditions, there is no loading mechanism causing a stress at the bond interface. Therefore, selection of the primer was not based on a requirement for exceptional adhesive qualities.

It is concluded that the 310 psi (216 N/cm²) differential pressure across the grain found a path to the chamber wall in the area of the equator and rapidly peeled the insulation away from the case. In effect, a condition approaching a free-standing grain existed over a large portion of the motor just prior to failure.

In an attempt to determine whether a gross bonding inadequacy existed within the steel/primer/IBT-106 interface, several doubleplate-tensile (DPT) and shear specimens were prepared. Primer from the actual lot of 162-Y-22 material used in the motor was brushed on 2 x 2 in. (5.1 x 5.1 cm) test plates and cured prior to IBT-106 application. Motor processing procedures were followed except where the surfaces were deliberately contaminated or the primer put on in an excessive (4X) thickness. The results (Table 27) show a minimum bond strength of 371 psi (256 N/cm²) with nearly all failures occurring within the IBT-106. Some primer came off with the IBT on selected samples, but not to the extent that might have been expected, based on the appearance of the chamber fragments. The 0.10-in.-thick (0.25 cm) steel test plates bent on all tensile samples prior to final separation of the two halves of the specimen, attesting to the strength of the bond and probably contributing to premature failure of the samples. Unfortunately, there is no convenient laboratory method of realistically duplicating the peel-type failure or of characterizing the peel strength of the primer-case bond. In summary, a potential motor processing technique which could have resulted in poor insulation bond strength could not be duplicated in the laboratory.

c. Significance of the Failure

Even though the nozzle was recovered intact, and essentially undamaged, no valid ablative performance data were obtained. The extended and severe heat soak caused by residual propellant burning in the aft section of the motor produced charring in the ablatives that is inconsistent with any service condition and is undefinable.

The failure of Motor LCAN-01 raised questions concerning the condition of the second motor, which was processed in an identical fashion.

To eliminate the chance of an insulation or boot defect initiating another malfunction, several modifications were proposed and accomplished with the approval of the NASA-LeRc program manager. A decision was also made to rebuild the second nozzle to permit evaluation of the carbon-silica throat and entrance section. These changes were discussed in Section III.B.3.d.

3. Motor LCAN-02 Test Results

a. Summary of Test Results

The second nozzle evaluation motor (LCAN-02) was statically test fired on 2 July 1970. Motor performance was normal for the first 28.6 sec of operation. A burnthrough on the nozzle entrance section occurred at this time, and the throat-and-exit cone assembly was ejected near the end of the tailoff phase. Sufficient data were obtained to allow evaluation of the materials under consideration and the accomplishment of most test objectives.

Performance of the propellant grain/insulation system was satisfactory, demonstrating the potential of the trowelable insulation and boot concept.

The nozzle failure was the result of an abnormally high material loss rate in the carbon-silica phenolic entrance section at the area of maximum exhaust stream impingement (in line with the grain valleys). The average erosion at the nozzle throat was essentially as predicted, as evidenced by recovered throat fragments and the results of a computer calculation of throat area based on measured chamber pressure and thrust. Performance of the silica- and canvas duck-phenolic exit cone liner was very satisfactory. Erosion and char rates were obtained from the recovered and relatively undamaged sections of this assembly.

Despite the four burnthrough areas forward of the nozzle throat section, the remainder of the nozzle and exit cone assembly remained attached to the structural shell until 45.8 sec, well into the tailoff portion

of the firing. The actual time of separation was established by a disturbance seen in the thrust trace and was confirmed by review of the movie film. The chamber pressure was about 90 psig (62 N/cm^2) at the time of nozzle separation.

Several hot spots on the case, notably at 90 and 270 degrees (1.57 and 4.71 rad) (0 degree being at the top) and generally in the aft 1/4 portion of the motor, appeared during the posttest heat-soak period. The nozzle malfunction rendered the quench system inoperable so that no posttest internal cooling was achieved as programed.

b. Discussion of the Test Results

(1) Ignition

Ignition was smooth and nearly identical to both the predicted pressure-time trace and the ignition transient of Motor LCAN-01. A maximum pressure of 616 psia (425 N/cm^2) was recorded at 0.280 sec.

(2) Motor Performance

Ballistic performance of the motor during the first 28.6 sec was normal, although the chamber pressure during the initial portion of the test was lower than expected. This is the result of the erosive burning effect, as programed in the ballistic prediction analysis, not being as severe or prevailing as long as anticipated. Otherwise, performance was smooth and essentially as predicted. For example, at T + 28 sec, just prior to the nozzle burnthrough, the predicted pressure and thrust were 525 psia (362 N/cm^2) and 107,685 lbf (479 KN), respectively; measured values were 520 psia (358 N/cm^2) and 107,928 lbf (485 KN). There was no evidence of any anomaly in the grain-insulation-boot system as was experienced on the first motor test, verifying the adequacy of the rework performed. The pressure- and thrust-vs-time plots are shown in Figure 37.

At approximately T + 28.6 sec the first burnthrough of the nozzle occurred just forward of the throat insert at the 180 degree

(3.14 rad) position (bottom of the nozzle). This initial failure was almost immediately followed by similar burnthroughs at the other three locations in line with valleys of the propellant grain at 0, 90, and 270 degrees (0, 1.57, and 4.71 rad). The average chamber pressure over the duration prior to failure was 522.5 psia (360 N/cm 2). Web burnout occurred at T + 38.4 sec, slightly less than the desired 40 sec. Ballistic performance data are summarized in Table 28.

(3) Nozzle Material Evaluation

The photograph shown in Figure 38 documents the nature of the nozzle failure. The orientation of the nozzle relative to the valleys of the propellant grain is obvious and is a major cause contributing to the burnthrough.

(a) Exit Cone

The entire exit cone was recovered in three major pieces and was in very good condition considering the thermal and dynamic environments to which it was exposed. The erosion of the MX-2600-96 silica and the 4KXDO2 canvas-phenolic flame liner was less than predicted with little evidence of local high loss rates (or gouging). No delaminations were present. The silica forward insulator blended smoothly into the canvas section indicating a common loss rate at this interface. The exit cone was sectioned at two longitudinal locations, 45 degrees apart (0.79 rad), and measurements were taken of the remaining virgin material and char depth. Because of the charring of the exit cone exterior surface, the overwrap interior interface was used as the reference in determining the remaining material thickness.

The measured exit cone performance data, including total material loss, char depth and regression rate are presented in Table 29. The total time the exit cone was attached to the motor (45.8 sec) was the duration used to arrive at the basic loss rate. There was no appreciable difference between measurements made at the same axial station but 45 degrees apart. A more conservative loss rate, which assumes that all material loss

occurred during web time (38.4 sec) is also included for comparison. These erosion rates are plotted vs area ratio along with data from other programs in Figure 39. No. attempt was made to adjust the data for differences in motor operating pressure or nozzle size.

A heavy, uniform, and rather fragile char was formed on the interior of the canvas portion of the exit cone. This char could be easily displaced from the surface. The sectioned exit cone is shown in Figure 40.

(b) Nozzle Throat

The actual erosion and char depth at one location on the MXSC-195 carbon-silica nozzle throat insert was determined from fragments recovered after the test. The recovered pieces (Figure 41) were sectioned, and the remaining material thickness and char depth determined. As seen on the nozzle performance data summary (Table 29), a surface regression of 0.39 in. (0.99 cm) at the throat plane occurred on this part. Only one fragment that could be identified as representing a complete section through the throat was found, all others being from random sections of the insert. Most pieces show evidence of severe localized erosion and gouging on the forward surface, indicating that little protection was provided by the entrance insert at locations in line with the grain valleys.

The 0.39-in. (0.99 cm) material loss measured on the section discussed above most probably represents the best performing portion of the throat insert, probably in line with a grain ray, such as at 45 degrees (0.79 rad). It is difficult to arrive at an accurate material loss rate because of the change in flow conditions that occurred subsequent to burnthrough (28.6 sec). However, the throat was exposed to the exhaust gases until nozzle separation at 45.8 sec. Using this duration to determine the erosion on the recovered throat fragment results in a loss rate of 8.5 mils/sec (0.022 cm/sec), which is well below the predicted overall average rate of 11.7 mils/sec (0.030 cm/sec). A more realistic approach is to use the web-duration (38.33 sec), which results in 10.2 mils/sec (0.026 cm/sec). It must be remembered, however,

that a substantial amount of the exhaust products were exiting forward of the throat for nearly 10 sec prior to web burnout. The average pressure over this period was 499 psia (344 N/cm^2) , essentially the same value as was used in the thermal analysis of the nozzle. It is logical to expect that higher erosion was experienced in areas in line with the propellant grain valleys.

A computer analysis, which calculates throat area vs time based upon the measured chamber pressure and thrust was conducted for the portion of the test prior to nozzle burnthrough. A nozzle efficiency constant (K_f) of 0.97 was assumed for this analysis. The results indicate that the material loss at the throat was essentially as predicted. The calculated increase in throat area at 28 sec was 14.2 sq in. (36.1 sq cm), or an average surface loss of 0.345 in. (0.88 cm). This represents a loss rate of 12.3 mils/sec (0.031 cm/sec) as compared to the 12.7 mils/sec (0.032 cm/sec) predicted over this duration.

(c) Entrance Section

The MXSC-195 carbon-silica portion of the entrance insert was the location of the nozzle failure. A very high, localized material loss rate at the four positions coincident with the grain valleys, where maximum gas flow and impingement occurs, was the cause of the failure. A nonstreamlined or turbulent flow condition, caused by uneven erosion of the IBT-100 or silica insulators ahead of the carbon silica may have aggravated this already severe flow condition. The motion pictures show the first burn-through occurring adjacent to the 180 degree (3.14 rad) (bottom) position near the upstream 2:1 area ratio. Failure at the other three radial locations of the entrance section in line with grain valleys came shortly after the initial event. At two locations on the entrance shell, where the grain rays provided protection from direct impingement, full-length sections of the entrance insert remained in place for the entire firing duration and were available for analysis. A section taken from the location of the initial burnthrough, about 200 degrees (3.45 rad), is shown in Figure 42.

At the projected point of failure, a surface regression rate of about 53 mils/sec (0.135 cm/sec) would have been experienced

for the failure to have occurred when it did. This rate is nearly five times as great as was expected and no previous industry-wide experience with carbon-silica phenolic composites has resulted in comparable performance. There were no known fabrication deficiencies in the part, and the density of the cured material met specification requirements.

It is apparent that some mechanism other than those normally present, and considered in the Aerojet Charring Material Ablation computer program, was the reason for the abnormally high loss rate. Direct impingement of the high velocity exhaust gases coincident with the grain valleys can cause radial as well as axial flow conditions, with resultant turbulence and localized high impact pressure conditions where the exhaust stream reattaches to the nozzle entrance surface. Nonsymmetrical or severe erosion of the IBT-100 or silica insulation forward of the carbon silica would aggravate this condition and could result in a gas flow parallel to the ply orientation of the carbon-silica entrance insert. This effect could cause progressive peeling or delamination of the plies. A tendency of the carbon sílica to delaminate during charring was observed during the material evaluation program conducted by the Battelle Memorial Institute. Most fragments of the throat insert exhibited a forward face that was broken parallel to the plies and showed some evidence of gas flow on the exposed forward surface which lends credence to this theory.

Some portion of the silica-phenolic forward insulator remained at all stations forward of the failure points, thus eliminating this section as the source of the failure, as was initially suspected. The IBT-100 trowelable insulation performed well, with a substantial thickness of virgin material remaining. A very heavy, loose char completely covered this portion of the entrance section. The posttest nozzle insulation profile at 45 and 200 degrees (0.79 and 3.49 rad) is shown in Figure 43.

Investigation of Carbon-Silica Char Strength

In an attempt to ascertain the reasons for the excessively high erosion rate of the MXSC-195 carbon silica phenolic in the

entrance section of nozzle No. 2, specimens cut from the test ring of the parent billet were charred and subjected to compression tests. A section of an MXSC-195 throat billet from another program (Low Cost Fabrication Techniques) was also tested to provide data for comparison.

The samples of material were enclosed in a metal retort and heated in an atmosphere of flowing argon to a temperature of 1500°F (1090 °K) for 1 hour and then cooled in argon. After charring, the samples were examined visually. While no actual cracks or separations were observed, the char did not have the uniform, tightly knit appearance of a normal, dense composite char. Both ring and throat samples were similar in appearance after charring. A sample typical of the charred LCAN nozzle entrance material is shown in Figure 44.

Compression specimens, $1/4 \times 1/4 \times 1/2$ in. $(0.64 \times 0.64 \times 1.27 \text{ cm})$ were machined from the charred materials and tested to destruction. The results are shown in Table 30. The average compressive strength of the ring specimens was 2020 psi (1393 N/cm^2) , and that of the throat specimens was 1946 psi (1342 N/cm^2) . The average compressive strength of the charred material at room temperature compares favorably with that of charred carbon and silica specimens, 2500 psi (1725 N/cm^2) for MX-4926 and 1800 psi (1240 N/cm^2) for FM-5131. The range of values is much greater than has been observed previously, however, and the minimum values are so low as to indicate that some material or processing discrepancies were present. Since the samples for testing were taken from parts fabricated by two different sources, the material is the most likely offender.

As part of the Task I effort, nozzle materials were characterized with regard to physical and mechanical properties. It was not possible to measure the elevated-temperature strength of MXSC-195 specimens because they delaminated during charring.

AVCERAM reinforcements were used in entrance sections of nozzles for the Air Force Low Cost (NOMAD) Nozzle Program (2), as well as in the throat inserts. WB-8251, 4C 2530, and X-5571 pre-pregs,

supplied by Western Backing, Coast Mfg. and Supply Co., and U. S. Polymeric Corp., respectively, were used in that program. The performance of the materials was uniformly acceptable. The elevated-temperature compression strength of one of the charred composites (X-5571) was on the order of 6000 psi (4140 N/cm^2) at 2500°F (1647°K).

In view of the information noted above, conclusion is made that the excessive erosion rate observed in the MXSC-195 was most probably caused by a lack of mechanical strength in the charred composite.

Comparison of Production Algol and LCAN Motor Conditions

The production Algol II-A and II-B nozzles also show, to a lesser degree, the effects of exhaust impingement due to the grain configuration. The nozzle entrance section on these motors is fabricated from a high-silica-content glass laminate (Refrasil) with the approach to the graphite throat inclined at 55 degrees (.94 rad) to the gas stream. Early tests resulted in higher than expected erosion of this section. A subsequent reorientation of the wrap angle from perpendicular-to-center line to perpendicular-to-gas flow was accomplished that reduced the erosion to an acceptable value. A comparison of motor and nozzle conditions between the Algol II-B and the LCAN-02 motor is shown in Table 31. The higher solids loading of the ANB-3347 propellant and the higher gas velocity at the end of the LCAN grain both contribute to a more severe environment in the LCAN motor. In addition, the graphite throat insert of the Algol motor extends outboard of the inner diameter of the grain valley, thus it receives the direct exhaust impingement during the initial portion of motor operation, when flow conditions are the worst.

(4) Chamber Internal Insulation System

The areas of chamber overheating were correlated with sections of the insulation that were of less than design thickness, generally about 0.10 in. (0.25 cm), or are associated with small voids or gaps between

adjoining passes of the sidewall insulation dispenser. The individual discrepant areas were concealed from visual detection during the processing by a thin surface covering of IBT-106. When detected by ultrasonic or X-ray inspection, they were repaired.

X-ray inspection of the insulated case sidewall section was not extensive enough to reveal all the areas that had less than the desired thickness. Ultrasonic inspection was intended as the primary method of detecting flaws within the sidewall insulation, but material thickness cannot be determined by this technique. In-process physical measurements ("tooth-pick" gage) were made periodically during application of the insulation to verify correct positioning of the dispenser blade. Apparently the occasional slippage of the motor on the turning rollers resulted in thin areas not discernable by visual inspection and only discovered during the posttest review of the loaded-motor X-ray film.

For a normal duration tailoff, a 0.10 in. (0.25 cm) thickness of insulation would provide adequate protection for the case. However, on this test the exposure period at the more critical locations (at the grain valleys in the aft section) was at least 22 sec and no internal quench or cooling was actuated for about 8 to 10 min after web burnout. The most severe area of case heating was first detected at about the time of nozzle ejection (~46 sec) and was located on the aft 5 ft (1.27 m) of the case at the 90 degree (1.57 rad) position. The case was deformed adjacent to weld No. 7, precluding its reuse as a pressure vessel. The original insulation thickness at this location was about 0.10 in. (0.25 cm) and obviously not detected by pretest radiographic inspection. Unfortunately, none of the 16 case thermocouples was at an area of maximum heating, thus indicating near-ambient temperatures throughout the firing. Thermocouple No. TCC-080-289 was adjacent to a small hot spot at the forward end of the chamber and did sense a maximum temperature of about 350°F (450°K) as shown in Figure 45. Figure 46 shows the posttest condition of the case.

A thick, irregular and very flaky char similar to that noted in previous small-motor tests, covered all the remaining internal

insulation. The interior of the chamber steel wall was exposed in large areas where the most severe hot spots were located. These areas are all in grain valley locations, generally at 90 and 270 degrees (1.57 and 4.51 rad). A small portion of the aft boot, charred completely through, remained in the chamber along with some of the MK-599 potting material. No forward boot material remained. Both the forward- and aft-head insulation were in very good condition with a substantial thickness of virgin material remaining.

A tabulation of the actual amount of insulation remaining at selected stations within the chamber and the original material thickness at these locations is presented in Figure 47.

Sidewall insulation erosion from Stations A through L (see Figure 47) ranged from 0.018 to 0.29 in. (0.046 to 0.74 cm). The expected thickness loss in this area was 0.072 in. (0.18 cm). Because of the longer tailoff and after-burn, the expected thickness loss could be as high as 0.16 in. (0.41 cm). At the area of the largest hot spot (Station L) the initial insulation thickness was 0.075 in. (0.19 cm) as measured from radiographic negatives. Motion picture coverage shows the first indication of case heating at this location at about 46 sec. Since web burnout occurred at 38.4 sec, the exposure time for this area was approximately 8.6 sec, resulting in a thickness loss rate of about 0.009 in./sec (0.023 cm/sec), or three times greater than the expected rate of 0.003 in./sec (0.008 cm/sec).

This excessive rate can be accounted for in part by the fact that subsequent to web burnout the nozzle effective throat area was continuously and rapidly increasing, thus reducing the motor port-to-throat ratio. This in turn resulted in an increase in the gas velocity over the aft section of the case. After nozzle ejection at 45.8 sec the gas velocity was estimated to be about Mach 0.15. This condition imposes a severe environment on the IBT-106 insulation. This material is not intended to be used in areas where any significant erosion or gas velocity is expected; IBT-100 is normally used in such locations.

c. Conclusions Based Upon Test Results

- (1) The test is considered a success in that valid performance data were obtained on the low-cost ablative nozzle materials of principal interest for full-scale motor application.
- (2) Performance and processability of the canvas duck-phenolic (4KXD02) and heavy-weight silica-phenolic (MX-2600-96) materials were very satisfactory. The erosion rates of these materials were less than expected.
- (3) Carbon-silica phenolic (MXSC-195) was found to provide poor performance in regions of high exhaust stream impingement and disturbed flow. The failure of the carbon-silica entrance insert is attributed to an extremely high loss rate resulting from poor mechanical properties, particularly interlaminar shear strength, of the charred composite.
- (4) Performance of the trowelable chamber insulation system was satisfactory over the action time duration. The chamber hot-spots that occurred near the end of tailoff and during the extended heat-soak period were the result of undetected defects in the insulation and the abnormal thermal environment experienced.
- (5) The quality of the IBT insulation system is directly dependent upon the degree of tooling sophistication. The processing methods utilized were demonstrated to be satisfactory and applicable to 260-FL class motors.

D. TASK III - FULL SCALE NOZZLE DESIGN AND FABRICATION PLANNING

1. Evaluation of High Nozzle Throat Erosion Rates on Motor Performance and Cost

An important consideration in the design or planning stages of a low-cost full-scale nozzle is whether an actual overall motor cost savings is achieved when the lower-cost, yet poorer-performing ablative materials are

incorporated in the nozzle throat. As the throat area increases, the thrust coefficient decreases with a corresponding loss in total impulse. To maintain the same mission capability as with a baseline case, additional propellant (and inert materials) must be added to the motor. This additional motor cost must then be compared with the savings realized through the use of the low-cost ablative materials to determine the net savings (or loss) achieved.

Considering the above, a study was made of the effects of high nozzle-throat erosion rates on 260-in.-dia (6.6 m) motor performance. The full-length 260-in.-dia (6.6 m) motor defined in Reference (6) was used as the basis for this evaluation. The ballistic performance of this motor was calculated using assumed nozzle throat erosion rates of 10, 15, 20, and 25 mil/sec (0.025, 0.038, 0.051, and 0.063 cm/sec). The payload capabilities of 260/SIVB vehicles with these various first-stage nozzle erosion rates were then determined for comparison with the payload delivered by the baseline vehicle with a 6 mil/sec (0.015 cm/sec) nozzle erosion rate.

The effect of the nozzle throat erosion rate on the payload capability of 260/SIVB vehicles launched from the Eastern Test Range into 105 nautical mile (195 km) circular orbit is shown in Table 32. The vehicle payload decreases with increasing nozzle throat erosion rate. The 25 mil/sec (0.063 cm/sec) erosion rate results in a 5% payload loss, as compared with the baseline 6 mil/sec (0.015 cm/sec) erosion rate. The effect of the throat erosion rate on 260-FL motor thrust performance is shown in Figure 48. The 25 mil/sec (0.063 cm/sec) erosion rate results in reduced total impulse and extended burning duration compared with the baseline performance. This, together with the increased weight of the high erosion rate nozzle causes the reduction in calculated payload.

A study was made of the propellant grain design modifications that could be made to compensate for high nozzle throat erosion rates. It was found that a 20 in. (51 cm) reduction in the length of the finned section and an equal increase in the length of the cylindrical section of the full-length motor grain, combined with a 2% increase in propellant burning rate (0.606 to 0.618 in./sec at 600 psia) (1.54 to 1.57 cm/sec at 413 N/cm²), provides the

same peak thrust and burning duration with a 25 mil/sec (0.063 cm/sec) erosion rate as is obtained in the baseline design with a 6 mil/sec (0.015 cm/sec) erosion rate. The thrust performance of this modified version is also shown in Figure 48. Evaluation of the payload capability of a 260/SIVB vehicle with this modified first stage indicates that the payload loss is about 23% less than with the unmodified grain design at the highest erosion rate. Similar improvements can be achieved at the intermediate erosion rates.

The trajectory analysis used to obtain the payload comparisons also provides exchange ratios as part of its output. The exchange ratios relating change in burnout velocity to change in first stage inert materials, first stage propellant, and vehicle payload were used to establish the increase in first stage weight required to achieve the baseline vehicle payload with the higher nozzle erosion rates. It was assumed that the motor size increase would not affect the propellant mass fraction. The resulting weight increases, together with the estimated corresponding cost increases are shown in Table 33. The cost values provide a basis for evaluating the economics of high-erosion rate nozzle materials. The savings realized through use of low-cost ablative nozzle materials must exceed the cost of the necessary motor size increase.

To further define the cost advantages of using the lower cost materials in a 260-FL nozzle, a study was conducted using four different nozzle configurations. Actual current material costs were obtained for 1000 lb (454 kg) lots from the principal suppliers of the materials considered. Previous work has shown that the difference in fabrication costs from one material to another in a large nozzle is not significant and was not considered in this study.

The baseline nozzle was a standard carbon and silica design, similar to that of the 260-SL-3 nozzle originally prepared for a low-cost study conducted under Contract NAS7-513. The Alternative No. 1 nozzle was defined during the same study and incorporated carbon-silica and canvas-phenolic materials to replace the higher-priced carbon and silica of the baseline design. Alternative No. 2 was a silica and canvas design, whereas Alternative No. 3 combined a carbon throat with lower cost materials in the other liner inserts. The component weights previously determined for the baseline and Alternative No. 1

designs were adjusted for differences in the density and thickness requirements of Alternatives No. 2 and 3. Table 34 summarizes the material costs for these four nozzles, and compares the apparent savings with the added motor cost required to provide the same payload capability as the baseline design. A plot of additional motor cost vs nozzle erosion rate is shown in Figure 49. These data were the output of the trajectory and performance analysis discussed in the preceding paragraphs.

Examination of Table 34 shows that if the silica-throat erosion in a 260-FL motor is as predicted, no significant cost advantage in its use would be realized. The use of a carbon-silica throat, however, would result in a net saving of \$79,200. A nozzle such as Alternative No. 3, incorporating a carbon throat and with maximum use of the lower cost materials in other areas, is by far the most economical design. This conclusion and the results of the LCAN-02 test firing are the most significant influencing factors in the material selections and design of the low-cost full-scale nozzle.

2. Design Criteria

The full-scale, low-cost nozzle design is based on the 260-FL motor defined in the Douglas 260/SIVB study. The motor contained 3.4 million lb $(1.54 \times 10^6 \text{ kg})$ of propellant and its operating characteristics are summarized below:

Action Time 147.5 sec

MEOP 764 psia (526 N/cm^2)

Average Thrust, web 6.34×10^6 lbf (28.2 MN)

Flame Temperature 5742°F (at 1000 psia) 3440°K (at 690 N/cm²)

These criteria meet or exceed the reference parameters established in Exhibit "A" to the Contract NAS3-12038 Work Statement.

The exhaust gas composition of ANB-3374 (the HTPB propellant that is expected to be used in any future large solid booster) is given in

Table 35. These data, along with the pressure-time curve shown in Figure 50, were used as input data for the ablative performance analysis program.

The nozzle is designed to permit a \pm 2 degree (0.035 rad) TVC capability, at a rate of 3 degrees/sec (0.052 rad/sec) by incorporating the flexible seal assembly designed under Contract NAS3-12049.*

A primary design requirement was the use of resin-impregnated fabrics, which are less expensive than the conventional carbon and silica composites used in all large solid booster nozzles fabricated to date. These materials must also have been evaluated to the extent and at a scale adequate to provide assurance of success on the 260-FL motor nozzle. Fabrication of the ablative liners by proven tape wrapping and pressure/heating cure processes was a further requirement. The design and nozzle processing sequence have been established with a goal of providing an economical manufacturing plan, within the state-of-the-art, while maintaining a high product reliability.

The initial thicknesses of the ablative liner were established using a minimum safety factor of 1.50 over and above the expected surface material loss and char penetration. The location of the 100°F (312°K) isotherm further defined the total ablator thickness, with the criteria that the overwrap inner surface does not exceed this temperature. The design safety factor at the nose was increased to 2.0, where analysis is complicated, and reduced to 1.25 in the aft exit cone section, where material loss is minimal and easily defined.

Structural members were designed to prevent strain in the plastic parts from exceeding 0.25%. A safety factor of at least 1.25 was also imposed on the minimum allowable material properties.

3. Other Factors Affecting the Design

In addition to the basic objective of using lower cost materials in the nozzle assembly,, several other important factors must be considered that affect the overall cost and performance of the nozzle or full-scale motor. These are discussed below:

^{*}Design, Fabrication, and Test of Omnidirectional Flexible Seals for Thrust Vector Control of Large Solid Rocket Motors (Contract NAS3-12049; Aerojet Solid Propulsion Company, from Lewis Research Center).

a. Effect of Throat Erosion Rate on Motor Performance

Trade studies of motor performance vs throat erosion rate were conducted to determine the actual cost differential achieved when throat surface regression rates of up to 0.025 in./sec (0.064 cm/sec) were experienced. The cost savings gained by the use of low cost ablative materials were compared to the cost of the additional propellant and inert motor components required to produce the same performance as the baseline motor with a throat erosion rate of 0.006 in./sec (0.015 cm/sec). The conclusion, as discussed in Section III.D.1, is that the greatest potential for cost savings is realized when carbon phenolic (or an equivalent material) is used in the throat and the low cost materials are incorporated elsewhere in the nozzle and exit cone assembly.

b. Material Selection and Qualification

The practice followed on previous 260-SL nozzle designs of specifying a single manufacturer's product (pre-preg carbon or silica) has resulted in artificially inflating the price paid for these raw materials. A more desirable practice, and one which allows more competitive pricing, is the establishment of a qualified products listing (QPL) for each material that is considered essentially equivalent in performance and processability. Therefore, for the full-scale nozzle design three or more acceptable alternatives are listed for each generic material.

c. Facility and Equipment Limitations

The availability of existing equipment and facilities for the wrapping, machining, and curing of very large nozzle components influences the design and limits the number of competing fabricators. Both of these factors have an impact on the overall cost of the end product. On a large production order, to reduce the costs of a new facility, it may be desirable to enable more than one qualified fabricator to participate in the nozzle manufacture. To accomplish this objective, the maximum outer diameter (OD) of most parts must be limited to 130 in. (3.3 m). This results in a variation from some accepted design practices in the nozzle nose and submerged sections where

a minimum area ratio of about 2:1 at the nose is considered desirable and has proven to be satisfactory with 260-SL motors. Reducing the OD in this area to be compatible with process equipment limitations will expose the nose to a more severe environment; however, insert thicknesses may be increased accordingly at comparatively little additional cost.

Initially, a three piece exit cone was proposed. This was done primarily to allow more fabricators to be considered for supplying the forward section, which was compatible with the 130-in.-dia (3.3 m) limitation of most existing wrapping and curing facilities. This concept, however, did not result in the greatest overall savings. With a two piece design, additional cost savings (less tooling, processing time, etc.) resulted that overshadowed the advantages of the three-piece unit. The forward section of the resulting two-piece configuration may still be wrapped and cured in existing facilities, and the aft section of either design necessitates the same new facilities and presents the same logistical problems.

d. Confidence in Nozzle Performance

Very little actual performance data exist for some of the low cost materials that would appear to be attractive for use in 260-size nozzles. Available data are generally from subscale test firings (D $_{\rm t}$ $^{\sim}$ 8 in. (20.7 cm) or less) where nozzle configuration, grain geometry, or propellant exhaust composition varies from a typical 260 motor condition to the extent that little performance correlation may be expected. A conservative philosophy was followed in the design of the low cost full-scale nozzle; medium risk or high risk materials were not considered, despite the apparent possibility of cost savings.

Task II test results from the LCAN-02 firing demonstrated the poor performance of carbon-silica in the nozzle entrance section (although gas thermal dynamic conditions were more severe than would be present in the 260-FL motor), the area where this material had potential for cost-effectiveness. As a result of the LCAN-02 test, the full-scale nozzle will incorporate carbon phenolic in this region; the cost will be greater, but maximum confidence in

successful operation and the ability to predict ablative performance will be gained.

The LCAN-02 test also provided additional data confirming the desirability of canvas duck and the heavyweight silica-phenolic materials in the less severe environments of the nozzle and exit cone. The better-than-expected performance of canvas in the exit cone and its excellent processing qualities enable its use in the 260-FL nozzle design without reservations and at a considerable material savings over the conventional silica material normally specified.

4. Design Description

a. Nozzle

The full-scale nozzle design is shown in Figure 51. The nozzle is of the submerged type, having a throat diameter of 89.1 in. (2.26 m). The nose and approach section have a 3:2 elliptical shape, with the major axis equal to 75% of the throat radius and the leading edge being at an area ratio of 1.81:1. This configuration provides a streamlined gas flow transition into the throat area and has been shown by analysis and test results to be a very satisfactory design. The flexseal will permit a minimum of \pm 2 degrees (0.035 rad) nozzle deflection for TVC. The seal assembly incorporated in this nozzle was designed, structurally analyzed, fabricated, and tested under Contract NAS3-12049.

Carbon phenolic pre-preg materials having a minimum carbon assay of 92% and a phenolic or polyphenylene resin solid content of from 31 to 37% will be used as the basic ablative material in the nozzle. The aft portion of the submerged liner and all insert overwrap insulation will be made of canvas duck phenolic. The reinforcement pre-preg will consist of 8-oz double-fill cotton duck with a 38 to 44% phenolic resin solids content.

The nozzle shell and throat support structural components will be made from HY-150 steel. Roll-formed and welded assemblies will be

utilized as a cost reducing fabrication method with the thicker flange sections and the forward portion of the throat support machined from ring-rolled forgings.

A brief description of each ablative component is given in the following paragraphs:

(1) Nozzle Shell Insulation

The nozzle shell thermal protection consists of an inboard canvas duck phenolic section with IBT-100 trowelable insulation on the less critical outboard area. The canvas piece is wrapped of bias tape at an 80 degree (1.40 rad) to center line orientation. The cured and machined insert would be bonded into the HY-150 steel shell with an ambient curing epoxy adhesive. The IBT-100 would be mixed and applied at the motor assembly site.

(2) Submerged Insert

This component provides protection for the flexseal and the submerged backside of the throat support structure. It is a two material composite, having a canvas duck phenolic aft insulator cantilevered from the steel shell to a position adjacent to the aft closure canvas insulation where it protects the seal from the thermal radiation of combustion gases. The forward portion of the piece is made from carbon-phenolic and extends to the nose cap at a diameter of 120.0 in. (3.05 m) or an ϵ = 1.81:1. Warp-cut tape may be used for both materials as the wrap-angle is from 0 to 3 degrees (0 to 0.053 rad) of the nozzle center line.

(3) Nose Insert

This insert is wrapped of bias-cut resin-impregnated carbon tape at an angle of 97 degrees (1.69 rad) to the nozzle center line. A canvas duck phenolic overwrap, parallel to the surface, is applied to the machined backside of the preformed billet and simultaneously cured.

(4) Entrance Insert

The entrance insert also incorporates carbon (biascut) tape with a parallel-to-surface canvas duck insulator. The nominal 67 degrees (1.17 rad) to center line wrap angle makes this part very similar to its 260-SL-3 counterpart.

(5) Throat Insert

This piece is also similar to the 260-SL-3 throat insert, having a 50 degree (0.87 rad) nominal wrap angle. Bias-cut carbon tape is used for the exposed flame liner section, which may experience a thermal or erosive environment. An unusually thick canvas back-up is used to provide material cost savings where excessive thickness is necessary due to the geometry of the steel support assembly.

A weight summary for the nozzle is provided in Table 36. The total weight of the entire nozzle assembly, including the exit cone and flexseal is 43,676 lb (19,830 Kg).

b. Exit Cone

The two piece exit cone, shown in Figure 52, is of a contoured or bell-shaped design having an exit plane diameter of 267.30 in. (6.78 m) and an overall length of 247.16 in. (6.27 m). The expansion ratio of 9:1 provides a thrust coefficient ($\mathbf{C}_{\mathbf{f}}$) very nearly the same as a conventional conical exit cone having an 11:1 expansion ratio. The contoured design results in economy of materials, while maintaining the overall diameter and length to dimensions compatible with reasonable fabrication-tooling and facility requirements, shipping limitations, and the aft-flare envelope of the 260/SIVB motor.

The exit cone forward section extends to an area ratio of 3.72 and is designed to take maximum advantage of the low cost canvas duck material while maintaining the better performing and well-characterized carbon in the more critical areas. Carbon phenolic was selected for the forward

section for the following reasons:

- (1) The low area ratio (1.1:1) at the forward end of this component requires a material with good erosion resistance.
- (2) The other leading material candidate for this part was carbon-silica phenolic and little or no performance data are available on this material at this location.
- (3) Using the estimated material loss for carbon-silica at an area ratio of 1.38:1 and actual 260-SL carbon phenolic test data in a cost-effectiveness comparison results in a definite advantage (over 2 to 1) for carbon. Similar results were obtained when either canvas or heavyweight silica were investigated for use at the more severe environments.

The parallel-to-center line carbon phenolic wrap increases to a slightly thicker than necessary section near the 2.15 area ratio to allow a smooth transition into the adjacent canvas duck material, which requires a greater cross-section. The two materials would be wrapped and further processed as a common liner on a net-contoured mandrel. A canvas duck overwrap, nominally 0.30 in. (0.76 cm) thick, is incorporated over the portion of the exterior surface which is bonded to the steel housing. This overwrap blends into the structural glass phenolic overwrap, which extends to the aft face of the part. A 4130 steel attachment flange is bonded to the glass structure at the aft end; the flange is further secured with an overwrap of a room-temperature curing epoxy resin/glass system. The AISI 4130 steel shell would be a weldment joining the machined-forging forward flange to the roll-and-welded conical segment. The aft portion of the shell has the additional thickness needed to resist and distribute the TVC actuation loads. Two actuator attachment brackets, 90 degrees (1.57 rad) apart, would be welded to the shell.

The exit cone aft section has an all canvas duck phenolic liner and a glass-epoxy resin structural overwrap. No insulative overwrap of ablative material (canvas, silica, etc.) is used on the part. The

glass tape, wrapped parallel to surface, will assume the functions normally associated with the ablative overwrap (insulator and gas path barrier) in addition to its structural function. The flame-liner thickness is designed to maintain the glass-canvas interface at a temperature of 100°F (312°K) or lower. The structural analysis indicates that the glass-epoxy system has adequate stiffness in the axial mode so that no additional structural reinforcement (such as honeycomb) is required. The relatively low TVC loads make this possible.

The forward attachment ring would be bonded to the machined surface of the glass structure and overwrapped with a glass-epoxy ambient curing system.

The use of canvas duck phenolic at an area ratio as low as 2.26 is the most notable departure of this exit cone from previous designs, where a transition from carbon to silica has generally been made near the 2.3 to 2.5 area ratio station. Canvas has been successfully used in subscale motors (8.2-in.-dia (21 cm) throats) in the programs described in References (2) and (3) and most recently on Task II of this program where excellent performance of the canvas was experienced at an area ratio as low as 1.95. The extensive use of canvas in the full-scale nozzle design represents the most-significant, single factor in material savings.

In addition to the fabrication considerations, the aft flange location of the forward section was selected to enable either surface or air transportation of this part within present carrier size limitations and DOT regulations.

The aft section must either be manufactured near the motor assembly site (A-DD) or shipped from the west coast via the Panama Canal.

The weight of the exit cone assembly is shown in Table 37.

5. Design Verification

a. Thermal Analysis

A thermal evaluation was conducted of the proposed low-cost full-scale nozzle design. This analysis utilized the estimated ballistic performance and provided analytical predictions of local erosion, char depth, and total thermal zone growth in the ablative liners as a function of elapsed firing time. Discussions of the pertinent data and analytical techniques used in this analysis follow:

The analysis consists of a series of one-dimensional transient thermal analyses performed at various preselected axial stations of the preliminary nozzle design. These locations are chosen so that all critical areas receive special attention and are of sufficient number that a smooth post-firing erosion and thermal gradient contour may be prepared over the entire nozzle profile. The analytical techniques have been used on previous large motor programs. This procedure considers the actual thermal response of a material that reacts at the surface with the propellant exhaust products (erosion) and decomposes in depth (charring). The input data required for this program include material properties, dimensions, and surface heat-transfer conditions. The latter are established using a boundary layer growth technique which considers the local flow surface Mach numbers, nozzle contour, and propellant transport properties. The resulting boundary conditions used in this analysis are summarized in Table 38.

In addition, the heat transfer coefficients were varied according to the schedule shown in Table 39 to better account for the chamber pressure variation that occurs during the firing.

Based on these data, the expected erosion, char depth, and total thermal zone growth were determined and are tabulated in Table 40. In the table, the erosion represents the material loss resulting from either chemical corrosion and/or melt removal. The char zone depth is defined as the location of the 1100°F (865 °K) isotherm, while the total thermal zone represented

by the 100°F (312 °K) isotherm. As noted, the thermal erosion at the throat is predicted to be 0.88 in. (2.24 cm), which represents a loss rate 6.3 mils/sec (0.016 cm/sec) over the motor web time. This compares to a measured value of 5.8 mils/sec (0.015 cm/sec) for the 75 sec web time of 260-SL-3. The difference is attributed to a higher average chamber pressure and a slightly increased chemical corrosion potential for the HTPB type propellant.

The expected ablator surface loss and char zone at the end of the firing, as tabulated in Table 40, is shown plotted on the nozzle layout in Figure 53 (forward section) and Figure 54 (exit cone). The thermal response at the throat and at the most critical location on the exit cone canvas liner is plotted vs motor duration in Figures 55 and 56, respectively. Erosion in the canvas exit cone liner is plotted vs area ratio in Figure 57.

The exit cone represents a nearly optimum design in relation to the liner thicknesses selected. The $100^{\circ}F$ (312 °K) isotherm is just outside of the overwrap interface. The nozzle section is more conservatively designed as may be seen in Figure 53. The combined effects of erosion, char, and thermal zone growth, as determined by the computer analysis, were not as severe as was assumed for the preliminary design. Therefore, the actual minimum safety factor on the Task III nozzle design is somewhat higher than the target value (2.1 vs 1.5) at the most critical location ($\epsilon = 1.13$).

Although it would be possible to further refine the full-scale nozzle design to reduce the liner thicknesses forward of the exit cone, this task was considered beyond the scope of this program. In an actual production program any modification to this design would most probably not be made until firing data confirmed the expected performance and a lower safety margin could be justified.

b. Stress Analysis

A stress analysis was conducted to determine the design adequacy of the 260-FL motor nozzle. The Aerojet E11405 finite element computer routine was used for the analysis (see Section III.B.2.d).

The design loads for input into the analysis included the following:

Motor maximum expected operating pressure (MEOP) of 750 psia (517 N/cm^2) .

Axial ejection force of 1,000,000 lb (4.45 MN) in the flexible seal.

Thermal gradient in the nozzle ablator at motor burnout as determined from the heat transfer analysis.

On the basis of the design loads, safety factors of 1.25 on structural components and 1.00 on ablative components were imposed. In addition, the strain within the ablative components was limited to 0.25%.

HY-150 steel was selected for the conical closure and throat support nozzle structure. Normalized 4130 steel was selected for the exit cone housing and attach flanges. The exit cone structural overwrap was fabricated of 184 glass/phenolic resin. Ablative liner materials were carbon phenolic and canvas phenolic. Material properties that were used in the analysis are shown in Tables 41, 42, and 43. Elevated temperature property values obtained from the material characterization task of this program are included.

Detailed analysis of the nozzle was performed by dividing the nozzle into three basic parts: (1) conical closure with the flexible seal aft ring, (2) nozzle throat support with the flexible seal forward ring, and (3) the exit cone assembly.

(1) Part A: Conical Aft Closure

In analyzing Part A, the structure was modeled by the gridwork shown in Figure 58. The flange at Point A was assumed to be fixed, and a design pressure of 938 psia (647 N/cm^2) (1.25 MEOP) was applied to the inside surface of the closure. In addition, the ejection force was distributed over the forward surface of the seal aft ring. In actual operation, torque is applied to the seal ring as a sinusoidally varying edge load and has the effect

of increasing or decreasing the uniformly distributed ejection force on this surface. Since the computer program is limited to axisymmetric loading conditions, the design values of the distributed axial load was taken as the ejection force plus the maximum value due to torque. A breakdown of this loading is indicated below:

Ejection force: $1,000,000 \times 1.25/2\pi = 199,000 \text{ lb/radian}$ (885,000 N/rad) Torque: $5,000,000 \times 1.25/56\pi = 35,500 \text{ lb/radian}$ (158,000 N/rad) Design Load = 234,500 lb/radian (1,043,000 N/rad)

Results of the analysis indicated that the maximum stress occurred at Element 31 (Figure 58). The principal stresses in this element were:

Radial stress - 2,250 psi (1550 N/cm^2) (tension) Axial stress - 8 psi (5.5 N/cm^2) (tension) Hoop stress - 63,206 psi $(43,500 \text{ N/cm}^2)$ (tension)

The margin of safety based on maximum stress theory was +0.107. The margin of safety based on the distortional energy failure (Von Mises) theory yielded a slightly larger margin of safety (+0.127) as all the principal stresses were in tension.

(2) Part B: Nozzle Throat Support

In the Part B analysis, the HY-150 throat support was conservatively assumed to take all the structural loads without contribution from the ablative liner. The structural shell also limited strain in the ablative liner to within 0.25%. The pressure distribution calculated from compressible, isentropic (γ = 1.2) flow on the nozzle surface based on a chamber pressure of 938 psi (647 N/cm²) was applied on the steel shell surface. This pressure was found to vary from 320 psi (221 N/cm²) at flange A (see Figure 59) to 938 psi (647 N/cm²) at surface B. A load was also applied to flange A so that the resultant horizontal reaction at C would equal the design

III.D. Task III - Full Scale Nozzle Design and Fabrication Planning (cont) ejection force of 1,250,000 lb (5.56 MN).

In addition to these loads, two possible loading conditions, with and without chamber pressure in area D (see Figure 59), were considered in the analysis. The more critical stress condition was without pressure in area D; it therefore controlled the design.

From the computer analysis, all stresses in Part B were below the allowable yield and allowable buckling of the material. For the most part, however, strain was the governing factor. The highest strain of 0.23% was at element 29, showing a margin of safety of +0.087.

The relative movement at the bearing joint between the nozzle shell and seal forward ring is shown in Figure 60. No joint separation existed even at full chamber pressure.

At the attachment joints between the seal and the nozzle structure, the interface load is normally in compression from the ejection force. Even with the maximum torque of 5,000,000 in.-lb (565,000 J) that can be applied, the separating force at the joint is small. The design and spacing of the attachment bolts were, therefore, governed by good design practices considering vibration and handling conditions.

(3) Part C: Exit Cone Assembly

In the stress analysis of the exit cone assembly, the effects of ablation were considered by using the ablated geometry of the liner at burnout time as predicted by heat transfer analysis. Complete anisotropic (hoop, meridional, and radial) properties of the materials were used in the analysis. Properties shown in Tables 42 and 43 were input for each finite element in accordance with the temperature profile predicted from the heat transfer analysis. For conservatism, static pressure along the nozzle wall, calculated from compressible isentropic flow, based on MEOP pressure, was combined with the temperature profile at motor burnout in the analysis.

Two regions in the nozzle exit cone that were expected to result in maximum stress were analyzed in detail. These regions were at the carbon phenolic-to-canvas phenolic interface (area ratio of 2.3) and at the mechanical joint between the two exit cone assemblies (area ratio of 3.85). Stresses in the three orthogonal directions for each element were obtained. A summary of the maximum stresses and strains is tabulated in Table 44. The results indicated that minimum safety factors of 2.0 existed in all locations.

Distribution of the maximum stress and strain in the exit cone liner and structural support were plotted. Stress and strain plots in the region of the 2.3 area ratio are shown in Figures 61 and 62. Maximum stress and strain data for the region of 3.85 area ratio are shown in Figures 63 and 64. The results confirm the structural adequacy of the proposed full-scale nozzle design.

6. Fabrication Plan for Ablative Components

A description of the fabrication methods planned for each component of the full-scale low-cost nozzle assembly is presented in the following paragraphs. Detailed requirements for the production of this nozzle are included in the material and processing specifications that were prepared during the Task III portion of this program and submitted previously to the NASA-LerC project manager. These specifications are:

ASPC Development Specification No.	<u>Title</u>
AGC-34467	Molding Tape, Carbon Fabric, Resin Impregnated
AGC-34468	Molding Tape, Canvas Duck Fabric, Resin Impregnated
AGC-36595	Ablative Components, Tape Wrapped, Process Control of
AGC-36596	Nozzle Assembly, Process Control of
AGC-36597	Exit Cone Assembly, Process Control of
AGC-36598	Glass Fabric, Epoxy Impregnated, Application of

a. Closure Insulator

The closure insert is a single-material (canvas) component that, because of its relatively mild thermal environment, can tolerate a wide range of laminate orientation. The selection of the tape-wrapping angle, therefore, is essentially limited to the ease and cost of fabrication. This component has no 260-SL-3 counterpart, but is roughly comparable to the 260-SL-1, -2 entrance piece.

The obvious choice of a parallel-to-center line orientation offers the advantages of a high as-wrapped density and the lower material costs that are available when using warp-cut tape. However, the maximum radial thickness of the as-wrapped billet would be approximately 9 in. (22.8 cm). This thickness would result in severe wrinkling during a hydroclave (or autoclave) cure cycle, unless the billet were subjected to intermediate debulk cycles every 3 to 4 in. (7.6 to 10.2 cm) during wrapping. Since the total projected radial thickness of the finished part is approximately 15 in. (38 cm), the innermost wrap would be subjected to three or four debulk cycles prior to the final cure cycle. The additional cost of the debulk cycles and the risk of advancing the resin system to this degree prior to final cure make this wrap orientation undesirable.

Therefore, an 80 degree (1.4 rad) wrap angle was selected for use with a net-molded mandrel contour as shown in Figure 65. Maximum re-orientation of the plies is expected to be of the order of 10 degrees (0.17 rad) at the small diameter end of the part, resulting in a minimum orientation of approximately 70 degrees (1.22 rad). This laminate orientation permits a more efficient wrapping operation since only half as many tape width changes are required to achieve the same material economy. The insert would be cured at either hydroclave or autoclave pressure and machined to mate with the closure contour.

b. Submerged Insert

The submerged insert, which also serves as a thermal protection for the flexseal, is essentially a parallel-to-center line component of

both canvas and carbon cloth. No overwrap is required. The part is similar to the 260-SL-3 submerged insert, which had an 82 degree (1.43 rad) laminate orientation, but includes the nose-cap (area ratio 1.81:1) which previously was a part of the nose insert (see Figure 66 for billet configuration).

Two potential fabrication problems are evident in this component. The maximum ply width of the canvas is in excess of 16 in. (40.7 cm), and the maximum as-wrapped ply thickness would be nearly 5 in. (12.7 cm). The wrapping of 16 in. (40.7 cm) tape has not been demonstrated and would very likely require significant development if uniform roller compaction and tape tension were to be achieved. Therefore, a spiral wrap pattern, such as was used for the 260-SL-3 overwrapping, is the logical choice to obtain a uniformly high as-wrapped density.

The excessive as-wrapped thickness could result in an undesirable degree of wrinkling, particularly in the carbon nose piece, because of limitations on the ability of the larger diameter plies to compress circumferentially. This would be alleviated by an intermediate debulk cycle during wrapping. Incorporation of methods to control wrinkling may be necessary during the debulk and final cure cycles. The forward face of the canvas section would be machined after debulking, prior to initiation of the carbon wrap, to provide a suitable interface between the two materials. The part size will permit curing at hydroclave or autoclave pressures of about 300 psi (207 N/cm²). The as-wrapped billet is shown in Figure 66.

c. Nose Insert

The nose insert is similar to the corresponding 260-SL-3 component and would be fabricated in a like manner except that the piece does not include the outer nose cap, which was separately wrapped, debulked, machined, and then cured with the aft section of the insert. As a result, this part would be much easier to fabricate than its 260-SL-3 counterpart.

The laminate would be wrapped at 90 degrees (1.7 rad)
(Figure 67) and debulked. The backside contour would be machined and overwrapped

with canvas phenolic. Following a 300 psi (207 N/cm²) cure, the insert would be final machined on the back face. The flame contour would be machined after assembly.

d. Entrance Insert

This part would be essentially the same as the corresponding 260-SL-3 component. The insert would be wrapped with bias-cut carbon tape at an angle of 67 degrees (1.17 rad) on a net-contoured mandrel (see Figure 68). It would be preformed, machined, overwrapped with warp-cut canvas tape on a spiral pattern, cured, and final machined.

e. Throat Insert

The throat insert would be fabricated in the same manner as its 260-SL-3 counterpart. The carbon bias-cut tape would be wrapped at a normal 50 degree (0.87 rad) to center line angle on a two-piece net-contour mandrel as shown in Figure 69. The preforming and subsequent operations would be similar to those for the entrance insert. Application of the canvas overwrap to the three-cone surface would require careful wrapping techniques to avoid excessive roller-edge compaction at the conical interfaces. Conventional cure procedures would be utilized.

f. Forward Exit Cone Liner

The forward exit cone liner provides the internal contour between the area ratios of 1.10 and 3.72, including the transition from the throat radius contour to the exit contour at a maximum divergence angle of 34.5 degrees (0.6 rad). This part is roughly comparable to the throat extension inserts of the 260-SL motors, and uses both carbon— and canvas duck—phenolic liners with a canvas—phenolic overwrap in the forward section where the liner bonds to the steel shell.

The laminate orientation of this component is parallel to the center line. Although the 260-SL throat extensions were wrapped at

30 degrees (0.53 rad), other large nozzles have performed successfully with parallel orientation at these area ratios. The selection is therefore a matter of fabrication consideration and not ablative performance.

angle would present unique fabrication difficulties. Because of the geometry, wrapping must be done from the small end with the large diameter up. In this position there is a tendency for the in-process billet to slump away from the mandrel. While this may be alleviated by careful selection of material wraping properties and the in-process use of shrink tape or carbon dioxide coolant, the contour of the forward exit cone liner is much more severe, having a maximum divergence angle of 34.5 degrees (0.6 rad) compared with the 17.5 degrees (0.31 rad) of the earlier components. The feasibility of wrapping bias tape with the small end of the mandrel up and the wrapping head inverted is not known but appears undesirable.

Wrapping parallel to the center line over the contoured mandrel should present no special fabrication problems and this is the technique selected. The liner would be wrapped, debulked, machined, overwrapped, and final cured. A hydroclave or autoclave cure process would be used for this component. The size of the part is within existing facility wrapping and curing capabilities.

g. Aft Exit Cone Liner

Fabrication of the aft exit cone liner should present no unusual problems. Although there is only limited experience with canvas phenolic material, it appears to be similar to silica phenolic in ease of fabrication. The configuration of the part is not unusual, but the maximum diameter is beyond existing autoclave or hydroclave capabilities. A simple vacuum bag oven cure has been considered, but subscale results to date have not been encouraging. Maximum liner density is probably not required for this part, therefore a low-pressure cure procedure would be adequate. The use of nylon tension-wrap would be utilized for controlling laminate orientations and for providing the desired cure compaction. A final density of about 98% of that

expected from an autoclave cured part could be expected. The processing sequence would include parallel-to-center line tape wrapping, machining of the as-wrapped liner, parallel-to-surface overwrapping of the glass tape, nylon tension-wrap cure, and final machining of the forward surface where the attachment flange would be bonded to the structure. Although the component is extremely large, no special fabrication requirements are envisioned. No nozzle fabricator presently has the equipment or facilities required to wrap, machine, or cure a plastic component of this large size, 270 in. dia (6.86 m).

7. Full-Scale Nozzle Cost Estimate

A production cost estimate for the full scale 260-FL nozzle design (Figures 51 and 52) was prepared and is discussed in the following sections. The estimate is based on the assumption of a 30 motor program, with a nozzle production rate of 6 units/year for 5 years. The selection of the production quantity has a significant effect on the per-unit nozzle cost. Tooling, facility, and nonrecurring labor costs on a prorated basis vary from \$62,500 to \$187,700 per unit depending upon whether a 30 or a ten motor program is being considered. No transportation costs have been included in the estimate, as this item is normally handled by Government Bill-of-Lading (GBL).

As shown in the full-scale nozzle cost summary (Table 45), the nozzle assembly unit cost is \$899,334, of which \$565,844 is attributable to the nozzle and \$333,490 to the exit cone. The addition of a flexseal for TVC would increase the cost by \$62,300 for a total of \$961,634, exclusive of any necessary actuators, hydraulic-power system, or related subsystems.

The incorporation of the low-cost ablative materials in the full-scale nozzle, notably the canvas duck phenolic and lower-cost carbons, results in an overall savings of approximately \$80,200, in comparison with a comparable design using the conventional MX-4926 carbon and FM-5131 silica phenolics. The cost of the ablative pre-preg materials represents about 25% of the total nozzle cost, therefore the savings realized by the use of low cost materials results in an overall nozzle cost reduction of about 9%.

The estimated cost of the nozzle steel components is the most subject to uncertainty. There are no 260-SL components that are sufficiently similar in design to permit an accurate comparison of manufacturing cost data. The two large steel fabricators that were solicited for an ROM estimate on the major structural parts declined to provide any cost information on an informal and unfunded basis. Therefore, the general rule-of-thumb of using a \$20/lb (\$44/kg) figure for the approximate cost of the finished part was applied. Because of the inherent toughness of HY-150 steel, welding standards may be relaxed, which, when combined with the initial lower cost of the material (compared with maraging steel), may result in a reduction of the \$20/lb estimate. In addition, the proposed production rate allows optimization of forging design and for tooling for all flanges and thicker sections, thus reducing machining time and material scrap loss.

The estimated cost of ablative materials is not comparable to the material costs of the nozzle design used in the trade study discussed in Section III.D.1. This is because of the considerable difference in the complexity of the two nozzle designs, the low-cost ablative nozzle being by far the easiest to fabricate.

An explanation of how each item in the cost summary (Table 45) was derived is included in the following sections. The total cost is believed to be the most realistic that has been published to date for a 260-FL motor nozzle, particularly in view of the fact that this nozzle represents a flight-weight design, utilizing state-of-the-art materials and fabrication techniques, and has been verified by thermal and structural analyses.

a. Ablative Material Costs

The cost of the resin-impregnated ablative and glass tapes used in the full-scale nozzle has been determined in a manner that insures maximum accuracy consistent with the fluctuating quotations obtained by the major suppliers over the past few years. Contrary to the design practice used on the 260-SL nozzles where the materials were specified by trade name or designation, the low-cost nozzle pre-preg specifications are written so as to enable the use

of tape from any one of several suppliers. The cost-per-pound of most materials being considered for use in the full-scale design were solicited early in this program. These costs, for warp-cut carbon and canvas duck tape in 1000 lb (454 kg), minimum, lots are shown below.

Carbon *	Canvas-Duck*
\$25.36	\$2.25
21.10	1.60
21.90	1.80
19.90	
18.75	
\$21.40 Average	\$1.88 Average

While \$21.40 was the average price for the carbon tapes of interest, it is felt that because of the quantities that would be required for a 30 nozzle order and the competition for a program of this scope, a more realistic cost of \$20.00 lb (\$44/kg) could be expected. A cutting charge of \$1.50/lb (\$3.30/kg) for bias tape is assumed. Thus, \$20.00 and \$21.50/lb (\$44.00 and \$47.30/kg) (warp and bias) were used for the costs of the carbon pre-preg raw material used in the cost estimate. Likewise, values of \$1.80 and \$3.30/lb (\$3.97 and \$7.30/kg) were used for the warp and bias-cut canvas duck-phenolic material; which is essentially the average price noted above for the warp-cut material.

The amount of material required was obtained by determining the volume, and subsequently, the weight of the as-wrapped billet for each component. (The billet configurations are shown in Figures 65 through 69.) An additional 5% (of the billet weight) was added to each part for scrap-loss and contingencies. Each billet has sufficient material to account for cure shrinkage

^{*}The material designations have been omitted at the request of certain suppliers to protect their competitive position.

and test specimen removal. Weight and cost data of each material required for the nozzle and exit cone are summarized in Table 46.

The prices shown in Table 47 are provided for information only and are based on the purchase of 5000 lb (2273 kg) minimum lots and delivery in 1000 lb (455 kg) releases. Generally, like products and grades sell within a narrow price range in a freely competitive market. For this reason, the prices of the commercially available tape and molding grades are listed against generic systems rather than specific trade names. In order for prices to be truly competitive, applicable material specifications should be broad enough to cover equivalent materials, and should include only those requirements that are specifically related to the expected performance.

b. Labor Costs

Direct labor costs associated with the manufacture of the full-scale nozzle were determined from a cost estimate in support of the Phase I Cost Study (7). This estimate was based on the omnivector, movable-nozzle design (Aerojet Drawing 1005017). As mentioned previously, this nozzle, while having the same throat diameter and a similar exit cone, is considerably more complicated in all sections forward of the throat. Therefore, the labor estimates for production of the low-cost nozzle have been adjusted accordingly. For example, the omnivector nozzle has five more ablative inserts than the low-cost design. The exit cone had a honeycomb structural reinforcement overwrapped with glass tape and roving, as compared with a simple glass tape overwrap.

A rating scale was applied to the two designs in order to arrive at a relative complexity factor which would take into consideration the manufacturing operations of both nozzles. This factor was then applied to the estimate of man hours required to produce the omnivector nozzle, at the six unit/year delivery rate.

Results of this comparison indicate that the low-cost nozzle should require only 63.5% as great a manpower expenditure as the base-line unit, while the exit cone labor would be about 94% of its counterpart. Thus, the unit labor cost was calculated as follows:

(1) Nozzle Throat Assembly

14,470 Hours (Phase I Study Estimate)

x <u>0.635</u> Factor of Relative Complexity

9,188 Direct Labor Hours/Unit

+ 300 Prorated Nonrecurring Direct Labor

9,488 Total Direct Labor Hours

(2) Exit Cone Assembly

4,015 Hours (Phase I Study Estimate)

x 0.94 Factor of Relative Complexity

3,774 Direct Labor Hours/Unit

+ 300 Prorated Nonrecurring Direct Labor

4,074 Total Direct Labor Hours

The direct labor basic hourly rate of \$5.87 and the overhead rate of \$10.20 (174%) used herein is an Aerojet estimate based on information provided by a major nozzle fabricator.

c. Tooling Costs

A production rate of six nozzle assemblies per year does not require more than one set of tooling for any individual insert or component. The same tooling items would be required for the manufacture of a single nozzle assembly, although the degree of design sophistication would naturally be less.

The identification of required tooling and the estimated cost of each item listed in Table 48 is based on the cost study previously mentioned. These estimates have been adjusted to reflect actual 260-SL-3 tooling costs, 260-FL nozzle design differences, and the projected 1971-72 dollar value. As may be seen from the listing, the cost of tooling is a significant percentage of the total nozzle cost, with the exit cone mandrels contributing the major share of this expense. No attempt has been made to optimize mandrel design or to conceive new mandrel fabrication concepts. However, this is an area where tooling cost reductions of up to 40% may be possible.

d. Facility Requirements

The 260-FL nozzle and exit cone assembly consists of seven individual tape-wrapped parts. Assuming a production rate of six complete assemblies per year, a total of 42 components must be fabricated annually. This requirement exceeds the facility capacity of any ablative component fabricator presently engaged in this specialty.

The wrapping, machining, and autoclave/hydroclave cure facilities and limitations of the three major nozzle fabricating firms in the Southern California area were surveyed as a part of this study. The significant results of this investigation are summarized below:

- (1) All three firms have the ability to manufacture parts up to and including 130 in. in dia (3.3 m), which excludes the two exit cone sections and the closure insulator. None can meet the production rate requirement with their existing facilities.
- (2) Only one firm has the capability to wrap, machine, and autoclave cure the forward exit cone section and closure insulator.
- (3) None of the firms can wrap or machine the aft exit cone section.

(4) A 36-ft. (11 m)-dia autoclave, capable of pressures to 100 psi (69 N/cm 2) at 350°F (450°K), is available and is accessible to a barge loading dock. No wrapping, machining, or overhead lifting equipment exists at this facility, however.

To arrive at the most realistic new facility cost, the required program schedule for a 30 motor program (six nozzles per year) was projected on the basis of the fabricator who presently has the best capability in regards to the number and size of wrapping/machining and cure facilities and equipment. The Rohr Corp., Space Products Division, of Riverside, California (manufacturer of the 260-SL-3 nozzle) is prominent in this regard. Rohr presently has two vertical turning machines that can be used to process all ablative components forward of the aft exit cone section. Their cure facilities include two large hydroclaves of 175 and 96 in. in diameter (4.45 and 2.44 m) and an autoclave of 180 in. in diameter (4.57 m). A new vertical turning machine with a capacity of approximately 280 in. in diameter (7.12 m) will be required and represents the major facility expenditure. A new curing oven that can accommodate the aft exit cone and maintain a controlled temperature environment of at least 350°F (450°K) is also needed.

Even with the addition of the new turning machine and assuming optimum facility utilization and a multiple shift operation, the production capacity at Rohr would be barely adequate to meet nozzle delivery schedules (see Figure 70). To provide some degree of scheduling flexibility and to allow for equipment maintenance and manufacturing contingencies, a plan whereby at least one and possibly two of the smaller nozzle inserts would be fabricated by another firm should be considered. This more realistic approach, when combined with manufacture of the aft exit cone at A-DD, results in a schedule (Figure 71) that is not so sensitive to slippage due to machine breakdown or other unforeseen problems.

Essentially, \$1,000,000 of the new-facility requirement is associated with equipment needed for fabrication of the aft exit section. This cost was based on installation of equipment in an existing building at the

Rohr plant that has the necessary supporting facilities (crane, heating/air-conditioning, etc.) It would be more desirable from a logistics standpoint to fabricate this part at the motor processing site (A-DD). The cost of a building to house the fabrication equipment at A-DD would be an additional \$300,000, which would be less than the cost of shipping 30 aft exit cone sections from California to Florida via the Panama Canal.

The very high financial outlay for the facility and tooling required for production of the extremely large tape-wrapped exit cone aft section provides a strong argument for further development of alternative nozzle fabrication methods discussed in Section III.D.9.

8. Other Factors Influencing Large Nozzle Fabrication Costs

a. Effect of Processing Defects

As a result of previous investigations conducted for NASA and reported in Reference $^{(4)}$, the effects of defects on the performance of the tape-wrapped carbon and silica flame liners can be predicted with greater assurance. Defects in the canvas duck components have not been studied in the same detail, but may be inferred from the results observed for the carbon and silica composites.

This added knowledge as to what constitutes a defect (whether or not it will have an adverse effect on nozzle performance) will permit the acceptance of parts previously rejected or subjected to costly rework. In addition, the manufacturing specifications may be written with wider tolerances on material properties and acceptance criteria, and this will also lead to an overall less-expensive nozzle.

The findings of the referenced program were incorporated in the material and process specifications (discussed on Page 84) to the extent that back-up data were sufficient to justify a modification of existing acceptance criteria. The specific areas where these recent findings have been applied, or will be when additional data are available, are:

- (1) Minimum cured density
- (2) Resin segregation
- (3) Delaminations
- (4) Wrinkles
- (5) Volatile content

b. Dimensional Tolerances

A careful study of any final design of a large nozzle should be made to determine where dimensional tolerances may properly be relaxed, without adversely affecting the function or performance of the nozzle or motor. It appears reasonable to assume that on the extremely large exit cone parts, an increase of dimensional tolerances would be feasible except at mating interfaces.

9. Alternative Exit Cone Fabrication Methods

The extremely large size of the full-scale aft exit cone section imposes some unique problems in the tooling and facilities required for tape wrapping, curing, and machining of the part. It would be almost a necessity, from the transportation aspect alone, to fabricate the exit cone aft section at the motor assembly site. Rather than acquire all the necessary facilities and technical skills necessary to tape-wrap this part at A-DD, it would appear feasible to consider less complicated methods of manufacture as a means of achieving a cost savings.

Other fabrication methods that may have future potential as a cost-effective alternative to the conventional tape-wrapping procedures are discussed briefly below. These methods are not endorsed at this time since very little experience or performance data are available to substantiate their use. Work is currently in progress* at Aerojet that should provide a greater insight as to which new techniques show the greatest promise for the large exit cone sections.

^{*}Development of Low-Cost Fabrication Techniques for Ablative Nozzles (Contract NAS3-12064, Aerojet Solid Propulsion Company, from Lewis Research Center).

a. Molded Exit Cone

In this method, it is proposed to mold full length panels (15 degrees of arc by 14 ft (4.3 m) long) using a selected, low-cost ablative molding compound. Using a sheet metal or wooden mold assembly form, the 24 exit cone panels would be bonded together along axial, interlocking joints. Circumferential wrappings (either tape or pre-preg roving) would be applied to secure the panels against pressurization loads and to attach structural fittings at the forward end. The entire exterior surface of the exit cone would then be sprayed with a glass or asbestos/resin mixture, applied with the same tools and in the same manner as used for FRP boat hulls.

Molding will be performed by commercially available sources not requiring further facility capitalization. At a total production of 30 booster motors, the minimum requirement of 720 panels will justify a matched die set to control size and dimensions.

b. Shingle Lap

Using this method, panels would be made up as in the molded process; circumferential reinforcement, structural attachment, and overspraying with glass or asbestos would be similar to that already discussed.

The panels themselves would be fabricated using a hand lay-up procedure with interply bonding and final curing to be effected in steam-jacketed or electrically heated forming dies pressurized with hydraulic cylinders. The forward end of each panel would be formed from an ablative molding compound to prevent ply removal, and this would be bonded in position during the lay-up.

c. Wet Lay-Up

With the wet lay-up technique, the dry, uncoated reinforcing fabric is applied in precut patterns over a male form and a catalyzed

resin is brushed or bladed into the fabric. This technique is closely allied to the hand lay-up method used in fabricating boat hulls. A catalyzed, unfilled resin of low viscosity is a prerequisite, so that air entrapment in the resin is held to some reliably low level.

This method differs from the others in that all work could be performed at A-DD. It has the advantage of requiring the least amount of tooling, but requires the greatest amount of skill from the available labor.

IV. CONCLUSIONS AND RECOMMENDATIONS

- A. Incorporation of the low-cost ablative materials in large solid propellant rocket motor nozzles can result in cost-savings of up to \$80,200 when compared with a nozzle of the same design using conventional materials.
- B. A flight-weight nozzle for a 260-FL motor may be manufactured for about \$961,600 (based on a 30 unit production contract) including flex seal.
- C. It is feasible to fabricate the full-scale nozzle components using conventional and proven manufacturing techniques, although advanced processing concepts for the large exit cone section should be further investigated and developed.
- D. It was shown that the canvas duck-phenolic (4KXD02) material has excellent performance characteristics when used in the less-severe locations of the exit cone and nozzle. This material represents the single most important cost-reducing element in the design and fabrication of large ablative components.
- E. Carbon-silica phenolic (MXSC-195) demonstrated undesirable processing traits and unacceptable performance characteristics when used in the entrance section of the subscale test nozzle. Its use in the throat of full-scale nozzles does not provide any overall motor cost savings.

IV. Conclusions and Recommendations (cont)

- F. Results of the trade-studies reveal that the most practical low-cost full-scale nozzle design would use a carbon-phenolic (or equivalent) throat section and incorporate the lower-priced materials in other parts of the nozzle. This is the result of loss in motor performance at the higher throat erosion rates.
- G. The quality of a trowelable chamber internal insulation system was shown to be dependent upon the degree of tooling sophistication.
- H. Valuable insight was gained on the problems associated with the processing and inspection of a trowelable insulation system. Performance of the insulation was demonstrated on a scale significant enough to warrant its further consideration for 260-FL motor application.
- I. The technology gained in this program on the use and qualities of low-cost ablative materials and the trowelable insulation system could be combined advantageously with other technology elements in a demonstration of the cost-effectiveness of a "state-of-the-art" solid booster motor.

TABLE 1. - IBT-100/IBT-106 INSULATION SYSTEM DESIGN SUMMARY FOR LCAN MOTOR

Location	Dia, in.	Area,	<u>A/A*</u>	Mach No.	<u>Material</u>	TLR in./sec(3)	Exposure, sec(4)	Correction Factor(5)	Calculated Thickness, in.	Design (6)(7) Thickness, in.
Nozzle/Aft Dome	13.00(1)	132.73								
	20.00	314.16	2.367	0.26	(2)	N/A	40.1/24			
	22.00	380.13	2.864	0.21	(2)	0.023/0.003	40.1/24	0.95	0.922 (0.95) + 0.072 = 0.948	2.00
	24.00	452.39	3.408	0.18	IBT-100	0.018/0.003	40,1/24	0.95	0.722 (0.95) + 0.072 = 0.758	1.55
	26.00	530.93	4.000	0.15	IBT-100	0.015/0.003	40.1/24	0.95	0.602 (0.95) + 0.072 = 0.644	1.30
	28.00	615.75	4.639	0.13	IBT-100	0.013/0.003	40.1/24	0.95	0.521 (0.95) + 0.072 = 0.567	1.15
	30.00	706.86	5.326	0.11	IBT-100	0.011/0.003	40.1/24	0.95	0.441 (0.95) + 0.072 = 0.492	1.00
	32.00	804.25	6.059	0.10	IBT-100	0.010/0.003	40.1/24	0.95	0.401 (0.95) + 0.072 = 0.453	0.95
	34.00	907.92	6.840	0.09	IBT-100	0.008/0.003	40.1/24	0.95	0.321 (0.95) + 0.072 = 0.377	0.80
	36.00	1017.9	7.669	0.08	IBT-100	0.007/0.003	40.1/24	0.95	0.281 (0.95) + 0.072 = 0.339	0.70
ļ	38.00	1134.1	8.544	0.07	IBT-100	0.007/0.003	40.1/24	0.95	0.281 (0.95) + 0.072 = 0.339	0.70
Ť	40.00	1256.6	9.467	0.06	IBT-100	0.006/0.003	40.1/24	0.95	0.240 (0.95) + 0.072 = 0.300	0.60
Forward Dome	-	_	_	-	IBT-106	0.003/0.003	40.1/24	0.95	0.120 (0.95) + 0.072 = 0.186	0.40
Sidewall		_	-	_	IBT-106	0.003	0/24	N/A	0.072	0.15
Propellant Boots	- ,	_	-	-	IBT-106	0.003	40.1/0	N/A	0.120 (0.95) = 0.114	0.25

⁽¹⁾ Algol motor nozzle diameter for Contract NAS3-12038.

Data not converted to S.I. units for sake of clarity.

⁽²⁾ Silica-phenolic at these diameters.

⁽³⁾ Thickness loss rate at full pressure/thickness loss rate at reduced pressure.

⁽⁴⁾ Exposure at full pressure/exposure at reduced pressure.

⁽⁵⁾ $\left(\frac{502}{600}\right)^{0.3} = 0.95.$

⁽⁶⁾ Required thickness x 2.0 safety factor.

⁽⁷⁾ Tolerance: +0.05, -0.00 in.

TABLE 2. - CALCULATED WEIGHT SUMMARY OF IBT-100/IBT-106 INSULATION SYSTEM FOR ALGOL NOZZLE TEST MOTORS

Forward Dome	IBT-106	30	(13.6)
Sidewall	IBT-106	380	(173)
Aft Dome	IBT-100	170	(75.6)
Nozzle	IBT-100	45	(21.1)
Forward Boot	IBT-106	50	(22.7)
Aft Boot	IBT-106	30	(13.6)
	Total Weight	705 1ъ	(319.6) Kgm

TABLE 3. - EFFECTS OF CURING AGENT LEVEL, CURE TEMPERATURE, AND CURE TIME ON THE MECHANICAL PROPERTIES OF ANB-3347

Batch No. 106P-	DER 332 Equiv.	Cure Temp, °F (K)	Cure Time, Days	σ,	hanical F	roperti ^e m' <u>%</u>	es at 7	Ε,,	299 K) (N/cm ²)
9938	90	110 (317)	11 18	36 36	(25.2) (25.2)	28 28	38 42	175 170	(121) (117)
		135 (331)	11 18	38 39	(26.2) (26.9)	32 35	49 52	173 158	(119) (109)
9939	95	110	11 18	38 40	(36.2) (37.6)	25 21	39 34	221 286	(152) (197)
		135	11 18	44 43	(30.3) (29.7)	30 28	43 38	210 246	(145) (170)
9940	100	110	11 18	45 47	(31.0) (32.4)	22 21	33 26	282 315	(195) (217)
		135	11 18	54 55	(37.2) (37.9)	29 27	38 36	265 282	(183) (195)
9941	105	110	11 18	54 57	(37.2) (40.0)	21 20	28 24	352 392	(243) (270)
		135	11 18	66 69	(45.5) (47.6)	26 25	33 31	400 392	(276) (270)
9954	110	110 135	10 10	66 77	(45.5) (53.1)	20 24	26 32	501 479	(345) (330)

(Oxidizer Blend: 80/20 +48/MA)

TABLE 4. - EFFECT OF PBAN TERPOLYMER LOT ON MECHANICAL PROPERTIES OF ANB-3347 PROPELLANT

Batch No. 106P-	PBAN Lot No.	Cure Temp, °F (K)	Cure Time, Days	Mechanical om, psi (N/cm²)	ε,,	ties at εb', <u>%</u>	77°F (299°K) E _o , psi (N/cm ²)
9971	691	110 (317)	13	47 (32.4)	22	28	307 (212)
		135 (331)	13 20	56 (38.1) 58 (40.9)	26 25	34 35	307 (212) 330 (228)
9972	725A	110 (317)	13	44 (30.3)	20	28	296 (204)
		135 (331)	13 20	53 (36.4) 54 (37.2)	25 24	34 33	301 (208) 326 (225)

(Curing Agent Concentration 100 equivalents DER-332)

TABLE 5. - EFFECT OF OXIDIZER BLEND RATIO ON MECHANICAL PROPERTIES OF ANB-3347 PROPELLANT

Batch No. 106P-	Oxidizer Blend, +48/Ung/MA	Cure Temp, °F (K)	Cure Time, Days	o _m ,	nanical Pr	coperti ϵ_{m} ,	es at ε _b , <u>%</u>	Eo,	(299K) (N/cm ²)
9940	80/0/20	110 (317)	11 18	45 47	(31) (32)	22 21	33 26	282 315	(195) (217)
		135 (331)	11 18	54 55	(37) (38)	29 27	38 36	265 282	(183) (195)
9975	50/30/20	110 (317)	11 18	47 -	(32)	25 -	32	258 -	(178)
		135 (331)	11 18	54 57	(37) (40)	28 27	36 37	273 282	(188) (195)
10019	0/80/20	135 (331)	13	58	(41)	28	32	282	(195)

(Curing Agent Concentration 100 equiv. DER-332)

TABLE 6. - SUMMARY OF SIGNIFICANT ANB-3347 PROPELLANT CHARACTERISTICS

Flame Temperature in chamber at 500 psia, °F (at 345 N/cm ² , K)	5463 (3290)
Burning Rate (r _b) in./sec at 500 psia (cm/sec at 345 N/cm ²)	0.215 (0.546)
Burning Rate Pressure Exponent, n	0.23
Density, 1b/cu in. (gm/cu cm)	0.0626 (1.73)
Standard Specific Impulse, ** 1bf-sec/1bm (N-sec/Kg)	244.6 (2405)
Gamma	1.20

^{*} Average solid strand burning rate from nine full scale batches. ** 10KS-2500 motor, 1000/14.7 psia, 15° half angle.

TABLE 7. - GRAIN STRESS SUMMARY

Condition		Bore Tensile op Strain (%)	2	В	ond Shear Stress (psi)	ess		Bond Tensile Stress (psi)		
	Maximum	Allowable**	M.S.	Maximum	Allowable**	M.S.	Maximum	Allowable**	M.S.	
Storage 1 Year at 75°F (297K)	5%	13%***	+1.6	1.0	5.6	+4.6	3.0	7.0	+1.3	
Firing p = 600 psig (414 N/cm ²) at T = 75°F (297°K) t = 0.15 sec	10%	∿20%	+1.0	6.5	450	High		Compressive		

^{*} T_{cure} = 135°F (331°K)

^{**} Based on ANB-3241-2 Data.

^{***} From "Smith-Type" Failure Envelope.

TABLE 8. - NASA-LeRC NOZZLE AND TEST MOTOR DESIGN CRITERIA

Throat Diameter

Expansion Ratio

Expansion Angle

Nozzle Type

Port-to-Throat Ratio

Chamber Pressure

Web Action Time

Propellant Aluminum Content

Propellant Combustion Temperature

Propellant Type

13 to 16 in. (33 to 41 cm)

6:1

17.5° (0.297 rad)

Nonsubmerged, conical

1.3 (min)

 $600 \pm 100 \text{ psig } (413 \pm 69 \text{ N/cm}^2)$

40 sec (min)

 $15 \pm 1\%$ (by wt)

5500° + 100°F (3310 + 312°K)

PBAN

TABLE 9. - CANDIDATE LOW COST ABLATIVE MATERIALS FOR THE ALGOL TEST NOZZLES

Material Designation	Type
WB-8251	Carbon-silica phenolic
4C-2530	Carbon-silica phenolic
SP-8057	Carbon phenolic
4C-1686	Silica phenolic
MXS-198	Silica phenolic
SP-8030-96	Silica phenolic
F-502	Silica phenolic
KF-418	Canvas-duck phenolic
23-RPD	Asbestos phenllic
MXA-6012	Asbestos phenolic
FM-5272	Paper phenolic

TABLE 10. - COST EFFECTIVENESS COMPARISON OF ABLATIVE MATERIALS CONSIDERED IN 13-IN.-DIA (33 CM) NOZZLE

Component	Area Ratio	Material	Cost Effectiveness Index (CEI)*
Entrance	-2.11	Silica	9
		Carbon	12
	-1.23	Carbon-Silica	18
		Carbon	19
Throat	1.00	Carbon	16
		Carbon-Silica	18
		Silica	12
Fwd Exit Cone	1.60	Carbon	12
		Carbon-Silica	12
		Silica	8
Aft Exit Cone	2.40	Silica	4
		Canvas-Duck	1.5
	5.50	Silica	1.9
		Canvas-Duck	0.8

^{*}CEI = (erosion + char) x specific gravity x cost/1b.

Cost data used in CEI calculations:

Carbon Phenolic - \$21.50 (bias) Carbon-Silica Phenolic - \$16.50 (bias)

Silica-Phenolic -\$ 7.00 (bias) \$5.50 (warp) Canvas-Duck Phenolic -\$ 1.80 (warp)

TABLE 11. - INITIAL BOUNDARY LAYER CONDITIONS

Area Ratio	Heat Transfer Coefficient Btu/hr-ft2-°F	Surface <u>Mach Number</u>
-3.0	630	0.26
-2.0	950	0.40
-1.5	1250	0.47
-1.2	1540	0.68
-1.08	1660	0.92
1.00 (Throat)	1520	1.20
+1.20	1020	1.75
+1.50	9 30	1.83
+2.00	740	2.05

 $T_{c} \sim 5845^{\circ}R (3250^{\circ}K)$ $P_{c} \sim 600 \text{ psia } (413 \text{ N/cm}^2)$ $D_{t} = 13.00 \text{ in. } (33 \text{ cm})$

TABLE 12. - HEAT TRANSFER ANALYSIS SUMMARY, NOZZLE NO. 1

Station (Area Ratio)	<u>Material</u>	Depth from Erosion	Original Sur	face, in. (cm) 100°F** (312°K)
-2.10	Silica Phenolic	0.61 (1.55)	0.76 (1.93)	1.10 (2.79)
-1.71	Carbon/Silica	0.427 (1.08)	0.589 (1.50)	0.88 (2.24)
-1.23	Carbon/Silica	0.584 (1.48)	0.729 (1.85)	1.02 (2.59)
1.00 (throat)	Carbon/Silica	0.586 (1.49)	0.726 (1.84)	1.01 (2.58)
1.23	Carbon/Silica	0.370 (0.94)	0.534 (1.36)	0.83 (2.11)
1.60	Carbon/Silica	0.302 (0.77)	0.477 (1.21)	0.78 (1.98)
2.40	Canvas Phenolic	0.47 (1.19)	0.63 (1.60)	0.92 (2.34)
6.00	Canvas Phenolic	0.14 (0.36)	0.34 (0.86)	0.64 (1.62)

^{* 750°}F (673°K) isotherm.

^{**} At 75 seconds from fire switch.

TABLE 13. - HEAT TRANSFER ANALYSIS SUMMARY, NOZZLE NO. 2

Station (Area Ratio)	<u>Material</u>		pth from		nal Sur: ar*	face, in 100°F**	
-2.10	Silica Phenolic	0.61	(1.55)	0.76	(1.93)	1.10	(2.79)
-1.71	Silica Phenolic	0.70	(1.78)	0.86	(2.18)	1.15	(2.92)
-1.23	Silica Phenolic	0.91	(2.31)	1.06	(2.72)	1.17	(2.97)
1.00 (throat)	Silica Phenolic	0.89	(2.26)	1.04	(2.71)	1.15	(2.92)
1.23	Silica Phenolic	0.60	(1.52)	0.76	(1.93)	0.90	(2.28)
1.60	Silica Phenolic	0.45	(1.14)	0.62	(1.57)	0.77	(1.95)
2.40	Canvas Duck Phenolic	0.50	(1.27)	0.65	(1.65)	0.83	(2.11)
5.50	Canvas Duck Phenolic	0.15	(0.37)	0.35	(0.87)	0.55	(1.40)

^{* 750°}F (673°K) isotherm.

^{**} At 60 seconds from fire switch.

TABLE 14. - HEAT TRANSFER ANALYSIS SUMMARY, CARBON PHENOLIC THROAT, CANDIDATE NOZZLE

Station (Area Ratio)	Material	Depth from Original Surface, in. (Erosion Char* 100°F** (3)							
-2.10	Silica Phenolic	0.61 (1.55)	0.76 (1.93)	1.10 (2.79)					
7 1	Carbon/Silica Phenolic	0.427 (1.08)	0.589 (1.50)	0.88 (2.24)					
-1,23	Carbon/Silica Phenolic	0.584 (1.48)	0.729 (1.85)	1.02 (2.59)					
1.00	Carbon Phenolic	0.18 (0.46)	0.535 (1.36)	0.82 (2.08)					
1.23	Carbon/Silica Phenolic	0.370 (0.94)	0.534 (1.36)	0.83 (2.11)					
1.60	Carbon/Silica Phenolic	0.302 (0.77)	0.477 (1.21)	0.78 (1.98)					
2.40	Canvas Phenolic	0.47 (1.19)	0.63 (1.60)	0.92 (2.34)					
6.00	Canvas Phenolic	0.14 (0.36)	0.34 (0.86)	0.64 (1.62)					

^{* 750°}F (673°K) isotherm.

^{**} At 75 seconds from fire switch.

TABLE 15. - STRUCTURAL ANALYSIS SUMMARY, NOZZLE NO. 1

Component	<u> Material</u>	St psi	ress (N/cm ²)		t rature (°K)		timate ble Stress (N/cm ²)	Design Safety Factor (max)	Actual Safety Factor
Approach	Silica	C2915*	(2010)	343	(446)	3800	(2620)	2.0	1.31
Entrance	Carbon-Silica	1044	(720)	138	(333)	6000	(4130)		5.77
Throat	Carbon-Silica	C2195	(1513)	443	(502)	5250	(3620)		2.39
Fwd Exit Cone	Carbon-Silica	C2384	(1645)	430	(495)	5250	(3620)		2.20
Aft Exit Cone	Canvas Duck	1334	(921)	430	(495)	4000	(2775)	•	2.30
Overwrap	Asbestos	3831	(2640)	80	(300)	15000	(10340)	1.3	4.00
Steel Shell	4130 Stee1	29295	(20200)	80	(300)	70000	(48250)		2.80
Bond Line	Epon 913	384	(2645)	80	(300)	3000	(2068)		6.01
Bolts	tona.	18150	(12520)	80	(300)	38000	(26200)		1.61

^{*} The sign C preceding value indicates compressive stress.

TABLE 16. - STRESS ANALYSIS SUMMARY, NOZZLE NO. 2

Component	Material	Str	mit Stre)* At erature (°K)		imate 1e Stress (N/cm ²)	Design Safety Factor (max)	Actual Safety Factor
Approach	Silica	C2664**			(402)	4500	(3100)	2.0	1.70
Entrance	Silica	C3666	(2528)	363	(456)	6000	(4130)		1.64
Throat	Silica	C3955	(2727)	463	(512)	5300	(3652)		1.34
Fwd Exit Cone	Silica	C2678	(1831)	175	(352)	6500	(4480)		2.40
Aft Exit Cone	Canvas Duck	443	(305)	100	(312)	8500	(5860)	V	High
0verwrap	Canvas Duck	2019	(1391)	80	(300)	8500	(5860)	1.3	4.15

^{*}Along outside fiber at 40.5 sec.

 $[\]mbox{\ensuremath{\mbox{\scriptsize **The}}}$ sign C preceding value indicates compressive stress.

TABLE 17. - QUALIFICATION DATA FOR LCAN-02 INSULATION SYSTEM

Batch	Formulation	Liquid	Density	Rex Hardness at 200°F (367°K)					
No. 69-	No.	g/cc	(1b/in.3)	100 min.	150 min.	200 min.			
183	IBT-106	1.420	(0.0511)	0	20	45			
188		1.426	(0.0514)	0	30	50			
189		1.422	(0.0512)	5	40	60			
190		1.416	(0.0509)	0	35	60			
195		1.418	(0.0510)	10	45	55			
193	IBT-100	1.382	(0.0497)	5	40	55			

TABLE 18. - QUALIFICATION DATA FOR ANB-3347 PROPELLANT

Batch No. 22D-	MA Oxid.	Blend Surface H ₂ O %	Sul H ₂ 0 %	omix Acid Equiv.	PredH ₂ O %	mix Density g/cc	Pro Liquid Density g/cc	Dellant LSBR at 500 psig.in./sec at 85°F	Final Fuel % <u>FeAA</u>
Scale-Up Batc	<u>.h</u>								
203	5.0	0.005	0.068	0.0512	0.020	1.389	1.726	0.237	3.43
Motor LCAN-01	<u>.</u>								
205-1	6.8	0.005	0.059	0.0510	0.027	1.390	1.726	0.236	3.46
-2	7.1	0.005	0.059	0.0510	0.027	1.390	1.724	0.238	3.46
-3	8.8	0.006	0.059	0.0510	0.027	1.390	1.729	0.236	3.46
-4	6.3	0.004	0.059	0.0510	0.027	1.390	1.726	0.238	3.46
Motor LCAN-02									
206-1	4.3	0.008	0.065	0.0511	0.062	1.392	1.724	0.242	3.48
-2	4.2	0.007	0.065	0.0511	0.062	1.392	1.724	0.242	3.48
-3	4.3	0.008	0.065	0.0511	0.062	1.392	1.726	0.245	3.48
-4	4.2	0.006	0.065	0.0511	0.062	1.392	1.725	0.245	3.48

TABLE 19. - MECHANICAL PROPERTY DATA FOR ANB-3347 PROPELLANT BATCHES

		Cure			Mecha		perties a	t 77°F (298°K)	
Batch No.	Equiv. of DER-332	Time, Days	Bar Preparation	σ _m psi (N/cm ²)	ε _m <u>%</u>	ε _β	E _o psi (N/cm ²)	ECS
10CP-290	110	10	Die Cut	79	(54)	25	28	433 (299)	19
22D-203	110	10	Die Cut	66	(46)	24	32	385 (265)	18
			Milled	76	(52)	26	32	450 (310)	18*
22D-205-4	110	7	Die Cut	71	(49)	26	36	372 (256)	20
		8	Milled	77	(53)	27	33	442 (305)	19
22D-205-1	110	8	Milled	76	(52)	28	35	433 (299)	19
-2	110	8	Milled	80	(55)	27	34	461 (318)	18
-3	110	8	Milled	79	(54)	28	36	437 (301)	20
22D-206-1	110	8	Milled	71	(49)	26	31	409 (282)	19
-2	110	8	Milled	74	(51)	26	30	431 (297)	18
-3	110	8	Milled	76	(52)	25	31	459 (316)	17
-4	110	8	Milled	73	(50)	26	32	420 (290)	19

^{*}Propellant held 20% constant strain for 168 hours at 77°F (298°K)

TABLE 20. - PRE-PREG MATERIALS USED IN TEST NOZZLES

DESIGNATION	SUPPLIER	REINFORCEMENT	RESIN	WHERE USED
4KXD02 (4K9502)*	Hexce1	8.5 oz Canvas Duck	SC 1008	Entrance Overwrap (21,2f) Exit Cone (1,2) Exit O'wrap (2) Throat O'wrap (21, 2f)
MX-2600-96	Fiberite	C-100-96 Silica	SC 1008	Approach (2i,2f) Entrance (2i) Throat (2i) Throat Extension (2)
MXA-6012	Fiberite	Crocidolite Asbestos	SC 1008	Entrance O'wrap (1) Exit O'wrap (1) Throat O'wrap (1)
MXSC-195	Fiberite	Averam C/S (Carbon-Silica)	SC 1008	Entrance (1,2f) Throat (1,2f) Throat Extension (1)
SP-8030-96	Armour	C-100-96 Silica	EC 201	Approach (1)

^{*} A more recent designation of the same material.

TABLE 21. - PRE-PREG MATERIAL PROPERTIES

W-+	T . N		Volatile Content,	west of a CTV
Material	Lot No.	%	%	Flow, %
4KXD02 (4K9502)	50314	40.5 40.9 41.7	6.6 6.5 5.2	7.6 8.0 6.9
	50422	47.3 47.3 47.3 43.8	8.0 7.8 7.1	16.8 17.8 14.9
	50903	41.4	8.3	10.2
	DESIRED	36 - 44	7.5 Max	5 - 17
MX-2600-96	н-579	31.2 31.7 31.1	4.8 4.9 4.4	10.8 10.8 11.4
	J-267	31.5	4.5	11.3
	DESIRED	29 - 35	6.0 Max	8 - 15
MXA-6012	7786	45.6 45.6	8.9 9.0	11.0 10.3
	DESIRED	44 - 50	12.0 Max	7 - 14
MXSC-195	H-512 J-268	38.0 39.0 40.5 40.6 43.9 42.1	4.4 5.8 5.6 5.5	5.8 9.6 9.9 9.3 9.8 9.9
	DESIRED	37 - 44	9.0 Max	4 - 10
SP-8030-96	A-2294	30.5 29.7 30.9	5.4 5.4 5.5	18.2 17.1 14.9
	DESIRED	29 – 35	6.0 Max	8 - 15

TABLE 22. - FABRICATION DATA FOR NOZZLE COMPONENTS

Component		Material	Tape °F	Temp.	Roller lbf/in.		As-Wrappe	d Density gr/cu-cm	Debul °F	k Temp.,	Debul psi	lk Press.	Debulk Time, min		Temp.,	Cure	Press.	Cure Time, min.
																		
Approach	1*	SP-8030-96	200	366.5	275	480.4	0.051	1.41	175	352.6	250	172.4	150	300	422	250	172.4	180
	2 i	MX-2600-96	182	356.5	200	349.4	0.056	1.55	168	348.7	250	172.4	130	305	424.8	240	165.5	195
	2f	MX-2600-96	182	356.5	200	349.4	0.059	1.63	180	355.4	245	168.9	135	320	433.2	232	159.9	165
Entrance	1	MXSC-195	211	372.7	300	525.3	0.047	1.30	175	352.6	250	172.4	150	300	422	250	172.4	180
	2i	MX-2600-96	185	358.2	275	480.4	0.056	1.55	168	348.7	250	172.4	130	305	424.8	240	165.5	195
	2f	MXSC-195	190	360.9	150	262.6	0.048	1.33	180	355.4	245	168.9	135	320	433.2	232	159.9	165
Ent. O'wrap	1	MXA-6012	182	356.5	275	480.4								300	422	250	172.4	180
	2i	4KXD02	205	369.3	200	349.4								305	424.8	240	165.5	195
	2 f	4KXD02	190	360.9	200	349.4								320	433.2	232	159.9	165
Throat	1	MXSC-195	204	368.7	165	288.3	0.049	1.35	167	348.2	235	162.0	130	300	422	250	172.4	185
	2i	MX-2600-96	176	353.2	250	436.8	0.057	1.58	190	360.9	240	165.5	150	305	424.8	240	165.5	190
	2f	MXSC-195	184	357.6	200	349.4	0.050	1.38	175	352.6	240	165.5	150	320	433.2	232	159.9	165
Throat O'wrap	1	MXA-6012	208	370.9	300	525.3								300	422	250	172.4	185
•	2 i	4KXD02	209	371.5	300	525.3								305	424.8	240	165.5	190
	2f	4KXD02	190	360.9	200	349.4								320	433.2	232	159.9	165
Throat Ext	1	MXSC-195	180	255.4	167	291.7	0.050	1.38	1.70	349.8	240	165.5	130	300	422	235	162.0	165
	2	MX-2600-96	206	269.8	250	436.8	0.056	1.55	185	358.2	245	168.9	150	305	424.8	250	172.4	195
Exit Cone	1	4KXD02	215	374.8	180	314.5	0.045	1.24	170	349.8	240	165.5	130	300	422	235	162.0	165
	2	4KXD02	230	383.2	200	349.4	0.044	1.21	185	358.2	245	168.9	150	305	424.8	250	172.4	195
Exit O'wrap	1	MXA-6012	190	360.9	300	525.3								300	422	235	162.0	165
	2	4KXD02	200	366.5	300	525.3								305	424.8	250	172.4	195

^{*1 =} First Nozzle

²i = Second Nozzle, Initial Configuration 2f = Second Nozzle, Final Configuration

TABLE 23. - BILLET TAG-END PROPERTIES

Material	Component	S	pec. Grav.	Hardness,	Uncured Resin, %	Volatile Content, %
4KXD02	Entr. O'wrap	(2i) (2f)	1.33 1.33	109 106	0.78 0.70	4.88 4.9
	Throat O'wrap	(2i) (2f)	1.32 1.36	104 101	0.52 0.49	5.12 4.8
	Exit Cone	(1) (2)	1.32 1.34	107 104	0.71 0.57	5.2 5.09
	Exit O'wrap	(2) (2)	1.33 1.34	105 105	0.61 0.70	4.78 4.70
	Target		1.32(min)	111(min)	0.50(max)	4.0/6.0*
MX-2600-96	Approach	(2i) (2f)	1.72 1.70	123 123	0.31 0.17	0.58 0.76
	Entrance Throat	(2i) (2i)	1.72 1.71	123 123	0.31 0.22	0.58 0.75
	Throat Exten.	(2)	1.71	123	0.22	0.73
SP-8030-96	Approach	(1)	1.69	118	0.50	3.4
	Target		1.69(min)	120(min)	0.50(max)	4.0(max)
MXA-6012	Entr. O'wrap	(1) (1)	1.78 1.77	117 117	0.52 0.55	2.9 2.9
	Throat O'wrap Exit O'wrap	(1) (1)	1.73 1.74	114 116	0.56 0.54	4.0 3.6
	*	(1)	1.75	116	0.51	3.2
	Target		1.59(min)	112(min)	0.70(max)	4.0(max)
MXSC-195	Entrance	(1) (2f)	1.51 1.51	123 122	0.25 0.14	2.5 3.3
	Throat	(1) (2f)	1.52 1.52	117 124	0.23	1.9 3.3
	Throat Exten	(1)	1.53	125	0.19	1.02
	Target		1.50(min)	124(min)	0.50(max)	4.0(max)

^{*} Volatiles limit in cured part increased from 4.0% to 6.0% on second exit cone.

TABLE 24. - MECHANICAL PROPERTIES OF SP-8030-96 SILICA COMPOSITE

Property	Tempe°F	erature °K	Ply Orient.	Modulu psi x 10 ⁶		$\frac{0.2\% \text{ Yiel}}{\text{psi x } 10^3}$		Ult. St		Strain to
Troperty	- F		OTTERL.	psi x io	ruy/ Cin	ps1 x 10	KN/CM	ps1 x 10	KN/cm ²	Failure, %
Tension	75	297	Parallel	0.86	0.59	7.43	5.12	7.53	5.19	2.44
	75	297	Parallel*	1.9	1.3	-	-	6.8	4.7	- .
	75	297	Normal	0.20	0.14	Dadi	Prime .	1.04	0.72	0.59
	75	297	45-degrees	0.38	0.26	-	_	1.29	0.89	0.52
	1750	1227.5	Parallel	0.62	0.43	-	-	1.40	0.97	0.29
Compression	75	297	Parallel	1.54	1.06	9.03	6.23	16.35	12.72	2.92
	7 5	297	Parallel*	1.45	1.0	-		15.9	9.6	_
	75	297	Norma1	1.33	0.92	25.65	17.68	42.13	29.04	4.58
			45-degrees	1.23	0.85	19.90	13.72	32.50	22.41	4.52
Shear	75	297	Paralle1	0.0175	0.012	-	-	1.70	1.17	
	75	297	Norma1	0.075	0.052	-	-	>2.64	>1.82	_
	1750	1227.5	Paralle1	0.01	0.007	-	-	0.36	0.25	-

^{*}Report AFRPL-TR-67-310

TABLE 25. - MECHANICAL PROPERTIES OF MXSC-195 CARBON-SILICA COMPOSITE

	Temperature	P 1 y	Modulus		0.2% Yie		Ult. St	Strain to		
Property	°F	°K	Orient.	psi x 10 ⁶	MN/cm ²	psi x 10	3 KN/cm^3	psi x 10	$\frac{3}{\text{KN/cm}^2}$	Failure, %
Tension	75	297	Paralle1	1.39	0.96		-	9.51	6.56	0.70
	75	297	Paralle1*	2.2	1.5	•••	_	8.83	5.4	_
	75	297	Norma1	0.23	0.16	· _	-	1.08	0.74	0.49
	75	297	45-degrees	0.45	0.31	•••	-	2.17	1.50	0.65
Compression	75	297	Parallel	2.20	1.5	_	_	23.40	16.13	1.23
	75	297	Paralle1*	2.2	1.5		-	20.7	14.3	_
	75	297	Norma1	1.64	1.13	31.6	21.79	37.10	25.48	2.84
	75	297	45-degrees	1.56	1.08	-		22.50	15.51	1.58
	2500	1644	15-30** degrees		-		-	6.0	4.1	·
	3000	1922	15-30** degrees	_	_	_	-	1.76	1.2	<u>-</u>
Shear	75	297	Parallel	0.036	0.025	_	_	1.69	1.17	_
			Norma1		-	ecos	_			NLO

^{*}Report AFRPL-TR-67-310 (4C 2530 Material)
**Report AFRPL-TR-67-310 (X-5571 Material)

TABLE 26. - MECHANICAL PROPERTIES OF 4KXD02 CANVAS COMPOSITE

	Tempe	erature	P1y	Modulu		0.2% Yiel		Ult. St	cength	Strain to
Property	°F	°K	Orient.	psi x 10 ⁶	MN/cm ²	psi x 10 ³	KN/cm ³	psi x 10	KN/cm ²	Failure, %
Tension	75	297	Parallel	0.46	0.32	6.84	4.72	8.83	6.09	3.78
	75	297	Parallel*	0.84	0.58	-		8.59	5.9	_
	75	297	Normal	0.36	0.25	1.92	1.32	2.49	1.72	1.50
	1750	1227.5	Parallel	0.44	0.30	_		1.97	1.36	0.45
Compression	75	297	Parallel	0.95	0.65	5.69	3.92	21.3	14.68	10.29
	75	297	Parallel*	0.76	0.52			22.8	15.7	_
	75	297	Norma1	0.42	0.29	6.54	4.51	39.7	27.37	22.4
	1750	1227.5	Normal	0.61	0.42	-		8.31	5.73	1.58
	2750	1783	Normal	0.52	0.36	_		9.43	6.50	2.02
Shear	75	297	Parallel	0.038	0.026		-	2.26	1.56	_
			Normal	0.052	0.036	_		>4.77	>3.29	_
	1750	1227.5	Paralle1	0.012	0.008	_		>0.53	>0.37	

^{*}Report AFRPL-TR-67-310 (KF-418 material)

TABLE 27. - IBT-106 BOND TEST DATA

				DPT (N/cm ²)	_ P		ear (N/cm ²)
1.	IBT-106	(Uncured) to IBT-106 (Cured)	500	(345)	5	00	(345)
2.	V-44/Ep	oon 921/IBT-106 (Cured)	414	(285)	3	13	(216)
3.	IBT-106	(Uncured)/162-Y-22*/Steel	*			*	
	162-	-Y-22 Condition					
	a.	Untreated	423	(292)	4	26	(294)
	Ъ.	Contaminated	399	(274)	4	18	(289)
	С.	Uncontaminated and Tric Wipe	-			-	
	d.	Contaminated and Tric Wipe	431	(297)	4	77	(324)
	e.	Untreated (3 to 4 times normal thickness)	371	(255)	2	80	(193)
	f.	Apply directly to plates before normal 30 min. standing time.	-		4	85	(334)

NOTE: Plates on all samples bent during test. Failure occurred in the IBT-106 material.

* Fuller Epoxy Resin Primer

Lot	Mfg.
A-7-11N	5-14-68
A-7-11N	5-21-68

These materials were from the same lots as used in Motor LCAN-01 $\,$

TABLE 28. - BALLISTIC PERFORMANCE SUMMARY, MOTOR LCAN-02

Ignition Delay, sec	0.075	
Ignition Interval, sec	0.125	
Maximum Pressure, psia (N/cm ²)	616	(425)
Web Action Time (t _b), sec	38.33	
Action Time (t _a), sec	48.33	
Total Time (t _t), sec	59.42	
Average Chamber Pressure (web) (P _{cb}),psia (N/cm ²)	500	(345)
Average Chamber Pressure (action) (Pca), psia (N/cm²)	432	(298)
Impulse, Web (I _b), 1b-sec (N-sec)	3,877,531*	(17.25×10^6)
Average Thrust, Web, (F _{yb}), 1bf (N)	85,758*	(382,000)
Burning Rate (r _b), in./sec (cm/sec)	0.258	(0.655)
For First 28.6 sec of Operation (Prior to		
Nozzle Burnthrough)		
Average Pressure (P _{cf}), psia (N/cm ²)	522	(360)
Average Thrust (F _{vf}), 1bf (N)		(480,000)
Impulse, (I _f), 1b-sec (N-sec)	2,910,215	(12.9×10^6)
Specific Impulse (I s (mc)), sec (N-sec/kg)	207.95	(2080)
C _{f (mc)}	1.4194	

^{*}Not a valid indication of motor performance due to nozzle malfunction at 28.6 sec.

TABLE 29. - LCAN-02 NOZZLE MATERIAL PERFORMANCE SUMMARY

Component	Material (1)	Axial (2) Station	Initial Area Ratio	Radial Location	Orig. Thick. in.	Material Remain. (3)	Total Matl. Loss, in.	Char Thick. in.	Loss	Rate (mil	s/sec) b	ased on
Entrance	IBT-100	A	-3.37	45°	2.61	1.93	0.68	0.30			14.3	
	IBT-100	В	-2.97		2.61	1.70	0.91	0.32			18.8	
	IBT-100	C	-2.61		2.61	1.50	1.11	0.33			23.0	
	IBT-100	D	-2.32		1.66	0.35	1.31	0.18			27.0	
	Silica	_	2.52		0.81	0.81	0	0			0	
	IBT-100	E	-2.09		1.05	0	1.05	_			32.0	(5)
	Silica		2.07		0.78	0.59	0.19	0.20		35.0	52.0	(3)
	C-Si				0.37	0.37	0	-		0		
	IBT-100	F	-1.86		0.55	0.37	0.55			U	20 N	(5)
	Silica	1	1.00		0.52	0	0.52	11000			38.0	(5)
	C-Si				0.84	0.67		0.20		29.0		
	IBT-100	G	-1.75			0.67	0.17	0.20)	FO 0	(5)
		G	-1.75		0.24		0.24	-		2	50.0	(5)
	Silica				0.10	0	0.10	-		26.3		
	C-Si	77	1 22		1.31	0.53	0.78	0.53)	10.0	
	C-Si	H	-1.32		1.48	0.55	0.93	0.55		24.3	19.2	
	C-Si	I	-1.11	2008	1.49	0.58	0.91	0.58		23.8	18.8	
	IBT-100	A	-3.37	200°	2.61	1.60	1.01	0.27			20.8	
		В	-2.97		2.61	1.24	1.37	0.32			28.4	
		C	-2.61		2.61	1.03	1.58	0.25			32.7	
		D	-2.32		1.66	0	1.66			-	34.4	
	Silica				0.81	0.81	0	0.24	(6	0		
	C-Si	Pt. of Failure	-2.00 (est.)		1.25	0	1.25+ 0/W	/	53.5	· ·		
Throat	C-Si	J	-1.05	Area	1.42	0.68	0.74	0	25.8	19.3		
		K	1.00	of Least	1.42	1.03	0.39	0.16	13.6	10.2		
		L	1.06	Matl.	1.10	0.73	0.37	0.16	12.9	9.7		
		М	1.13	Loss	1.00	0.69	0.31	0.17	10.8	8.1		
xit Cone	Silica	N	1.23	Unknown	0.985 (7)	0.550	0.435	0.09		11.3		9.5
		0	1.42		0.960	0.540	0.420	0.10		11.0		9.2
		P	1.60		0.935	0.560	0.375	0.10		9.8		8.2
		Q	1.76		0.925	0.580	0.345	0.12		9.0		7.5
	Si/Canvas	R	1.95		0.910	0.550	0.360	0.08		9.4		7.9
	Canvas	S	2.40		0.870	0.665	0.205	0.11		5.4		4.5
		T	2.05		0.900	0.559	0.341	0.08		8.9		7.4
		U	3.50		0.750	0.660	0.090	0.14		2.4		2.0
		V	4.46		0.640	0.598	0.042	0.15		1.1		0.9
		W	5.50		0.590	0.555	0.035	0.15		0.9		0.8

NOTES:

⁽¹⁾ Silica phenolic was MX-2600-96; carbon-silica was MXSC-195; canvas-duck was 4KXD02.

⁽²⁾ Refer to Figure 43.

⁽³⁾ IBT-100 values reflect virgin material (char removed).

⁽⁴⁾ $t_{bt} = 28.6 \text{ sec (time of initial burnthrough)}.$

 $t_b = 38.3 \text{ sec (web action time)}.$

 $t_a = 48.4 \text{ sec (action time)}.$

 t_f = 45.8 sec (time of exit cone separation).

⁽⁵⁾ IBT-100 erosion rate estimated and used to calculate ablative liner exposure time.

⁽⁶⁾ Based on 23.6 sec (assumes 5 sec required to burn through overwrap and steel).

⁽⁷⁾ Excluding overwrap. Data not converted to S.I. Units for sake of clarity.

TABLE 30. - COMPRESSIVE STRENGTH OF CHARRED CARBON SILICA IN 45 DEGREE-TO-PLY DIRECTION

Specimen from		Strength, psi	(N/cm^2)
LCAN Entrance Ring (MXSC-195)		1800	(1240)
(IMOO 1)3)		2010	(1385)
		1180	(813)
		2320	(1600)
		2790	(1922)
	Average	2020	(1392)
LCFT Throat No. 16 (MXSC-195)		1560	(1075)
(IMOO 1)3)		990	(683)
		3330	(2293)
		1700	(1172)
		2150	(1481)
	Average	1946	(1341)

TABLE 31. - COMPARISON OF NOZZLE ENTRANCE CONDITIONS AND CONFIGURATION BETWEEN ALGOL IIB AND LCAN-02

	Algol		L	CAN
Nozzle Throat Diameter, in. (cm)	11.78	(29.9)	13.00	(33.0)
Motor Port-to-Throat Ratio (initial)	1.44		1.34	
Gas Velocity at End of Grain (Mach No.)	0.142		0.183	
Temperature of Combustion Gases at 1000 psia [690 N/cm^2], theoretical	5480°F	(3300°K)	5463°F	(3290°K)
Propellant Solids Content	80		84	
Ammonium Perchlorate	61		69	
Aluminum	19		15	
Nozzle Entrance Ins. Material	Refrasil (AGC-10803)		Silica and Carbon-Silica Phenolic	
Wrap Orientation, Ref to Nozzle Center Line	Perpe	Upstream ndicular s Flow)	70 <u>+</u>	5°

TABLE 32. - EFFECT OF NOZZLE EROSION RATES ON 260/SIVB VEHICLE PAYLOAD CAPABILITY

Nozzle Erosion mils/sec	Rate,	(195 K	for 105 NM m) Orbit, (Kg)	Change in Payload, %		
6 (Base	(94,675	(43,000)	0		
10	(0.025)	93,721	(42,500)	-1.0		
15	(0.038)	92,451	(42,000)	-2.3		
20	(0.051)	91,206	(41,300)	-3.7		
25	(0.063)	89,954	(40,800)	-5.0		
25 (Modif	(0.063) ied Grain)	91,045	(41,250)	-3.8		

TABLE 33. - 260-IN.-DIA (6.6 m) MOTOR WEIGHT AND COST INCREASE REQUIRED TO ACHIEVE BASELINE PAYLOAD

	le Throat ion Rate, c (cm/sec)	Inc	or Weight rease for ormance, 1b (Kg)	Motor Cost Increase, \$
6	(0.015)		0	0
(base	case)			
10	(0.025)	52,900	(24,000)	98,400
15	(0.038)	121,300	(55,200)	225,600
20	(0.051)	189,700	(86,100)	352,800
25	(0.063)	258,100	(117,200)	480,100
25 (Modii	(0.063) fied Grain)	181,500	(82,500)	337,600

^{*}Assumes motor cost increase at a rate of \$1.86 per 1b (\$4.10 per Kg)

TABLE 34. - ABLATIVE MATERIAL COST COMPARISON FOR 260-FL NOZZLE DESIGNS

	Material Costs for 260-FL Nozzle (1005017)							
			Adjusted	Alt.	Alt.	Alt.		
127 ** 1	Ablative	Baseline	Baseline	No. 1	No. 2	No. 3		
Where Used	<u>Material</u>	(1)	(2)	(3)				
Throat and	Carbon	\$223,540	\$203,000			\$ 57,100		
Hi Loss-Rate	Carbon-Silica		,	\$159,000		, ,,,,,,,,,,,,,,,,,,,,,,,,,,,,,,,,,,,,,		
Areas	Silica (Hvy wt)				\$ 75,550			
~ N	a 1 0111					70 070		
Medium Loss- Rate Areas	Carbon-Silica Silica (Hvy wt)					79,870		
Nate Aleas	Dirica (nvy wt)							
Exit-Cone,0/W,	Silica (Std)	210,950						
and Low Loss-	Silica (Hvy wt)		182,550			25,510		
Rate Areas	Canvas-Duck		•	48,250	55,340	52,340		
	Asbestos			8,000				
Tota	l Material Cost	\$434,490	\$385,500	\$215,250	\$130,890	\$214,820		
			·	·				
	a . a . (4)		/ 0 000	210 240	202 (00	210 (70		
Nozzle Mtl	Cost Savings (4)	_	48,990	219,240	303,600	219,670		
	(5)							
Added Mo	tor Cost for (5)	_	-	140,000	282,000	_		
Equal Pa	iy toad							
n 1	Not Cost Cost -		ė 40 000	ė 70 240	ė ai 600	¢210 670		
Kealized	Net Cost Saving		\$ 48,990	\$ 79,240	\$ 21,600	\$219,670		

NOTES: (1) From low cost study conducted on NAS7-513.

⁽²⁾ Baseline design adjusted for best current and competitive prices.

⁽³⁾ Alternate design from NAS7-513, adjusted for best current and competitive prices.

⁽⁴⁾ Compared to baseline design.

⁽⁵⁾ From Figure 49 based on expected throat loss rate.

TABLE 35. - EXHAUST GAS COMPOSITION - ANB-3374 PROPELLANT (HTPB)

HC1	0.4971
N ₂	0.3030
н ₂ о	0.7015
н ₂	0.8883
02	0.0009
0	0.0029
ОН	0.0408
C1	0.0425
NO	0.0032
Cl ₂	0.0001
Н	0.1113
CO	0.7873
co ₂	0.0772
PN	0.0015
PO	0.0071
A1	0.0002
A1C1	0.0085
Alcl ₂	0.0213
Alcl ₃	0.0006
A1203	0.2626
FeC1	0.0112

^{*}Moles/100 gm of propellant at 1000 psia (690 N/cm 2) chamber pressure and 5742°F (3440°K)

TABLE 36. - WEIGHT SUMMARY, FULL-SCALE NOZZLE

			Calculated Weight					
Component	Material	Fabric Cut	As-Wra Bille		Final Part			
			1b	(kg)	1b	(kg)		
Closure Ins.	Canvas-Duck	Bias	1,263	575	1,104	502		
Submerged Liner	Canvas-Duck Carbon	Warp Warp	804 630	365 286	675 517	306 235		
Nose Insert	Carbon	Bias	819	372	561	255		
Nose O/W	Canvas-Duck	Bias	33	15	28	13		
Entrance Insert	Carbon	Bias	777	353	599	272		
Entrance O/W	Canvas-Duck	Bias	58	26	48	22		
Throat	Carbon	Bias	1,647	•••	1,357	616		
Throat O/W	Canvas-Duck	Warp	567	257	515	234		
Aft Closure Insulator	IBT-100	-	-	-	3,035	1,380		
Nozzle Shell	HY-150	-	-	_	6,614	3,005		
Throat Support	HY-150	-		-	3,837	1,743		
Bolts; Adhesive; Misc.	<u>-</u> ·	-	_		64	29		
	Basic Nozzle	Weight			18,954	8,610		
	Flex Seal Ass	embly			4,426	2,010		
	Total Nozzle	Weight			23,380	10,610		

TABLE 37. - EXIT CONE WEIGHT SUMMARY

			Calculated Weight					
Component	Part	Material	As-Wra Bille		Fin Par			
			1ъ	(kg)	1b	(kg)		
Forward Exit	Housing	4130STL	_	_	3,558	1,617		
Cone	Aft Flange	4130STL	~	_	794	361		
	Fwd Liner	Carbon	1,483	675	1,143	521		
	Aft Liner	Canvas-duck	2,336	_	2,296	1,042		
	Insulator/ Overwrap	sulator/ Canvas-duck 415 -	377	171				
	Structural Overwrap	Glass	1,162	528	528 1,056	480		
	Adhesive; Misc.	· -	-	No.	40	18		
	Sub-tota	al			9,264	4,210		
Aft Exit	Fwd Flange	4130STL	_	-	899	408		
Cone	Liner	Canvas-duck	7,908	· <u>-</u>	6,823	Mate.		
	Structural Overwrap	Glass	3,575	-	3,250	****		
	Adhesive; Misc.	-	- -	-	60	ton.		
	Sub-tota	al.			11,032	5,020		
	Exit Cor	ne Total Weight			20,296	9,175		

TABLE 38. - THERMAL ANALYSIS STATIONS AND BOUNDARY CONDITIONS - FULL-SCALE NOZZLE

	Nozzle Lo	cation	Local Convec		ecovery		
Rad			Transfer Coe		Temperature		
in.	(cm)	<u>ε</u>	Btu/hr-ft ² °F	$(W/m^2$ °K)	•R	(°K)	
59.6	151.5	-1.80	1700	5350	6076	3380	
52.67	133.7	-1.40	1222	3840	6058	3370	
47.20	119.8	-1.13	1291	4070	6015	3350	
44.88	114.0	-1.02	1228	3865	5972	3320	
44.45	113.0	1.00 (Throat)	1110	3495	5929	3300	
45.78	116.3	1.06	829	2610	5820	3230	
47.03	119.4	1.12	728	2295	5783	3210	
59.46	151.0	1.79	567	1788	5728	3180	
65.12	165.3	2.15	464	1460	5667	3150	
70.2	178.0	2.50	390	1230	5648	3140	
76.7	194.8	3.00	317	997	5610	3120	
99.6	253.0	5.00	173	545	5520	3070	
123.9	315.0	8.00	105	331	5445	3030	

^{*} At chamber pressure of 514 psia (354 N/cm²)
** Chamber stagnation temperature = 6094°R (3390°K)

TABLE 39. - HEAT TRANSFER CORRECTION FACTOR SCHEDULE

Time, sec	Chamber Pr psia (essure N/cm ²)	Heat Transfer Factor - HTF*
0	620	427	1.161
35	650	448	1.207
55	505	348	0.985
112	700	482	1.280
140	400	276	0.820
148	14.7	10	

^{*}HTF = Ratio of heat transfer coefficient at any desired chamber pressure (P_c) to its value at P_c = 514 psia (354 N/cm²).

TABLE 40. - EXPECTED PERFORMANCE OF FULL-SCALE NOZZLE

				Depth from Original Surface					
Component	Station	Material	Area Ratio	Erosion in. (cm)	Char in. (cm)	100°F (515.23K)			
Nose Insert	1	Carbon Phenolic	-1.80	1.53 (3.87)	1.78 (4.52)	2.36 (5.99)			
Nose Insert	2	Carbon Phenolic	-1.40	1.06 (2.69)	1.36 (3.45)	2.05 (5.21)			
Entrance Insert	3	Carbon Phenolic	-1.13	1.09 (2.77)	1.38 (3.51)	2.10 (5.33)			
Throat Insert	4	Carbon Phenolic	-1.02	1.01 (2.57)	1.32 (3.35)	2.06 (5.23)			
Throat Insert	5	Carbon Phenolic	Throat	0.88 (2.24)	1.20 (3.05)	1.90 (4.83)			
Throat Insert	6	Carbon Phenolic	1.06	0.58 (1.47)	0.96 (2.44)	1.85 (4.70)			
Fwd Exit Cone	7	Carbon Phenolic	1.12	0.48 (1.22)	0.89 (2.26)	1.82 (4.62)			
Fwd Exit Cone	8	Carbon Phenolic	1.79	0.32 (0.81)	0.80 (2.03)	1.80 (4.57)			
Fwd Exit Cone	9	Carbon Phenolic	2.15	0.22 (0.56)	0.73 (1.85)	1.78 (4.52)			
Fwd Exit Cone	10	Canvas-Duck Phenolic	2.50	1.16 (2.95)	1.28 (3.25)	1.52 (3.86)			
Fwd Exit Cone	11	Canvas-Duck Phenolic	3.00	0.93 (2.36)	1.08 (2.74)	1.37 (3.48)			
Aft Exit Cone	12	Canvas-Duck Phenolic	4.00	0.35 (0.89)	0.59 (1.50)	1.04 (2.64)			
Aft Exit Cone	13	Canvas-Duck Phenolic	5.00	0.27 (0.69)	0.52 (1.32)	1.01 (2.57)			
Aft Exit Cone	14	Canvas-Duck Phenolic	6.50	0.19 (0.48)	0.48 (1.22)	0.97 (2.46)			
Aft Exit Cone	15	Canvas-Duck Phenolic	8.00	0.15 (0.38)	0.45 (1.14)	0.95 (2.41)			

TABLE 41. - STRUCTURAL MATERIAL PROPERTIES

Property	HY-150	Steel	4130	Stee1	1	.84 Glass Cloth Epoxy Resin
Yield Strength, ksi (KN/cm ²)	136	(93.7)	70	(48.2)		-
Ult. Tensile Strength, ksi (KN/cm ²)	149	(103)	90	(62.0)	47.4	(32.6) (hoop & axial)
					40.5	(27.9) (radial)
Ult. Shear Strength, ksi (KN/cm ²)	89.4	(61.5)	54	(37.2)	5.0	(3,5)
Young's Modulus, psi x 10 ⁶ (MN/cm ²)	29.5	(20.3)	29.0	(20.0)	3.9	(2.7) (hoop & axial)
					3.3	(2.3) (radial)
Poisson's ratio	0	.30	. (0.30		0.125

TABLE 42. - CARBON PHENOLIC MATERIAL PROPERTIES

					Temperat	ture, °F			
Proper	ty	80	100	200	600	1000	2000	3000	3900
Modulus, psi	x 10 ⁻⁶								
Axial and l	hoop (1)	2.30	2.18	1.86	1.40	1.27	1.10	0.30	0.001
	(2)	2.00	1.90	1.65	1.25	1.17	1.00	0.30	0.001
Radial	(1)	1.60	1.55	1.25	0.95	0.80	0.75	0.25	0.001
	(2)	1.68	1.60	1.39	1.05	0.98	0.84	0.25	0.001
Poisson Ratio	<u>o</u>								
Radial/axia	normalisessing generalise comments and deposits			0.0	08				
Radial/hoo	p	**************************************			0.3	15			
Coefficient of in./in./°F x		0.34	0.34	0.38	0.36	0.01	0.01	0.01	0.01
Ultimate Tens	sile Strength, ksi								
Parallel to	o ply	17.0	17.2	18.0	14.0	6.0		NIL -	
17° to ply		6.0	5.8	5.1	3.2	0.9	an garan ang pana ang pana an Alife ta mah ajada Masa ali	- NIL -	
Perpendicu	lar to ply	2.6	2.5	2.5	1.4	0.4		- NIL -	
Ultimate Com	pression Strength,	ksi							
Parallel to	o ply	44.0	43.0	36.5	13.0	4.0	emotivado na produción de la completa del la completa de la completa del la completa de la completa del la completa de la completa de la completa del	NIL -	
Ultimate Into Shear, ksi	erlaminar ————	2.6	2.5	2.2	1.4	0.4		— NIL —	

⁽¹⁾ Data from parts wrapped parallel to center line.(2) Data from parts wrapped 50° to center line.

(Data not converted to SI units for sake of clarity)

TABLE 43. - CANVAS DUCK-PHENOLIC MATERIAL PROPERTIES

					perature,	°F			
Property	_80	100	200	300	600	750	1000	1750	4000
Modulus, psi x 10 ⁻⁶									
Axial and hoop	0.95	0.92	0.81	0.75	0.65	0.59	0.50	0.29	0.00
Radial	0.43	0.41	0.31	0.25	0.15	0.12	0.08	0.03	0.00
Poisson Ratio									
Radial/Axial	*** VOIL TOT ADDRESSED		MD-manufactures and any open processing and any open processing and a second p		 0.25	when we will the control of the cont			nan or her more than the control of
Radia1/Hoop	N-000 0-000 0-000 0-000 0-000 0-000 0-000 0-000 0-000 0-000 0-000 0-000 0-000 0-000 0-000 0-000 0-000 0-000 0-		· ·		- 0.25				
Coeff. of Exp. in./in./°F	x 10 ⁵								
Axial and hoop	0.38	0.38	0.38	0.38	0.04	-0.056	-0.14	-0.114	-0.001
Radia1	0.015	0.015	0.015	0.015	-0.016	-0.022	-0.028	-0.021	-0.001
Ultimate Tensile Strength,	ksi								
Parallel to ply	8.83	8.75	8.34	7.93	6.68	6.08	4.72	1.97	NIL
Perpendicular to ply	2.49								
Ultimate Comp. Strength, ks	<u>si</u>								
Parallel to ply	21.3	21.1	20.0	19.1	16.0	14.5	12.0	4.46	NIL
Perpendicular to ply	39.7	39.2	37.3	35.6	30.1	27.4	22.6	8.3	NIL
Ult. Interlaminar Shear, ks	<u>2.26</u>	2.23	2.15	2.02	1.72	1.57	1.31	0.53	NIL

NOTE:

Data not converted to SI units for sake of clarity.

TABLE 44. - MAXIMUM STRESS AND STRAIN CONDITIONS IN EXIT CONE THERMAL STRESS ANALYSIS SUMMARY

				lated ess					
Component	Area Ratio Location	<u>Material</u>	psi	(N/cm^2)	Direction	°F	(°K)	Ultimate Stress	Factor of Safety
Fwd Liner	1.8	Carbon	2290	(1580)	Hoop Comp.	550	(566)	15940	6.96
	2.3	Carbon	840	(579)	Hoop Tens.	80	(300)	17000	High
	2.2	Canvas	340	(234)	Hoop Tens.	80	(300)	8833	High
	2.3	Canvas	1340	(923)	Hoop Tens.	1500	(1088)	2997	2.24
	2.4	Canvas	1300	(895)	Hoop Tens.	1000	(812)	4723	3.63
Overwrap	2.5	Glass	1950	(1345)	Hoop Tens.	80	(300)	47378	High
Steel Housing	2.4	4130	12000	(8260)	Hoop Tens.	80	(300)	90000	5.76
Aft Flange	3.6	4130	11500	(7930)	Hoop Tens.	80	(366)	90000	6.02
			Strain	, %			A	llowable Strain	
Fwd Liner Mtl. Transition	2.23	Canvas	0.206%		Hoop Strain	1500	(1082)	0.25%	1.21

NOTES: a. Ablative thermal gradient existing at end of firing in conjunction with MEOP loads earlier in firing used as input conditions.

b. Factor of safety = 1.3×1 imit stress-vs-ultimate for structural components. = 1.0×1 imit stress-vs-ultimate for ablative components.

TABLE 45. - FULL SCALE NOZZLE COST SUMMARY

I.	Nozz	<u>le</u>	•	
	Α.	Ablative Materials (1)		\$ 97,407
	В.	Steel Components (net wt x \$	20/1Ь)	209,020
	С.	Expendable Materials		2,500
	D	Direct Labor (9,488 hr at \$5	.87/hr)	55,695
	E.	Direct Labor Overhead at 174		96,778
	F.	Tooling for Ablative Compone	nts (2)	8,145
,	G.	Tooling for Steel Components	(2)	4,520
	н.	Facilities		1004
	I.	G&A at 8.5%		40,339
			Subtotal	\$514,404
			Profit (10%)	51,440
			Total	\$565,844
II.	Exit	Cone		
	Α.	Ablative Materials (3)		\$ 66,278
	В.	Steel Components		107,040
	C.	Expendable Materials		3,000
	D.	Direct Labor (4,074 hr at \$5	.87/hr)	23,914
	Ε.	Direct Labor Overhead at 174		41,555
	F.	Tooling for Ablative Compone	nts ⁽²⁾	9,639
	G.	Tooling for Steel Components	(2)	2,740
	Н.	Facilities (2)(4)		34,473
	I.	G&A at 8.5%		24,534
			Subtotal	\$303,173
			Profit (10%)	30,317
			Total	\$333,490
			UNIT COST	\$899,334
			WITH FLEXIBLE SEAL	\$961,600

⁽¹⁾ Includes IBT-100 Closure Insulation

⁽²⁾ Pro-rated on the basis of 30 units (6/yr for 5 yr)

⁽³⁾ Includes glass-phenolic structural overwrap(4) Some facilities included herein also will be used on nozzle fab.

TABLE 46. - ABLATIVE MATERIAL COST SUMMARY

				Total Wes	ight (1)(2)		
		<u>Material</u>	Cut	1b	(Kg)	Cost/1b	Cost
I.	Nozzle	Carbon Phenolic	Bias Warp	3,405 662	(1,550) (301)	21.50 20.00	\$ 73,208 13,240
		Canvas-Duck Phenolic	Bias Warp	1,422 1,440	(646) (654)	3.30 1.80	4,693 2,592
		IBT-100	_	3,340	(1,517)	1.10	3,674
			Sul	ototal			\$ 97,407
II.	Exit	Carbon Phenolic	Warp	1,557	(707)	20.00	31,140
	Cone	Canvas-Duck Phenolic	Warp	11,507	(5,230)	1.80	20,713
		Glass Phenolic	Warp	4,974	(2,260)	2.90	14,425
			Sul	ototal			\$ 66,278
			TO	ΓAL			\$163,685

 ⁽¹⁾ Gross as-wrapped billet weight plus 5% for scrap loss and contingency.
 (2) IBT-100 weight includes 10% scrap loss; cost includes application.

TABLE 47. - PRE-PREG PRICES APPLICABLE TO FULL-SCALE ABLATIVE NOZZLES

Reinforcement	Resin	\$ U.S./lbm
98% Carbon Fabric	Phenolic	20.00
98% Carbon Fabric Chopped	Phenolic	20.00
98% Carbon Fibers, Chopped	Phenolic	14.50
98% Carbon Fibers, Chopped	Epoxy-Novolac	12.50
98% Carbon Fabric	Polyphenylene	21.00
98% Carbon Fabric, Chopped	Polyphenylene	21.00
98% Carbon Fabric	Epoxy-Novolac	22.00
86% Carbon Fabric	Epoxy-Novolac	14.25
C-100-48 Silica Fabric	Phenolic	5.50
C-100-96 Silica Fabric	Phenolic	5.00
Silica Fabric, Chopped	Phenolic	6.00
Silica Fabric, Chopped	Epoxy-Novolac	9.50
C-100-96 Silica Fabric	Polyphenylene	5.00
AVCERAM C/S Fabric	Phenolic	15.00
AVCERAM C/S Fabric, Chopped	Phenolic	16.00
AVCERAM C/S Fabric	Polyphenylene	16.00
AVCERAM C/S Fabric, Chopped	Polyphenylene	16.00
Canvas	Phenolic	1.80
Canvas	Epoxy-Novolac	1.80
Canvas, Chopped	Phenolic	1.80
Glass Fabric	Phenolic	2.90
Glass Fabric, Chopped	Phenolic	2.00
KYNOL Fabric	Phenolic	3.00

^{*}Based on 5000 1bm (2273 kg) lots.

TABLE 48. - TOOLING REQUIREMENTS, 260-FL NOZZLE FABRICATION Sheet 1 of 2

Component	Tool Description		Estimated Cost
Fwd Exit Cone	Mandrel, Wrapping Mandrel Handling Aid Ablative Handling Aid Tracer Template (Wrap) Tracer Template (Mach), Ablative Storage Fixture		\$ 62,500 2,800 3,200 680 1,400 680
		Subtotal	\$ 71,260
Exit Cone Aft Section	Mandrel, Wrapping Mandrel Handling Aid Ablative Handling Aid Tracer Template (Wrap) 2 Tracer Template (Mach) 2 Ablative Storage Fixture Dam Ring	req'd	\$150,000 7,000 5,500 1,400 1,800 800 2,100
		Subtotal	\$168,600
Nozzle Assembly	Assembly Stand Tracer Template Machining Tool Stage Drawings Assembly Aids Inverting Fixture Leak Test Fixture		\$ 11,600 1,100 1,440 9,080 3,500 27,600 19,200
		Subtotal	\$ 73,520
Exit Cone Assembly	Assembly Fixture Flange Pos. and Bonding Tilt Stand Adapter Tracer Template (Mach) 3 Inspection Aids	•	\$ 12,500 15,000 12,600 1,200 8,000
		Subtotal	\$ 49,300
Closure Insulator	Mandrel, Wrapping Mandrel Handling Aid Ablative Handling Aid Tracer Template (Wrap) Tracer Template (Mach) Ablative Storage Fixture	Subtotal	\$ 28,800 1,600 2,160 450 720 300 \$ 34,030
		Dublocai	9 34,030

TABLE 48. - TOOLING REQUIREMENTS, 260-FL NOZZLE FABRICATION Sheet 2 of 2

Component	Tool Description		Estimated Cost
Submerged Liner	Mandrel, Wrapping Mandrel Handling Aid Ablative Handling Aid Tracer Template (Wrap) 2 Tracer Template (Mach) 3 Ablative Storage Fixture	req'd	\$ 19,300 1,800 2,250 800 1,950 400
		Subtotal	\$ 26,500
Nose Insert	Mandrel, Wrapping Mandrel Handling Aid Ablative Handling Aid Tracer Template (Wrap) Tracer Template (Mach) 2 Ablative Storage Fixture	-	\$ 21,600 1,700 1,850 400 750 400
		Subtotal	\$ 26,700
Entrance Insert	Mandrel, Wrapping Mandrel Handling Aid Ablative Handling Aid Tracer Template (Wrap) Tracer Template (Mach) Ablative Storage Fixture		\$ 22,320 2,000 2,100 340 600 500
		Subtotal	\$ 32,360
Throat	Mandrel, Wrapping Mandrel Handling Aid Ablative Handling Aid Tracer Template (Wrap) Tracer Template (Mach) 2 Ablative Storage Fixture	r	\$ 38,400 2,500 2,740 660 1,320 600
		Subtotal	\$ 46,220
	Total Too	ling Cost	\$528,490

TABLE 49. - NEW FACILITY REQUIREMENTS AND ESTIMATED COST

l.	Lathe tracer attachment	\$	4,200
2.	280-india vertical turning machine		625,000
3.	Curing oven		215,000
4.	Inspection standards		40,000
5.	Q. C. Laboratory testing equipment		120,000
6.	Raw material storage building		30,000
	Total	\$1	,034,200
	Fabrication Bldg and Crane (A-DD Fab only)		300,000
	Total if Aft Exit Cone Fab at A-DD	\$1	,334,200

I INTERPRET DRAWING PER MIL-STD-100.

APPLY MIL-C-16173, GRADE 3, CORROSION PREVENTIVE COMPOUND IN ACCORDANCE WITH AGC-36234 TO MATING STEEL SURFACES OF CHAMBER AND NOZZLE ASSEMBLIES.

LUBRICATE PACKING WITH VV-0-1078 SILICONE DAMPING FLUID&

FILL GAP WITH AGC-34076, CLASS 2 OR 3 SEALING COMPOUND,

LUBRICATE THREADS WITH MIL-A-907 ANTI-SEIZE COMPOUND,

FORGUE TO:

A. 100-110 FTA3 8. 25-30 IN/L8

C. 9- 13 FT/LB

INDEX HOLES OF MATING COMPONENTS SHALL BE ALIGNED AT ASSEMBLY.

LOCKWIRE IN ACCORDANCE WITH MS 33540.

FOR MOTOR FIRING, REMOVE AND DISCARD TWO (2) PLUGS (1128251-1) LOCATED AT FWD FACE OF THE GNITER ASSY (1128253-49) AND INSTALL TWO (2) INITIATOR CARTRIDGE ASSEMBLIES (1127506-1).

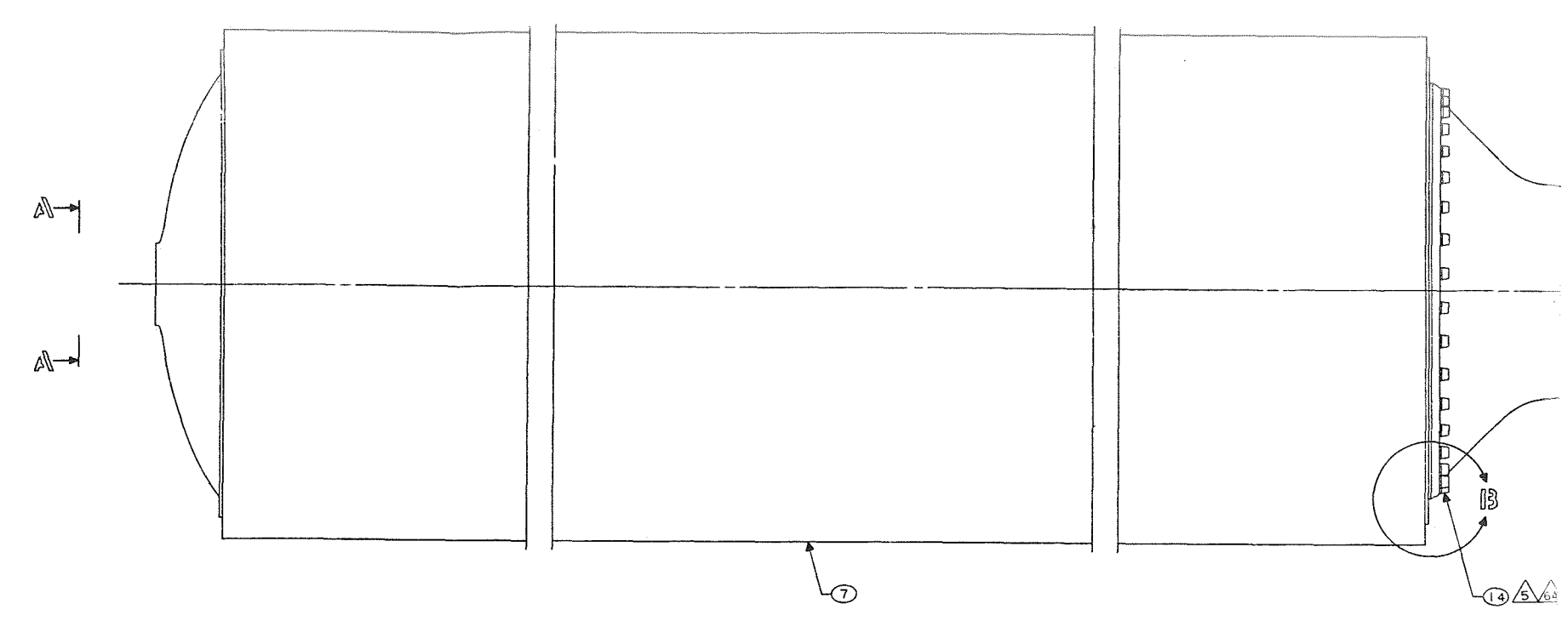
- 10 PRESSURE LEAK CHECK MOTOR AT 25-35 PSIG USING BB-H-411, TYPE 1, CLASS 1, GRADE B, DRY NITROGEN AND MIL-L-25567, TYPE 1, LEAK DETECTION SOLUTION. AREAS TO BE CHECKED FOR LEAKAGE ARE:
 - A. IGNITER ASSEMBLY PACKING (O-RING) SEAL.
 - 8. TWO (2) PRESSORE PORTS (INTERNAL IGNITER PRESSURE AND INTERNAL CHAMBER PRESSURE) AND THE TWO (2) INITIATOR CARTRIDGES ON THE FWD FACE OF THE IGNITER ASSEMBLY.
 - C. CHAMBER TO NOZZLE FLANGE JOINT, LEAKAGE LIMITS: NO VISIBLE EVIDENCE OF BUBBLE FORMATION.

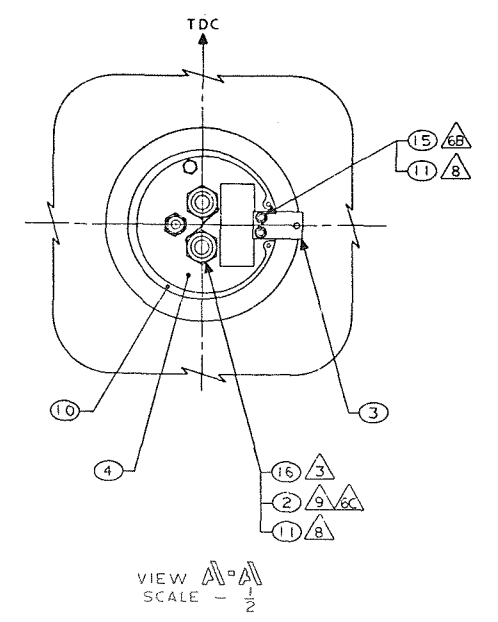
11 PAINTING INSTRUCTIONS:

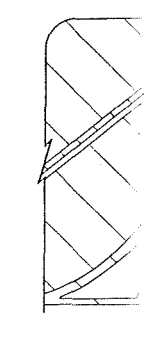
- A. PRIMEMOUTOUS:

 A. PRIMEMOUTH-UP ALL BARE EXTERIOR METALLIC SURFACES OF CHAMBER WITH MIL-P-8585 ZINC CHROMATE PRIMER COATING IN ACCORDANCE WITH AGC-36072. DELETE PRETREATMENT COATING REQUIREMENTS OF AGC-36072, SECTION 3.1. AIR DRY AT AMBIENT TEMPERATURE FOR TWO (2) HOURS MINIMUM.
- B. CLEAN ALL PREVIOUSLY PRIMED SURFACES WITH 0-1-620 1.1.1 TRICHLORGETHANE (METHYL CHEOROFORM).

 C. APPLY TWO (2) COATS (0.8 1.2 MILS THE TOTAL OF TY-L-32 WHITE TACQUER TO ALL PRIMED, UNPAINTED EXTERIOR SURFACES. DRYING HYERVAL SHALL BE 45 MINUTES BETWEEN COATS. AIR DRY FINAL COAT AT AMBIENT TEMPERATURE FOR EIGHTEEN (18) HOURS MINIMUM.
- DO NOT PAINT ELECTRICAL CONNECTORS, PRESSURE PORTS/PLUGS, OR ANY INTERIOR SURFACE.
- 12 APPLY MIL-C-16173, GRADE 1, CORROSION PREVENTIVE COMPOUND IN ACCORDANCE WITH AGC-36234 TO ALL EXTERIOR METALLIC SURFACES NOT PAINTED.







5-1 ASSY LG-2 ASSY HOLE SHOWN ROTATED VIEW B

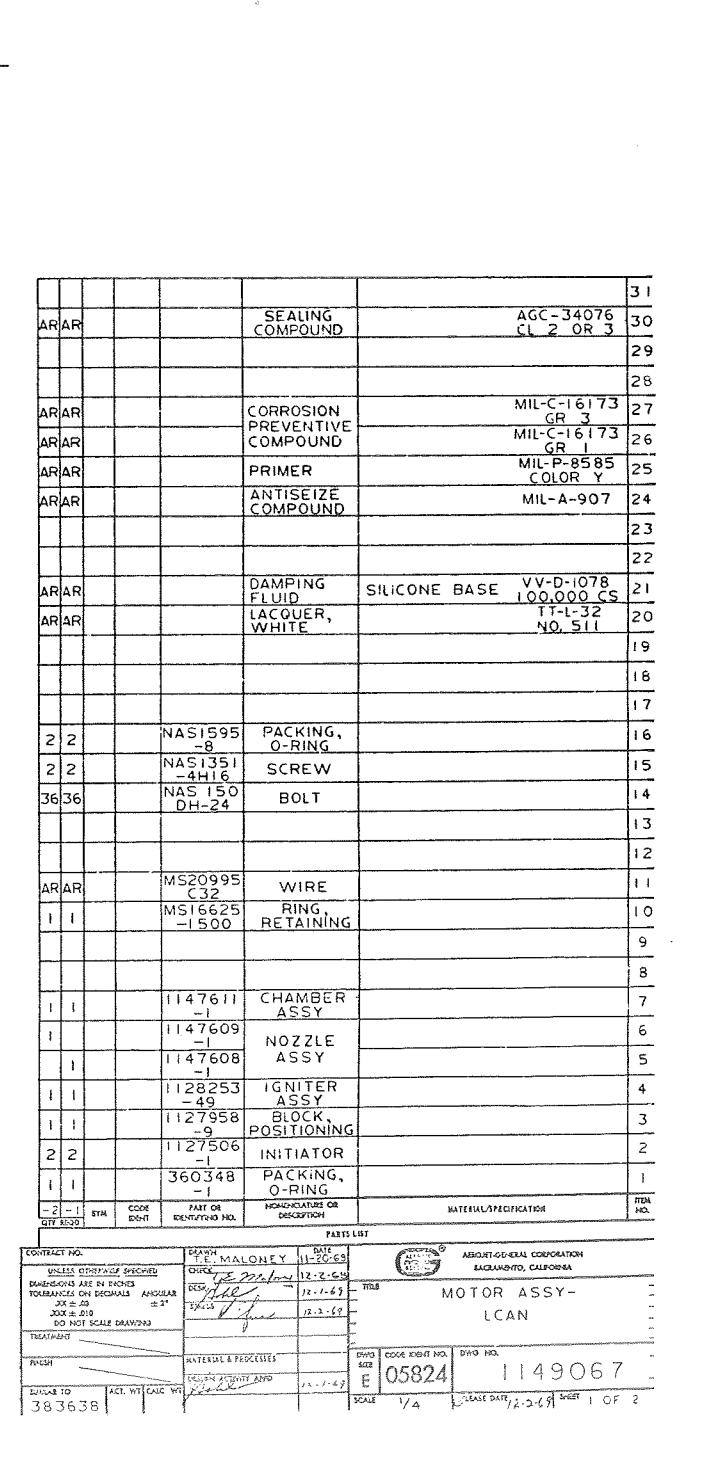


Figure 1. - LCAN Test Motor Assembly

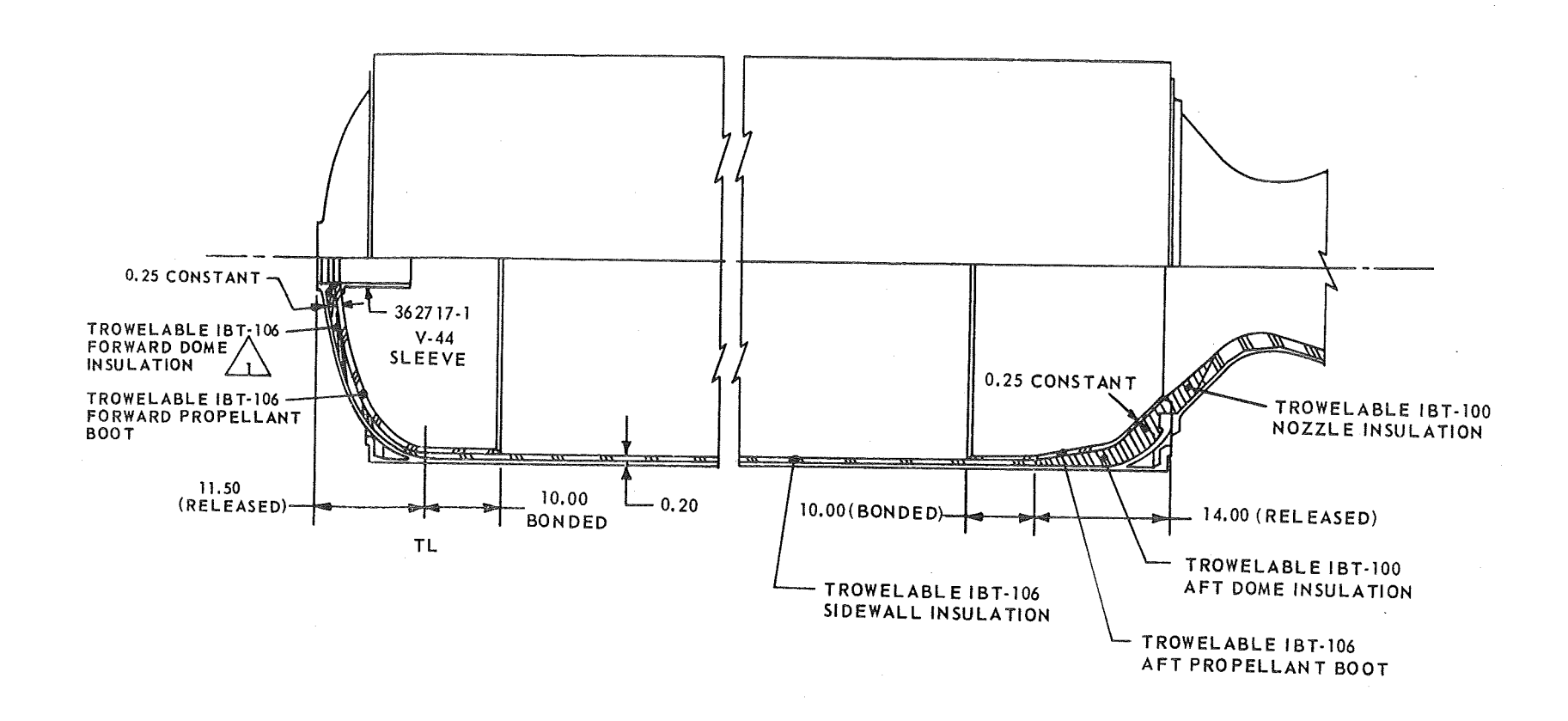


Figure 2. - Trowelable Insulation Configuration

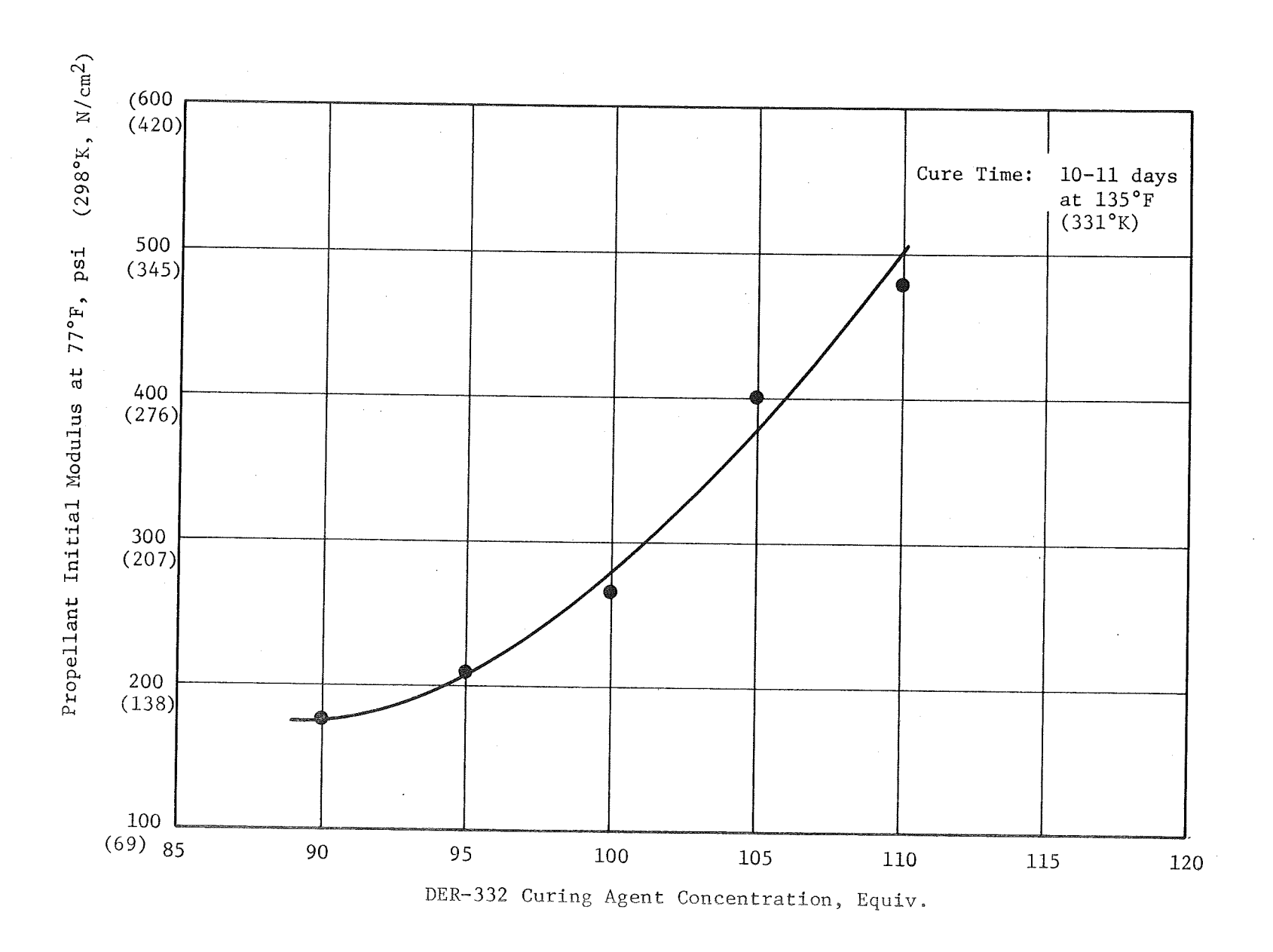


Figure 3. - Propellant Initial Modulus vs Cure Agent Concentration

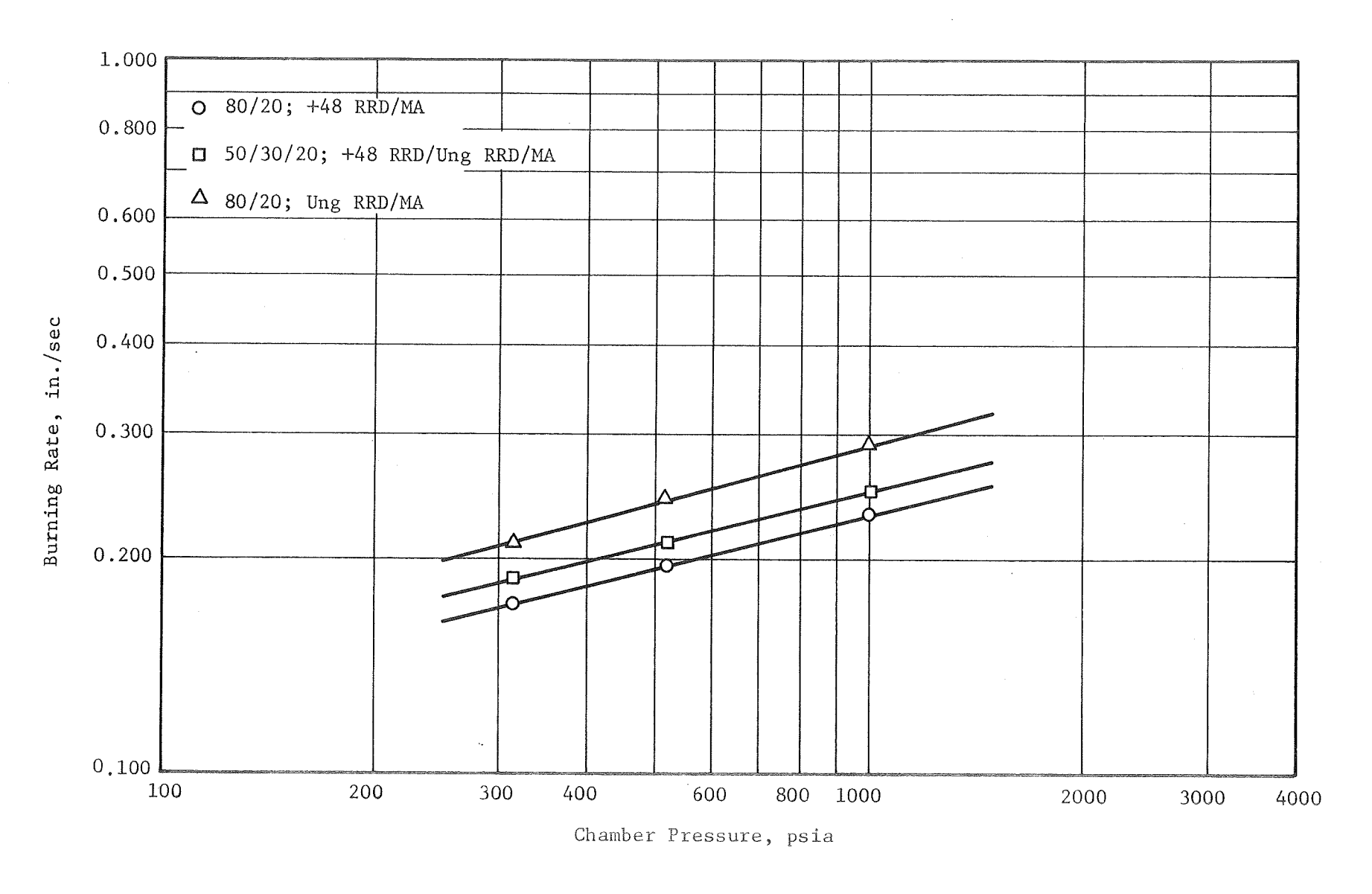


Figure 4. - Effect of Oxidizer Blend Ratio on the Solid Strand Burning Rates of ANB-3347 Propellant

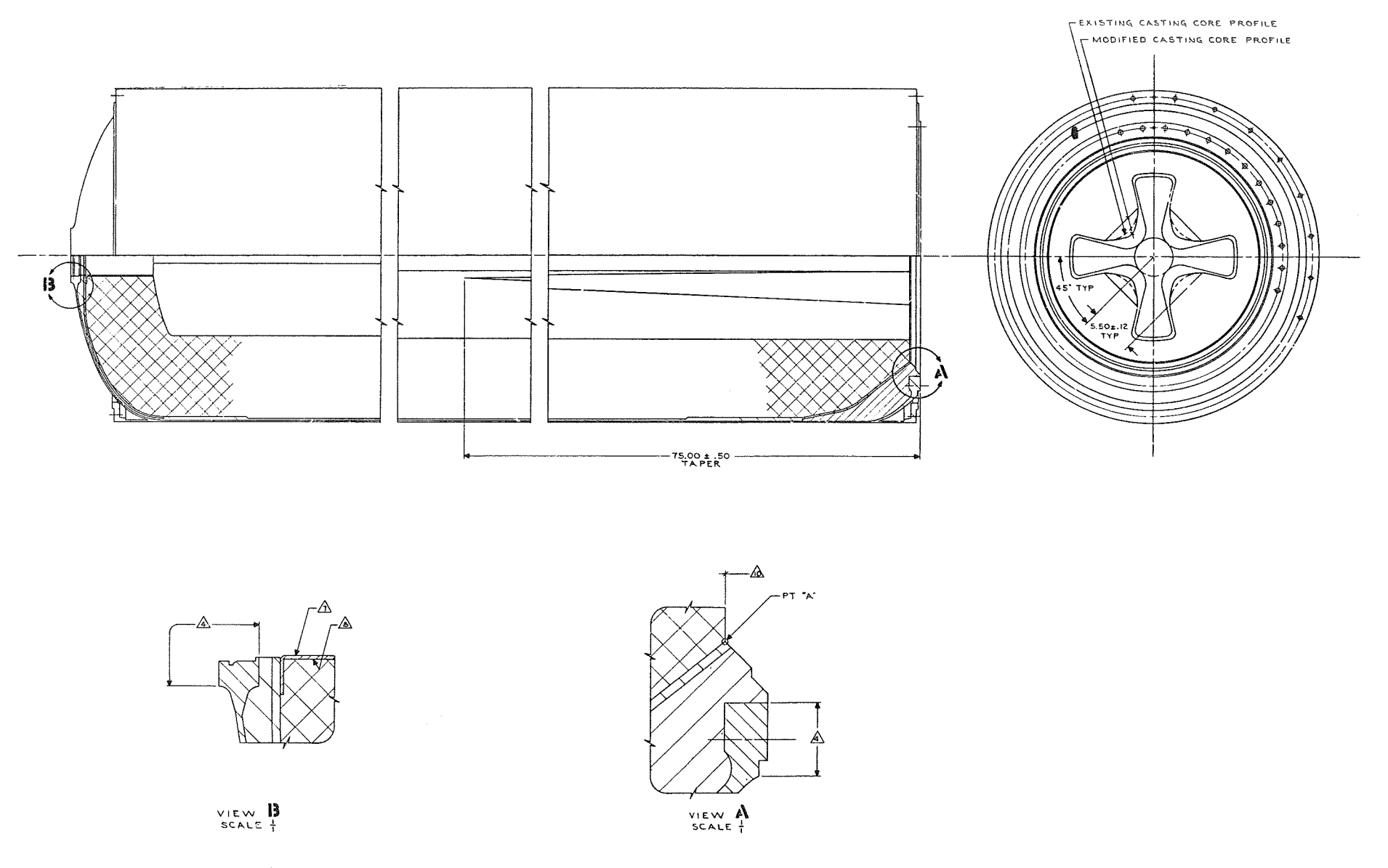


Figure 5. - Algol Test Motor Grain Design

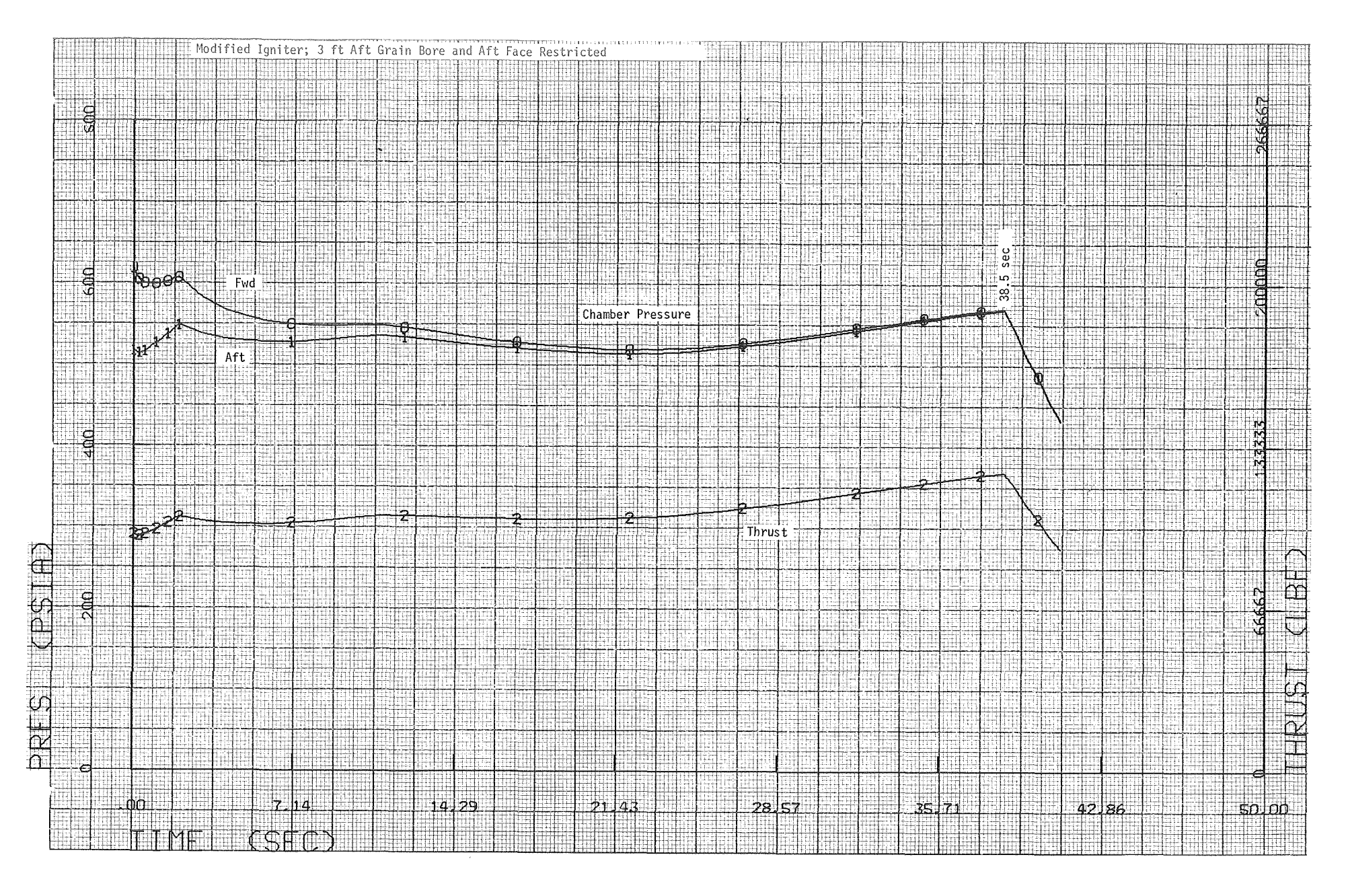


Figure 6. - Predicted Pressure and Thrust-vs-Time, LCAN Motors

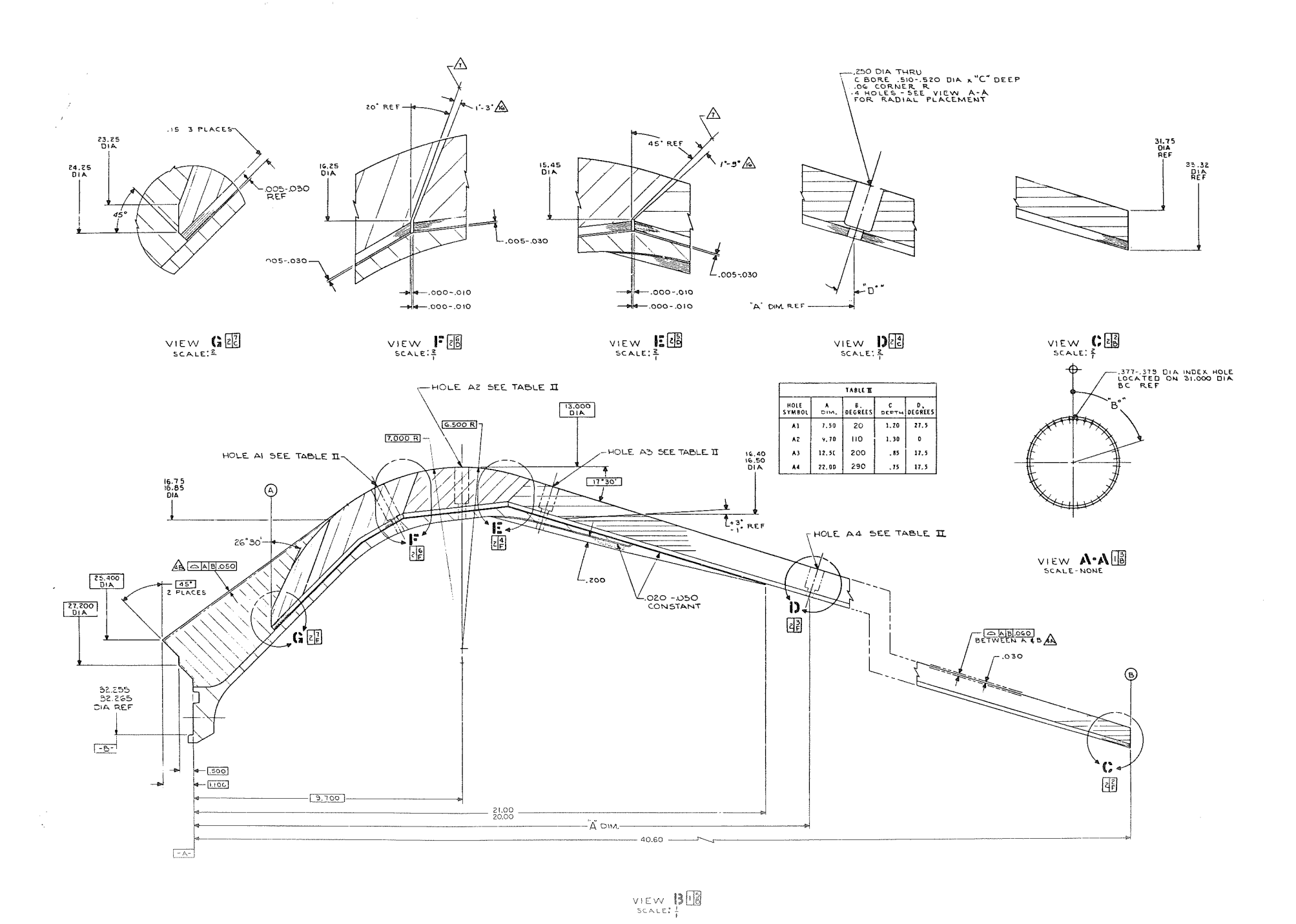


Figure 7. - Nozzle No. 1 (Sheet 2 of 2)

noits: 1 INTERPRET DRAWING PER MIL-STD-100.

REMOVE ALL BURKS AND SHARP EDGES EQUIVALENT TO .005 TO .015 R. UNLESS OTHERWISE NOTED.

SURFACE ROUGHNESS 125%, UNLESS OTHERWISE NOTED.

LAMINATE ORIENTATION HALF-ANGLE, MEASURED WITH RESPECT TO LONGITUDINAL CENTER LINE OF NOZZIE, SHALL BE:

LAMINATE ORIENTATION SHALL BE PARALLEL TO LONGITUDINAL CENTER LINE OF NOZZLE WITHIN 430 TO -10.

SURFACES SHALL BE COINCIDENTAL TO LAMINATE DRIENTATION WITHIN 2°.

ADJACENT LINERS AND TO BE TAPE-WRAPPED INTEGRALLY IN THE SAME OPERATION.

TAPE SHALL BE WRAPPED PARALLEL TO THE WRAPPING SURFACE(S).

10 EQUIVALENT MATERIALS, AS SHOWN IN TABLE 1, MAY BE SUBSTITUTED FOR ITEMS 10 THROUGH 16.

ACCORDANCE WITH OD 19258 AND TANGENTIAL-RADIOJEAPHICALLY INSPECTED IN ACCORDANCE WITH OLD NO. LEX-JOI. EVIDENCE OF SUMFACE AND INHIBNAL DEFECTS SHALL BE RECORDED. DEFECTS ARE SUBJECT TO ENGINEERING REVIEW ACTION.

12 LINERS AND BILLETS SHALL HAVE PHYSICAL AND MECHANICAL PROPERTIES IN ACCORDANCE WITH TABLE I AND:

A. BE TAPE-WRAPPED AND AUTOCLAVE CURED AT 225 TO 300 PSIG.

HAVE A MENIMUM AS-WRAPPED DENSITY OF:

1. 81 PERCENT OF CURED DENSITY, FOR BIAS-TAPE-WRAPPED BILLETS
2. 93 PERCENT OF CURED DENSITY, FOR STRAIGHT-TAPE-WRAPPED BILLETS

SPECIFIC GRAVITY AND HARBNESS PROPERTIES SHALL BE MEASURED ON EACH END OF EACH COMPONENT. VARIATIONS GREATER THAN 1.5 PERCENT SHALL BE SUBJECT TO ENGINEERING REVIEW ACTION.

ACTUAL PROPERTY VALUES SHALL BE DOCUMENTED.

TEST SPECIMENS SHALL BE OBTAINED FROM TEST RINGS MEASURING 1.50 BY 1.50 MINIMUM CROSS-SECTIONAL SIZE TAKEN FROM THE FOLIOWING CURED ABLATIVE COMPONENTS:

AFT END OF ITEM 10

END END OF ITEM 11

FAID END OF ITEM 12

D. AFT END OF ITEM 13

A MINIAUM OF 15 PERCENT OF-EACH TEST RING SHALL PE PROVIDED FOR DELIVERY TO AEROJET-GENERAL CORP.

INSTALL ENTRANCE, THROAT, AND EXIT CONE INSERTS, VSING AGC-34151-2 ADMESIVE. SURFACE CLEANING, COMPONENT FITTING, PROCESSING, AND BONDING PROCESS CONTROL SHALL BE IN ACCORDANCE WITH AGC 36497. AND AS FOLIOMS:

A. PROTECT IND FLANGE FACE DURING SANDBLASTING.

THE MACHINING CONTROL NOZZIE COMPONENT INSTALLATION, AND LEAK IEST CONTROL REQUIREMENTS OF AGC-36497 ARE NOT REQUIRED, AND SHALL BE DELETED.

ALL BONDLINES SHALL BE ULTRASONICALLY INSPECTED IN ACCORDANCE WITH OLD NO. LRU-10). EVIDENCE OF VOIDS AND UNBOXOLD AREAS SHALL BE SUBJECT TO EMGINEERING REVIEW ACTION.

AS PROCESS CLASS OVERWRAP IN ACCORDANCE WITH THE FOLLOWING PROCEDURE:

A. REINFORCED PLASTIC AND PRIMED STEEL SURFACES SHALL BE PREPARED FOR APPLICATION OF GLASS WRAP IN ACCORDANCE WITH AGC-36498.

IMPREGNATE GLASS CLOTH WITH EPON 828 RESIN. CATALYST MAY BE ADDED TO THE RESIN TO RESULT IN A RUOM-TEMPERATURE CURING SYSTEM.

THE EMPREGNATED GLASS CLOTH SHALL BE LAID UP CIRCUMFERENTIALLY WITH OVERLAPPING JOINTS, TO RESULT IN THE DESIGNED THICKNESS.

APPLY A VACUUM BAG OVER THE LAY-UP AND MAINTAIN A MINIMUM OF 20 IN. OF MERCURY.

CURE AT ROOM TEMPERATURE FOR A MINIMUM OF 48 HOURS. THE SURFACE FINISH OF THE GLASS WRAP SHALL BE "AS FABRICATED."

A FLAT TEST PAINT, REPRESENTING THE OVERWAPE CONSTRUCTION, SHALL BE PERPARED AND PROCESSED SIMULTANCOUSLY CITY THE CLASS WRAP. TENSILE STREAM AND MODULUS PROPERTIES SHALL BE DETERMINED FROM THE TEST PANEL AND RECORDED.

PRE-PREG MATERIAL RESIN CONTENT, WIS

FLOW. WTS

FINAL CURED BILLEY

EQUIVALENT MATERIALS

VOLATILES. NTS MAX

SPECIFIC GRAVITY, MIN

VOLATILES, HTS WAX

HARDNESS (ROCKWELL R), MIN

UNCURED RESIN CONTENT, MTS MAX

TABLE I

SILICA PHENOLIC (SP8030-96)

29 - 35 8 - 15

6.0

1,69

120

0.5

CANVAS

5 - 17

7.5

1,32

111

4.0 0.5

4KX007 CA-2213

PHENOLIC (KF-418)

G. THE QUALITY ASSURANCE PROVISIONS OF AGC-36515 SHALL APPLY.

FILE GAPS WITH AGC-34076, CLASS 5, SEALING COMPOUND.

ALL COMPONENTS SHALL BE PROTECTED FROM CONTAMINATION, CORROSION, AND DAMAGE DURING FABRICATION, HANDLING, AND STORAGE IN ACCORDANCE WITH MILT-Filb, METHOD III.

MARK PER ASD SZIS-H WITH 1/47GOB AND ASPLICABLE DASH NO. AND ASSIGNED SERIAL NUMBER	<u> </u>

Figure 8. - Nozzle No. 2 (Sheet 1 of 2)

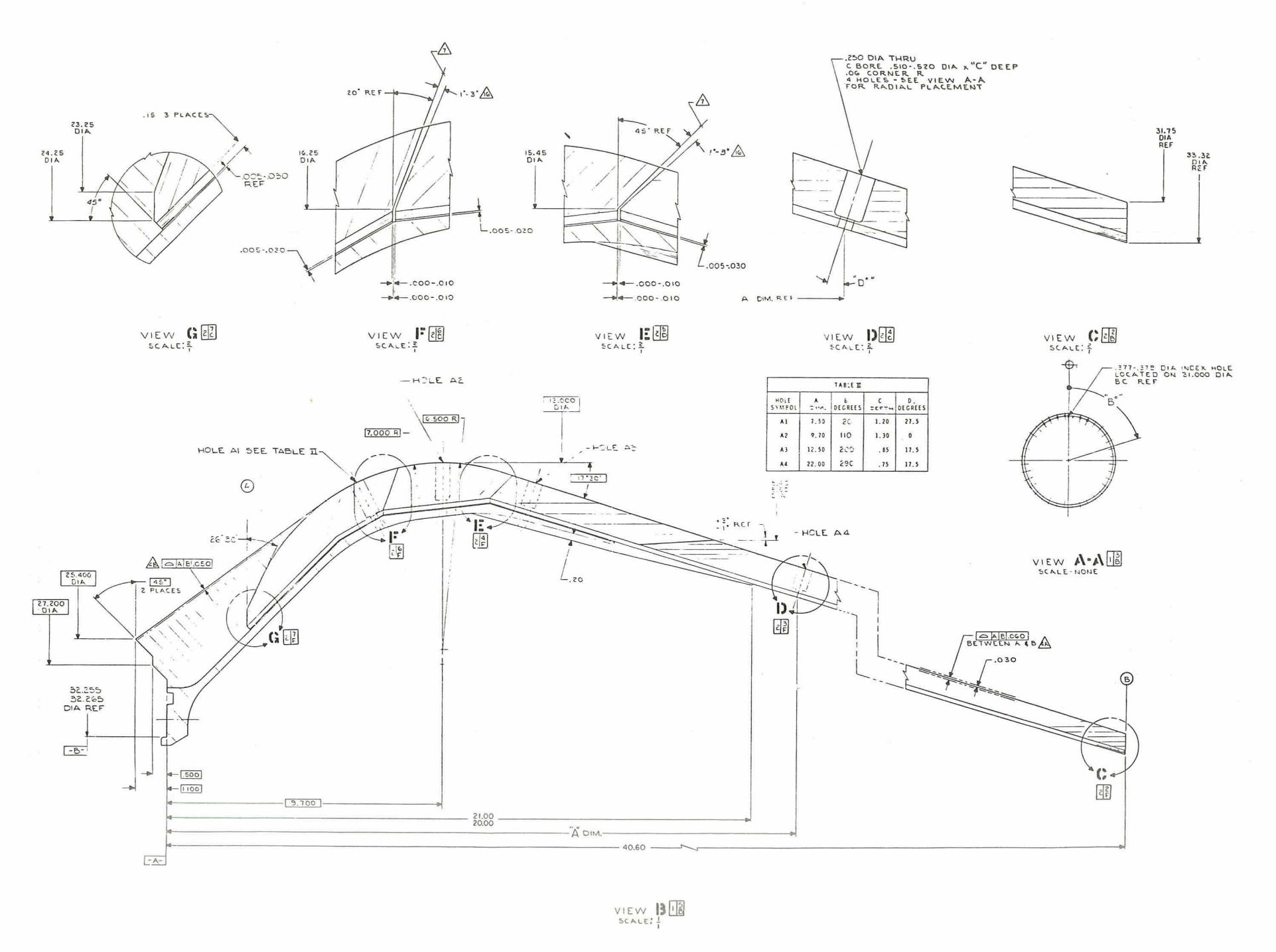
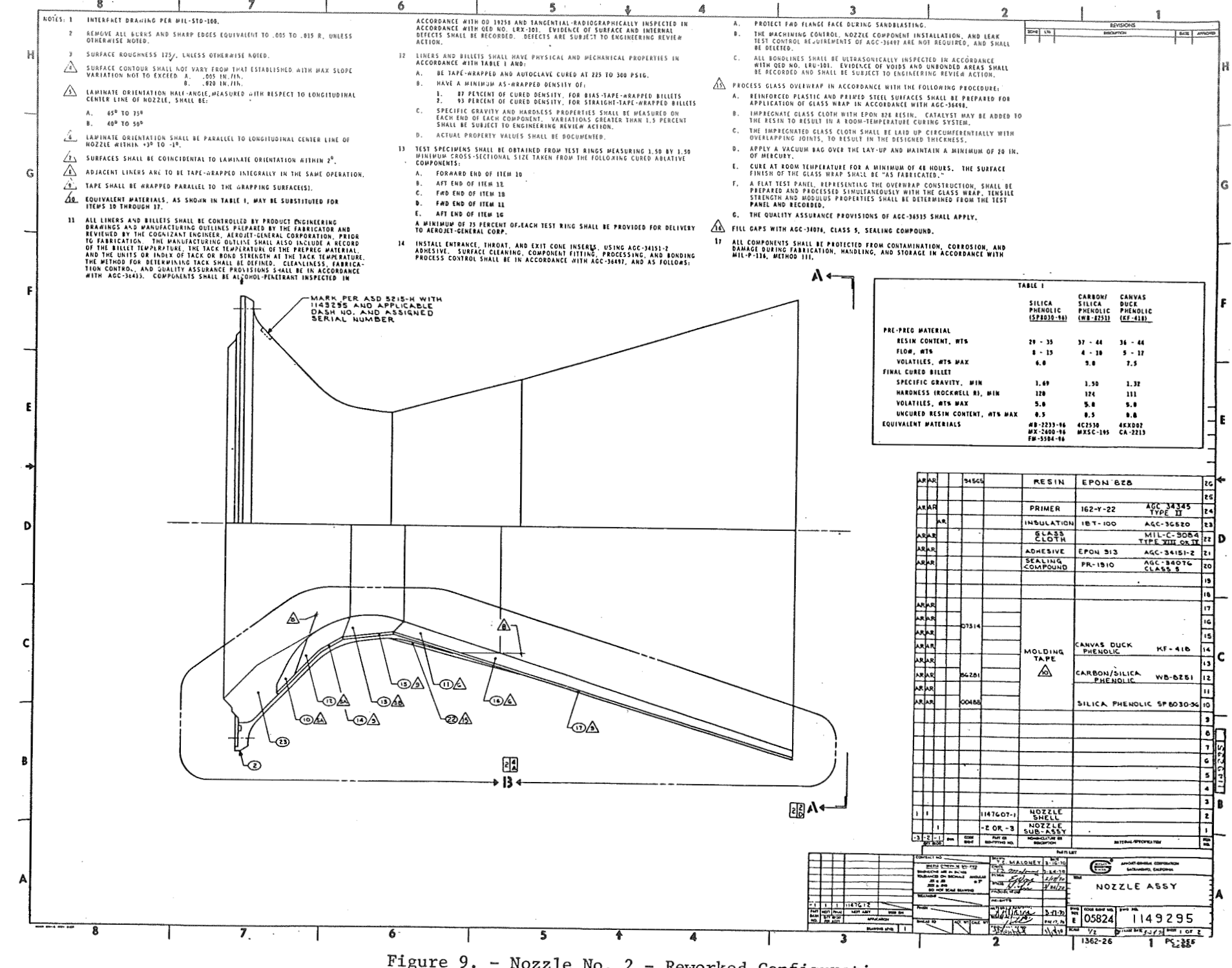
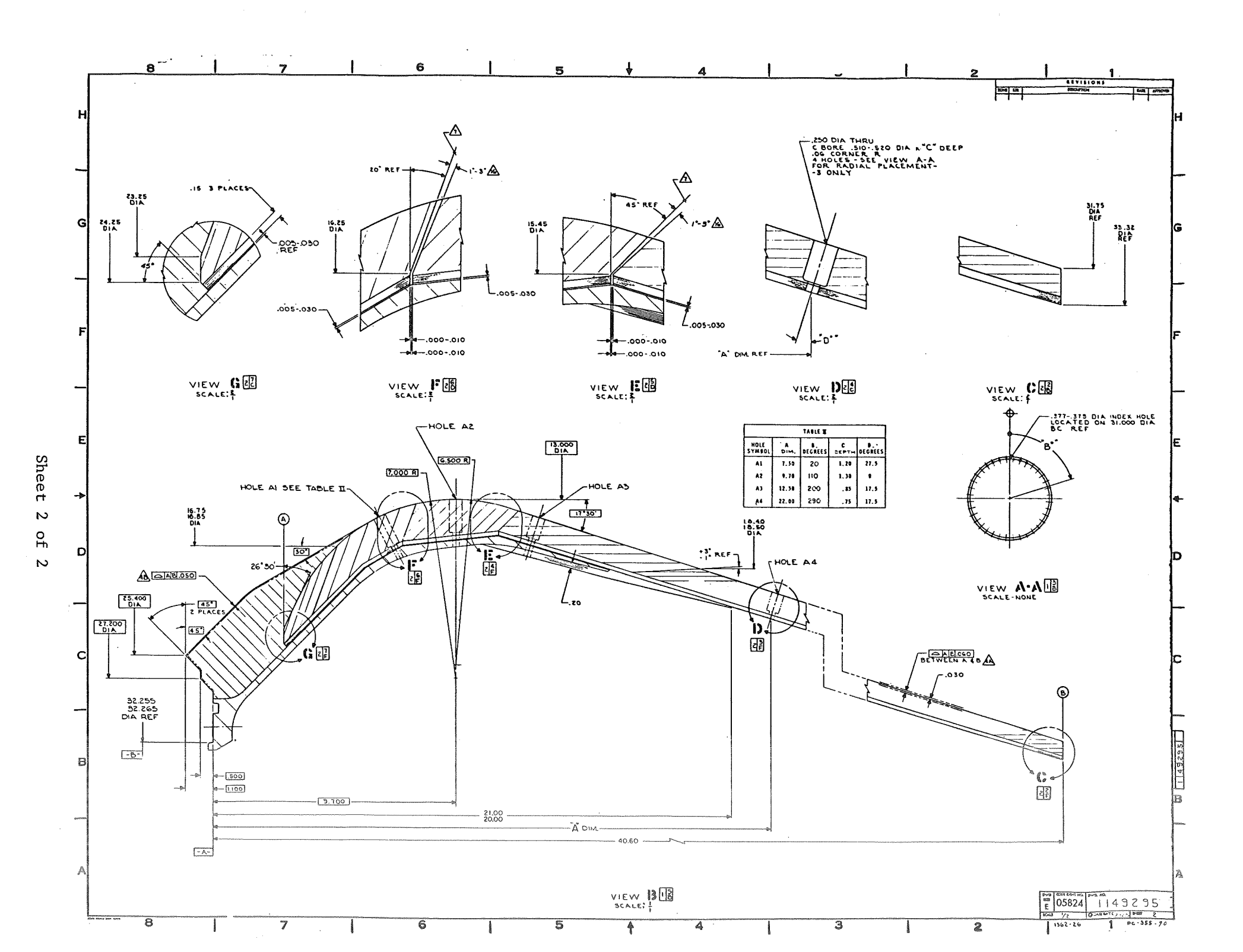


Figure 8. - Nozzle No. 2 (Sheet 2 of 2)



Ō Ö

Figure 9. - Nozzle No. 2 - Reworked Configuration



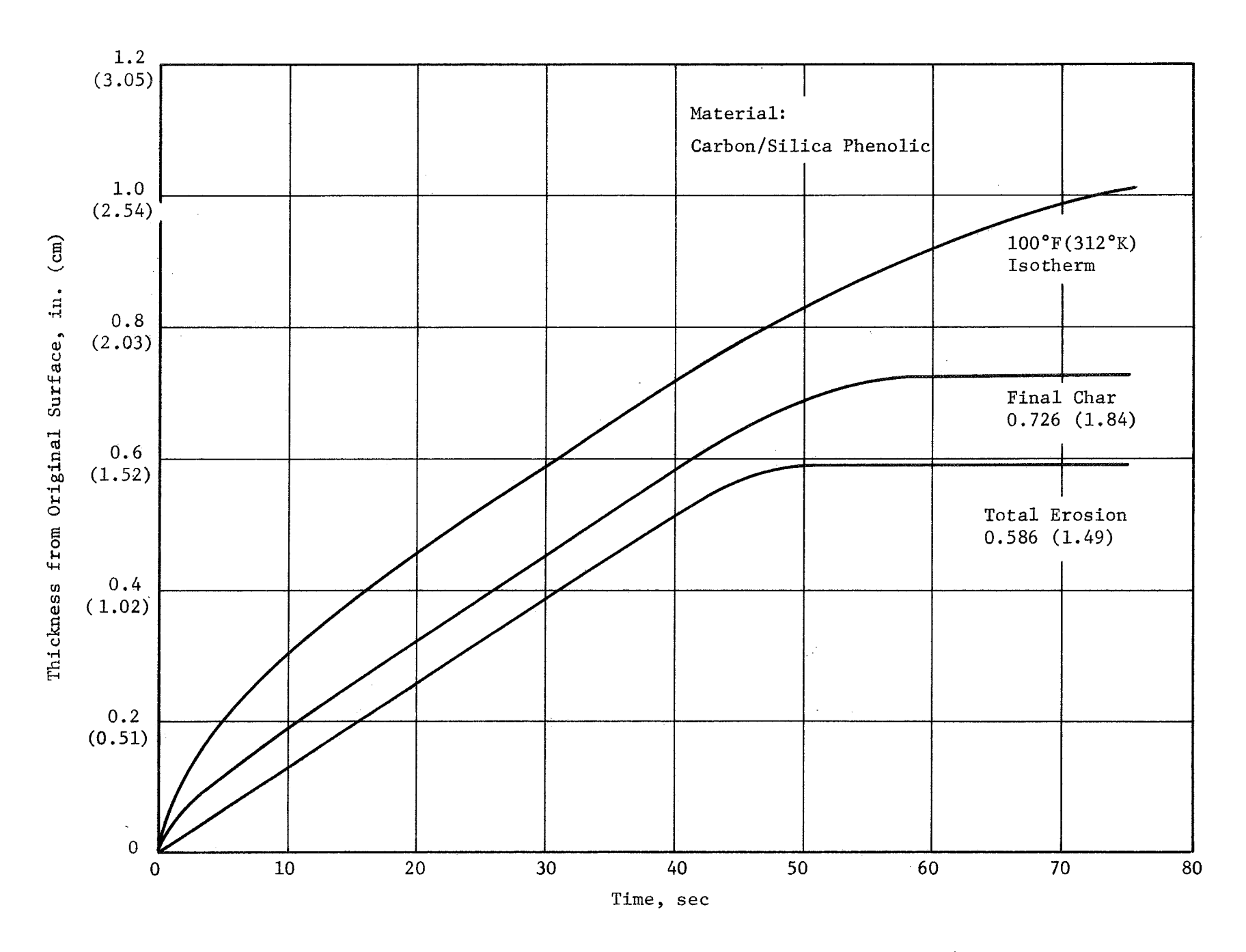


Figure 10. - Erosion, Char, and Thermal Zone at Throat, Nozzle No. 1

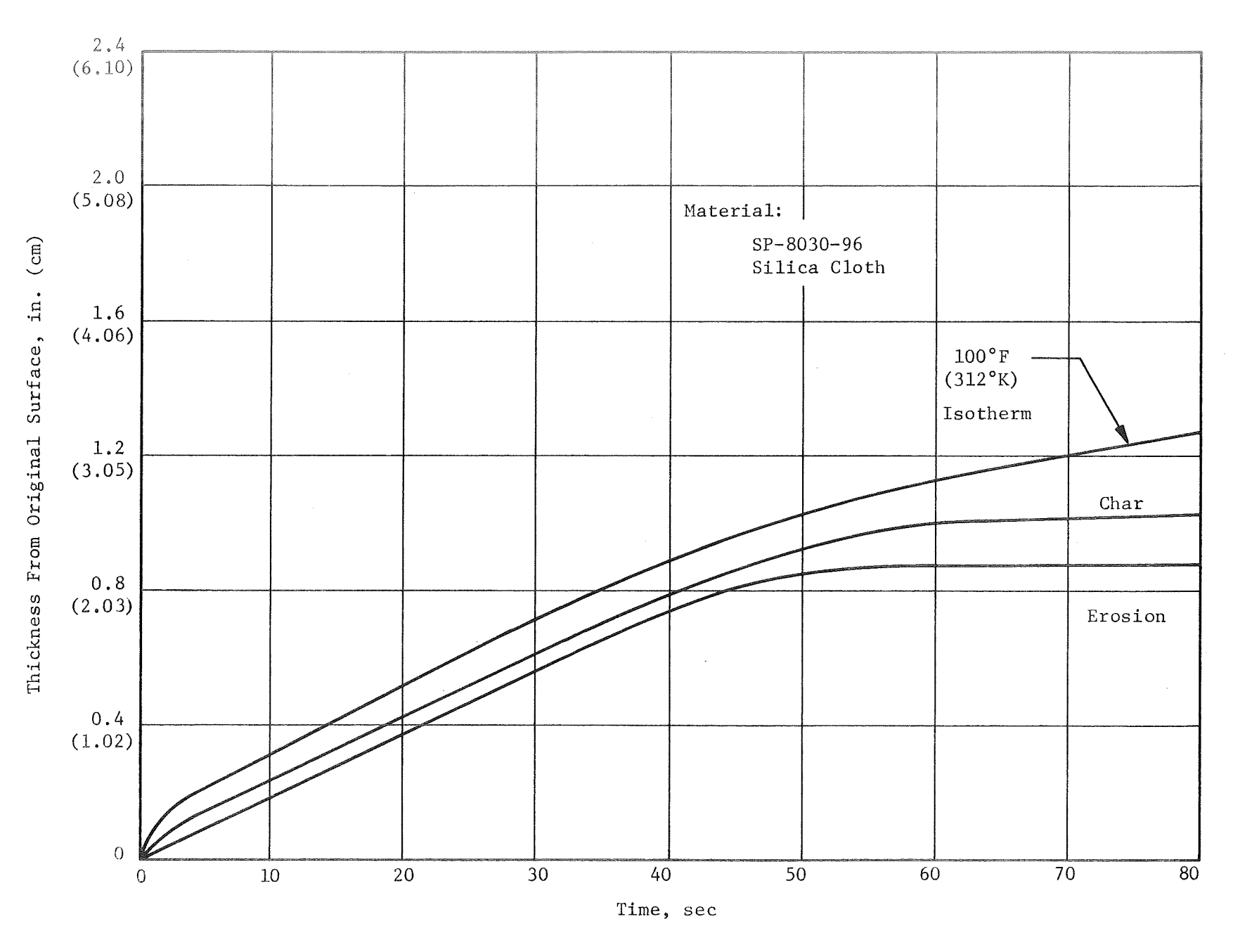


Figure 11. - Erosion, Char Depth and Thermal Zone Depth at Throat Station, Nozzle No. 2

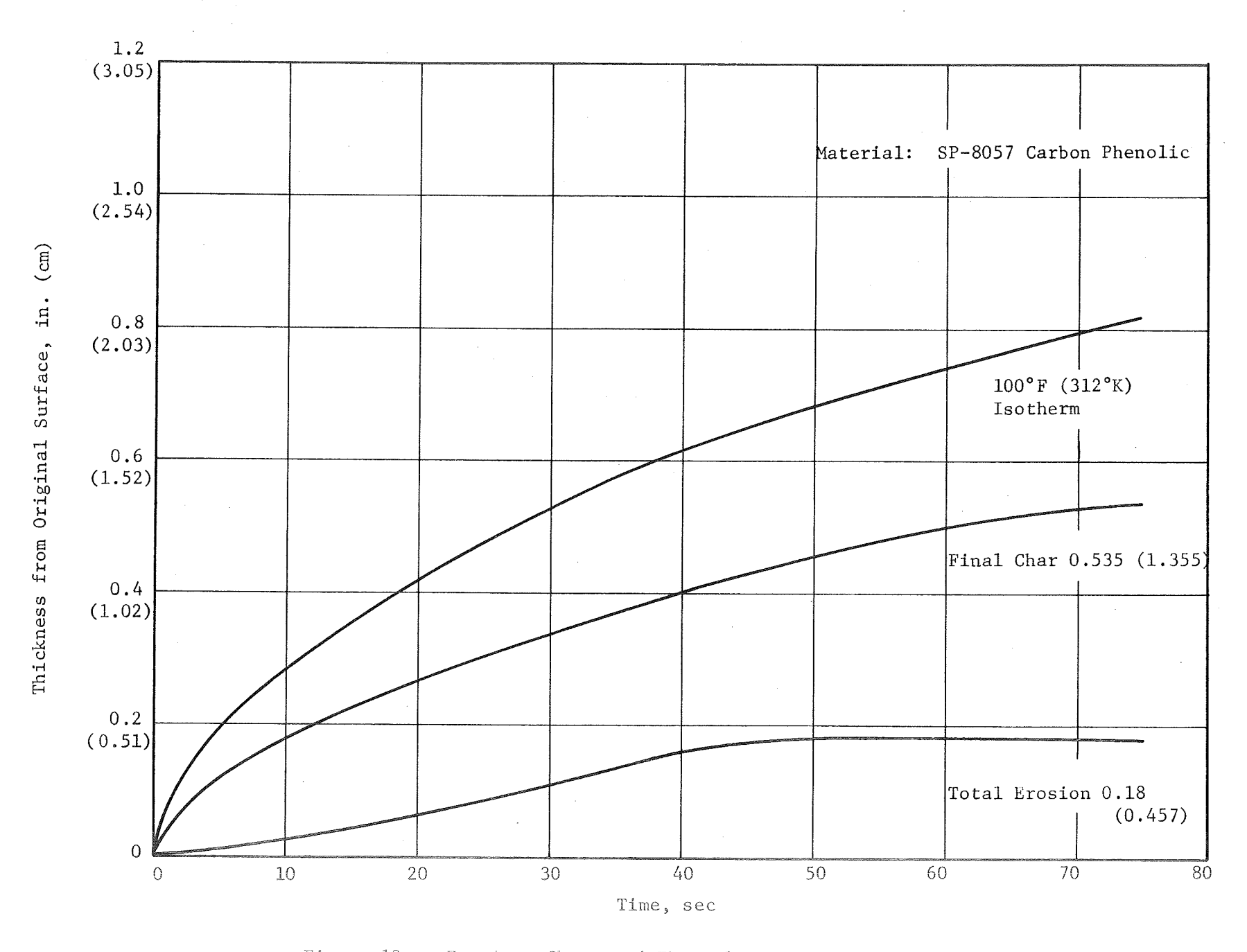


Figure 12. - Erosion, Char, and Thermal Zone Depth at Throat Station, Candidate Nozzle

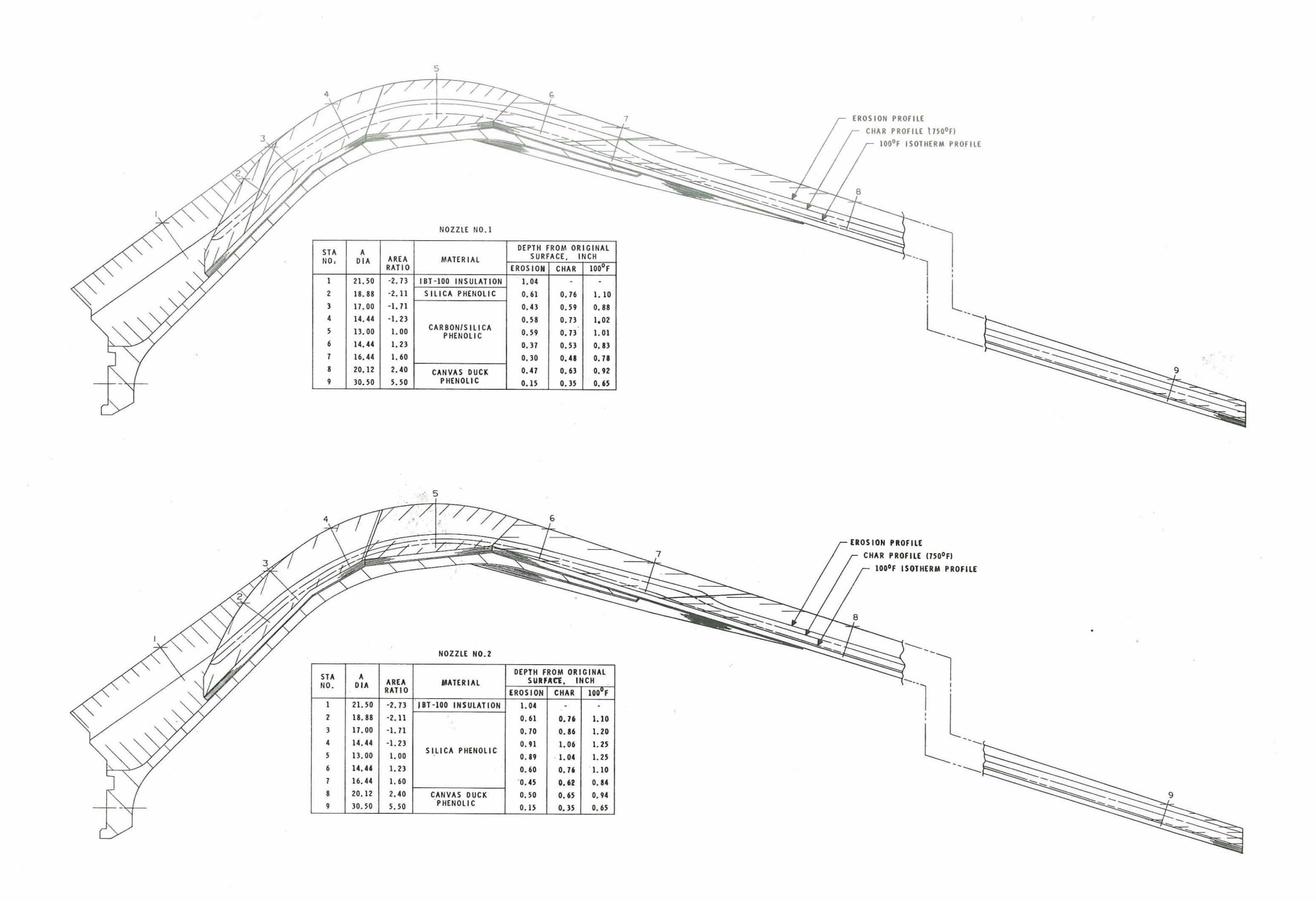


Figure 13A. - Thermal Response Profile, Nozzles No. 1 and 2

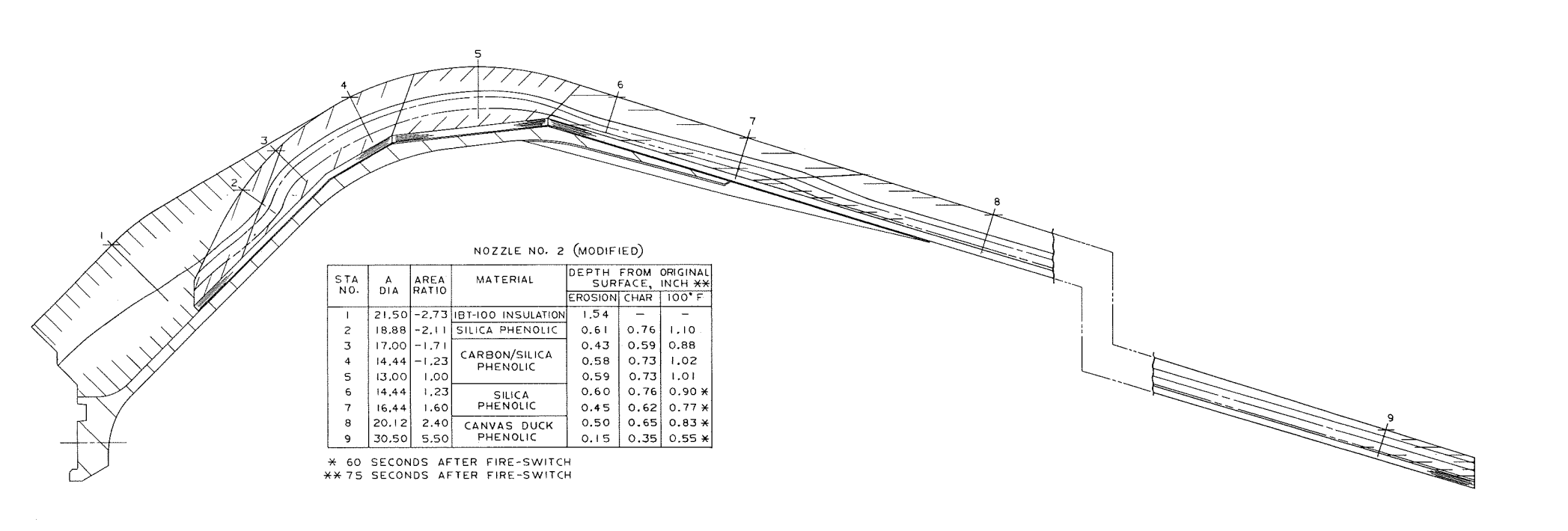
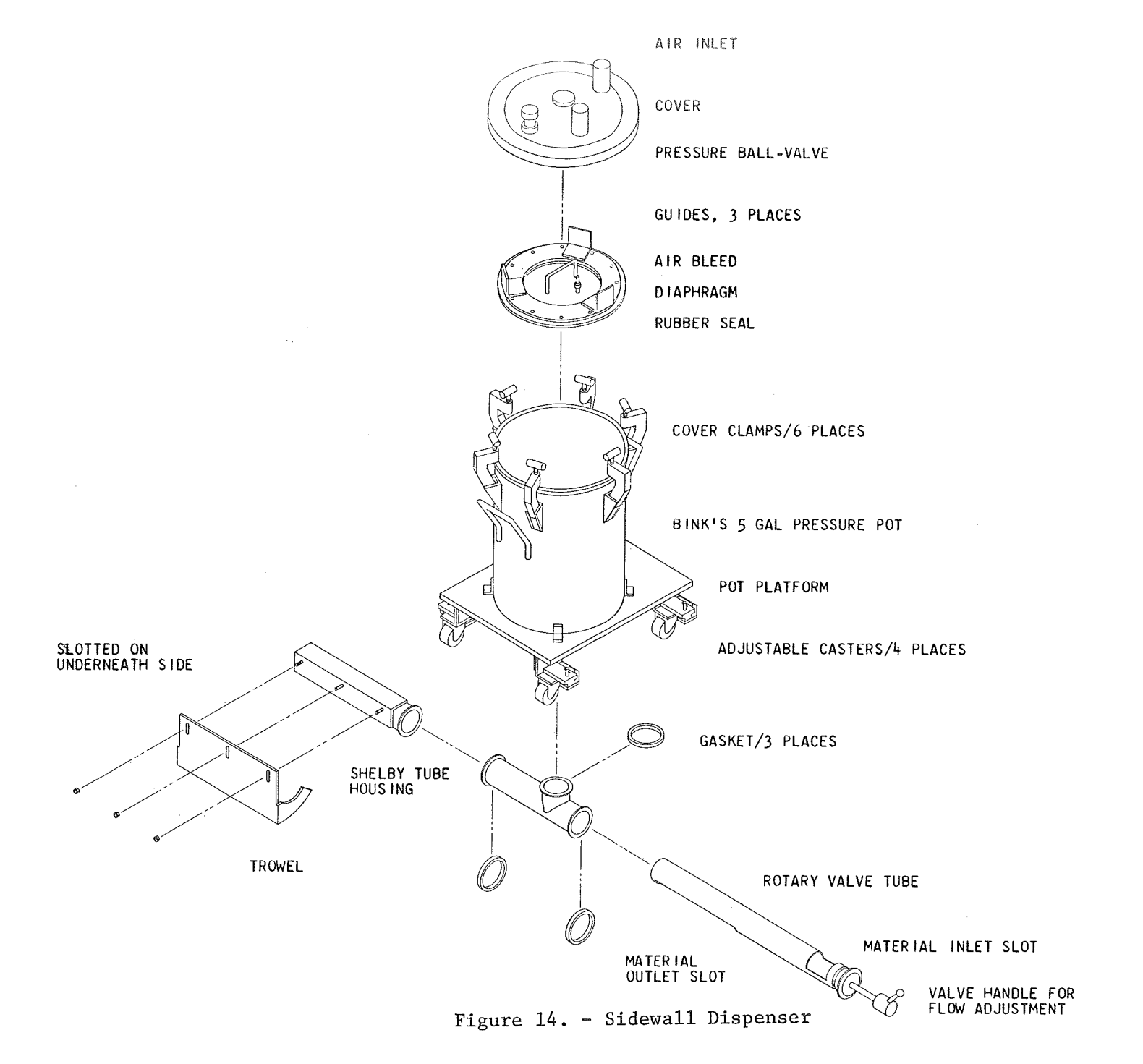


Figure 13B. - Thermal Response Profile, Nozzle No. 2



CENTER ING HUB

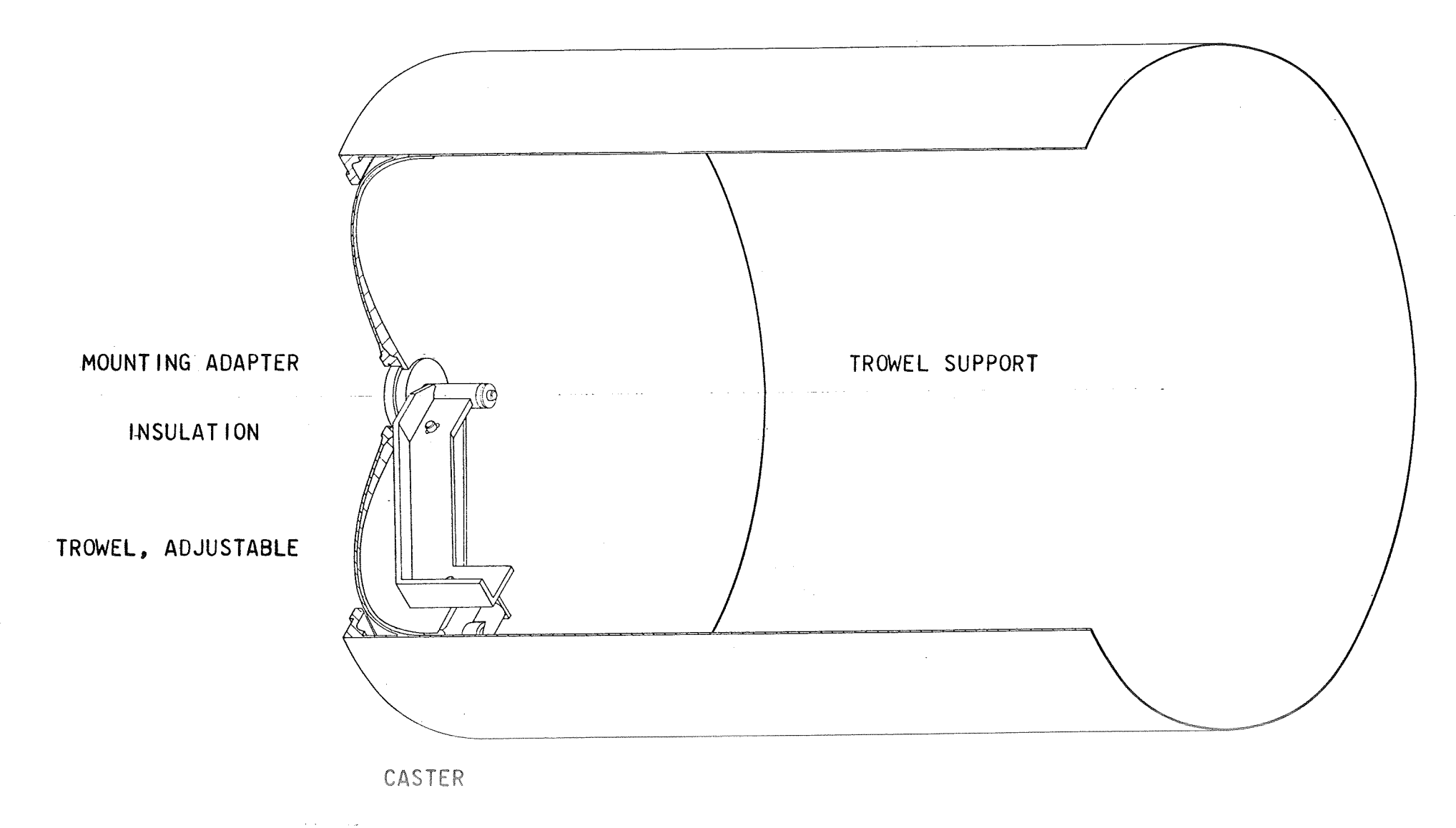
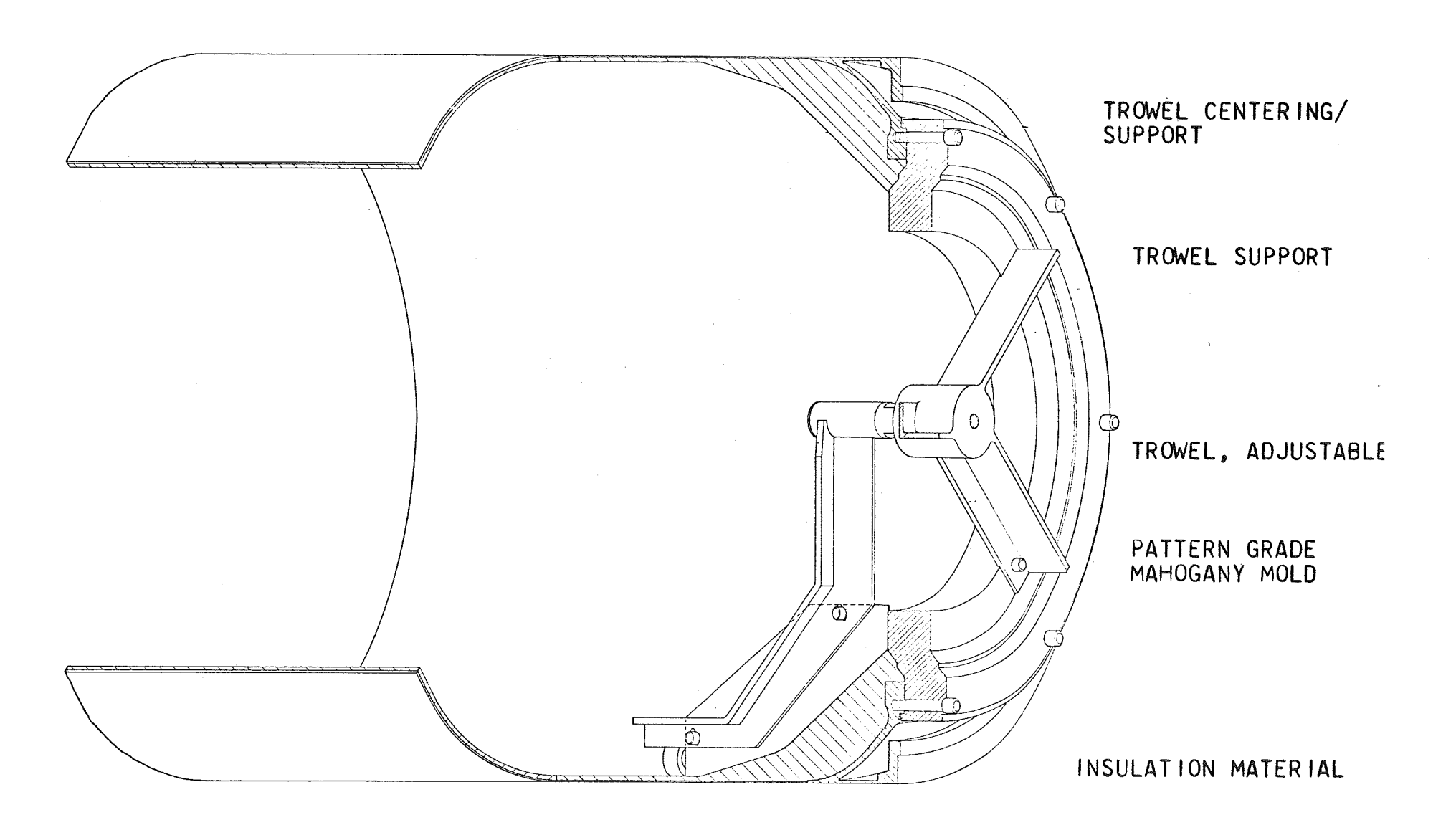


Figure 15. - Fwd Dome Sweep Template



CASTER

Figure 16. - Aft Dome Sweep Template

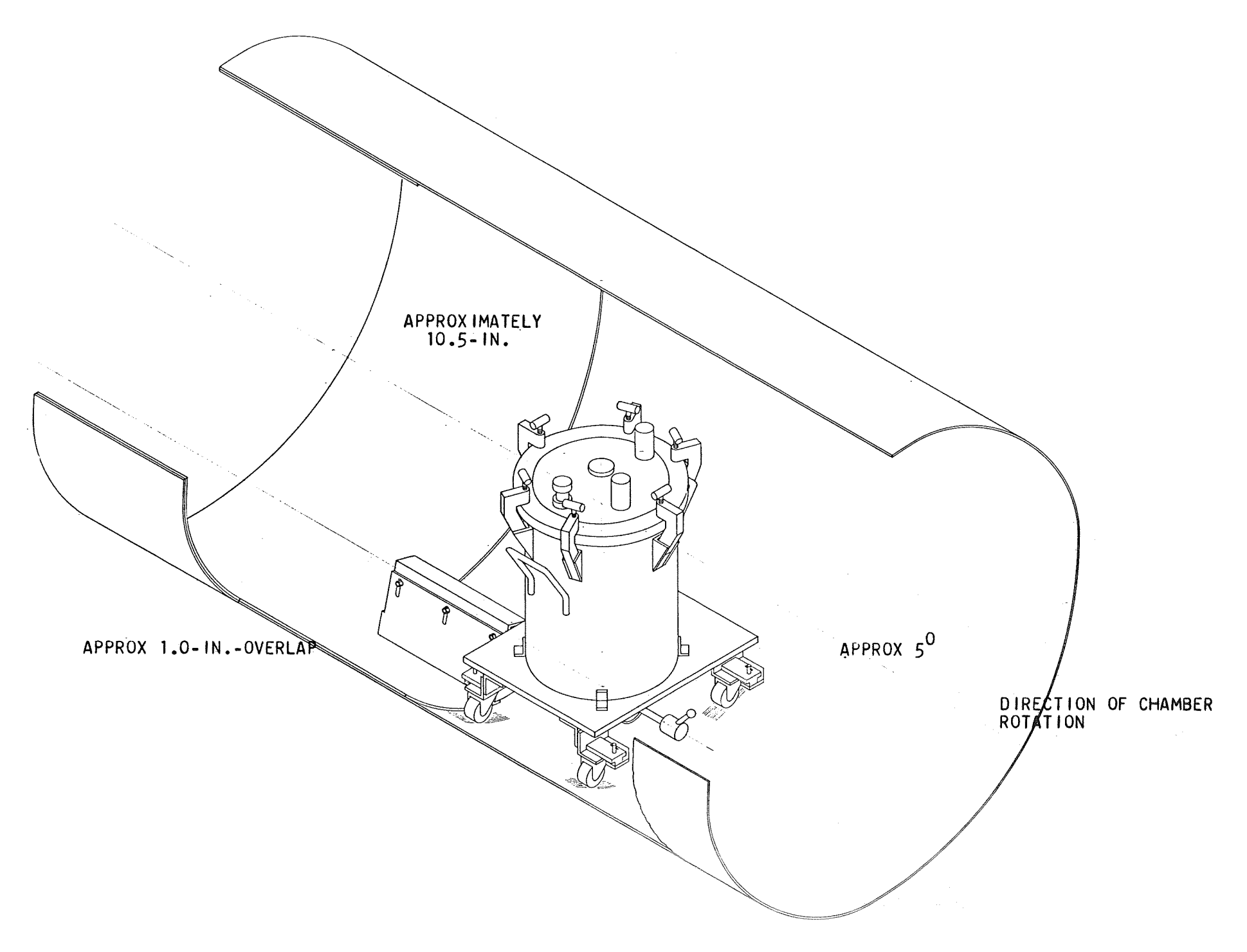


Figure 17. - Sidewall Dispenser Orientation

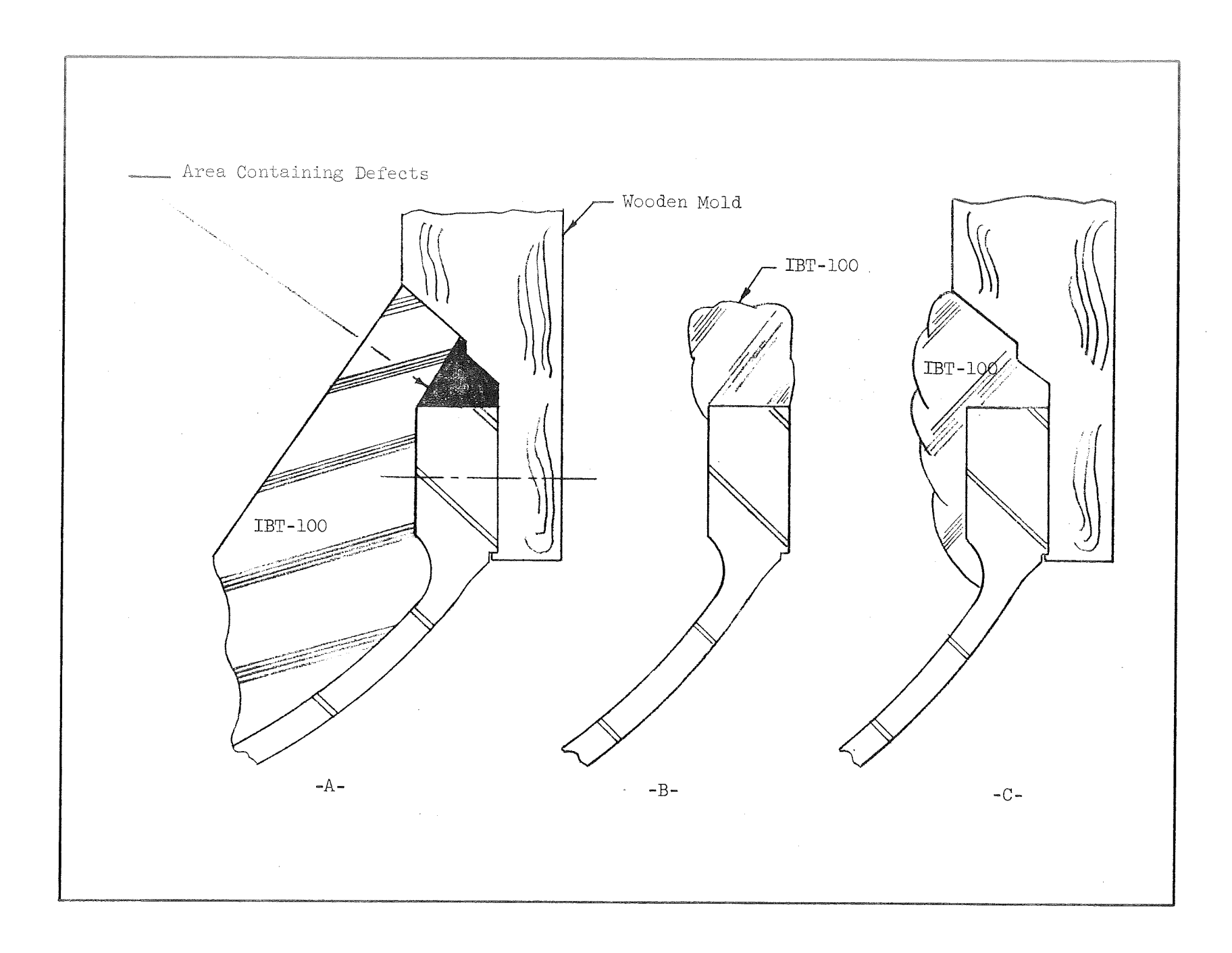


Figure 18. - Aft Flange Insulation Details

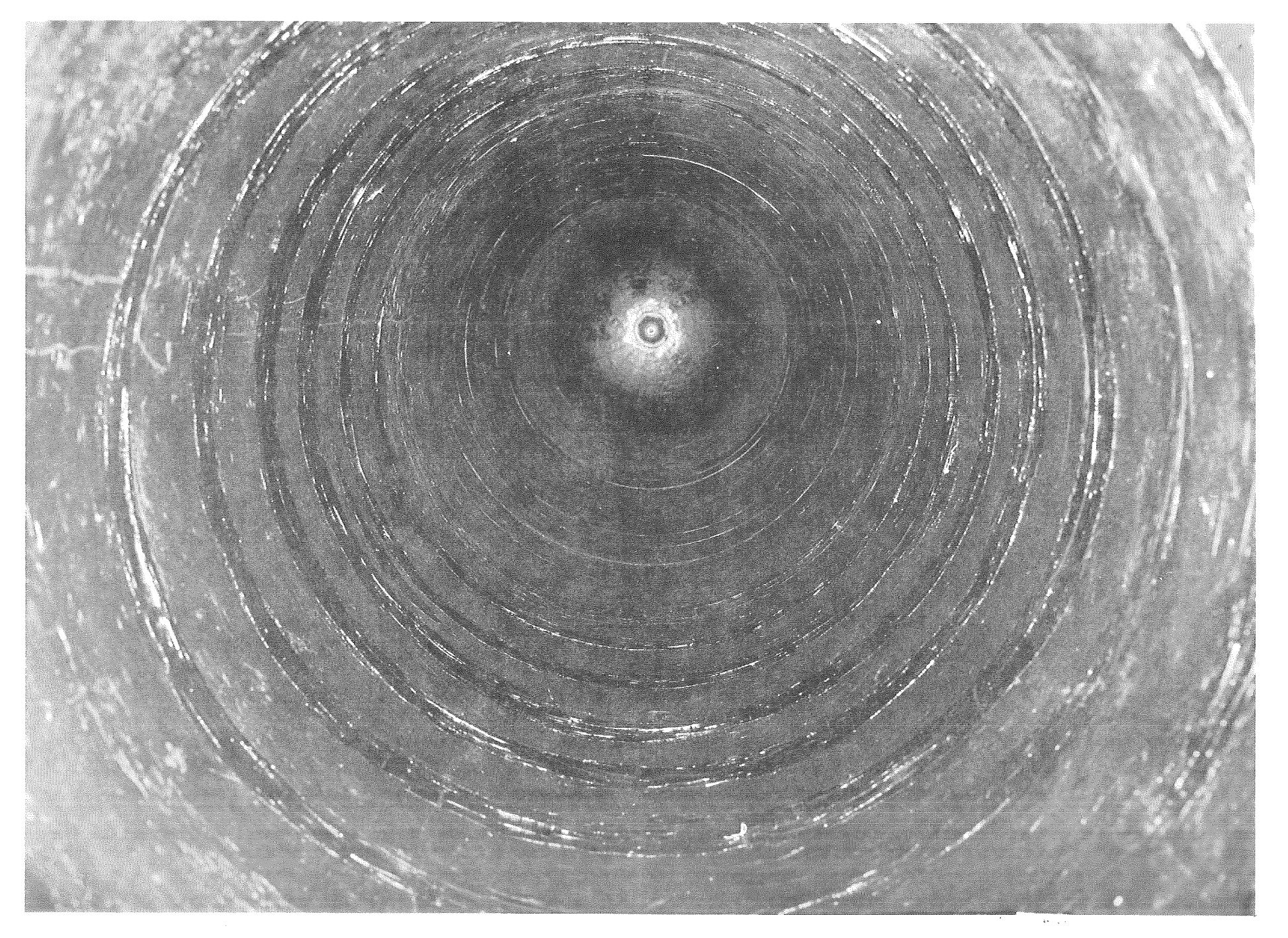


Figure 19. - View of Completed Insulation, Motor LCAN-01

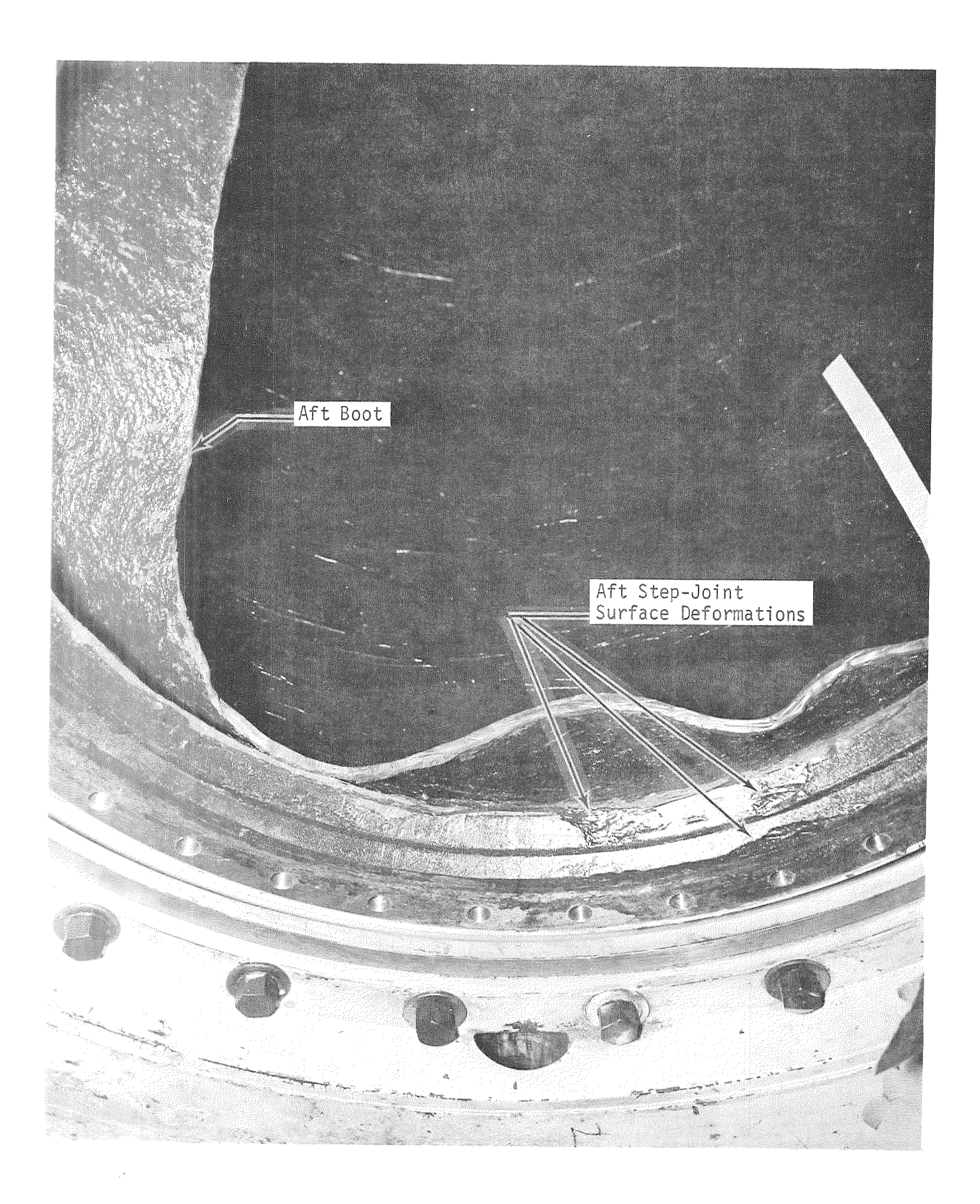


Figure 20. - Aft Step Joint and Boot, Motor LCAN-02

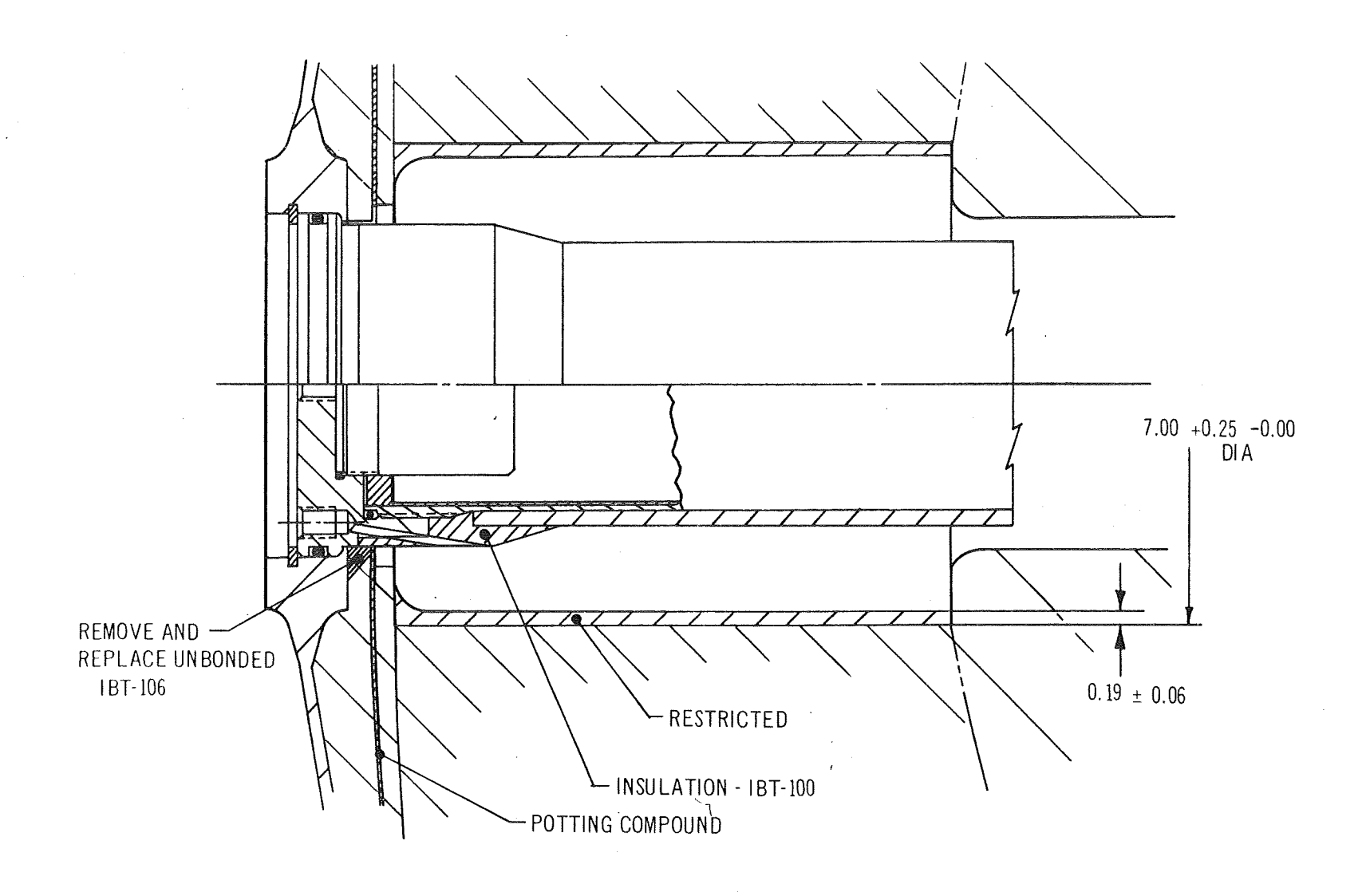


Figure 21. - Motor LCAN-02 Rework

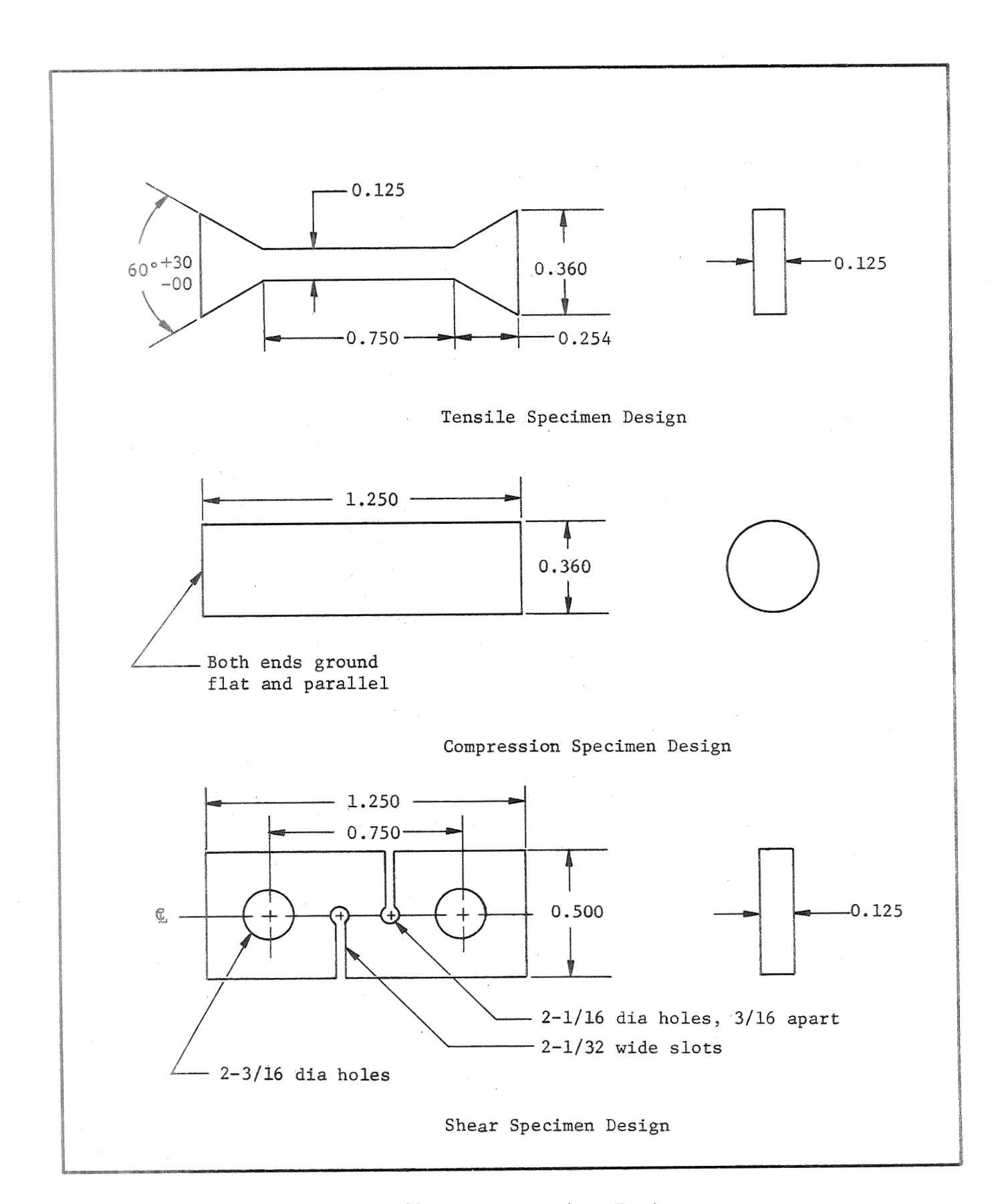


Figure 22. - Test Specimen Design

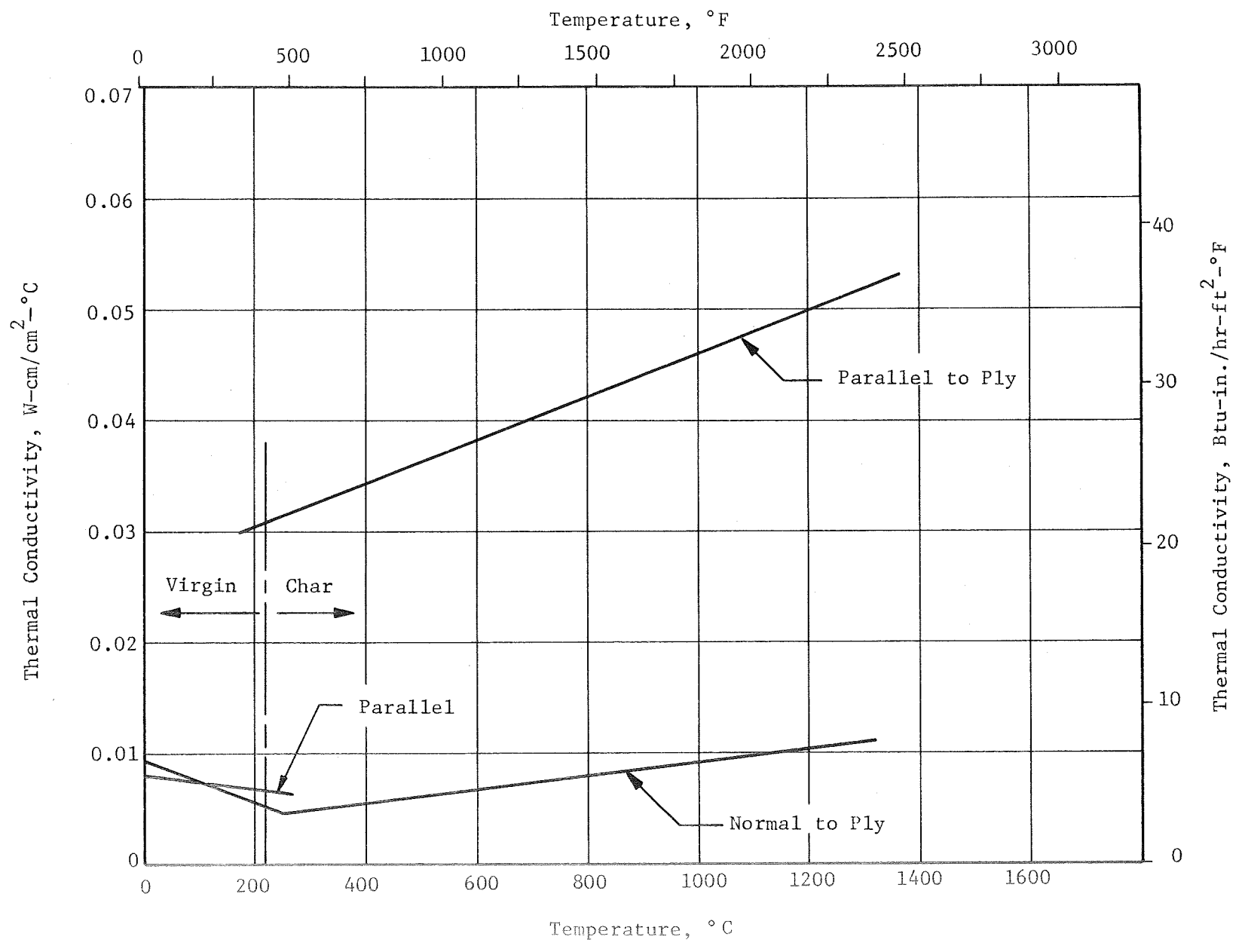


Figure 23. - Thermal Conductivity of MXSC-195 Carbon-Silica Composite



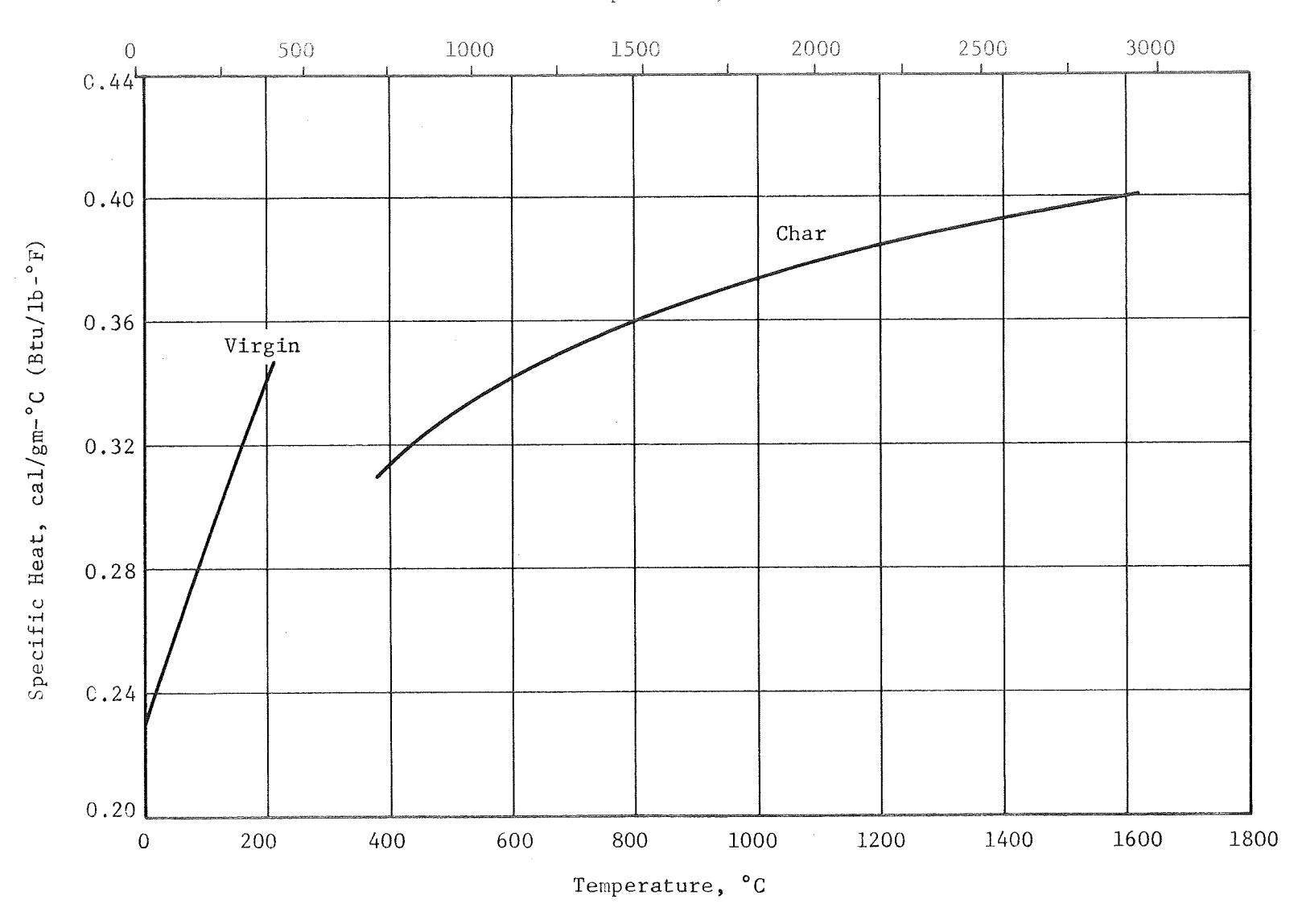


Figure 24. - Specific Heat of MXSC-195 Carbon Silica Phenolic Composite

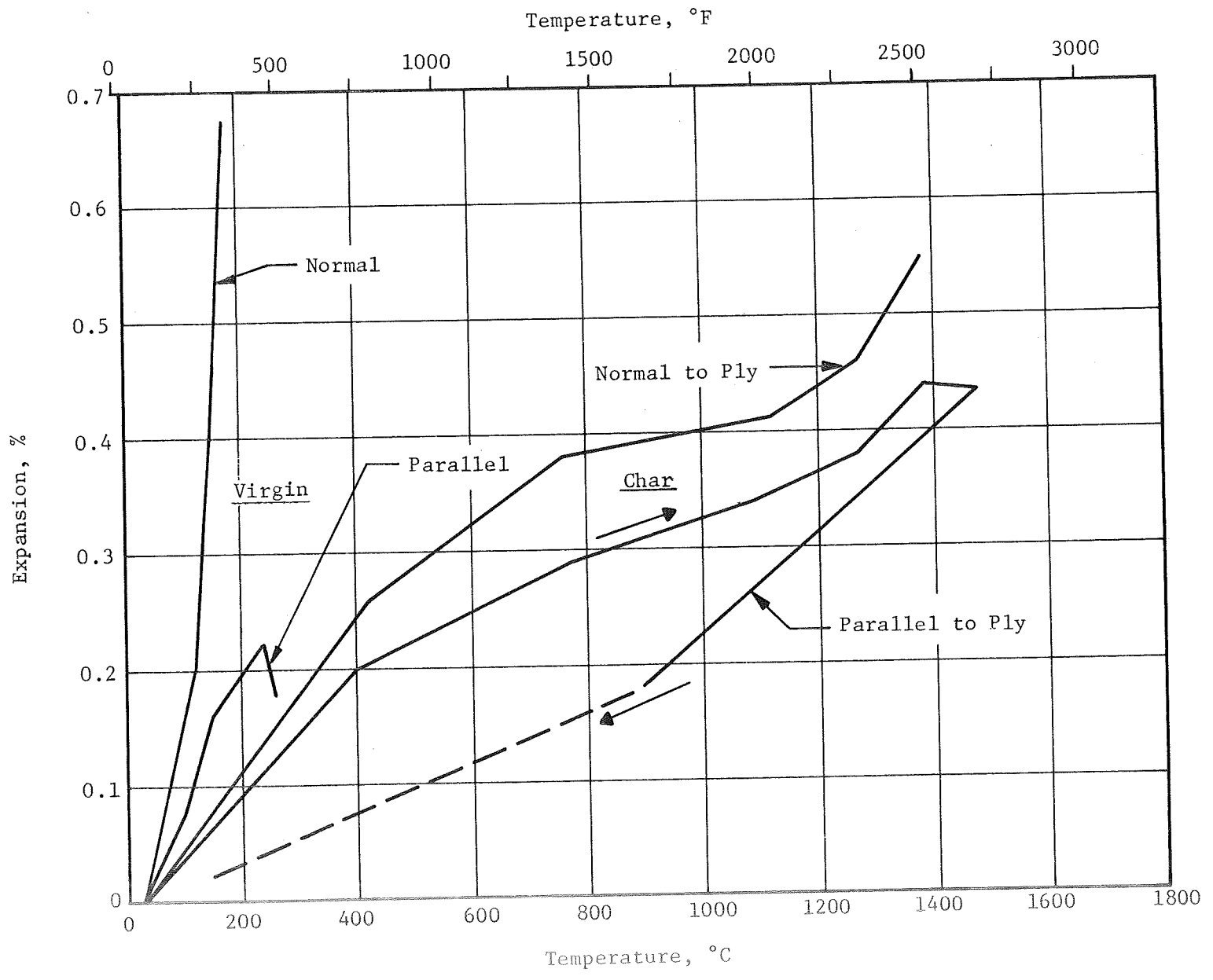


Figure 25. - Thermal Expansion of MXSC-195 Carbon-Silica Composite

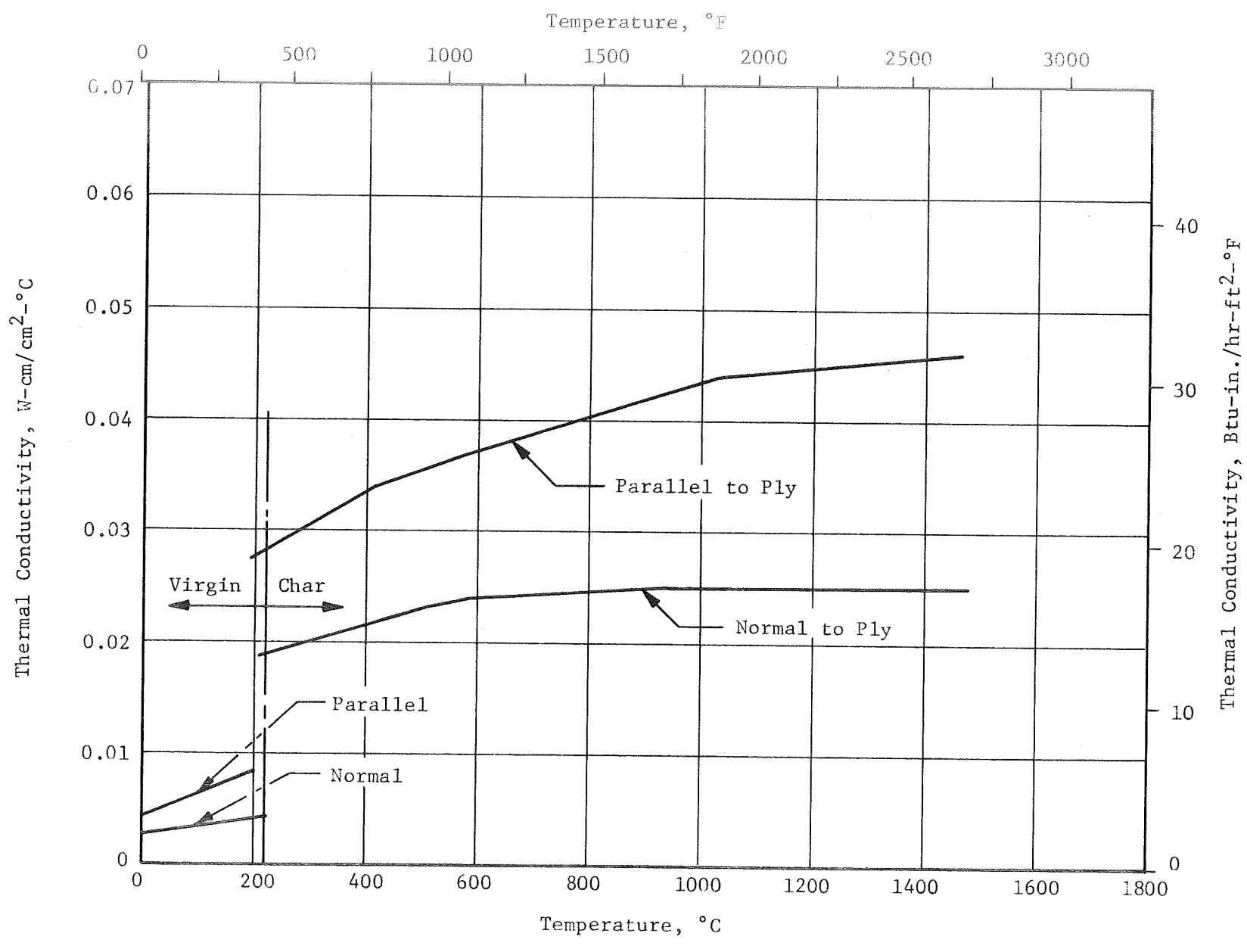


Figure 26. - Thermal Conductivity of 4KXD02 Canvas Composite

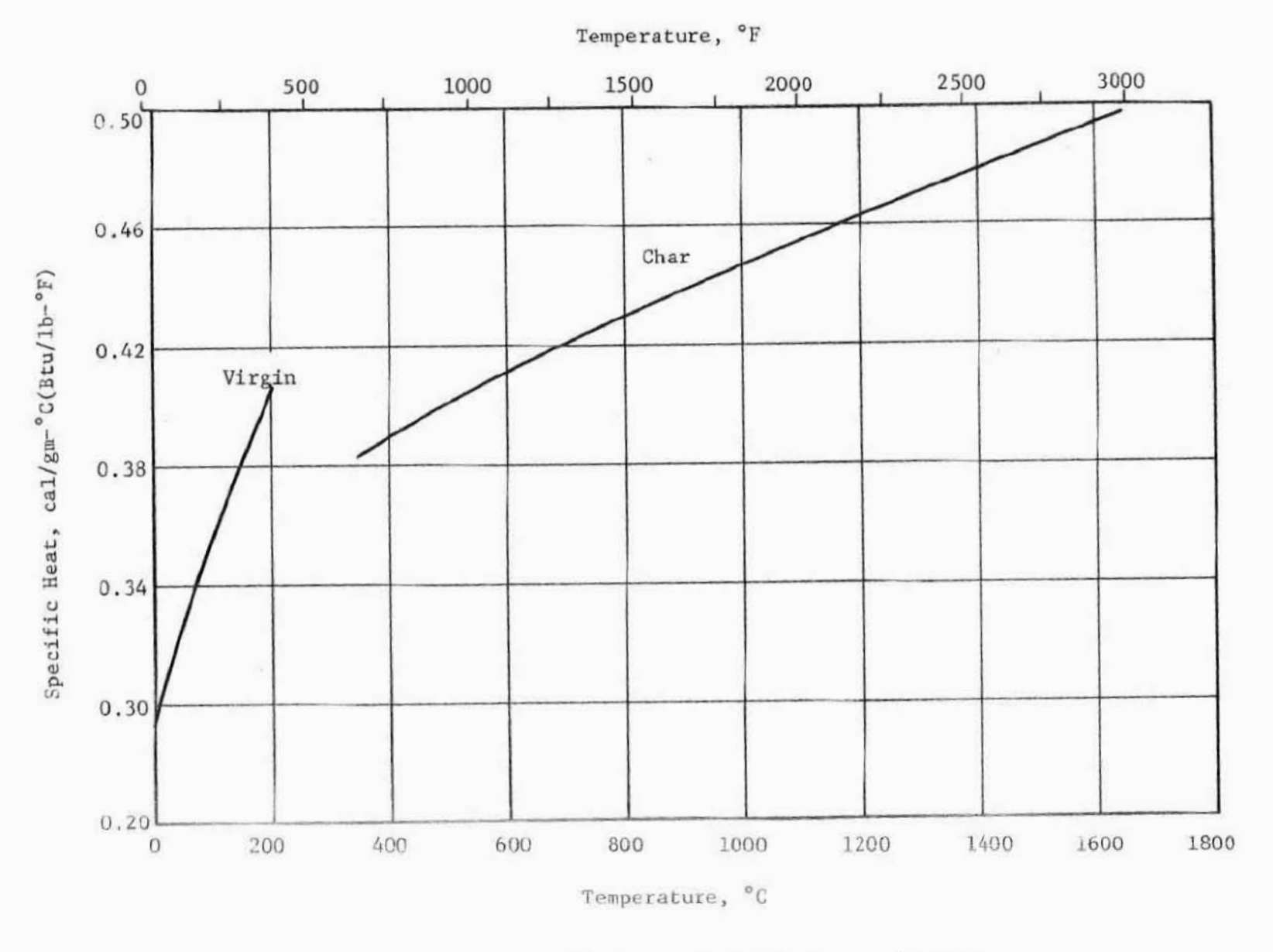


Figure 27. - Specific Heat of 4KXD02 Canvas Composite

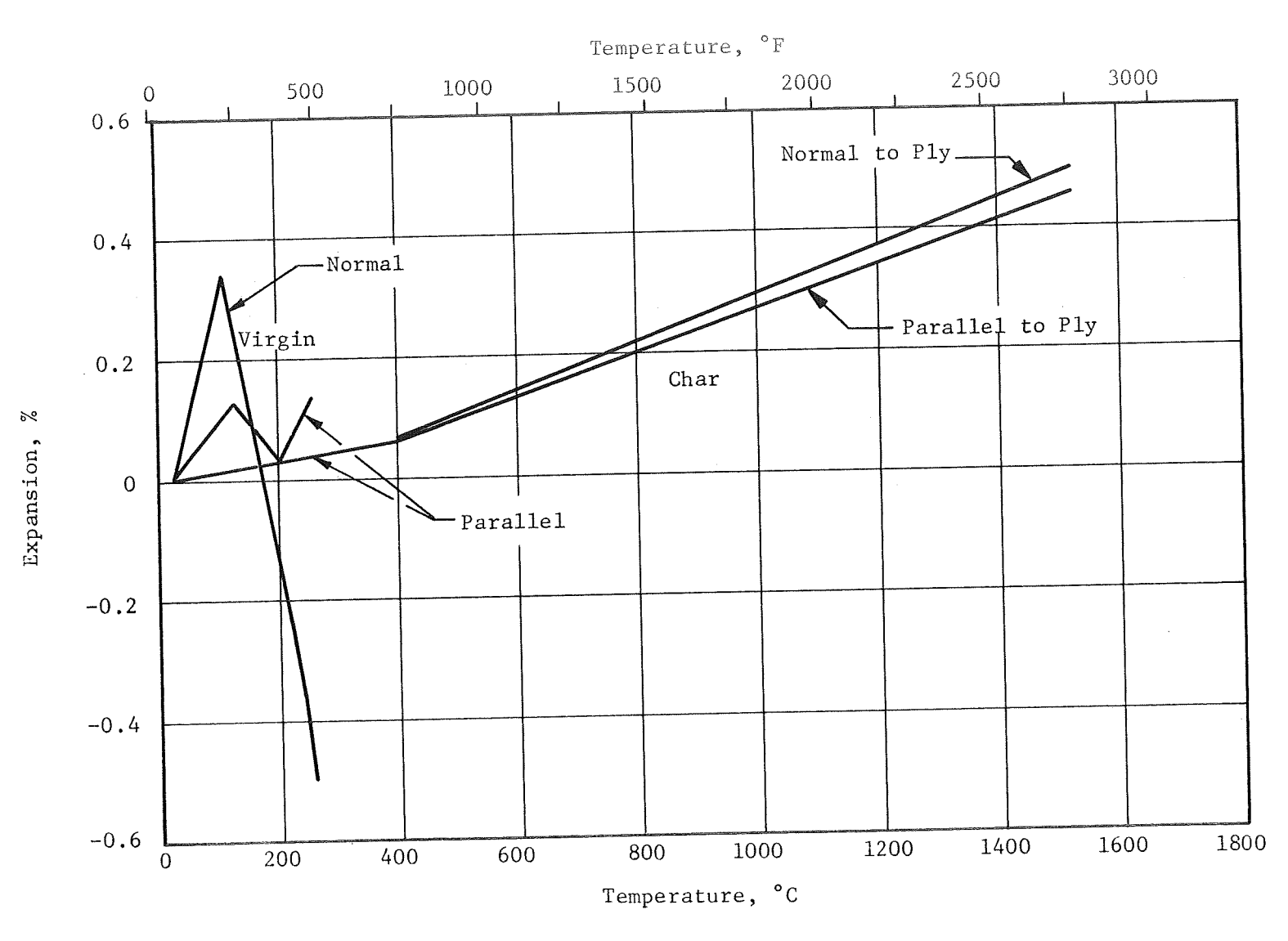


Figure 28. - Thermal Expansion of 4KXD02 Canvas Composite

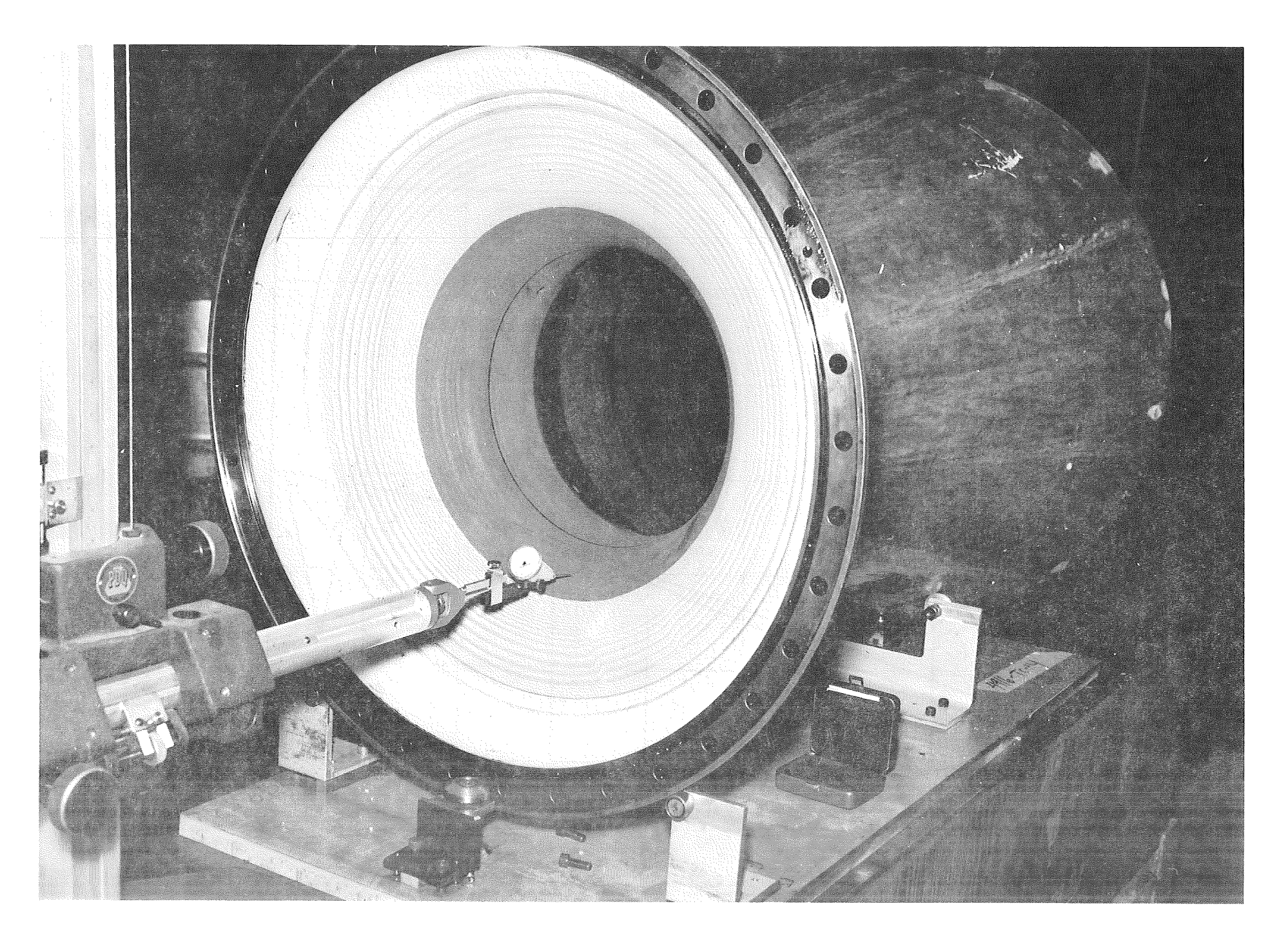
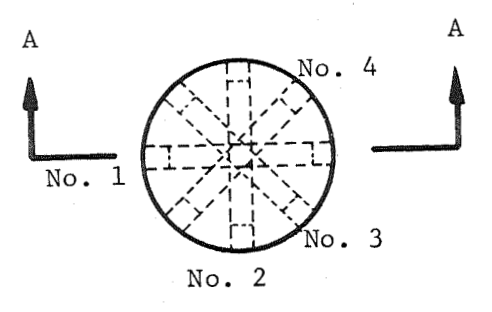


Figure 29. - Profile Mapping of LCAN-01 Nozzle



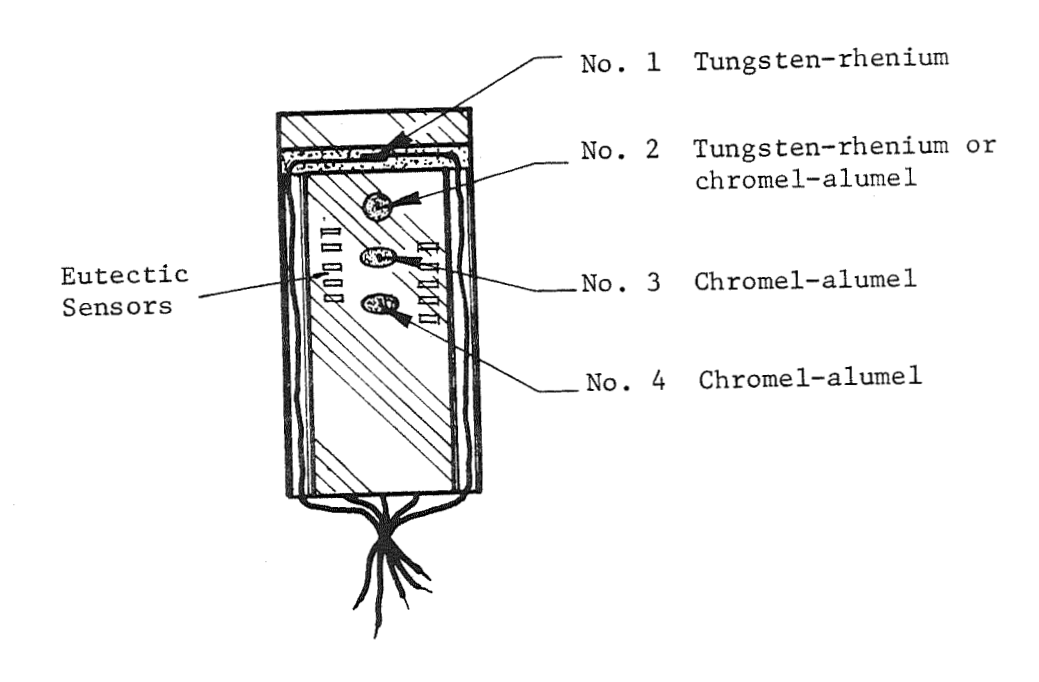


Figure 30. - Thermal Sensor Assembly

Section A-A

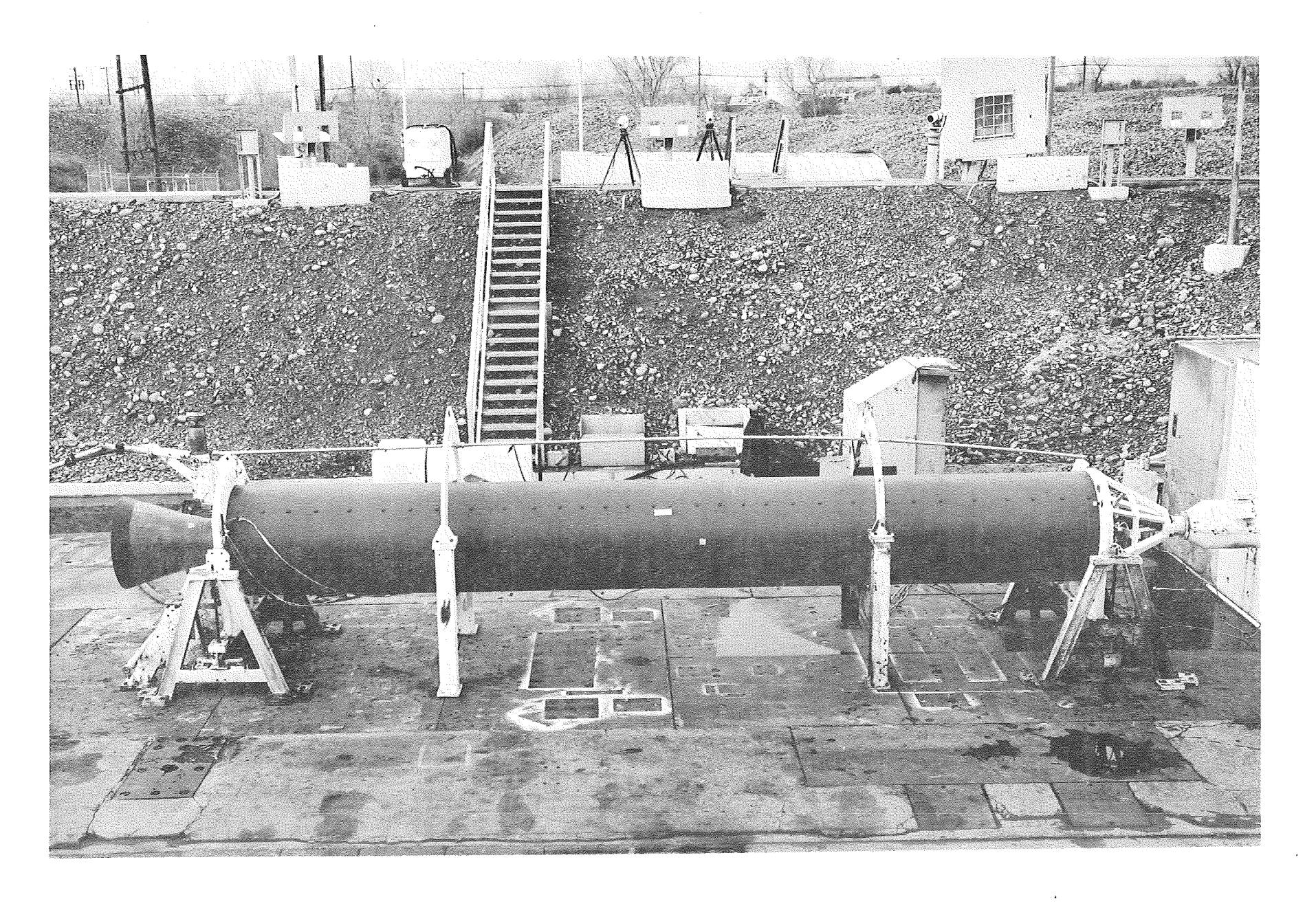


Figure 31. - View of Motor LCAN-01 Prior to Test Firing

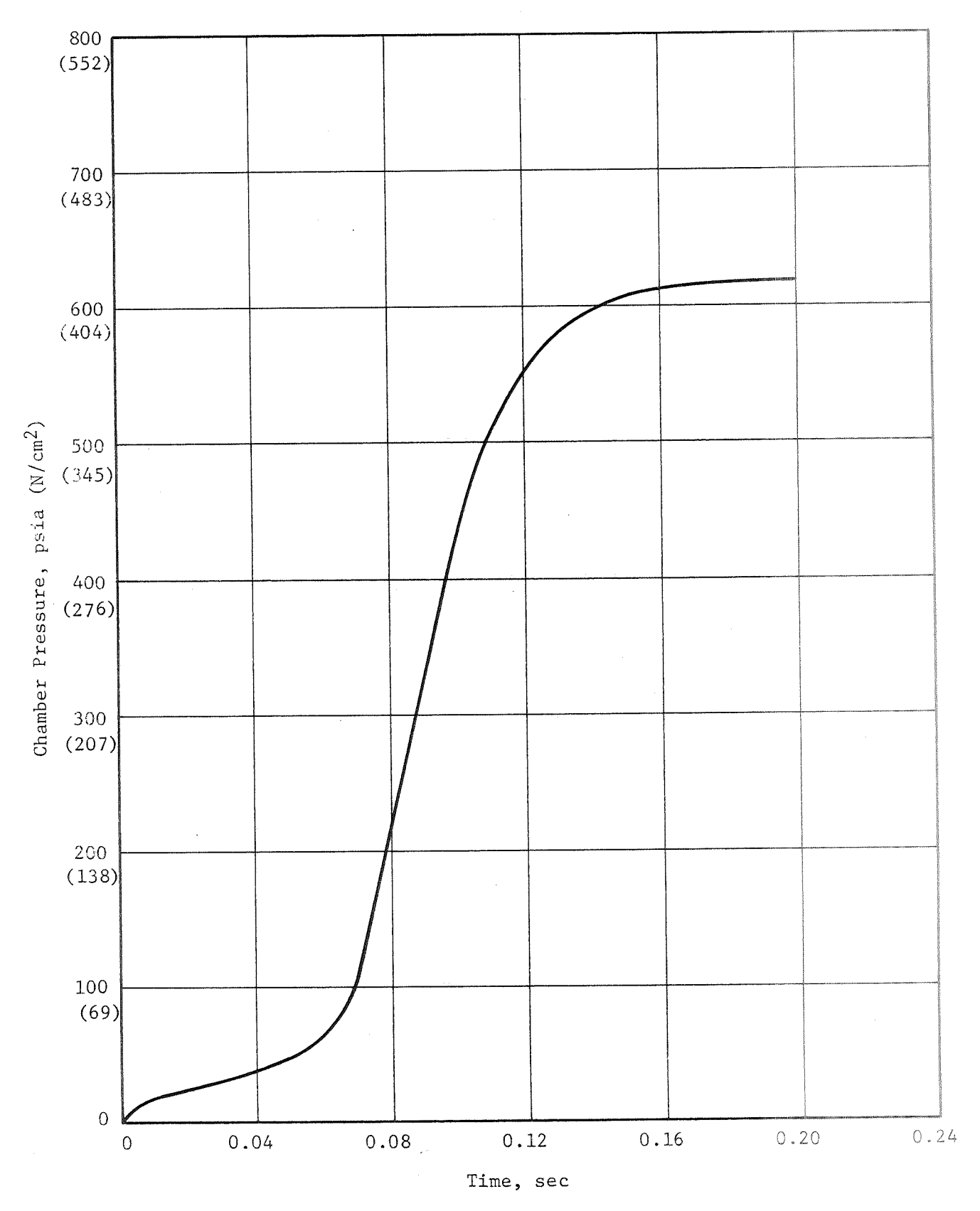


Figure 32. - Ignition Transient - Motor LCAN-01

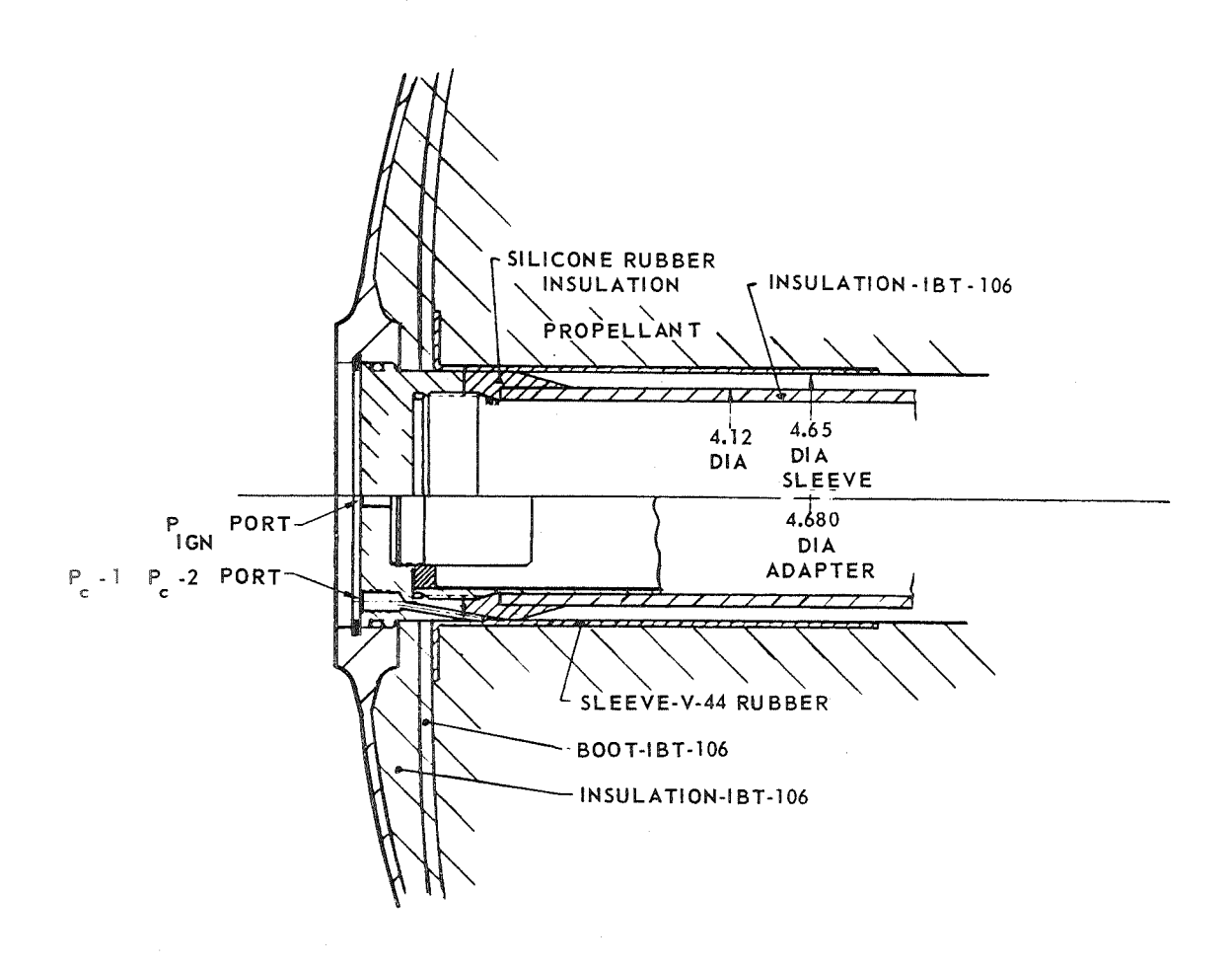


Figure 33. - Forward Head Configuration - Motor LCAN-01

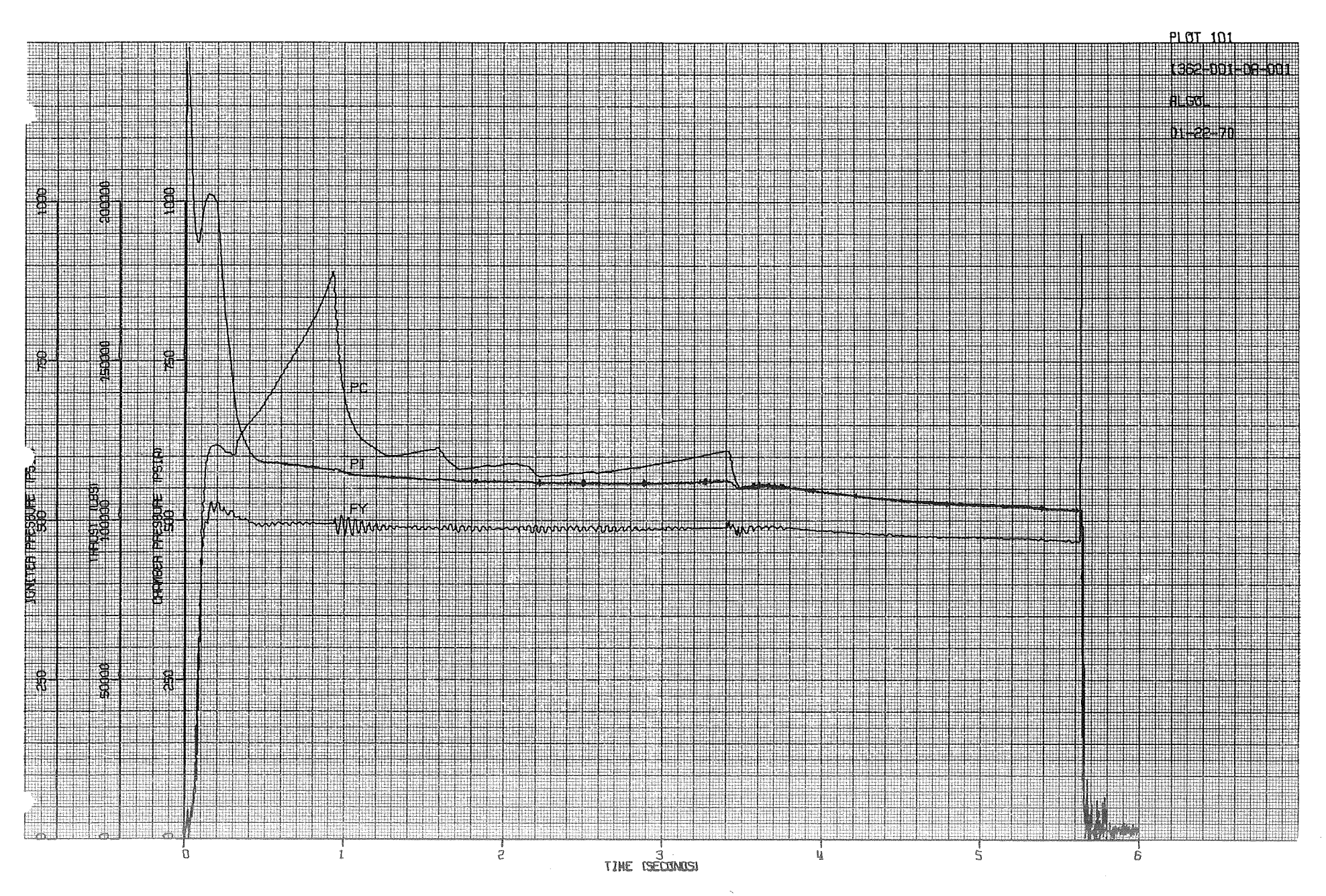


Figure 34. - Pressure and Thrust vs Time, Motor LCAN-01



Figure 35. - Posttest View of Motor and P-3 Test Facility



Figure 36. - Chamber Fragment From Area of Major Failure

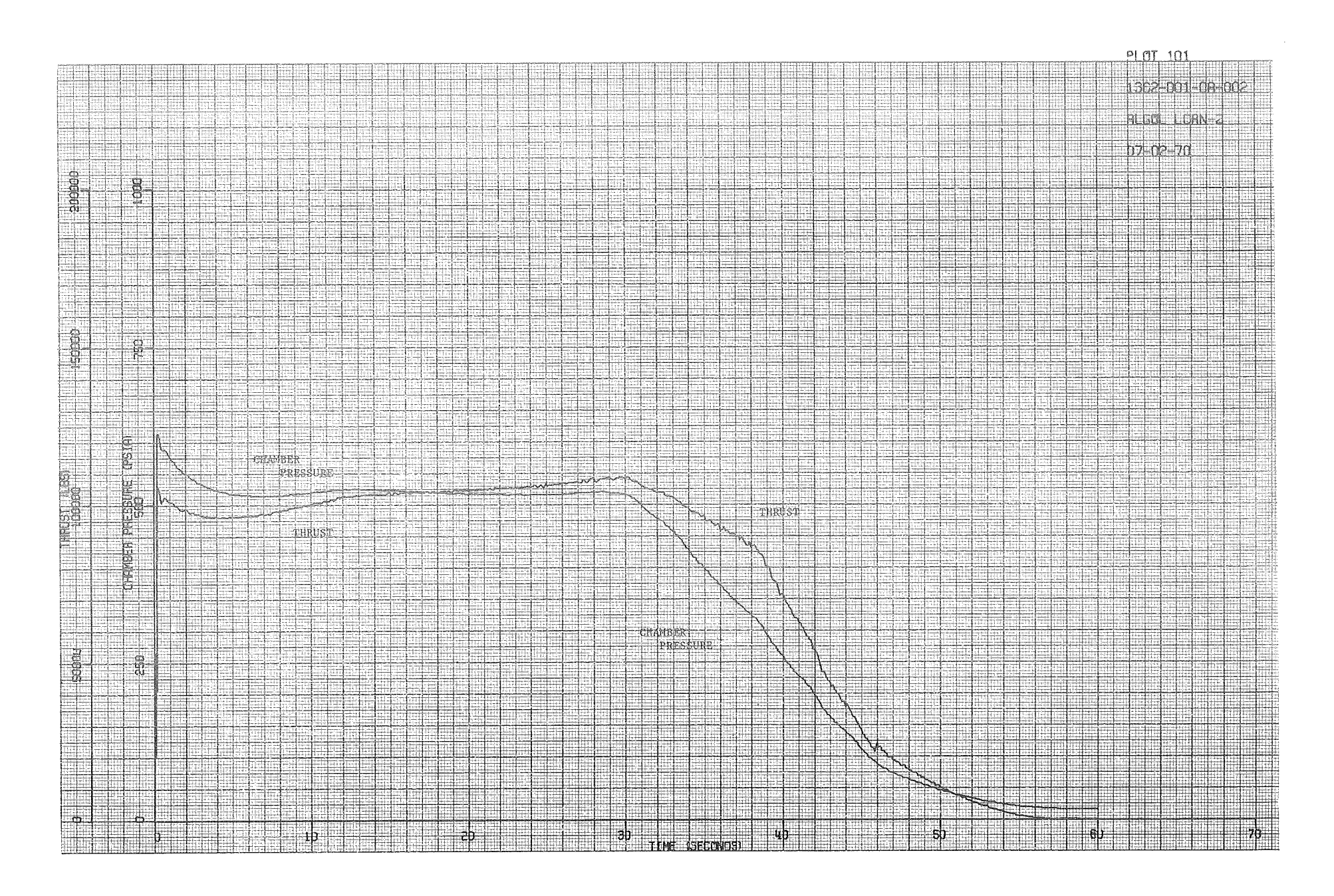


Figure 37. - Pressure and Thrust vs Time, Motor LCAN-02

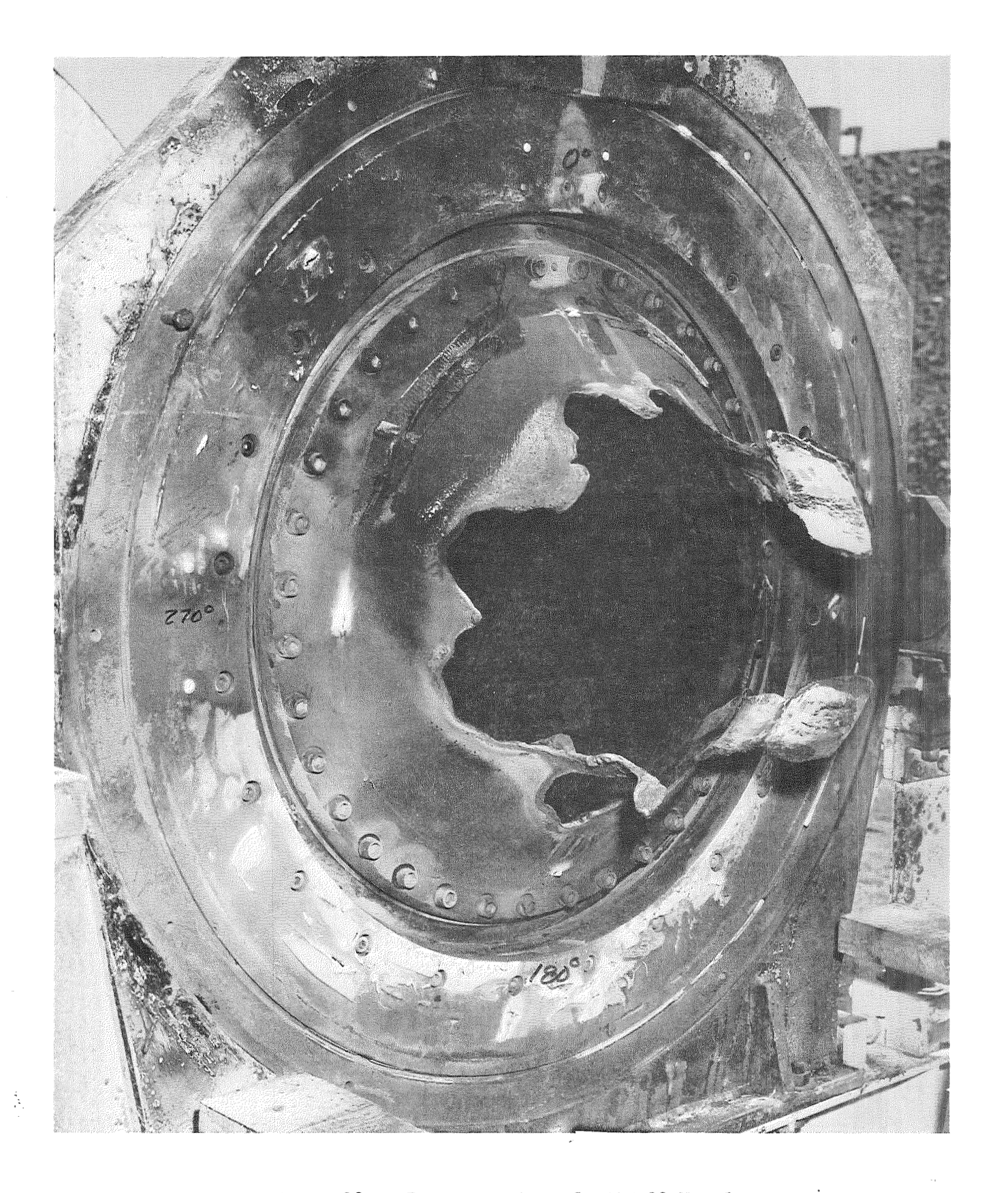


Figure 38. - Posttest View of LCAN-02 Nozzle

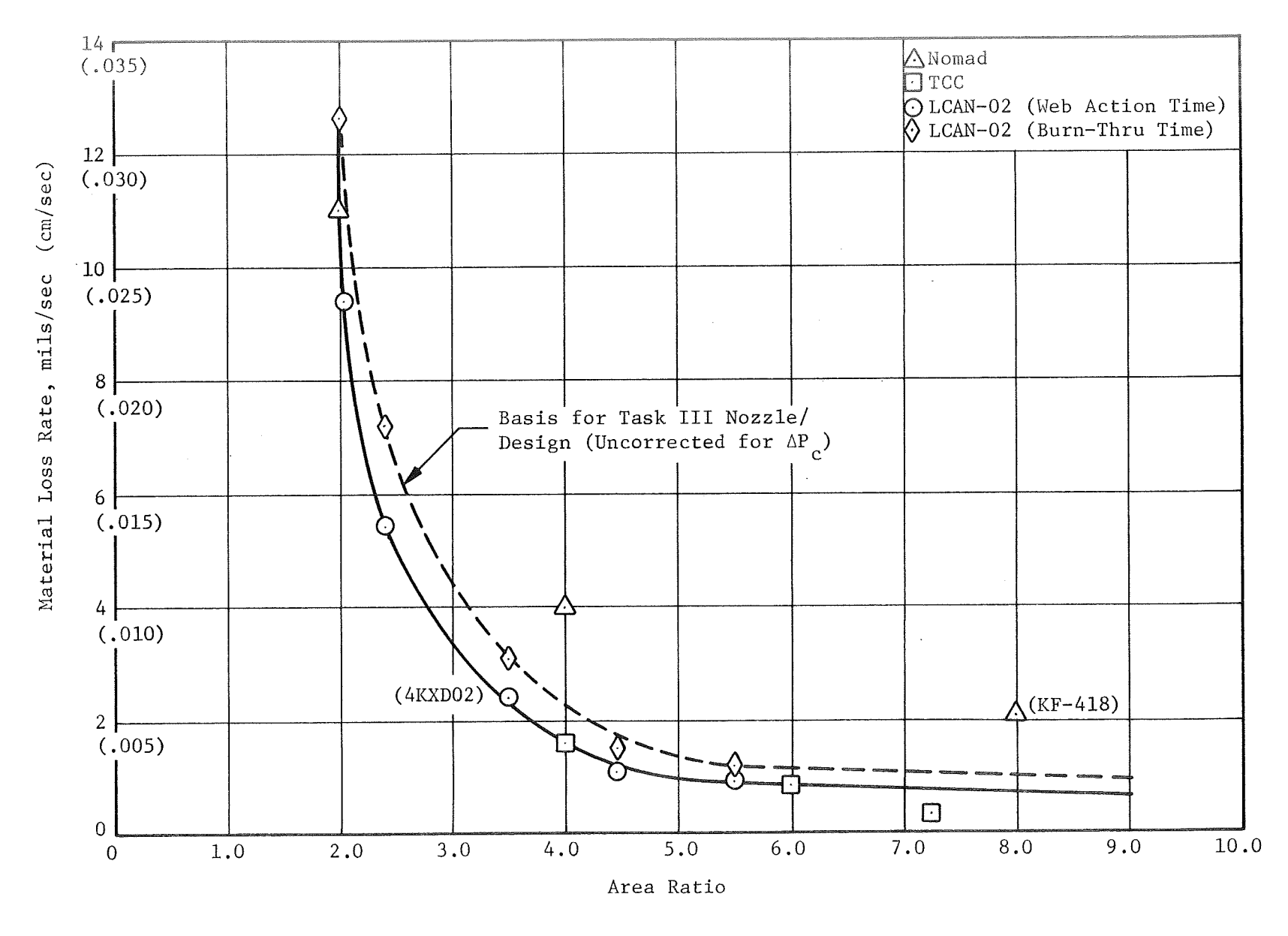


Figure 39. - Erosion Rate-vs-Area Ratio for Canvas-Duck Phenolic

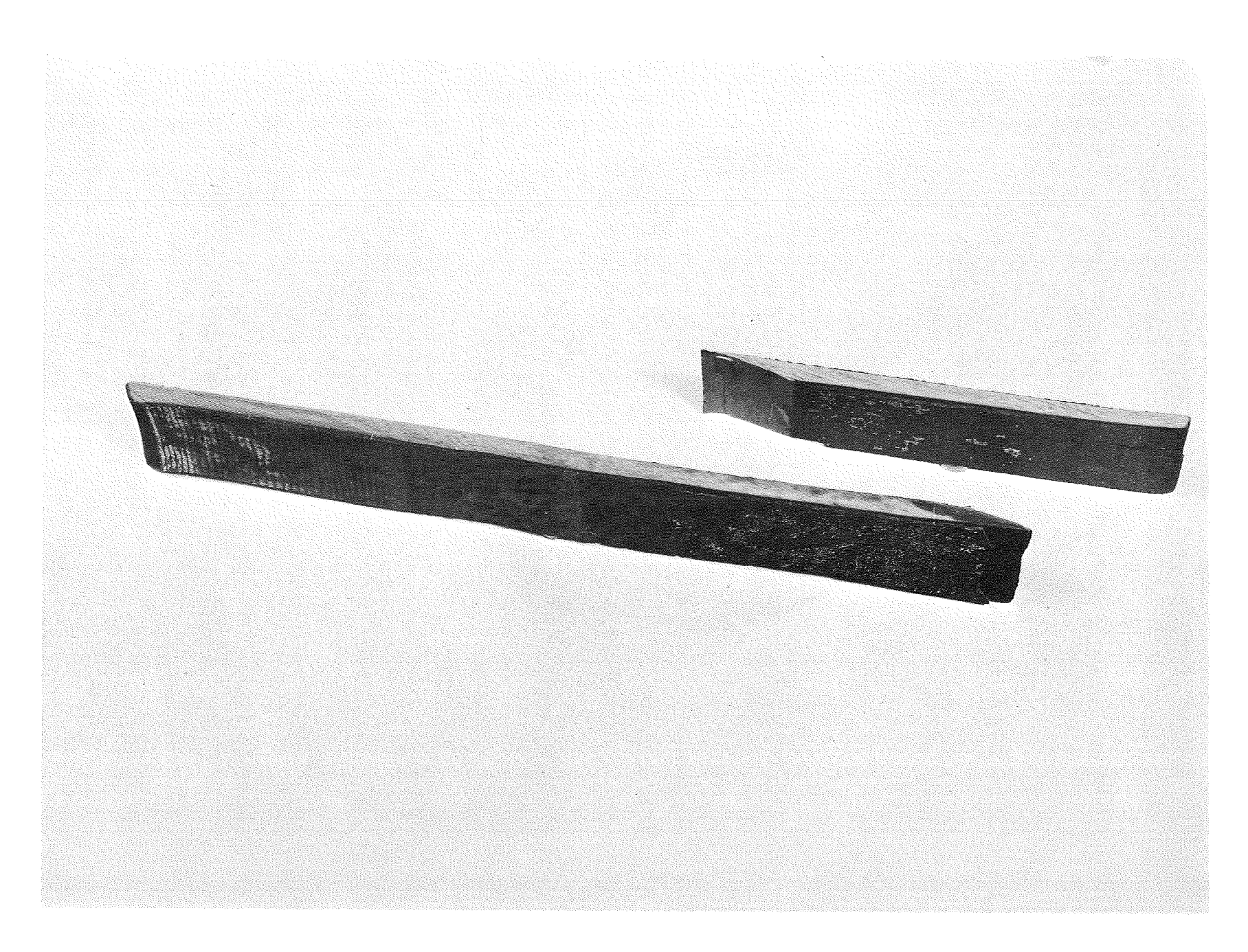


Figure 40. - View of Sectioned Exit Cone

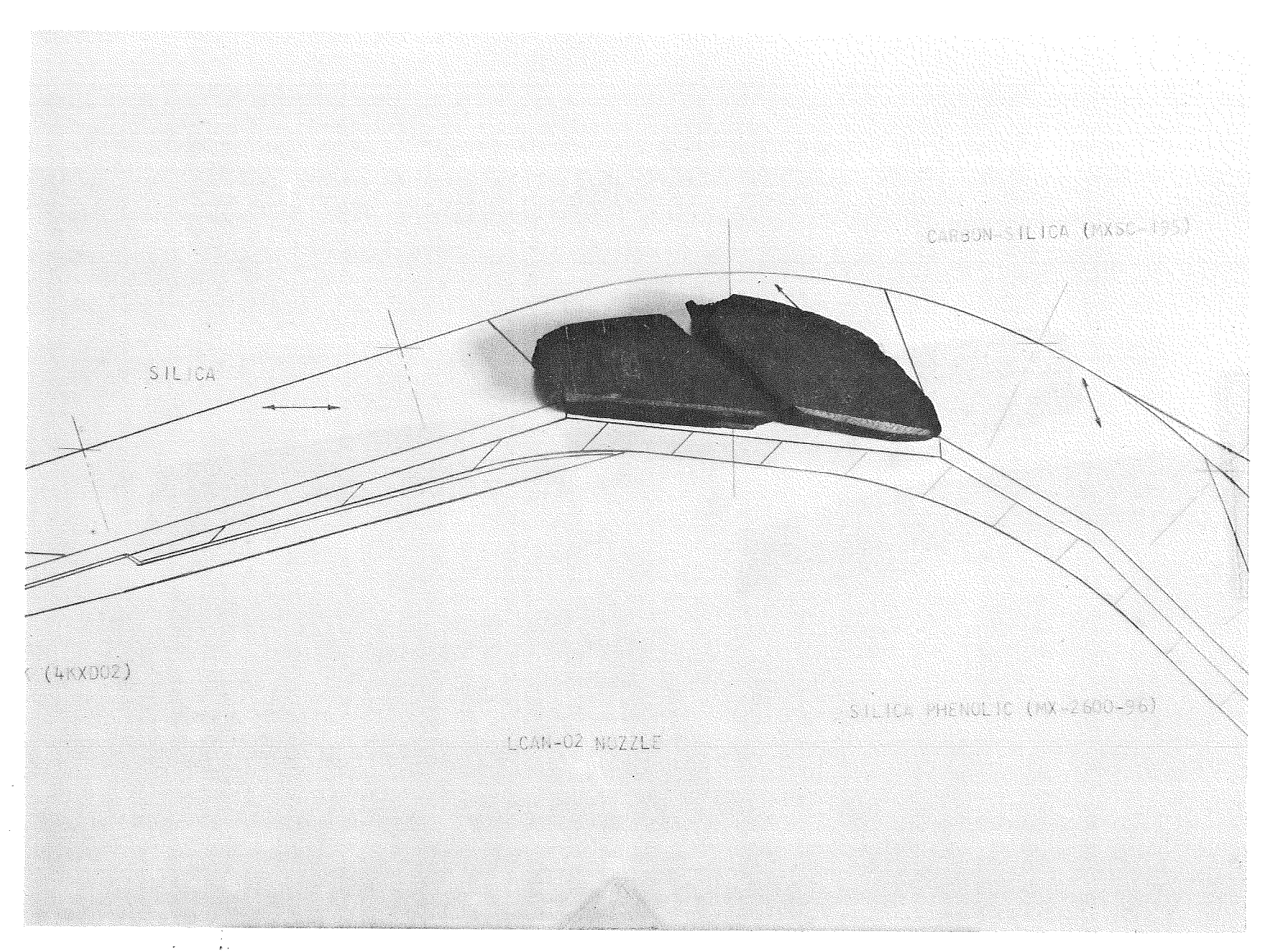


Figure 41. - Nozzle Throat Section Fragments

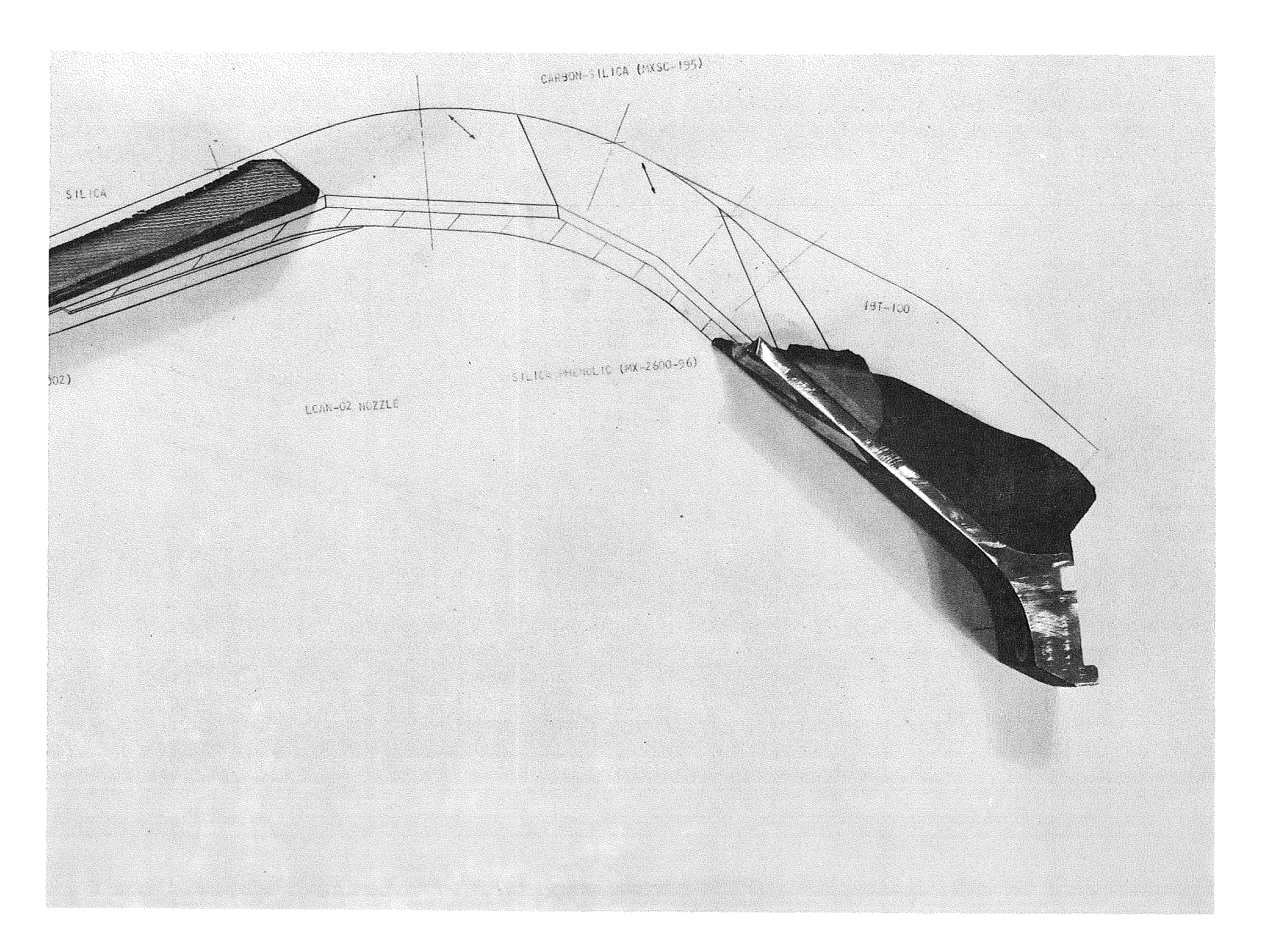


Figure 42. - Entrance Insulation at Location of Failure

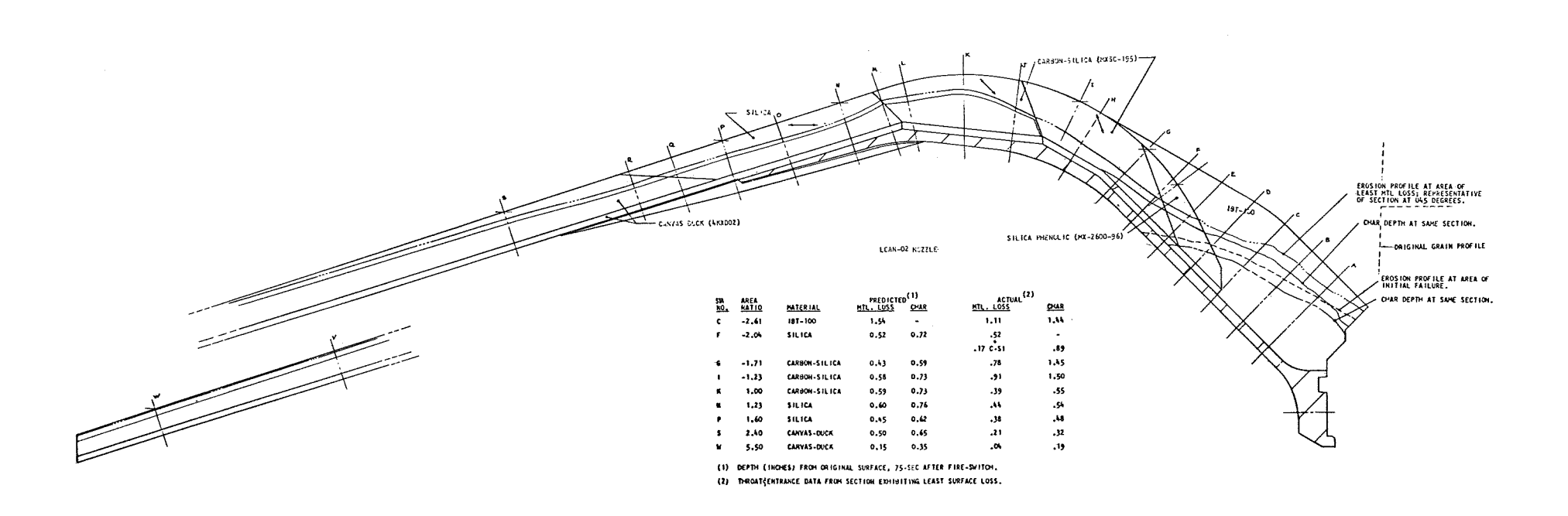


Figure 43. - Posttest Nozzle Insulation Profile

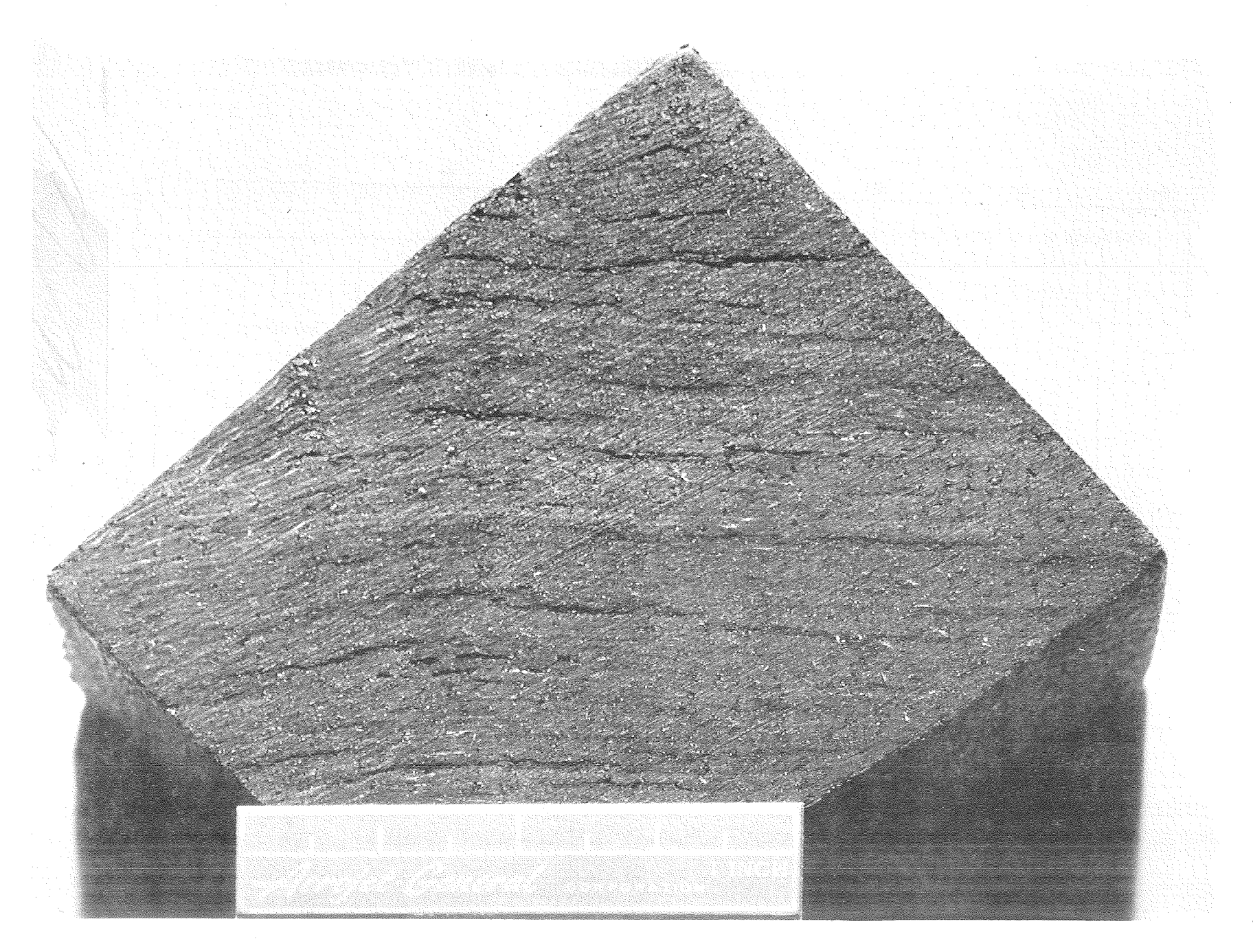


Figure 44. - Charred MXSC-195 From Entrance Section Tag-End

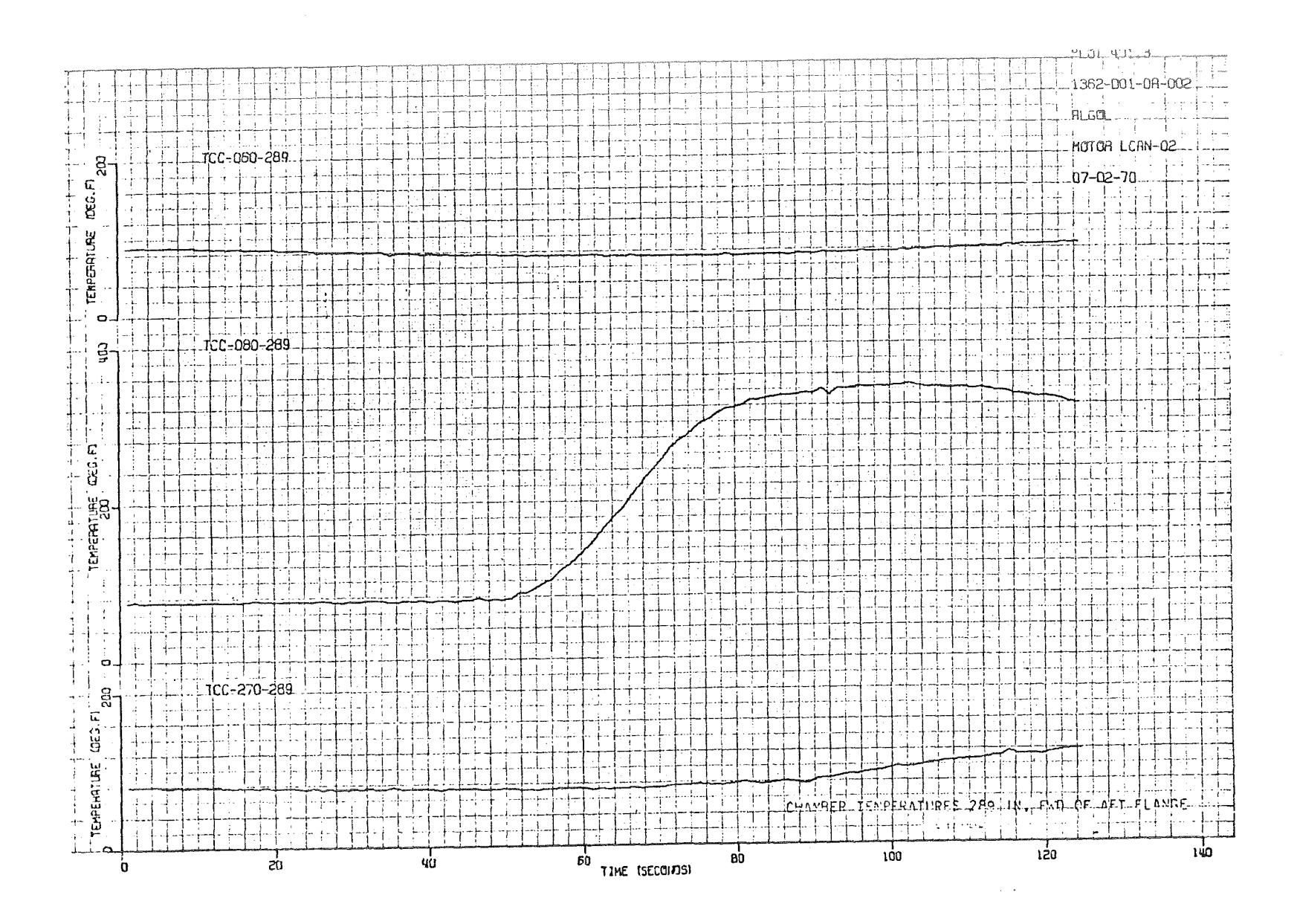


Figure 45. - Chamber Temperature 289 in. Forward of Aft Flange

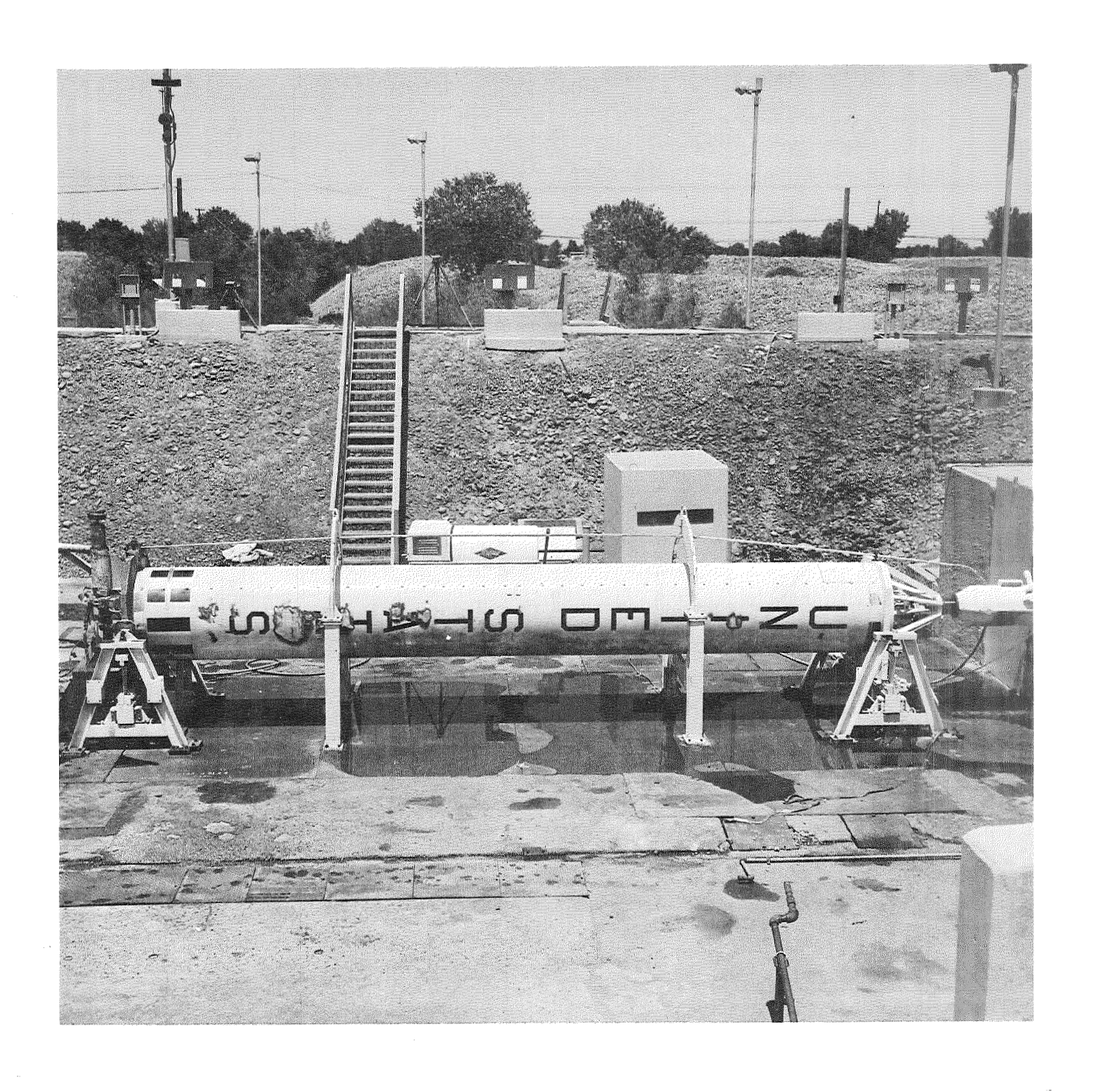


Figure 46. - Posttest View of LCAN-02 Chamber

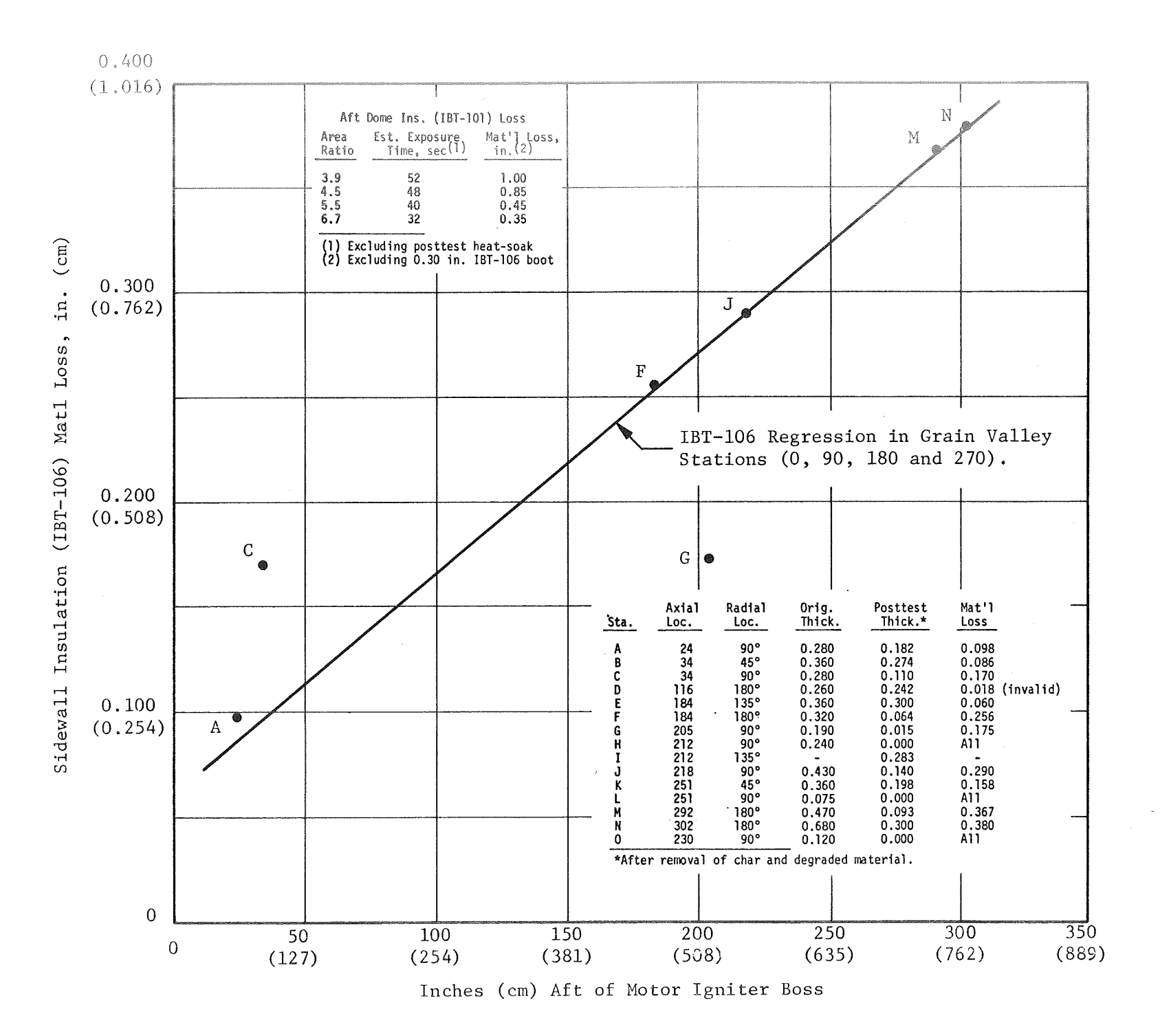


Figure 47. - Trowelable Insulation Performance Data

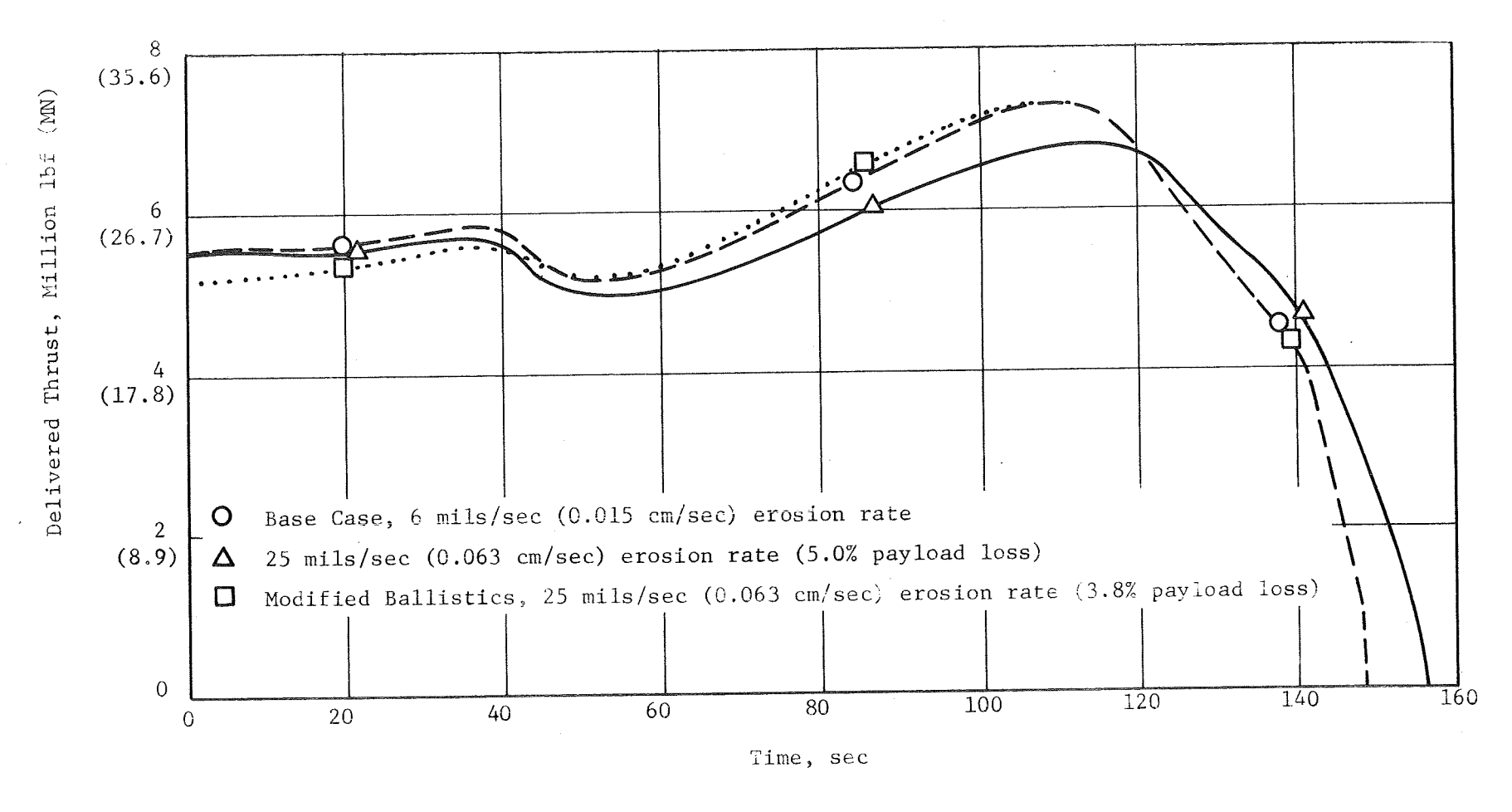


Figure 48. - Thrust-vs-Time Performance Comparison for Full-Length 260-in.-dia (6.6 m) Motors

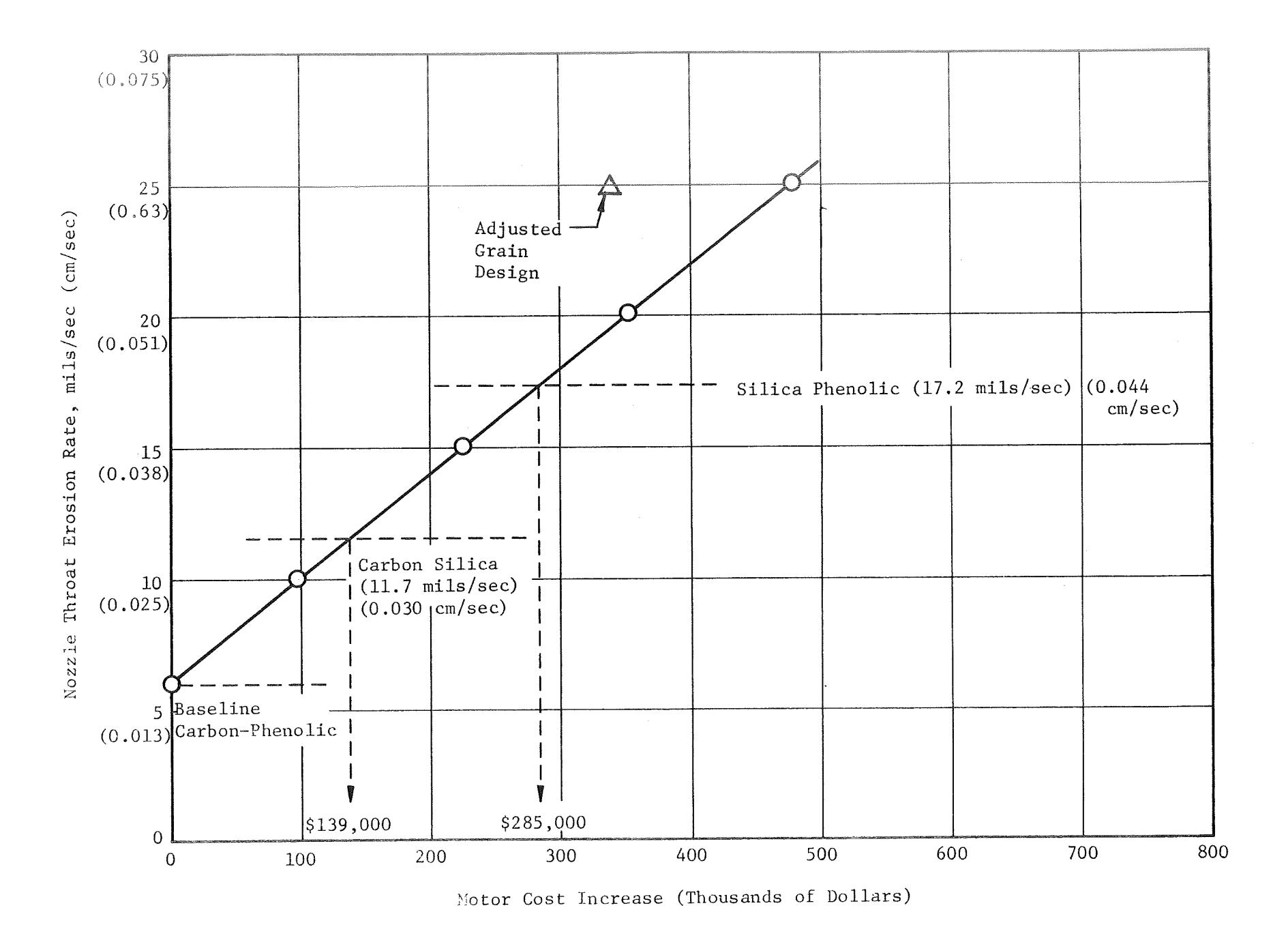


Figure 49. - First Stage Cost Increase vs Throat Erosion Rate

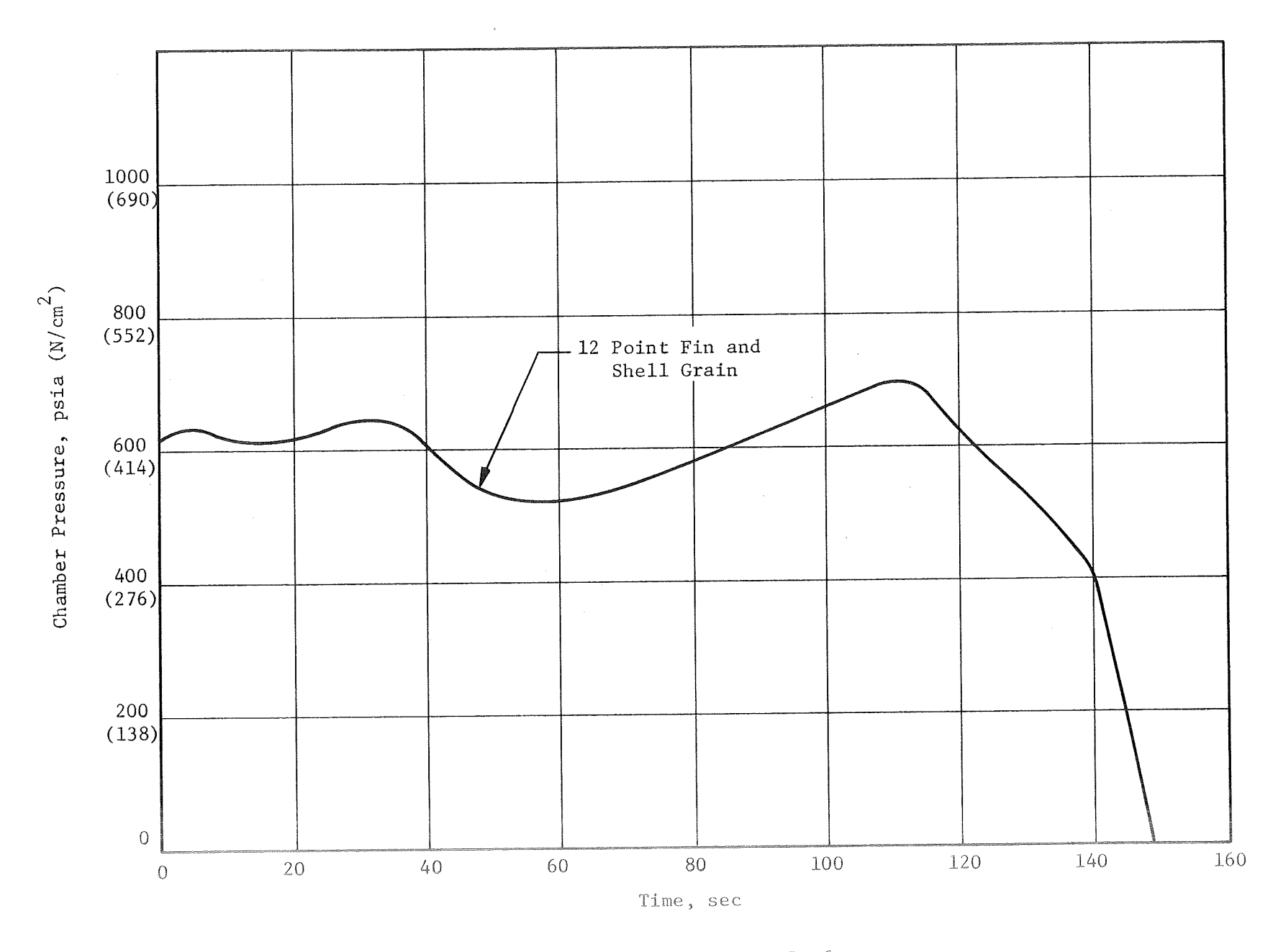


Figure 50. - Predicted Pressure vs Time Performance 260-FL Motor (260/SIVB Study)

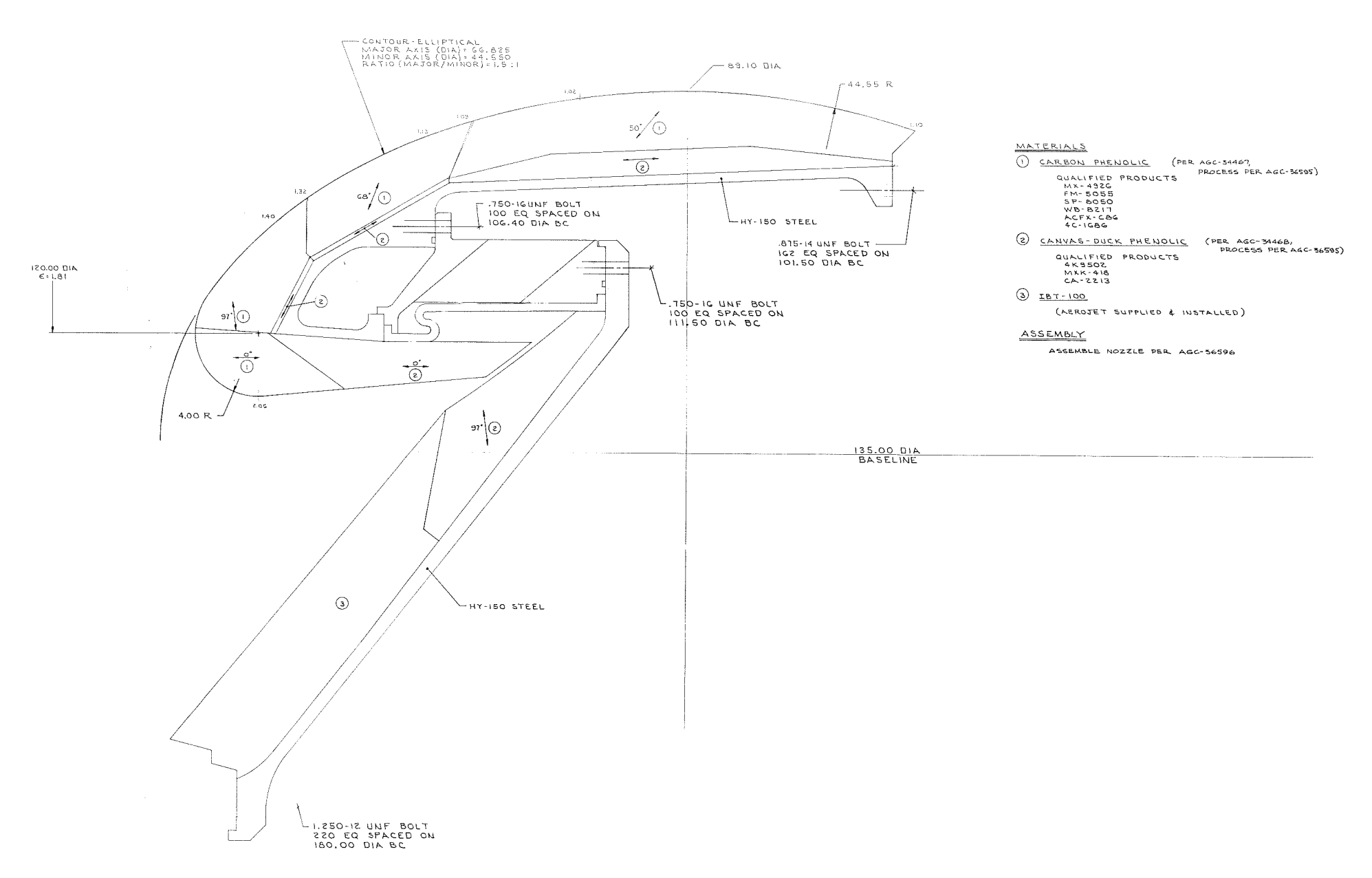
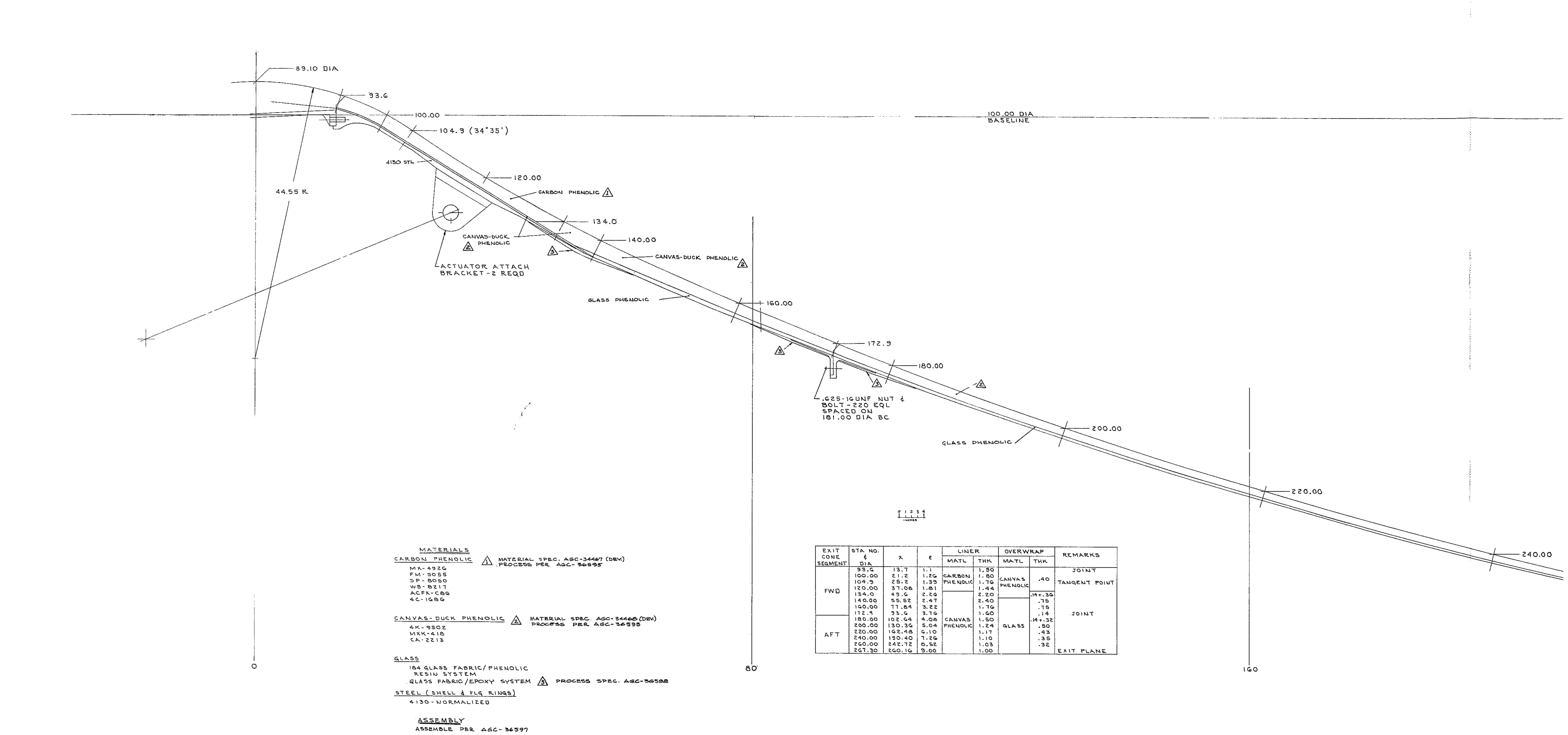


Figure 51. - Low-Cost Nozzle Design, 260-FL Motor



F010-000 #1

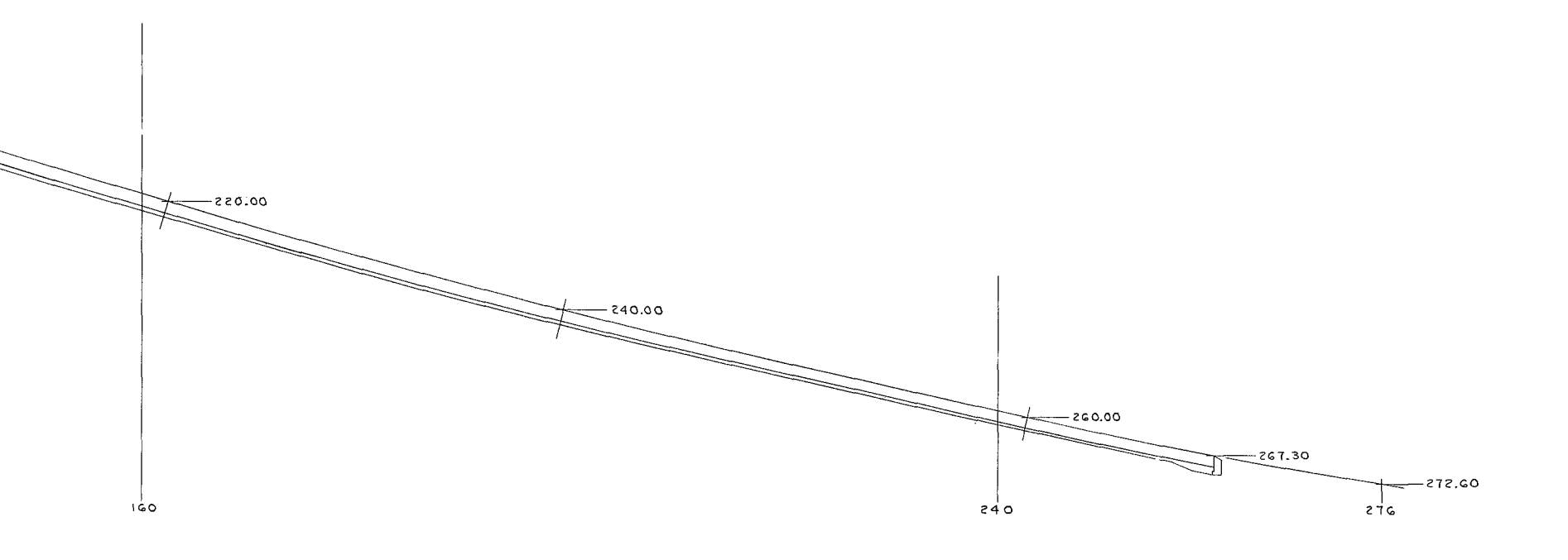


Figure 52. - Low Cost Exit Cone Design, 260-FL Motor

FOLD-OUT艺

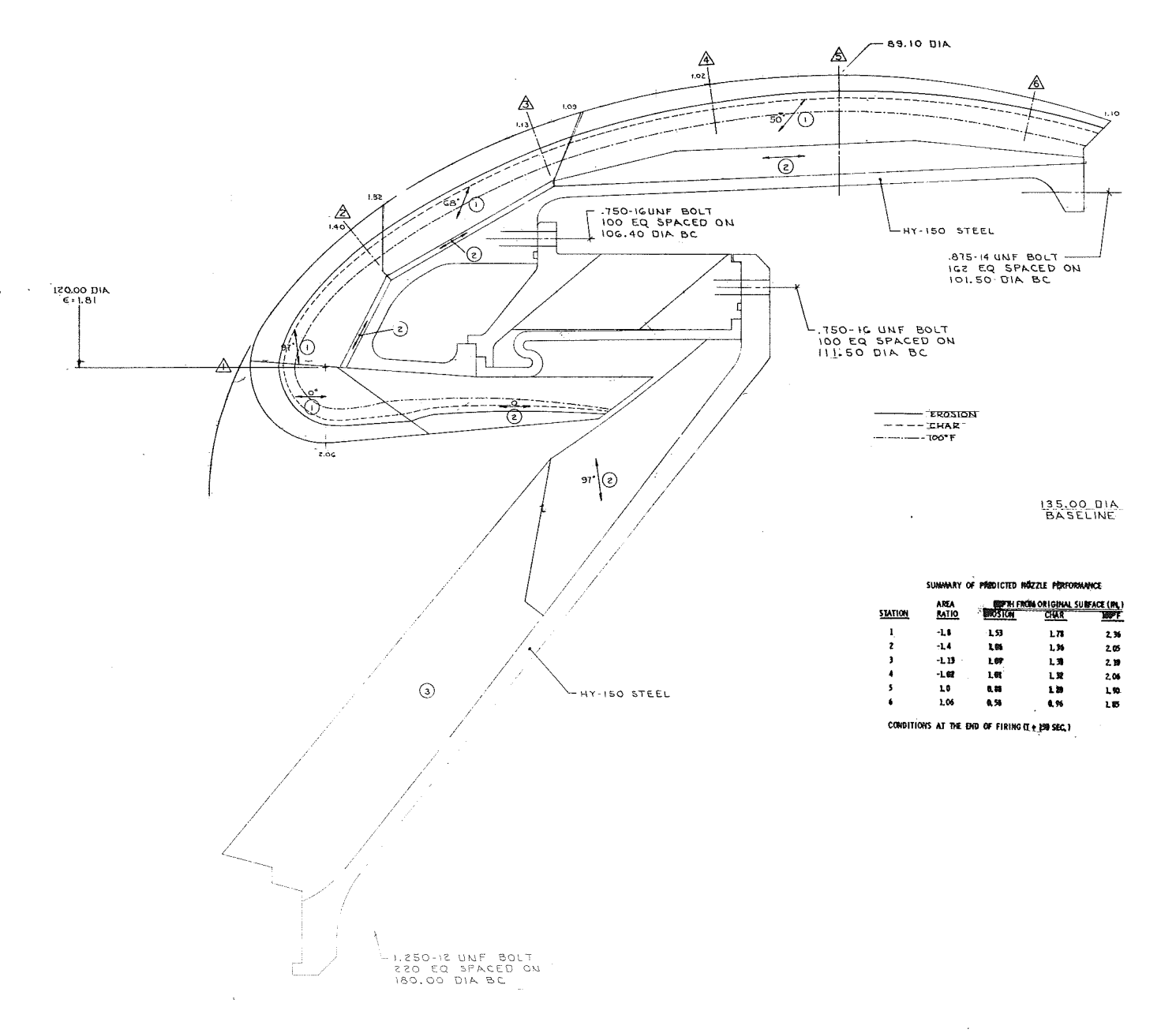


Figure 53. - Erosion, Char and Thermal Gradient - Full-Scale Nozzle

MATERIALS

1) CARBON PHENOLIC

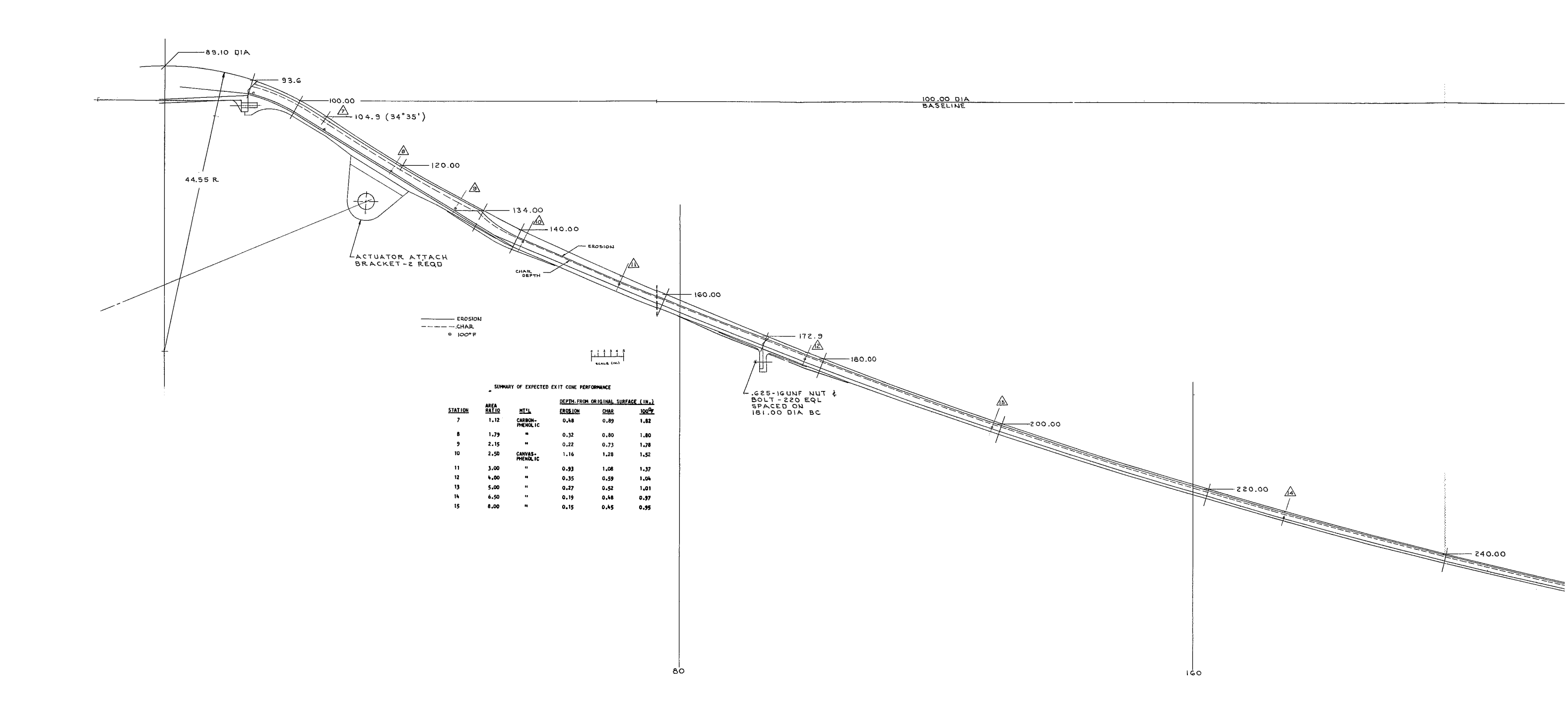
QUALIFIED PRODUCTS MX-4926 FM-5055 SP-8050 WB-8217 ACFX-C86 4C-1686

(2) CANVAS-DUCK PHENOLIC

QUALIFIED PRODUCTS
4K950Z
MXK-418
CA-2213

3 IBT-100

(AEROJET SUPPLIED & INSTALLED)



F040-OUT #1

Fold-ou

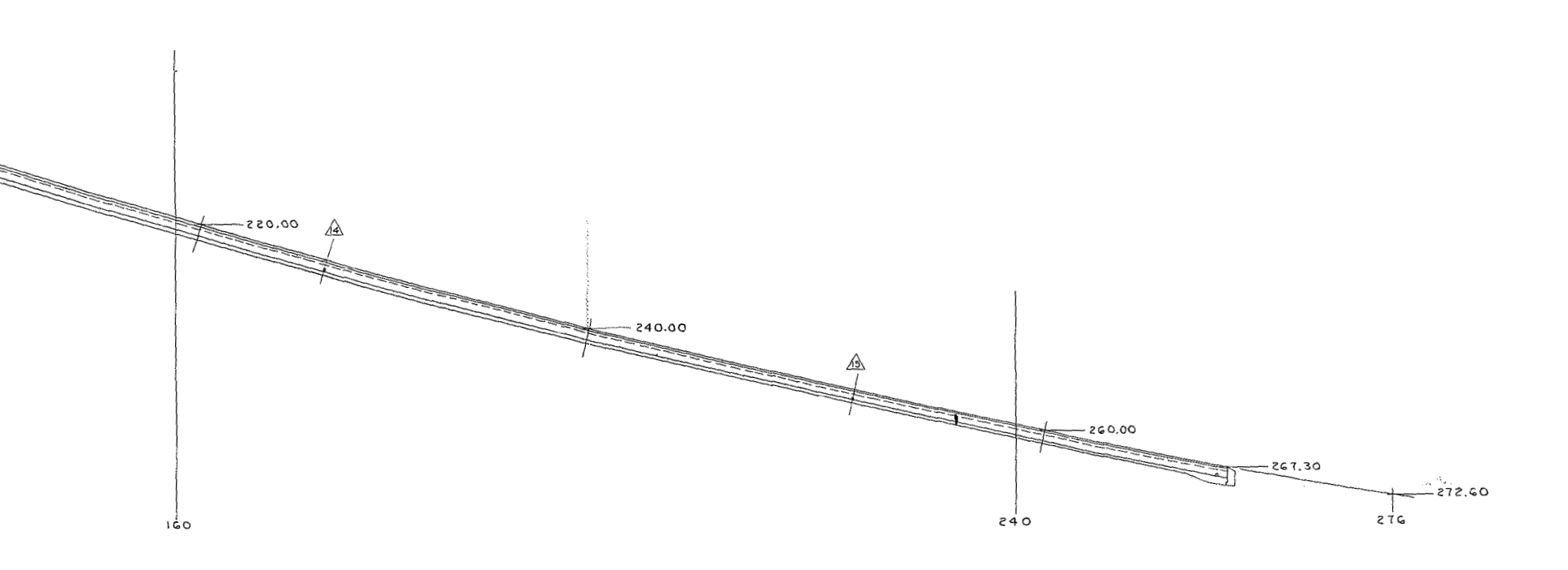


Figure 54. - Erosion, Char and Thermal Gradient - Full-Scale Exit Cone

FOLD-OUT#2

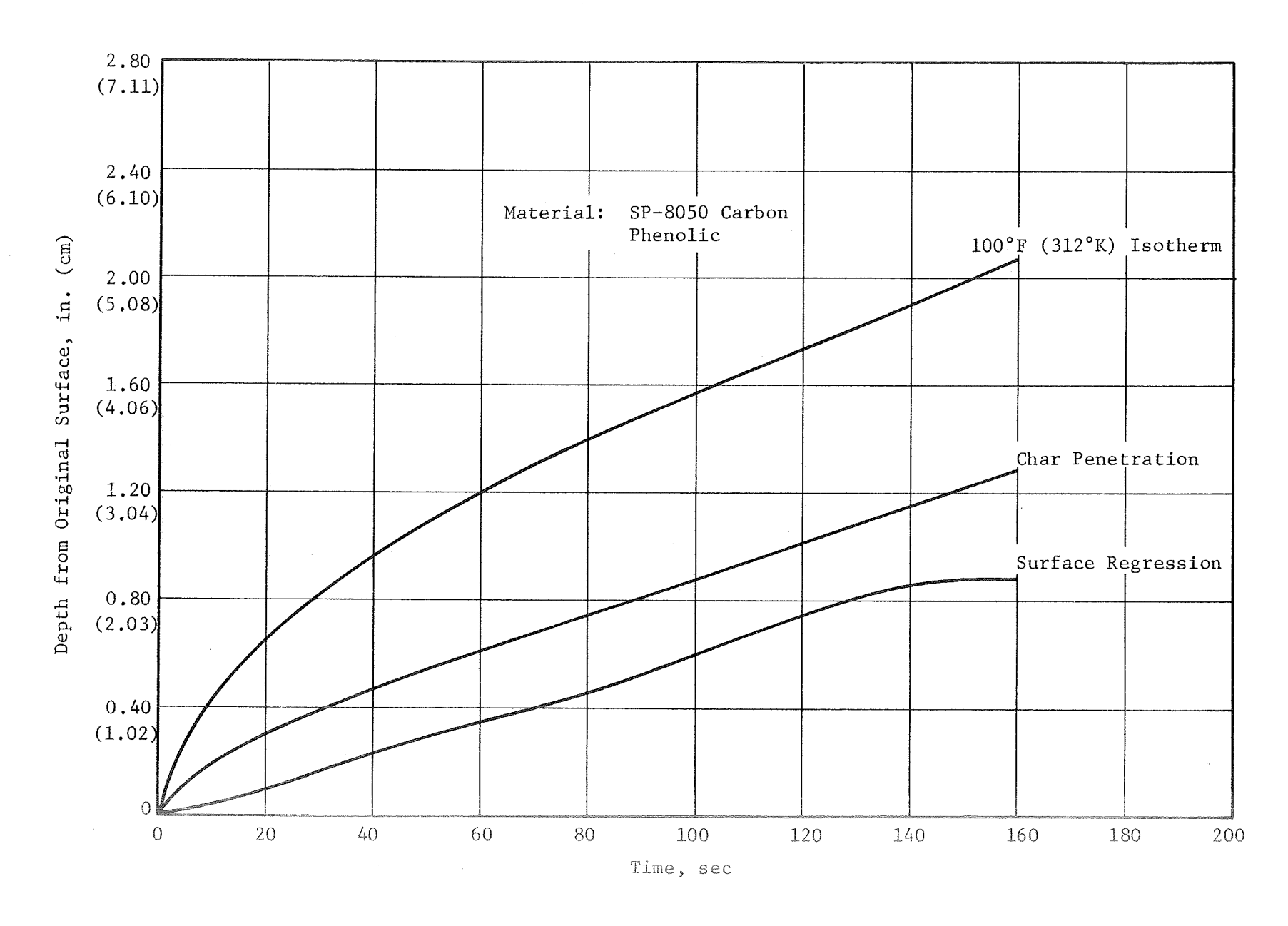


Figure 55. - Predicted Thermal Response at Throat Station - Full Scale Nozzle

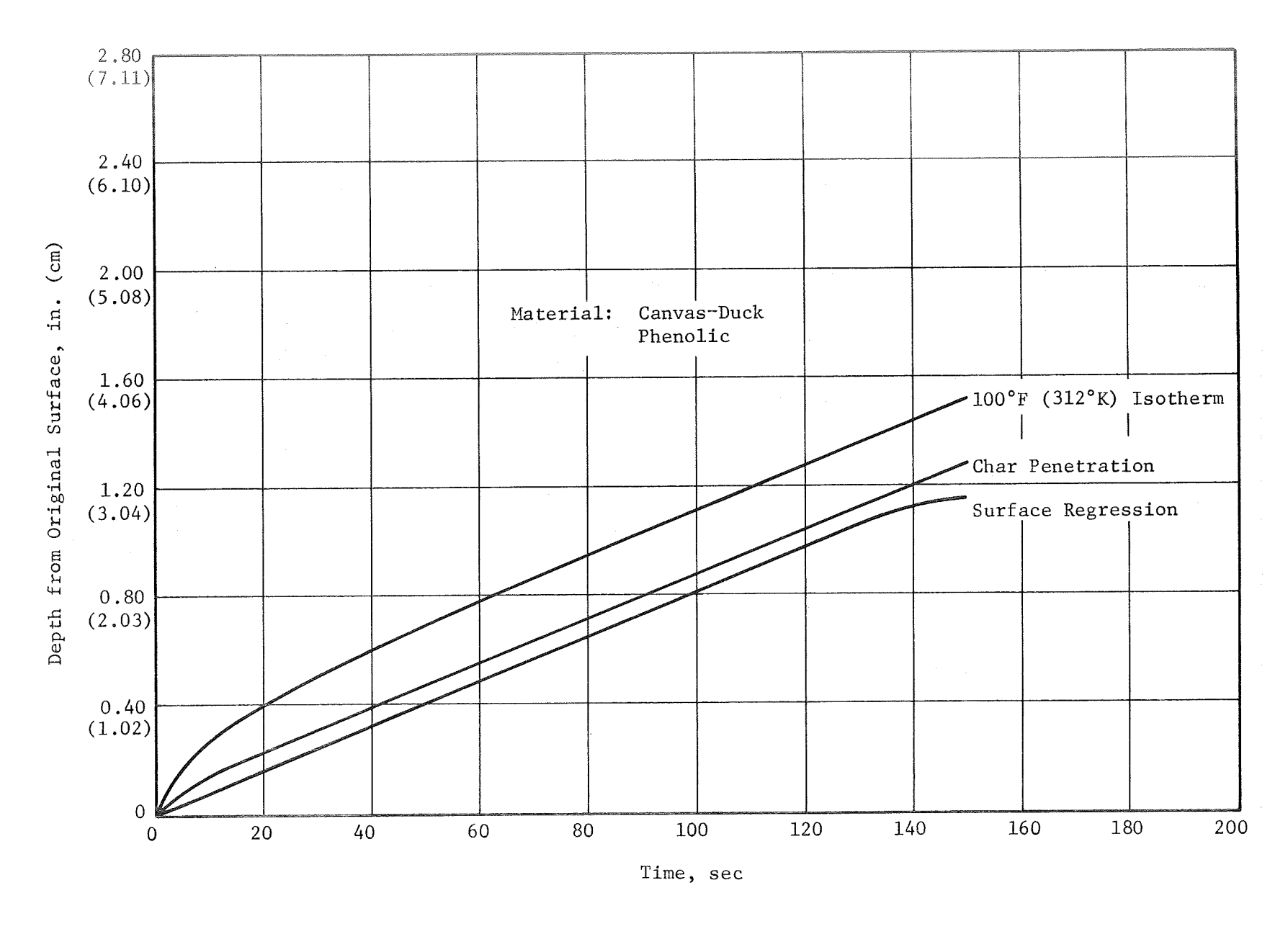


Figure 56. - Predicted Thermal Response at Exit Cone Area Ratio of 2.5:1

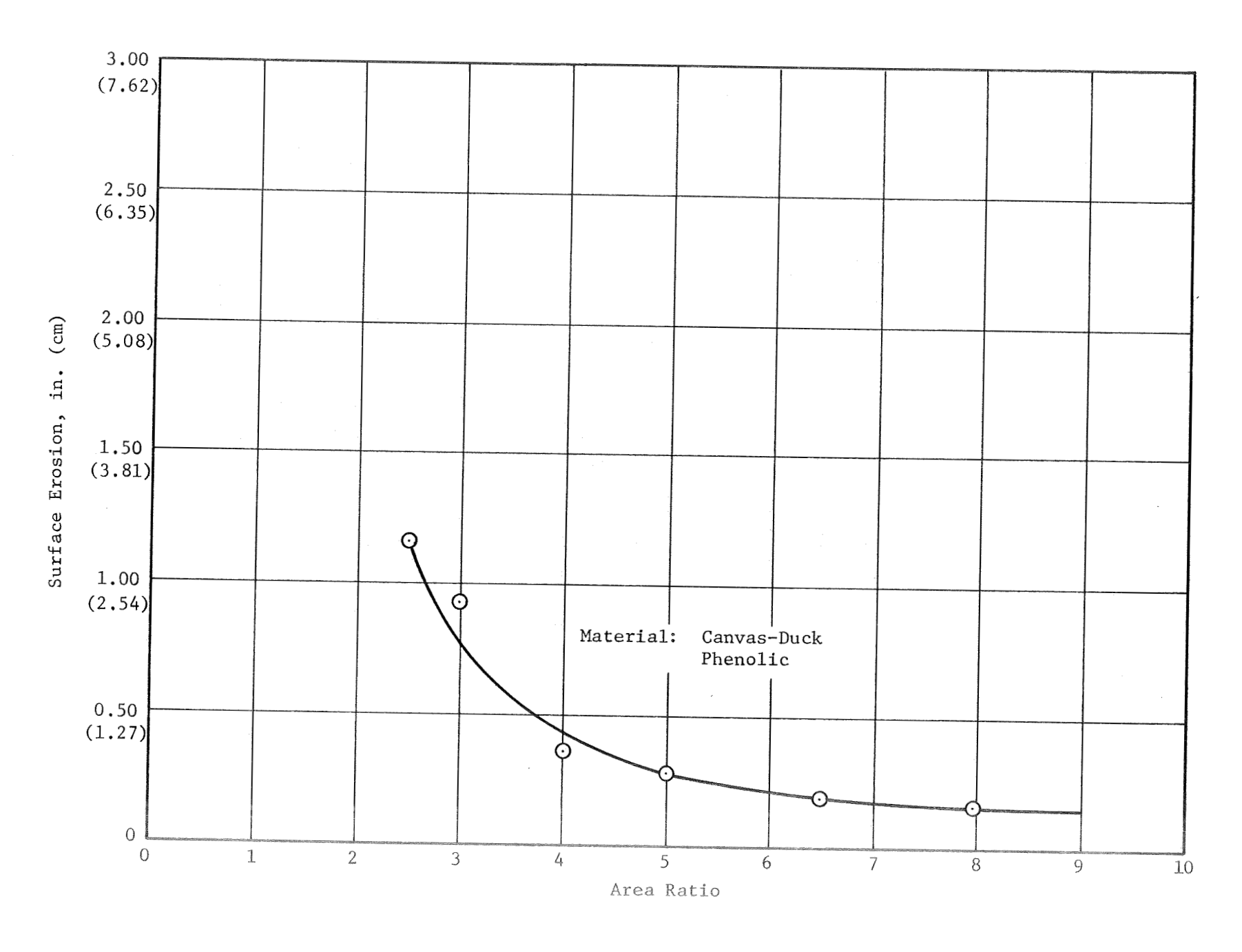


Figure 57. - Predicted Exit Cone Erosion vs Area Ratio at End of Firing

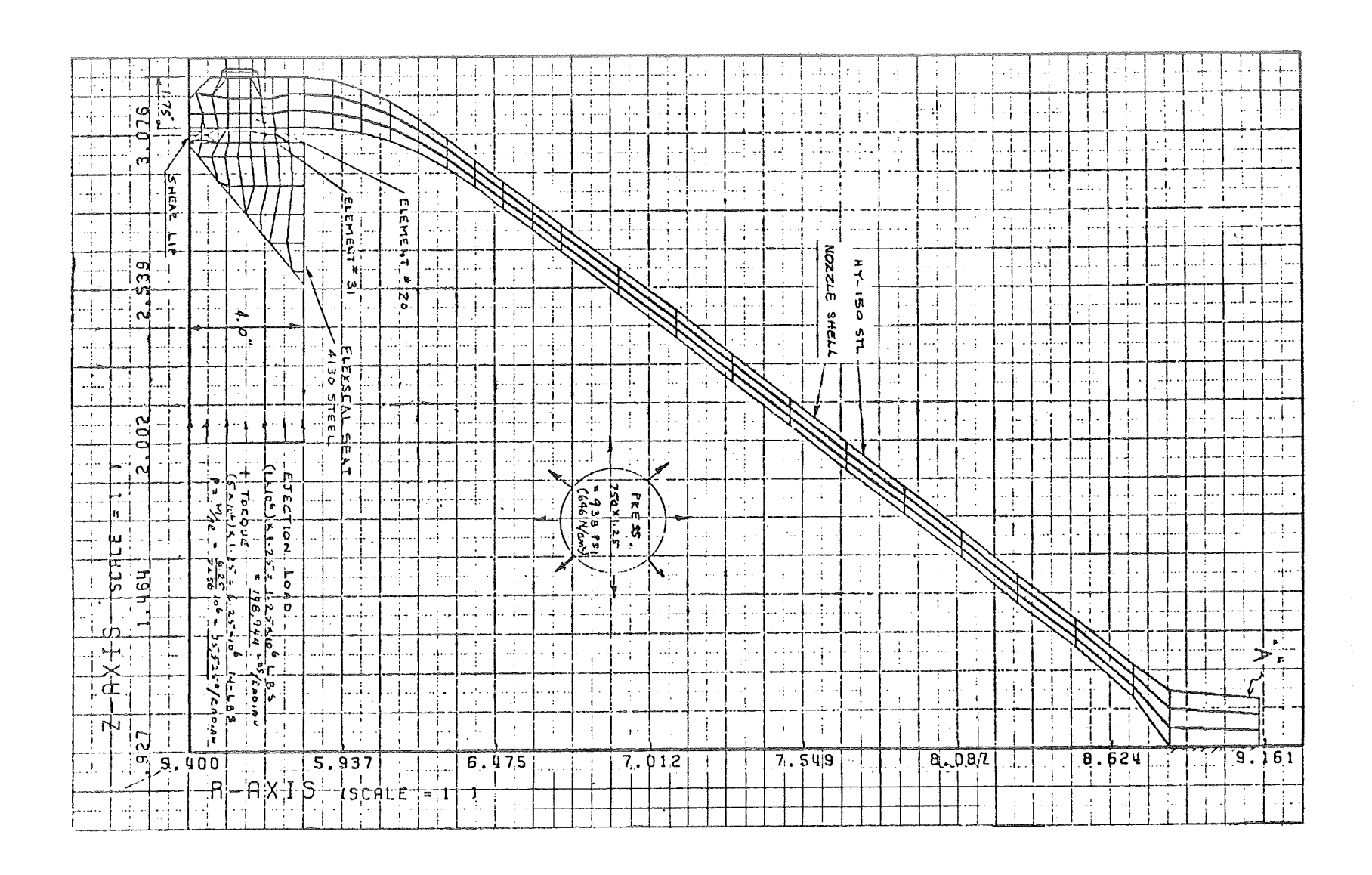


Figure 58. - Finite Element Model - Nozzle Shell

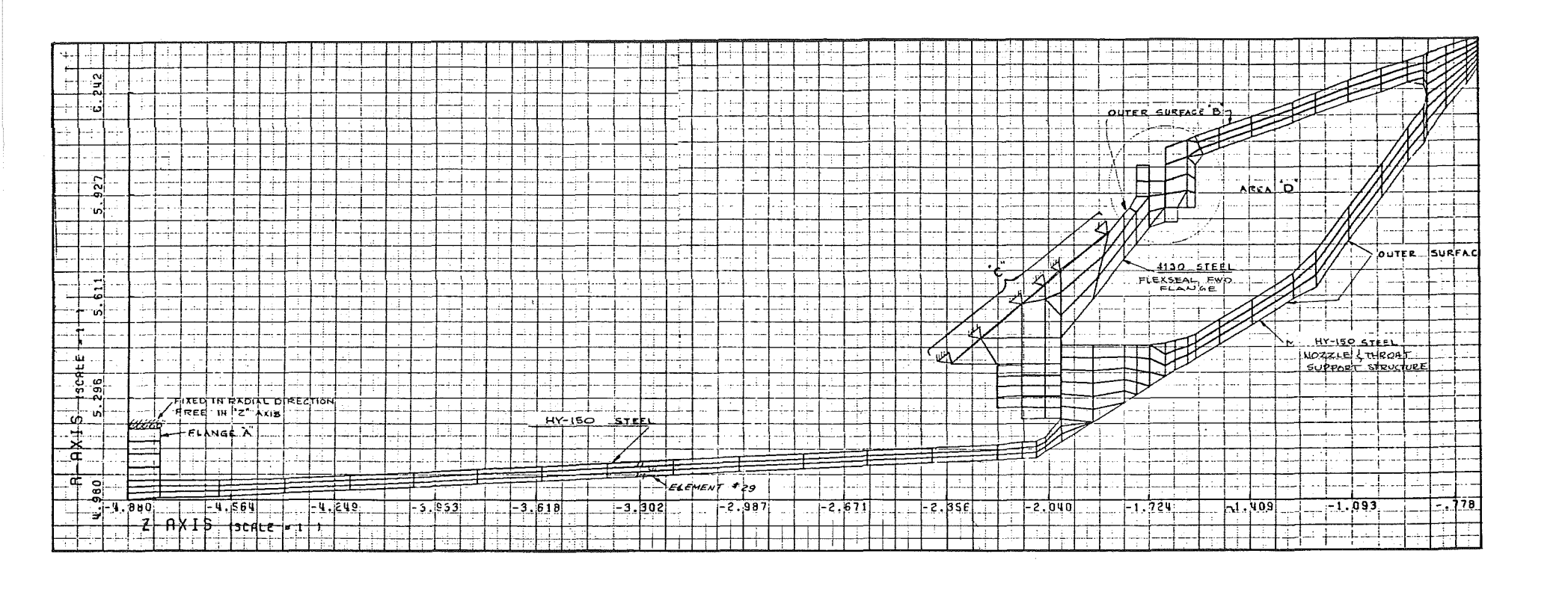
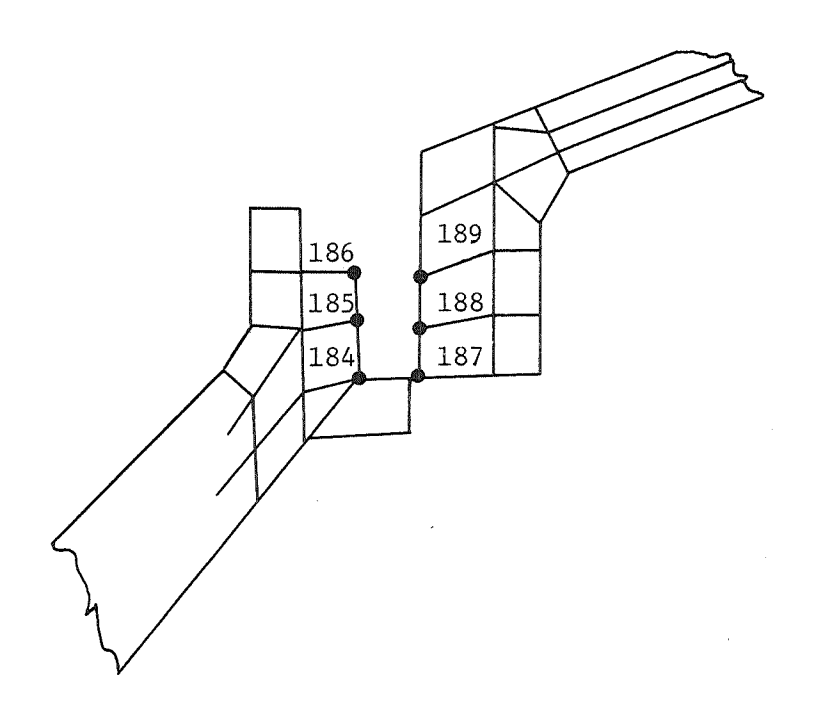


Figure 59. - Finite Element Model, Throat Support Structure



Pressure Outside Only

Nodal <u>Point</u>	Radial ↑ + Disp. ins. (mm)	Axial \leftarrow + Disp. ins. (mm)
184	-0.005091	-0.00248
187	-0.007573	-0.00248
185	-0.00518	-0.00445
188	-007878	-0.00445
186	-0.005284	-0.00643
189	-0.007987	-0.00643

Figure 60. - Calculated Deflections at Outer Joint

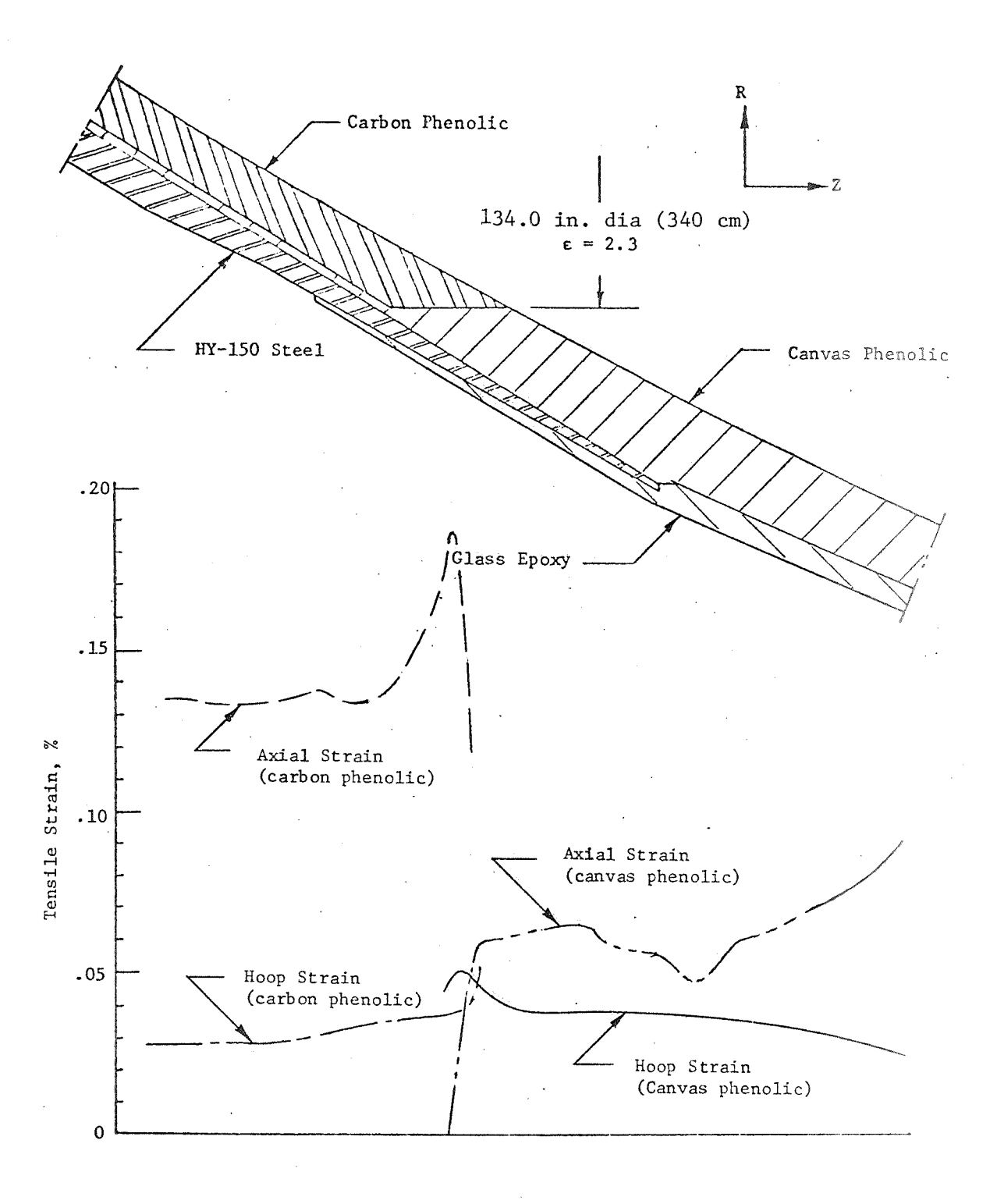


Figure 61. - Maximum Tensile Strain Distribution at Exit Cone ϵ = 2.3

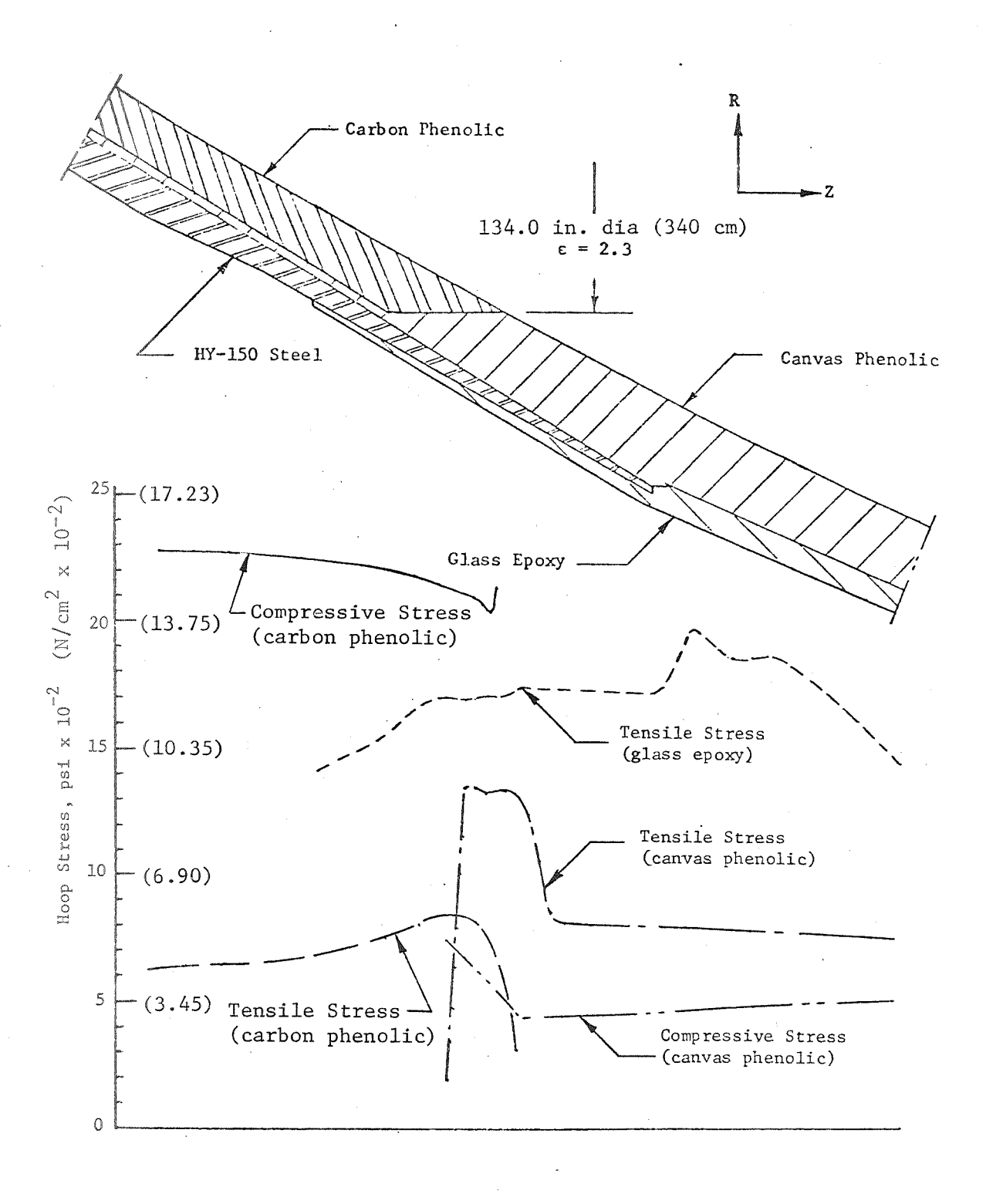


Figure 62. - Maximum Hoop Stress Distribution at Exit Cone ε = 2.3

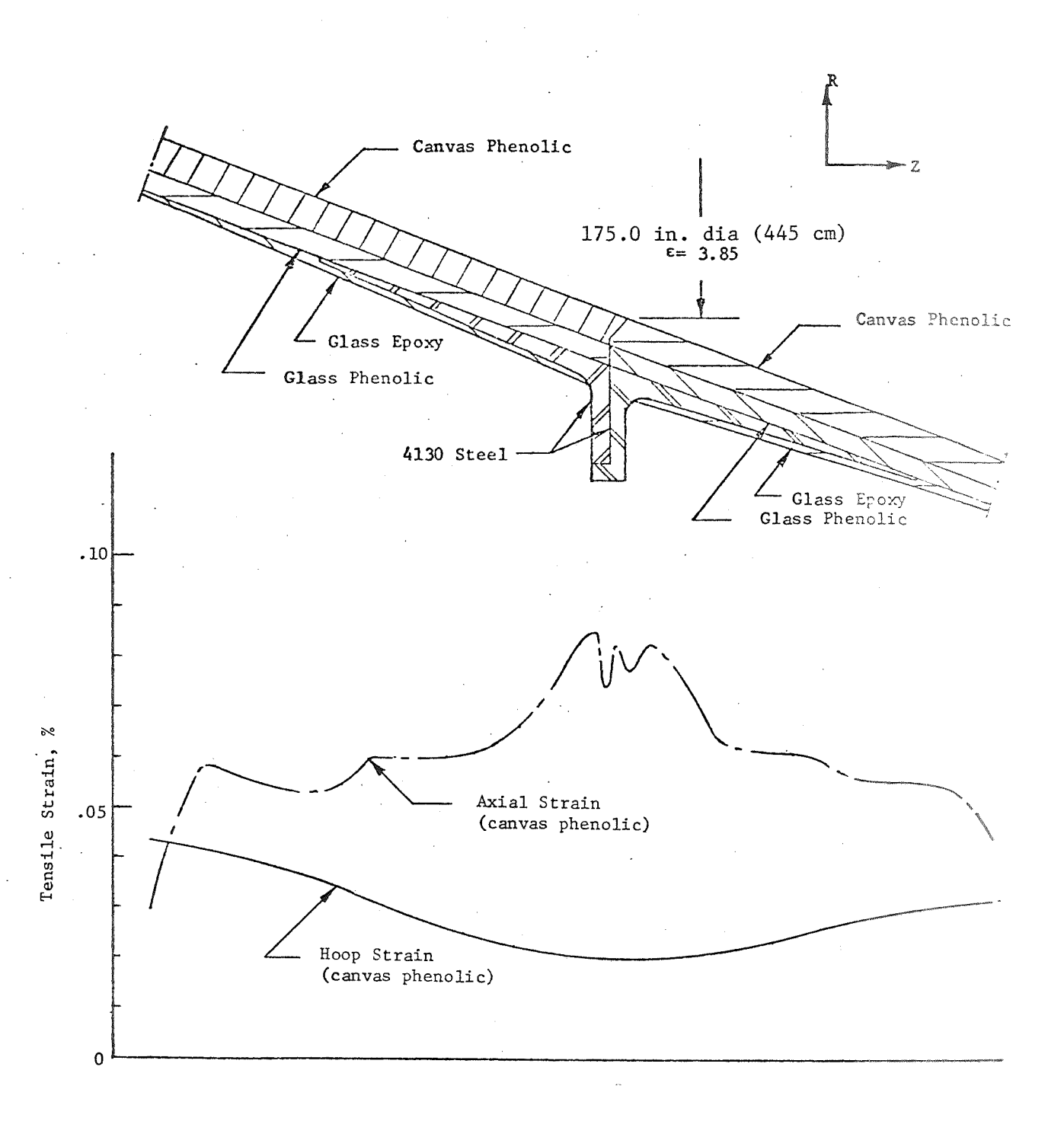


Figure 63. - Maximum Tensile Strain Distribution at Exit Cone ε = 3.85

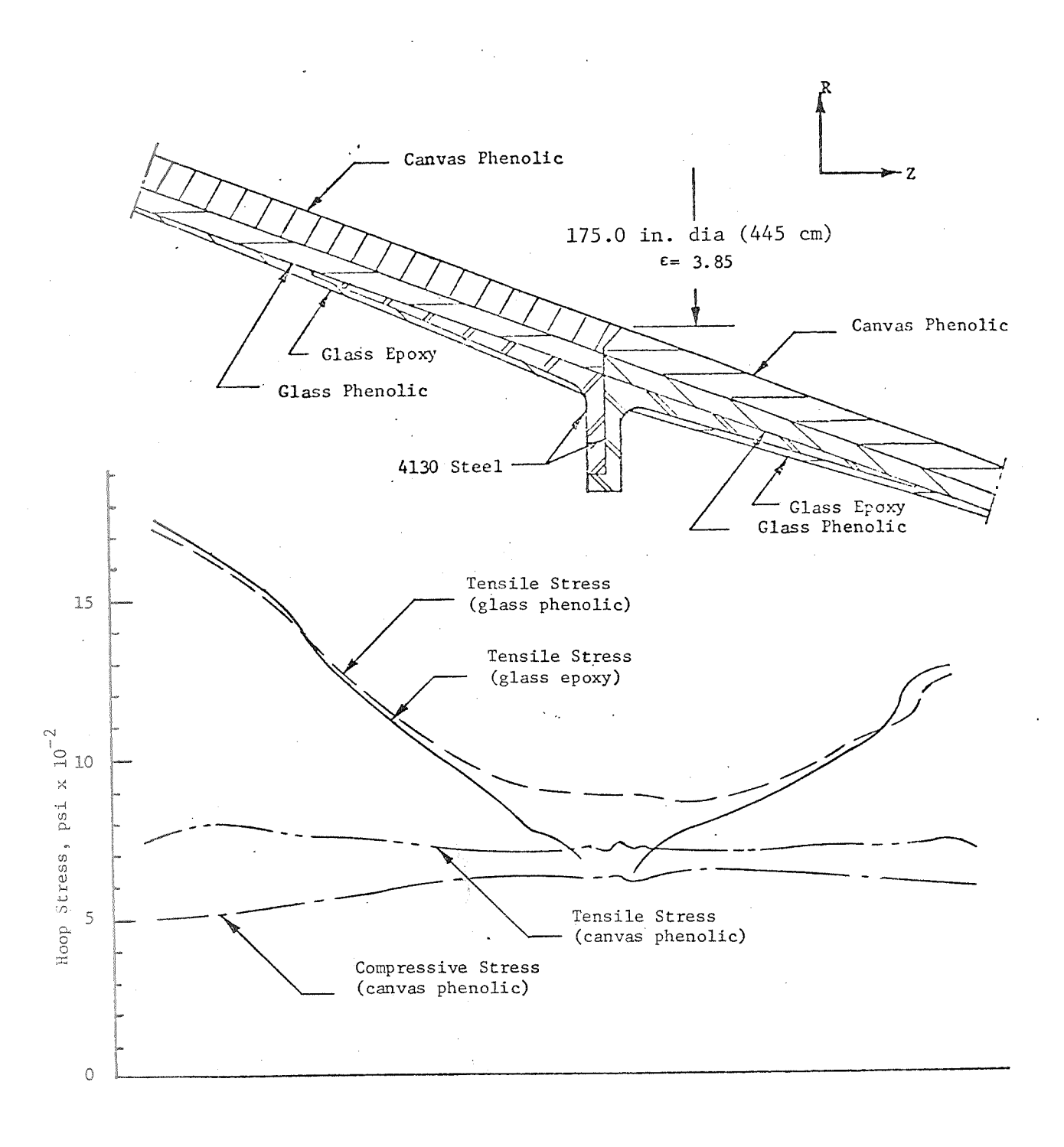


Figure 64. - Maximum Hoop Stress Distribution at Exit Cone ε = 3.85

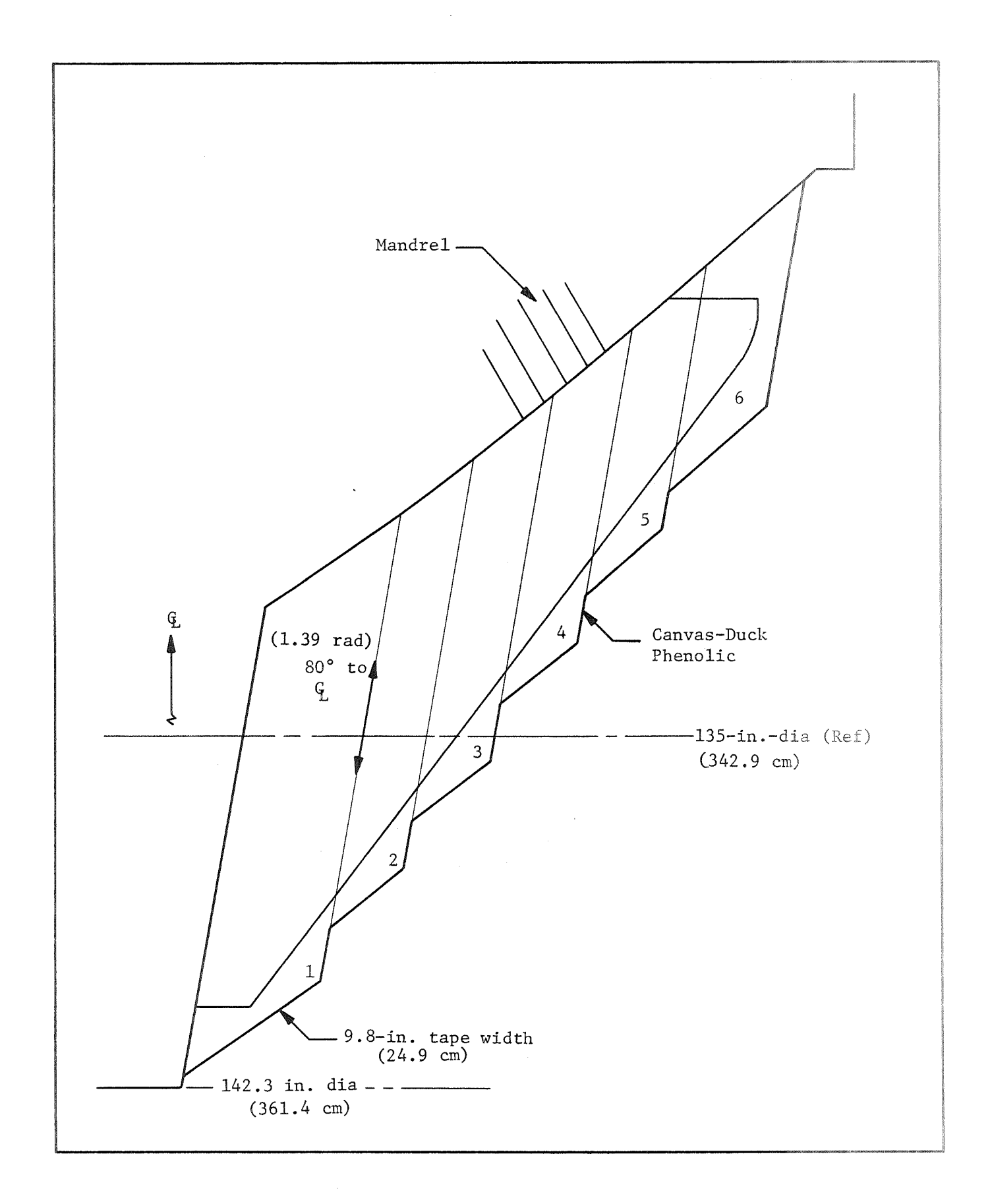


Figure 65. - As-Wrapped Closure Insulation Billet Configuration

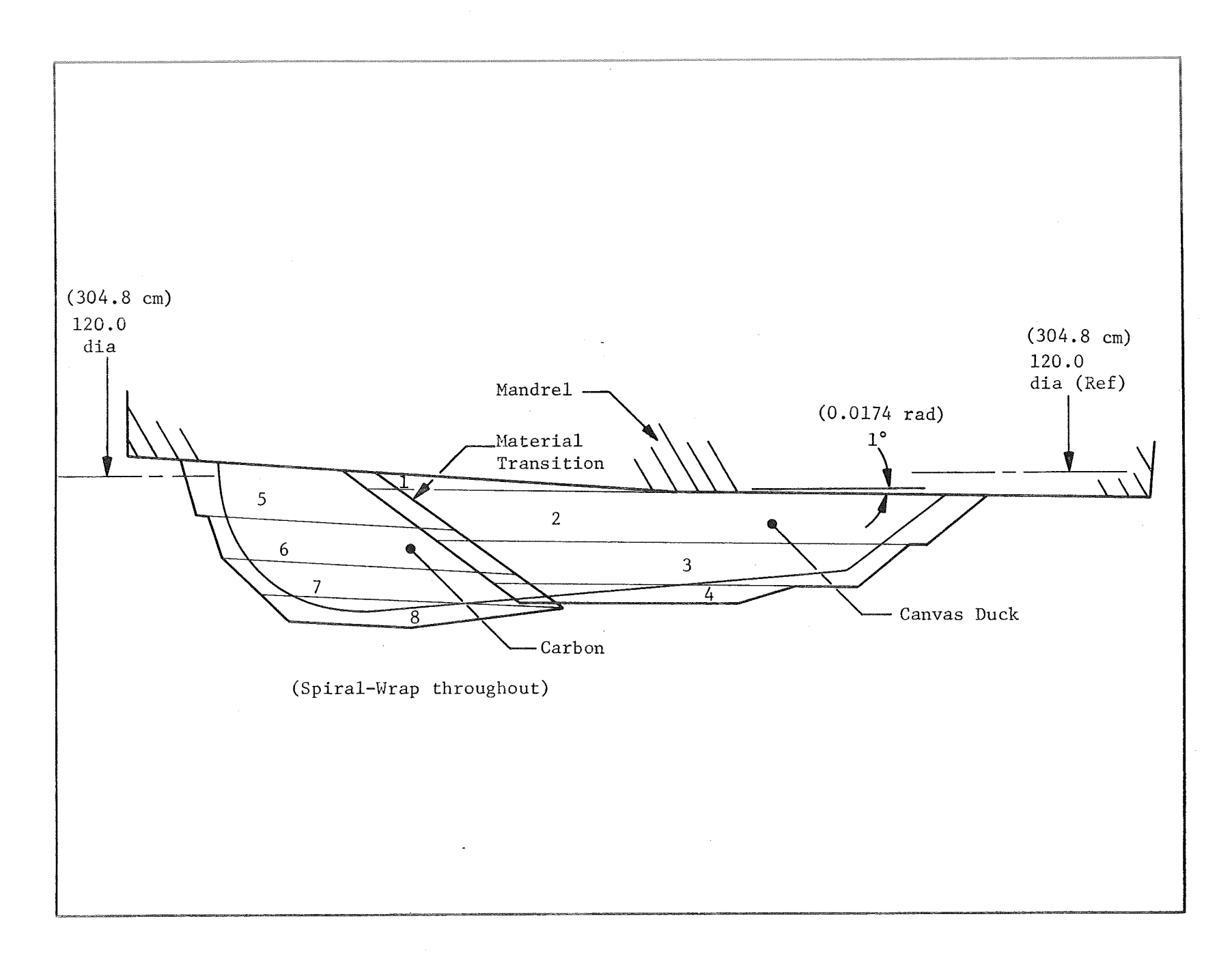


Figure 66. - As-Wrapped Submerged Insert-Billet Configuration

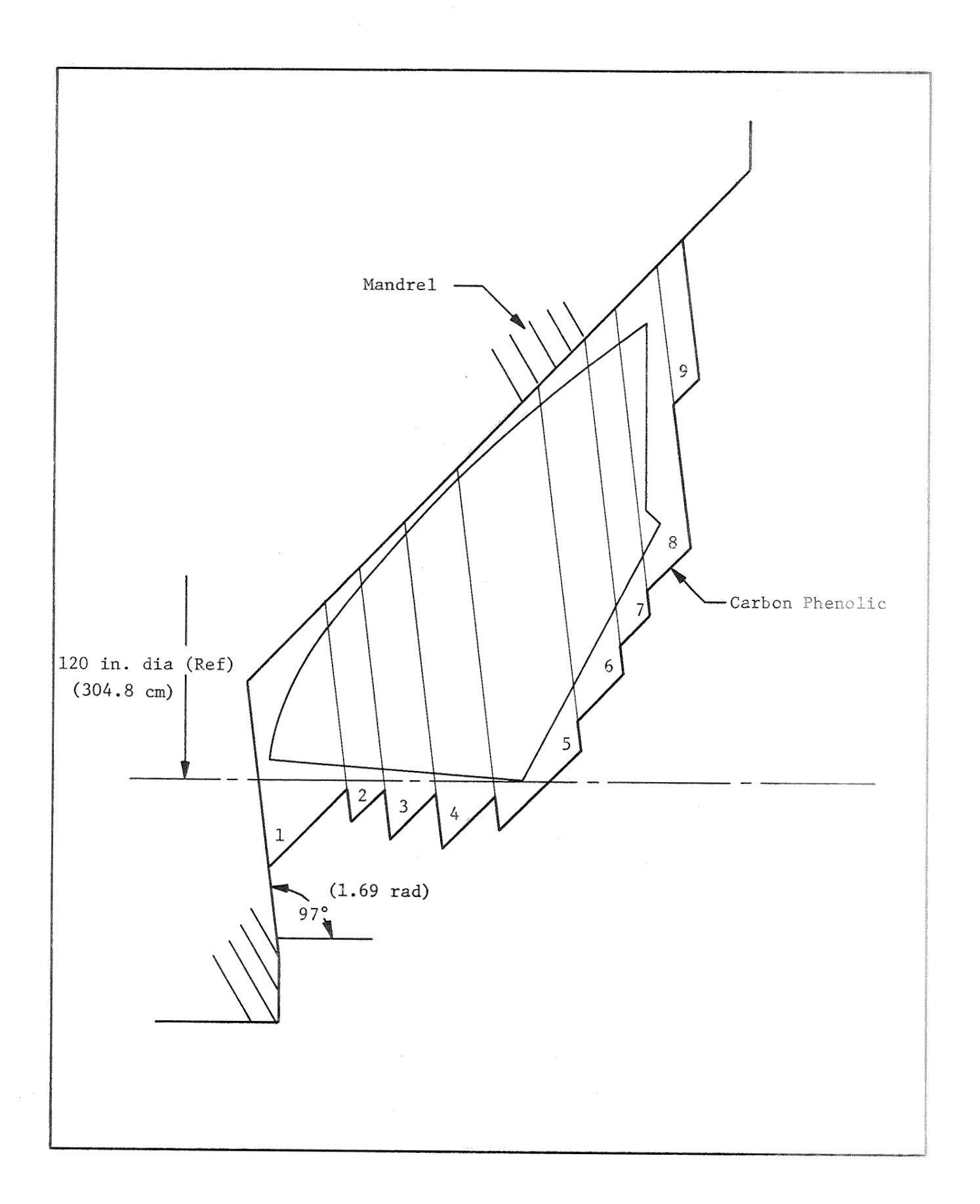


Figure 67. - As-Wrapped Nose Insert-Billet Configuration

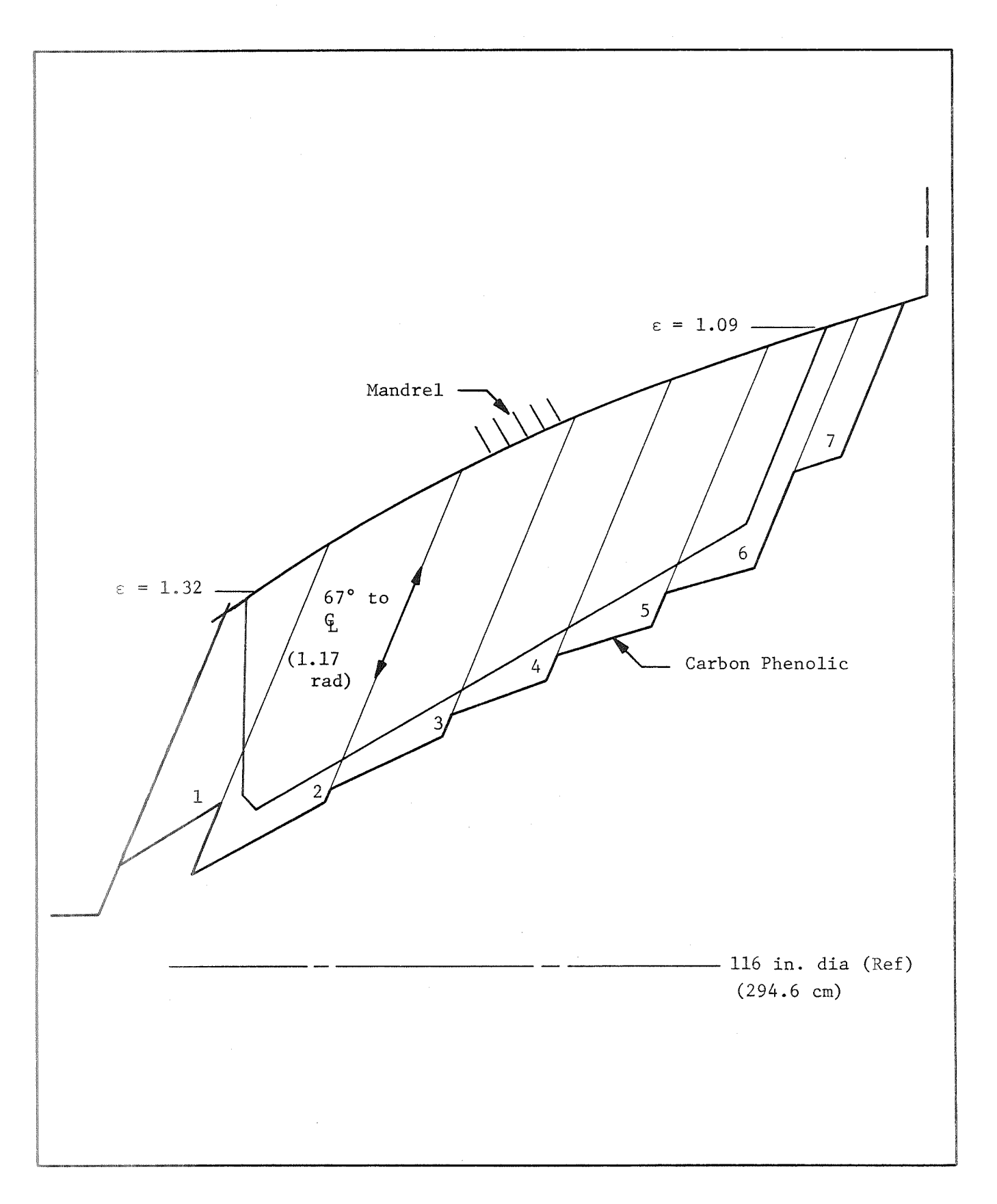


Figure 68. - As-Wrapped Entrance Insert - Billet Configuration

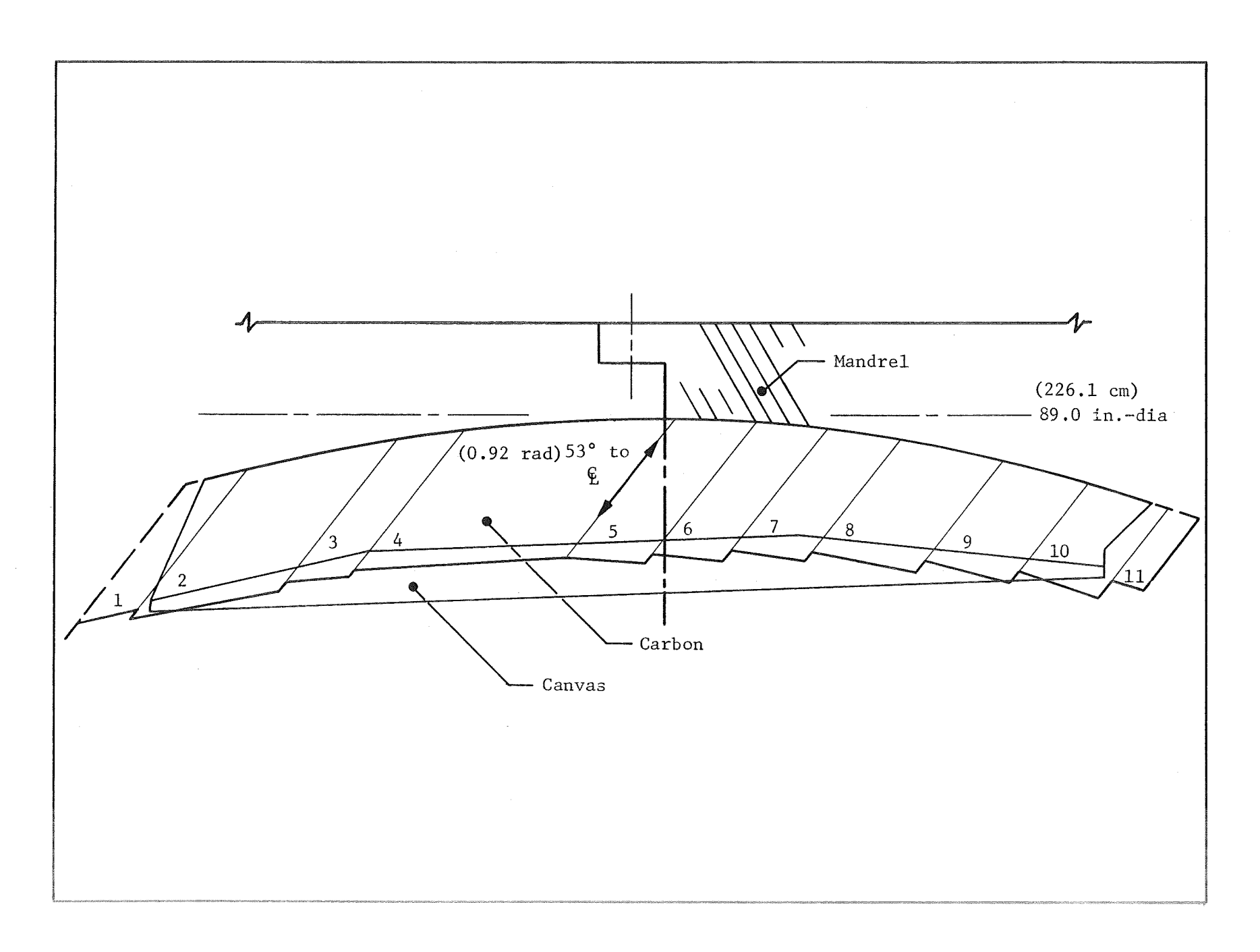


Figure 69. - As-Wrapped Throat Insert-Billet Configuration

Months	g-man-	2	3	4	5	6	7	8	9	10	77	12	13
Vertical Turning Machine (198-india)		ом приводательного почений в д 1949.											
Throat Insert**			2		3		4	7		5			
Approach Insert**		1		2		3		4			5		
Nose Insert**					2		3		4		5		
Vertical Turning Machine (240-india)													
Submerged Insert	1	2		3	4		5	6	ב				
Closure Insulator]	2		3	4		5	6				
Throat Insert										6			
Approach Insert						:					6		
Nose Insert				·								6	
Vertical Turning Machine (280-india) (new)													
Aft Exit Cone	1		2		3		4		5		6		
Fwd Exit Cone		1	The state of the s	2		3		4		5		6	
Nozzle Assembly Complete				企		थि				金		(

^{*}One New Vertical Turning Machine Required.

**One or more of these components could be subcontracted to another supplier.

Months	1	2	3	4	5	6	7	8	9	10	11	12	13
130-india Vertical Turning Machine (Subcontracted)													
Submerged Insert	1]		2		3		4		5		6		
Nose Insert		1		2		3		4		5	:	6	
198-india Turning Machine (Nozzle Prime Contractor)													
Throat Insert	1		2		3	i	4		5		6		
Approach Insert		1		2		3		4		5		6	
240-india Vertical Turning Machine (Nozzle Prime Contractor)												,	
Closure Insulator	1		2		3		4		5		6		
Forward Exit Cone Section		1		2		3		4		5		6	
280-india (New) Vertical Turning Machine at A-DD (Aerojet Prime)	·									,			
Aft Exit Cone Section	1		2		3		4		5		6		
Nozzle Assembly Complete			企		2		3		⑪		舒		얩

^{*}Subcontract 2 Components; Fab. Aft Exit Cone at A-DD

Figure 71. - Nozzle Fabrication Schedule - Option B*

LIST OF REFERENCES

- 1. Development of Cost-Optimized Insulation System for use in Large Solid Rocket Motors, Aerojet-General Corporation, Report NASA CR-72584, August 1969.
- 2. Evaluation of Low-Cost Materials and Manufacturing Processes for Large Solid Rocket Nozzles, Aerojet-General Corporation, Report AFRPL-TR-67-310, December 1967.
- 3. <u>Development of Low-Cost Ablative Nozzles for Solid Propulsion Rocket Motors</u>, Thiokol Chemical Co., Wasatch Division, Report NASA CR-72641, February 1970.
- 4. <u>Investigation of the Effects of Ablative Discrepancies on Nozzle</u>

 Performance Reliability, Aerojet-General Corporation, Report NASA CR72702, January 1970.
- 5. Development of a Temperature-Indicating Sensor for Use in Ablative Rocket Nozzles, Report AFRPL-TR-69-172, July 1969.
- 6. Saturn IB Improvement Study (Solid First Stage), Phase II, Douglas Missile and Space System Division, Report SM-51896, March 1966.
- 7. Development and Production Costs for 260-in.-dia First Stage Vehicle, Aerojet-General Corporation, Report NAS7-513, FR-2, April 1967.

DISTRIBUTION LIST FOR FINAL REPORT NASA CR-72973

NASA Lewis Research Center		Jet Propulsion Laboratory		
21000 Brookpark Road	Calif. Institute of Technology			
Cleveland, Ohio 44135		4800 Oak Grove Drive		
Attn: Contracting Officer		Pasadena, California 91103		
Mail Stop 500-313	(1)	Attn: Richard Bailey (1)		
J. J. Notardonato		Technical Library		
Mail Stop 500-205	(8)			
Technical Library		Scientific & Technical Information		
Mail Stop 60-3	(2)	Facility		
Tech. Report Control Office		NASA Representative		
Mail Stop 5-5	(1)	P. O. Box 33		
Tech. Utilization Office	(1)	College Park, Maryland 20740		
Mail Stop 3-19	(1)	Attn: CRT (6)		
Patent Counsel	(1)	0		
Mail Stop 500-311	(1)	Government Installations		
National Aeronautics and Space		AF Space Systems Division		
Administration		Air Force Unit Post Office		
Washington, D.C. 20546		Los Angeles, California 90045		
Attn: RPM/R. Wasel	(3)	Attn: Col. E. Fink (1)		
ATSS-AL/Technical Library	(2)			
,	` ,	AF Research & Technology Division		
NASA-Ames Research Center		Bolling AFB, D.C. 20332		
Moffett Field, California 94035		Attn: Dr. Leon Green, Jr. (1)		
Attn: Technical Library	(1)	()		
·	` ,	AF Rocket Propulsion Laboratory		
NASA-Langley Research Center		Edwards AFB, California 93523		
Langley Station		Attn: RPM/Mr. C. Cook (2)		
Hampton, Virginia 23365		•		
Attn: Robert L. Swain	(1)	AF Ballistic Missile Division		
Technical Library	(1)	P. O. Box 262		
		San Bernadino, California		
NASA-Goddard Space Flight Center		Attn: WDSOT (1)		
Greenbelt, Maryland 20771				
Attn: Technical Library	(1)	Army Missile Command		
		Redstone Scientific Info. Center		
NASA-Manned Spacecraft Center		Redstone Arsenal, Alabama 35809		
2101 Webster Seabrook Road		Attn: Chief, Document Section (1)		
Houston, Texas 77058	(1)			
		Ballistic Research Laboratory		
NASA George C. Marshall Space		Aberdeen Proving Ground,		
Flight Center		Maryland 21005		
Redstone Arsenal		Attn: Technical Library (1)		
Huntsville, Alabama 35812				
Attn: Technical Library	(1)	Picatinny Arsenal		
R-P&VE-PA/K. Chandler	(1)	Dover, New Jersey 07801		
		Attn: Technical Library (1)		

DISTRIBUTION LIST (cont)

Navy Special Projects Office Washington, D.C. 20360	(1)	Industry Contractors
Naval Air Systems Command Washington, D.C. 20360 Attn: AIR-330/Dr. O. H. Johnson	(1)	Aerojet Solid Propulsion Company P. O. Box 13400 Sacramento, California 95813 Attn: Dr. B. Simmons, 4800 (1)
Naval Ordnance Laboratory		Tech. Info. Center, (1) 4400
White Oak Silver Spring, Maryland 20910 Attn: Technical Library	(1)	Advanced Technology (8) Operations
Naval Propellant Plant		Aerojet-General Corporation P. O. Box 296
Indian Head, Maryland 20640 Attn: Technical Library	(1)	Azusa, California 91702 Attn: Technical Library (1)
Naval Ordnance Test Station China Lake, California 93557 Attn: Technical Library C. J. Thelen	(1) (1)	Aerospace Corporation 2400 East El Segundo Boulevard El Segundo, California 90245 Attn: Technical Library (1)
Naval Research Laboratory Washington, D.C. 20390	/3.	Solid Motor Dev. Office (1) Aerospace Corporation
Attn: Technical Library Chemical Propulsion Information Agency Applied Physics Laboratory	(1)	P. O. Box 95085 Los Angeles, California 90045 Attn: Technical Library (1)
8621 Georgia Avenue Silver Spring, Maryland 20910	(1)	Atlantic Research Corporation Shirley Highway at Edsall Road Alexandria, Virginia 22314
Defense Documentation Center Cameron Station		Attn: Technical Library (1)
5010 Duke Street Alexandria, Virginia 22314	(1)	Boeing Company P. O. Box 3999
Defense Materials Information Center Battelle Memorial Institute		Seattle, Washington 98124 Attn: Technical Library (1)
505 King Avenue Columbus, Ohio 43201	(1)	Chrysler Corporation Space Division Michoud Operations
Institute for Defense Analysis 1666 Connecticut Ave., N.W. Washington, D.C.		New Orleans, Louisiana Attn: Technical Library (1)
Attn: Technical Library	(1)	Hercules, Inc. Allegany Ballistics Laboratory
Advanced Research Projects Agency Pentagon, Room 3D154 Washington, D.C. 20354		P. O. Box 210 Cumberland, Maryland 21502 Attn: Technical Library (1)
Attn: Tech. Information Office	(1)	Accin. reconstruct bibliary (1)

DISTRIBUTION LIST (cont)

Hercules Company Bacchus Works P. O. Box 98 Magna, Utah 84044 Attn: Technical Library	(1)	Rohm and Haas Redstone Arsenal Res. Division Huntsville, Alabama 35807 Attn: Technical Library	(1)
Thiokol Chemical Corporation Wasatch Division Brigham City, Utah 94302 Attn: Dan Hess Technical Library	(1) (1)	Thiokol Chemical Corporation Elkton Division Elkton, Maryland 21921 Attn: Technical Library Thiokol Chemical Corporation	(1)
Lockheed Missiles & Space Company P. O. Box 504 Sunnyvale, California		Huntsville Division Huntsville, Alabama 35807 Attn: Technical Library	(1)
Attn: Technical Library Lockheed Propulsion Company P. O. Box 111 Redlands, California 93273	(1)	TRW Systems One Space Park Redondo Beach, California 90278 Attn: M. Kipow	3 (1)
Attn: Bud White Martin Marietta Corporation Baltimore Division	(1)	United Technology Center P. O. Box 358 Sunnyvale, California 94088 Attn: Technical Library	(1)
Baltimore, Maryland 21203 Attn: Technical Library Mathematical Sciences Corporation	(1)	Materials Advisory Board National Academy of Science 2101 Constitution Ave., N.W.	(1)
278 Renook Way Arcadia, California 91107 Attn: M. Fourney	(1)	Washington, D.C. 20418	(1)
Philco Corporation Aeronutronics Division Ford Road Newport Beach, California 92660 Attn: Technical Library	(1)		
Rocketdyne Solid Propulsion Operations P. O. Box 548 McGregor, Texas Attn: Technical Library	(1)		
Rocketdyne 6633 Canoga Avenue Canoga Park, California 91304 Attn: Technical Library	(1)		